



# LUND UNIVERSITY

## Combustion of selected alternative liquid fuels at oxy-fuel conditions: experiments and modelling

Nauc  r, Jenny D.

2016

*Document Version:*

Publisher's PDF, also known as Version of record

[Link to publication](#)

*Citation for published version (APA):*

Nauc  r, J. D. (2016). *Combustion of selected alternative liquid fuels at oxy-fuel conditions: experiments and modelling*. [Doctoral Thesis (compilation), Combustion Physics]. MediaTryck Lund.

*Total number of authors:*

1

*Creative Commons License:*

Unspecified

### General rights

Unless other specific re-use rights are stated the following general rights apply:

Copyright and moral rights for the publications made accessible in the public portal are retained by the authors and/or other copyright owners and it is a condition of accessing publications that users recognise and abide by the legal requirements associated with these rights.

- Users may download and print one copy of any publication from the public portal for the purpose of private study or research.
- You may not further distribute the material or use it for any profit-making activity or commercial gain
- You may freely distribute the URL identifying the publication in the public portal

Read more about Creative commons licenses: <https://creativecommons.org/licenses/>

### Take down policy

If you believe that this document breaches copyright please contact us providing details, and we will remove access to the work immediately and investigate your claim.

LUND UNIVERSITY

PO Box 117  
221 00 Lund  
+46 46-222 00 00



Combustion of selected alternative liquid fuels  
at oxy-fuel conditions: experiments and  
modelling



# Combustion of selected alternative liquid fuels at oxy-fuel conditions: experiments and modelling

Jenny D. Naclér



**LUND**  
UNIVERSITY

DOCTORAL DISSERTATION

by due permission of the Faculty engineering, Lund University, Sweden.

To be defended at Rydbergsalen, Fysicum, Professorgatan 1, 28<sup>th</sup> of  
October 2016 at 9:15.

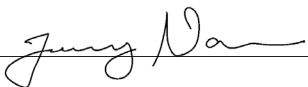
*Faculty opponent*

Professor Terese Løvås

Norwegian University of Science and Technology, Trondheim, Norway

Organization LUND UNIVERSITY Division of Combustion Physics Departement of Physics P. O. Box 118, SE-221 00 Lund, Sweden	Document name Doctoral disertation	
	Date of issue September 23, 2016	
Author(s) Jenny Nauc��r	CODEN LUTFD2/TFCP-198-SE	
Title and subtitle Combustion of selected alternative liquid fuels at oxy-fuel conditions: experiments and modelling		
<p>Abstract</p> <p>Combustion of fuels is a major source of energy and at the same time a threat to the environment. Carbon dioxide (CO<sub>2</sub>) emissions are one of the obstacles on the route to cleaner energy. Combining Carbon Capture and Storage-technology (CCS) with use of biofuels lead to a negative net release of CO<sub>2</sub> can be achieved. With some CCS-techniques the CO<sub>2</sub> is repurposed in the combustion process together with O<sub>2</sub>. However, use of CO<sub>2</sub> in the combustion process changes the prerequisites for the combustion process, and challenges our knowledge of fuel characteristics and chemistry.</p> <p>The first objective of the thesis was to increase the knowledge of fuels burnt under CO<sub>2</sub>-rich conditions. An increased understanding of alcohol chemistry under such conditions is of interest for its effect on fundamental combustion properties, such as the laminar burning velocity. Measurements of the laminar burning velocity were performed using the Heat flux method for ethanol and methanol flames with O<sub>2</sub>+CO<sub>2</sub> as the oxidizer. The experimental results were used as input to evaluate the performance of kinetic mechanisms from literature validated for combustion with air, at CO<sub>2</sub>-rich conditions and examining how the mechanisms interpret the chemistry in the examined mixtures.</p> <p>A second objective of the thesis was to study the ignition and flame characteristics of fuels with fuel-bound nitrogen, using nitromethane as a model-fuel. Nitromethane+O<sub>2</sub>+N<sub>2</sub> were examined for ignition characteristics in a shock tube, and the laminar burning velocity was examined for nitromethane burnt with air and with O<sub>2</sub>+CO<sub>2</sub>. From combining the experimental results with modeling and literature studies, the importance of knowledge of a fuel's combustion characteristics, when interpreting experimental results was highlighted. Both objectives of the thesis, on CO<sub>2</sub>-rich combustion and fuel-nitrogen combustion, were combined when nitromethane was studied at CO<sub>2</sub>-rich condition.</p> <p>Knowledge on important fundamental combustion properties under CO<sub>2</sub>-rich conditions was provided to the scientific community in the form of experimental results on laminar burning velocity and ignition characteristics. An evaluation of current knowledge of the underlying chemistry behind these fundamental combustion properties, was provided through kinetic modeling, highlighting gaps in our current understanding of combustion chemistry.</p>		
Key words fuel nitrogen, modeling, ignition, explosion, lamiar burning velocity, heat flux method, combustion, fuel, carbon dioxide		
Classification system and/or index terms (if any)		
Supplementary bibliographical information	Language English	
ISSN and key title ISSN 1102-8718	ISBN 978-91-7623-948-3 (Print) ISBN 978-91-7623-949-0 (Electronic)	
Recipient's notes	Number of pages 160	Price
	Security classification	

I, the undersigned, being the copyright owner of the abstract of the above-mentioned dissertation, hereby grant to all reference sources permission to publish and disseminate the abstract of the above-mentioned dissertation.

Signature  Date 2016-09-19

# Combustion of selected alternative liquid fuels at oxy-fuel conditions: experiments and modelling

Jenny D. Naclér



**LUND**  
UNIVERSITY

Copyright Jenny D. Naclér

Faculty of Engineering | Department of Physics

ISBN 978-91-7623-948-3 (Print)

ISBN 978-91-7623-949-0 (Electronic)

ISSN 1102-8718

ISRN LUTFD2/TFCP-198-SE

Printed in Sweden by Media-Tryck, Lund University  
Lund 2016



*If the apocalypse comes, beep me.*

*Buffy*

# Abstract

Combustion of fuels is a major source of energy and at the same time a threat to the environment. Carbon dioxide ( $\text{CO}_2$ ) emissions are one of the obstacles on the route to cleaner energy. Combining Carbon Capture and Storage-technology (CCS) with use of biofuels lead to a negative net release of  $\text{CO}_2$  can be achieved. With some CCS-techniques the  $\text{CO}_2$  is repurposed in the combustion process together with  $\text{O}_2$ . However, use of  $\text{CO}_2$  in the combustion process changes the prerequisites for the combustion process, and challenges our knowledge of fuel characteristics and chemistry.

The first objective of the thesis was to increase the knowledge of fuels burnt under  $\text{CO}_2$ -rich conditions. An increased understanding of alcohol chemistry under such conditions is of interest for its effect on fundamental combustion properties, such as the laminar burning velocity. Measurements of the laminar burning velocity were performed using the Heat flux method for ethanol and methanol flames with  $\text{O}_2+\text{CO}_2$  as the oxidizer. The experimental results were used as input to evaluate the performance of kinetic mechanisms from literature validated for combustion with air, at  $\text{CO}_2$ -rich conditions and examining how the mechanisms interpret the chemistry in the examined mixtures.

A second objective of the thesis was to study the ignition and flame characteristics of fuels with fuel-bound nitrogen, using nitromethane as a model-fuel. Nitromethane+ $\text{O}_2+\text{N}_2$  were examined for ignition characteristics in a shock tube, and the laminar burning velocity was examined for nitromethane burnt with air and with  $\text{O}_2+\text{CO}_2$ . From combining the experimental results with modeling and literature studies, the importance of knowledge of a fuel's combustion characteristics, when interpreting experimental results was highlighted. Both objectives of the thesis, on  $\text{CO}_2$ -rich combustion and fuel-nitrogen combustion, were combined when nitromethane was studied at  $\text{CO}_2$ -rich condition.

Knowledge on important fundamental combustion properties under  $\text{CO}_2$ -rich conditions was provided to the scientific community in the form of experimental results on laminar burning velocity and ignition characteristics. An evaluation of current knowledge of the underlying chemistry behind these fundamental combustion properties, was provided through kinetic modeling, highlighting gaps in our current understanding of combustion chemistry.

# Populärvetenskaplig sammanfattning

Förbränning är både vår största källa till energi och ett stort hot mot miljön i form av föroreningar och växthusgaser. Ett par av de stora bovorna i sammanhanget är koldioxid och kväveoxider och de stora mängderna av dessa i atmosfären. Där bidrar koldioxid till den globala uppvärmningen i egenskap av växthusgas. Kväveoxider påverkar både miljö och människors hälsa negativt genom att bilda marknära ozon. Tillsammans med vatten orsakar kväveoxiderna surt regn som skadar skogar och vattenbaserade ekosystem.

Försök till att begränsa koldioxidutsläpp görs genom Carbon Capture and Storage-tekniker (CCS). Dessa tekniker går ut på att separera ut koldioxiden och lagra den istället för att släppa ut den i atmosfären. I oxy-fuel-tekniker inom CCS kan koldioxiden återanvändas under förbränningsprocessen tillsammans med syre istället för luft. Kombinerat med biobränslen kan till och med ett negativt nettoutsläpp av koldioxid nås via oxy-fuel-tekniker. Att återanvända koldioxiden förändrar dock förutsättningarna för förbränningsprocessen jämför med konventionell förbränning med luft. Därmed skapas ett behov av grundläggande forskning angående förbränning av bränslen vid koldioxidrika förhållanden.

En viktig komponent för att förstå bränslen och dess kemi är att studera grundläggande egenskaper hos bränsleblandningar, som den laminära flamhastigheten. Det är den hastighet som en flamma rör sig genom att konsumera en bränsle/syreblandning. Det är en unik egenskap hos ett bränsle som i första hand är beroende av bränslet och dess kemi. Under arbetet som presenteras i denna avhandling har mätning av den laminära flamhastigheten varit en stor del av det experimentella arbetet.

Heat flux metoden användes för att mäta de laminära flamhastigheterna. Metoden tillåter att flammen stabiliseras på brännaren vid hastigheter nära den laminära flamhastigheten och utnyttjar därefter värmeutväxlingen mellan brännaren och flammen för att hitta den laminära flamhastigheten. De laminära flamhastigheterna ger inte bara information om bränslets förbränningsegenskaper, utan är värdefullt för att validera vår teoretiska förståelse för förbränningskemi.

På grund av de höga temperaturerna vid förbränning så är förbränningskemi komplext att studera experimentellt. Många reaktioner kan ske och under korta tidsförlöpp. Det gör det svårt att studera detaljer av förbränningskemin

experimentellt. Därför är kinetiska modeller ett bra komplement till experimentella studier för förbränningsprocesser och bränslekemi. Kinetiska reaktionsmekanismer är en samling av kemiska reaktioner som används tillsammans för att beskriva kemin av ett bränsle vid förbränning. Genom att använda kinetiska modeller kan både flamegenskaper förutspås vid förhållanden som inte studerats experimentellt, och information om kemin ser ut på detaljnivå fås. Kvaliten på resultaten från kinetiska mekanismerna är dock starkt beroende på hur väl mekanismerna kan förutspå förbränningsegenskaper där vi har experimentella resultat. Det är viktigt att jämföra de simulerade resultaten med experiment vid olika förhållanden. Därigenom fås mekanismer som reflekterar så realistisk kemi som möjligt och i förlängningen tillförlitligt kunna användas utanför förhållanden som täcks av experimentella resultat. Därför innehåller studierna i denna avhandling mekanism validering, inte bara mot de egna resultaten utan även mot experiment från litteraturen.

Det här forskningsprojektet fokuserar på att bidra med ny kunskap genom nya experimentella studier av grundläggande förbränningsegenskaper hos bränslen, under förhållanden som aldrig blivit undersökta för dessa bränslen tidigare. Flamhastigheter mättes för kända bränslen vid koldioxid rika förhållanden. Antändning undersöktes hos ett kvävebaserat bränsle. Kunskapsläget om kemin för de utvalda bränslena utreddes genom att testa prestationen hos väletablerade kinetiska mekanismer som presterar väl vid förbränning i luft, mot de nya experimentella resultaten.

Bränslena som studerats i denna avhandling valdes med tanke på dess relevans för biobränslen. Alkoholer är vanliga biobränslen med användningsområden i dagen samhälle. Alkoholer används som bränsle, med etanol som är ett vanligt bränsle för bilar och metanol som används till båtmotorer. De är även intressanta i egenskap av förstadier till aldehyder, vilka är vanliga komponenter under förbränning av många andra bränslen.

En positiv sidoeffekt vid användning av oxy-fuel-tekniker är att mängden kväveoxider minskar. Det är en effekt både av att inget kväve tillförs via luft och de ändrade förbränningsförhållandena som till exempel förbränningstemperatur och kemi. Då inget kväve tillförs via luft så återstår kväveoxiderna som ursprungligen från kväve bundet i bränsle. Ett kvävebaset bränsle som används idag är nitrometan, med tillämnningar inom till exempel dragracing. Förutom dess användning som ett bränsle, så är nitrometan framför allt utmärkt som modell för att studera bränslebundet kväve på grund av dess kväve-innehåll bundet till kolet och dess enkla struktur.

Laminära flamhastigheter för etanol och metanol tillsammans med  $O_2+CO_2$  mättes med hjälp av Heat flux metoden för första gången. Därefter används resultaten för att utvärdera hur väl etablerade kinetiska mekanismer från litteraturen klarar av att

beskriva alkoholkemin under koldioxidrika förhållanden. Där såg vi att mekanismer som presterar bra i konventionell förbränning med luft presterar sämre vid förbränning med koldioxid. Genom studien på etanol kom insikten att modellerna hanterar kemin under koldioxid-rika förhållanden liknande som de hanterar förbränning med luft. Intressant är att trots att de presterar väl för etanol+luft så skiljer sig prestationerna hos mekanismerna för etanol flammorna med mokyliärt syre+koldioxid skiljer i kvalitet både jämfört med luft och emellan mekanismerna. I studien om metanolförbränning så visades det på att enkla modifieringar av kemin kunde förbättra kvaliteten på prestationen vid CO<sub>2</sub>-rika förhållanden utan att kompromissa på kapaciteten för att beskriva förbränning vid luft för en etablerad mekanism från litteraturen.

För nitrometan studerades både den laminära flamhastigheten och trender i dess antändning. Med hjälp av de experimentella resultaten tillsammans med modelleringen och litteraturstudier bekräftades det att nitrometanförbränning har en ovanlig struktur, med två stadier både i flammor och under antändning. Den insikten användes till att utvärdera experimentella resultat från litteraturen och analysera de egna resultaten. Genom studien av antändningsfördröjningstiden i nitrometan+O<sub>2</sub>+N<sub>2</sub> kunde informations om egenskaper som tryck- och temperaturberoende och beroendet av blandningsförhållande utredas för båda stadierna av antändningen. Aktiverings energi kunde härledas från för båda stadierna. Studierna om nitrometan visade på att kemin av nitrometan är ännu inte fullt utredd. Egenskaper som tryckoberoende antändning och flamhastigheter vid CO<sub>2</sub>-rika förhållanden kunde inte förutspås genom modellering. Tillsammans visade nitrometan-studierna på att kunskapsläget om förbränning av bränslen med kolbundet kväve genom nitrometan inte är tillräckligt. För att framgångsrikt kunna beskriva nitrometans grundläggande förbränningsegenskaper och kemi korrekt behövs djupgående studier som täcker olika förhållanden och förbränningsegenskaper.

# List of papers

The thesis is based on the work presented in the following papers.

**Paper I.** J. D. Nauc  r, M. Christensen, E. J. K. Nilsson, A. A. Konnov, Oxy-fuel combustion of ethanol in premixed flames, *Energy and Fuels* 26 (2012) 4269-4276, DOI: 10.1021/ef3008085

**Paper II.** J. D. Nauc  r, L. Sileghem, E. J. K. Nilsson, S. Verhelst, A. A. Konnov, Performance of methanol kinetic mechanism at oxy-fuel conditions, *Combustion and Flame* 162 (2015) 1719-1728, DOI: 10.1016/j.combustflame.2014.11.033

**Paper III.** J. D. Nauc  r, E. J. K. Nilsson, A. A. Konnov, Laminar burning velocities of nitromethane+air: a comparison of flat and spherical flames, *Combustion and Flame* 162 (2015) 3801-3807, DOI: 10.1016/j.combustflame.2015.07.017

**Paper IV.** J. D. Nauc  r, Y. Li, E. J. K. Nilsson, H. J. Curran, A. A. Konnov, An experimental and modeling study of nitromethane+O<sub>2</sub>+N<sub>2</sub> ignition in a shock tube, *Fuel*, 186 (2016) 629-638, DOI: 10.1016/j.fuel.2016.09.003

**Paper V.** J. D. Nauc  r, E. J. K. Nilsson, A. A. Konnov, An experimental and modeling study of nitromethane flames at CO<sub>2</sub>-rich conditions, *submitted to Energy and Fuels*

## Related work

V. A. Alekseev, J. D. Nauc  r, M. Christensen, E. J. K. Nilsson, E. N. Volkov, L. P. H. de Goey, A. A. Konnov, Experimental uncertainties of the heat flux method for measuring burning velocities, *Combust. Sci. Tech.* 188 (2016) 853-894, DOI: 10.1080/00102202.2015.1125348

C. Brackmann, J. Bood, J. D. Nauc  r, A. A. Konnov, M. Ald  n, Quantitative picosecond laser-induced fluorescence measurements of nitric oxide in flames *Proceedings of the Combustion Institute* (2016), DOI: 10.1016/j.proci.2016.07.012

# Content

Abstract	iv
Populärvetenskaplig sammanfattning	v
List of papers	viii
Related work	viii
Content	ix
1    Introduction	1
1.1    Outline of thesis	3
2    Combustion concepts	4
2.1    Equivalence ratio	4
2.2    Premixed laminar flames	6
2.2.1    Laminar flame structure	6
2.2.2    Adiabatic laminar burning velocity	8
2.2.3    Temperature dependence of laminar burning velocity	9
2.2.4    Cellular structures	11
2.3    Ignition	13
2.3.1    Ignition delay time	13
2.3.2    Correlations of ignition delay time	14
3    Combustion chemistry	16
3.1    Flame- vs ignition-chemistry	18
3.2    The role of carbon dioxide in combustion chemistry	19
3.3    Kinetics	19
4    Combustion modeling	21
4.1    Detailed kinetic mechanisms	21
4.2    Modeling of combustion phenomena	22
4.3    Laminar burning velocity	23
4.4    Ignition	24
4.5    Evaluating the effect of carbon dioxide	24
4.6    Sensitivity to individual reactions and rate constants	25

4.7	Reaction path analysis	26
4.8	Rate of production	26
5	Experimental methods for quantifying combustion properties	28
5.1	Experimental methods for determining the laminar burning velocity	28
5.1.1	Heat flux method	29
5.1.2	Spherically expanding flames	33
5.2	Ignition	34
5.2.1	Shock tube	34
6	Results	37
6.1	Laminar burning velocity of alcohols at CO <sub>2</sub> -rich conditions	37
6.1.1	Ethanol+O <sub>2</sub> +CO <sub>2</sub>	38
6.1.2	Methanol+O <sub>2</sub> +CO <sub>2</sub>	40
6.2	Characterization of nitromethane combustion	44
6.2.1	Laminar burning velocity	45
6.2.2	Ignition	48
6.2.3	Nitromethane under CO <sub>2</sub> -rich conditions	51
7	Summary and outlook	55
	Acknowledgements	57
	References	58
	Summary of papers	65

# 1 Introduction

The work presented in the thesis aims at the following:

- Producing and presenting experimental data on the combustion of different fuels under conditions that have not been studied previously. (Papers I-V)
- Increasing the understanding of combustion taking place under CO<sub>2</sub>-rich conditions. (Papers I-II and Paper V)
- Presenting new information concerning the combustion behavior of nitrogen-containing fuels. (Papers III-V)
- Evaluating the performance of detailed kinetic mechanisms and their interpretation of the relevant chemistry for the examined fuels. (Papers I-V)

The thesis work is based on efforts to achieve these goals and to provide the scientific community with new knowledge.

The combustion of fuels has negative effects, from an environmental perspective. In light of the increasing need of energy in the world and the high degree of stress on the environment caused by climate change and pollution, environmentally friendly solutions for the combustion techniques employed are in high demand. At the same time, thermal and kinetic energy obtained from the combustion of fuels is presently the dominant energy product in the world, 80% of the energy consumption is based on fossil fuel [1]. Its popularity is due to the high levels of easily accessible energy that is released during combustion.

Unfortunately the output of combustion is not energy alone, but consists of such unwanted products as pollutants and greenhouse gases. One of the challenges for the scientific community in this respect is to increase the knowledge of combustion and of the role chemistry plays in the formation of pollutants. Even under ideal conditions with complete combustion, carbon dioxide (CO<sub>2</sub>) and water (H<sub>2</sub>O), two greenhouse gases are the final products. An important task in gaining an understanding of combustion is knowledge of how these products affect the combustion process and its chemistry. In real combustion scenarios side-products are formed in addition to the carbon dioxide and water. Many of these side-products act as pollutants and have strong implications for the environment.

Carbon dioxide is an abundantly produced greenhouse gas from anthropogenic activity. As a greenhouse gas it contributes to global warming, through absorbing heat and emitting it back into the atmosphere.

All combustion processes lead to emissions of carbon dioxide. In efforts to deal with the problem of carbon dioxide emissions, the scientific community is exploring techniques to capture and store the carbon dioxide instead of releasing it into the atmosphere. In CCS-techniques, carbon dioxide can be repurposed in the combustion process. The flue gas is used as a diluent for molecular oxygen ( $O_2$ ) in the combustion process. This technique generates a highly concentrated flue gas consisting mostly of carbon dioxide and water while at the same time reducing the amount of flue gas released into the atmosphere. Replacing air by a mixture of  $O_2+CO_2$  has implications for the combustion process, affecting combustion properties as the laminar burning velocity. Considerations of this sort motivated the work presented in Papers I-II and Paper V.

A secondary, yet important effect of oxy-fuel combustion is that nitrogen oxides are produced and released to a lesser extent as compared to combustion with air. The nitrogen containing oxide species nitrogen oxide (NO) and nitrogen dioxide ( $NO_2$ ) are commonly referred to collectively as NOx. The two species are in equilibrium with each other in the atmosphere, with their total amount relatively stable during the course of a day, but their individual concentrations varying depending upon the temperature and the sunlight. The presence of NOx in the atmosphere is problematic for both health and environmental reasons. Via photochemistry NOx participates in the formation of ground-level ozone ( $O_3$ ) and can therefore contribute indirectly to the greenhouse effect. In contact with water and hydroxyl (OH) in the atmosphere, nitrogen dioxide forms nitrous acid ( $HNO_2$ ) and nitric acid ( $HNO_3$ ), which are components of acidic rain.

When a nitrogen source in the form of air is removed from the combustion process, only the nitrogen bound to the fuel is left. The fuel-nitrogen is also a major combustion related source of NOx in the atmosphere. Thus, gaining a better understanding of the chemistry of nitrogen-containing fuels is an important step towards understanding of the formation of NOx, and being a motivation for the work that led to Papers III-V.

The development in combustion is moving towards the use of liquid biofuels as an alternative to fossil fuels. Biofuels are renewable fuels that formed from organic material. Biofuels are considered to be carbon dioxide-neutral since their carbon content has been absorbed from the atmosphere through photosynthesis. The fuels examined here were selected from established liquid fuels to reflect how the present knowledge on combustion of these fuels translates to carbon dioxide-rich conditions. Alcohols are common biofuels, which are frequently used as fuels for engines. Ethanol is often employed as an additive to gasoline for cars, and can also

serve as the primary fuel [2, 3]. Methanol is likewise gaining popularity as a fuel [4-6]. For nitrogen-containing fuels, nitromethane is an excellent model for understanding nitrogen-containing fuels as it is a known fuel-nitrogen species in emissions from fuels [7, 8], but promising monopropellant [9, 10], and a fuel used in real applications, such as burned together with methanol in drag racing cars [11, 12].

## 1.1 Outline of thesis

The outline of the thesis is as follows. First some general concepts connected with combustion, as well as fundamental physical properties of flames and ignition, are explained in Chapter 2. An overview of the principles of combustion chemistry is presented in Chapter 3. Chapter 4 concerns kinetic modeling and how it was applied during the work presented in the thesis.

After this background, the experimental methods employed during the work of this thesis are discussed briefly in Chapter 5. Various aspects of the experimental work that were of importance for the work in this thesis are explained in greater detail.

In Chapter 6, the results obtained during the thesis-work are presented and discussed.

Chapter 7 finally summarizes the thesis as a whole and provides an overview of possible future work.

## 2 Combustion concepts

Combustion research endeavors to deal with the negative aspects of combustion through gaining a better understanding of the physics and the chemistry involved in combustion on a fundamental level. The fundamental properties of combustion, as for example laminar burning velocity and ignition are controlled primarily by the chemistry of the fuel. Factors affecting fundamental properties do so by their influence on the chemistry of the fuel + oxidizer mixtures as opposed to external influence. This makes them particularly interesting for combustion research, both to learn about the fundamental behavior of the fuel, but also be used to indirectly study its chemistry through using these properties as input for theoretical studies of the chemistry.

Below some of the properties and general terms related to combustion are explained.

### 2.1 Equivalence ratio

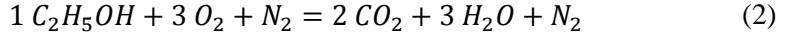
There are generally two components in a combustible mixture, the fuel and an oxidizer. The oxidizer consists of molecular oxygen and a diluting and usually inert gas. The molar ratio of the fuel to the molecular oxygen has a high influence in combustion. It affects the combustion through the chemical equilibrium of the global process. In experimental studies, it is an important variable, when examining combustion properties.

In the stoichiometric balance it is calculated the molecular ratio of reactants required for the reaction to go to completion. In ideal combustion, when a carbon based fuel reacts with molecular oxygen, the products are carbon dioxide and water. For combustion processes, the stoichiometry is considered balanced when the combustible mixture of fuel and oxidizer is fully converted to its final products.

The equivalence ratio ( $\phi$ ) is defined as the molar ratio of the fuel to molecular oxygen in relation to the same ratio of a stoichiometric mixture, prior to combustion occurring. The definition of equivalence ratio is as follows

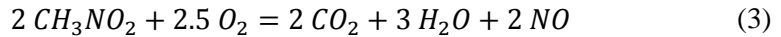
$$\phi = \frac{(fuel/O_2)}{(fuel/O_2)_{stoichiometric}} \quad (1)$$

The stoichiometric ratio is taken from the molar balance of the fuel and molecular oxygen in the stoichiometric balance, as exemplified below with the stoichiometric equation of ethanol with molecular oxygen.



Traditionally, the equivalence ratio is calculated with use of molecular nitrogen,  $N_2$ , as the final product for fuel-nitrogen chemistry. Such an approach is valid for most fuels, as the unreactive  $N_2$  from the air is often the most abundant nitrogen source. This approach was appropriate for the studies presented in Papers I-II.

When the fuel has nitrogen incorporated into its structure, the nitrogen participates in the chemistry through different paths, and other products are formed as compared to the molecular nitrogen from air. It also affects the choice of major nitrogen-containing product in the stoichiometric balance. The choice of definition of equivalence ratio is discussed further in Paper III and in Chapter 0. For part of the work in the thesis related to nitromethane, presented in Papers III-V, nitrogen oxide was used as the final nitrogen-species in the form of the stoichiometric equation below.



At equivalence ratio 1, the combustion is stoichiometric, and is going to completion with all of the reactants being converted to products. When there is an excess of fuel, equivalence ratio  $>1$ , the combustion conditions are termed “rich”, here there is insufficient oxygen to convert all fuel to its final products, but unburnt and partially burnt hydrocarbons, and accordingly emissions of carbon monoxide (CO) can be expected. When molecular oxygen is more abundant than the fuel, the conditions are termed “lean”. As there is more oxygen than fuel available, the fuel can be expected to be fully consumed, and radicals based on oxygen to be prevalent.

## 2.2 Premixed laminar flames

In a laboratory environment premixed laminar flames are widely studied because they are simple type of flames, designed to be governed predominantly by its chemistry, and isolated from external influence as for example turbulence. Through premixing the unburnt gas, fuel and oxidizer, are evenly spread in the volume of the gas, ensuring that the gas mixture is fed to the flame over the surface of the reaction zone. In a laminar flow, the unburnt gas moves in parallel layers, in a uniform flow, without lateral convection. A flame can be considered laminar if it is situated within a laminar flow. In a laminar flame the reaction zone is a one dimensional infinite planar sheet [13].

Movement in a laminar flow, as diffusion occurs along the direction of the flow, can cause local concentration gradients. However, it does not affect the definition of the flame as planar. The classification of the mixture as premixed is still valid, as it refers to the mixing together of the fuel and oxidizer prior to interaction with the flame.

### 2.2.1 Laminar flame structure

A flame can be seen as a self-sustaining reaction. It is visible because of the emission from burning gases. A flame can be divided up in different zones [14], as exemplified in Fig. 1. It is assumed there that the flame is premixed, ignited and stable. The zones are defined in relation to the flame itself, which is structured from the unburnt gas in the vicinity of the flame, through the preheat zone and the flame front to the post flame zone after the flame.

In the **unburnt zone** situated before the flame itself, not much is happening. The fuel and oxidizer are present but do not react here. The gas mixture is uniformly mixed. The temperature is not sufficiently high to initiate the combustion process.

Moving towards the flame the mixture enters the **preheat zone**. The mixture is still unburnt, but the temperature is rising through heat transfer from the flame. There is a large amount of unburnt species that acts as a heat sink, giving the temperature rise a concave shape in relation to distance to the flame front. The rising temperature can initiate the initial reactions, as the decomposition of the fuel. Because of the heating of the mixture in the preheat zone, thermal diffusion can create a concentration gradient along the direction of the flow, perpendicular to the flame front.

When the mixture has reached a sufficient temperature in the **inner layer** the fuel and the oxidizer are consumed and a radical pool builds up.

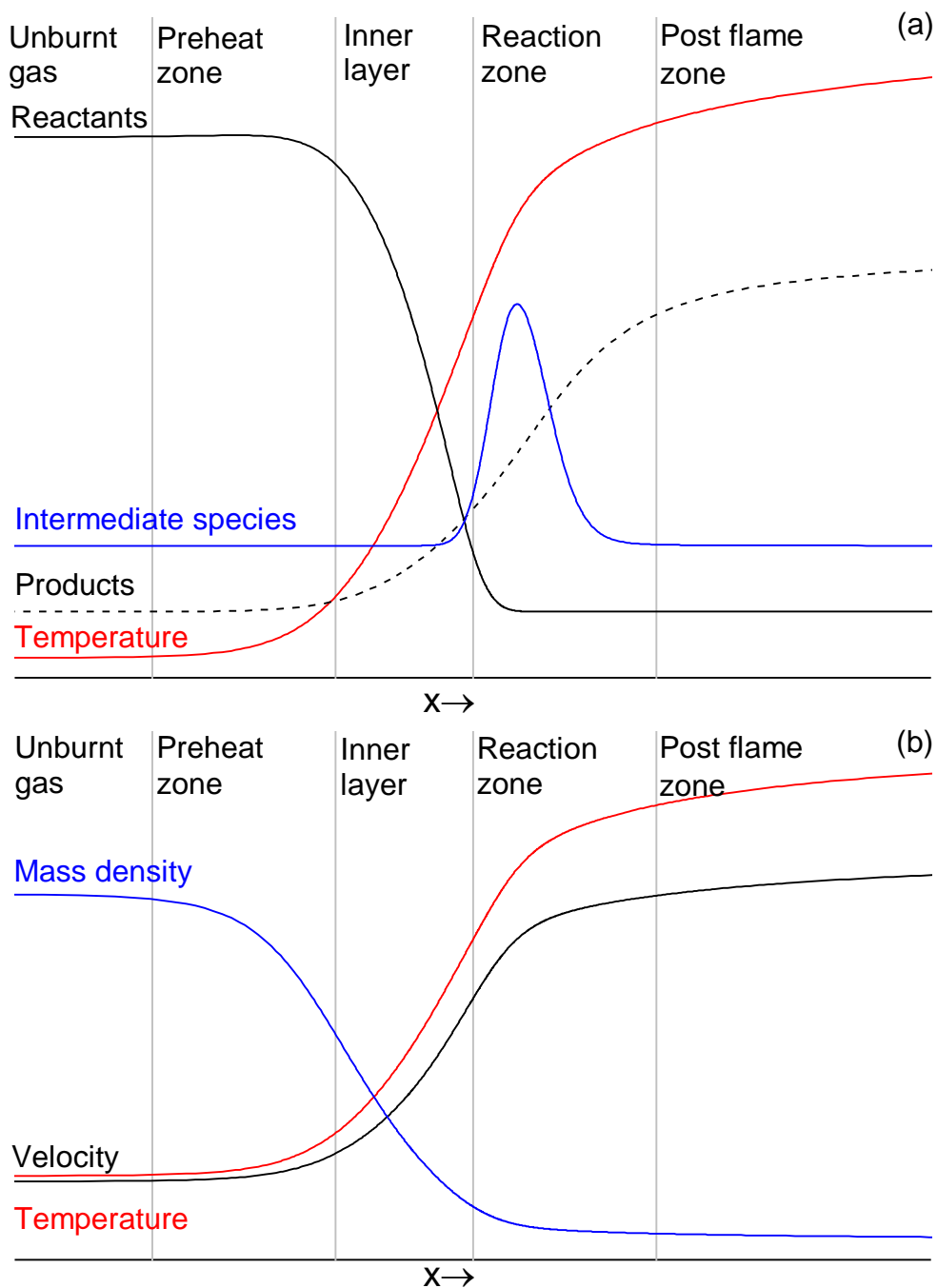


Figure 1: Schematic examples of (a) the flame structure across a flat laminar flame, with temperature and the main events taking place at the different zones related to distance across the flame, and in (b) the evolution of the gas velocity and the mass density across the structure of a flame are shown.

At the **flame front**, the radical pool that was built up in the inner layer is activated. Here the actual flame begins. Intermediate species are produced and are consumed at a high rate, driven by the high temperature. The temperature peaks in near proximity behind the reaction zone, and levels out to a plateau.

In **post flame zone** the majority of the reactions have already taken place. Stable species that are produced at the flame front, but were not consumed there are present in the post flame zone. This zone consists of hot gases, mostly carbon dioxide and water, but also unwanted side products, as pollutants. There the temperature is maintained by the product gases, and starts to decline as the product gases are cooled.

### 2.2.2 Adiabatic laminar burning velocity

The term adiabatic describes an ideal process, occurring without energy exchange with its surrounding. An adiabatic flame temperature is the temperature a flame would reach without any loss of heat to its surroundings. The velocity of a flame can also be described as adiabatic. In a real flame, the adiabatic velocity is the velocity where the net heat interactions with the surroundings are zero.

An unconstrained flame propagates at the rate of its consumption through a mixture of fuel and oxidizer. The laminar burning velocity ( $S_{LU}$ ) can be defined as the velocity at which flow of the unburnt gas is equal to the rate of consumption of the flame, creating a stationary flame unaffected by stretch.

The velocity of the gases is affected by the flame. The velocity starts to increase in the preheat zone, there being a strong increase as the gases pass through the flame front. In the post flame zone the increase in velocity levels off and eventually reaches a plateau. The increase in velocity is due to thermal expansion of the gas, and causes it to be higher on the burnt than on the unburnt side of the flame.

An illustration of how the gas velocity is related to the flame is presented in Fig. 1(b). As the propagation velocity differs depending on the position in the flame, defining the laminar burning velocity requires consideration to be taken to the flame. The laminar burning velocity is commonly referred to as the laminar burning velocity on the unburnt side of the flame ( $S_{LU}$ ), the velocity of the unburnt gas before it is affected by interaction with the flame.

The laminar burning velocity is one of the fundamental properties of a fuel+oxidizer when combusted in the form of a flame. It is dependent on the rate of the chemistry as a whole, the diffusion of radicals to the flame front and the flame temperature. The laminar burning velocity can be varied by changing external conditions as mixture composition, unburnt gas temperature, and pressure. The variations in laminar burning velocity based on changing such external conditions

as pressure and temperature are mainly an indirect effect of the flame temperature. The effects of mixture composition through varying the equivalence ratio, affect the chemistry through the ratio of reactants, thereby influencing the global chemical equilibrium.

For flames having a velocity less than the adiabatic laminar burning velocity its conditioned sub-adiabatic, whereas for flames having a higher velocity than the laminar burning velocity the conditions are super-adiabatic.

For the scientific community accurate data on the laminar burning velocity is imperative, as it is valuable not simply as information of the fundamental property itself, but also as a validation target for kinetic mechanisms. It is thus greatly valued because it enables validation of a mechanism as a whole and gives clues on the reactivity, the diffusive properties and the exothermicity of the mixture that is investigated. The laminar burning velocity is also valuable as input for understanding of other combustion phenomena, for example turbulent combustion.

### 2.2.3 Temperature dependence of laminar burning velocity

Given that the laminar burning velocity is dependent on the three independent variables: unburnt gas temperature, pressure and equivalence ratio; the laminar burning velocity can be evaluated as a function of unburnt gas temperature or pressure for each equivalence ratio.

The temperature dependence can be described by a correlation coefficient given by Eq. (4). In Eq. (4) the known laminar burning velocity ( $S_{LU,0}$ ) at a given temperature ( $T_u$ ) is used together with a power exponent ( $\alpha$ ) to calculate the expected laminar burning velocity at other temperatures  $T_{u,0}$ . The pressure dependence can also be described using (4), but not discussed further as it is outside the scope of the thesis.

$$S_{LU} = S_{LU,0} \left( \frac{T_u}{T_{u,0}} \right)^\alpha \left( \frac{P_u}{P_{u,0}} \right)^\beta \quad (4)$$

The experimental result for each equivalence ratio is processed on a logarithmic scale, where the power coefficient ( $\alpha$ ) is taken from the slope of the linear fit of the laminar burning velocity to temperature.

An example of a temperature dependence of laminar burning velocity is presented in Fig. 2, which illustrates the linearity of the laminar burning velocity

as a function of temperature on a logarithmic scale, and  $\alpha$  from Eq. (4) as a function of equivalence ratio is presented for both experimental results and modeling predictions. In Fig. 2(a) the linear fit is represented by line, while in Fig. 2(b) the lines represent modeling results.

By isolating the temperature dependence from variations in mixture composition, the effect of initial temperature on the flame is exposed. From  $\alpha$  as a function of equivalence ratio it can be seen how this temperature dependence is affected by mixture composition. Typically temperature dependence is stronger under lean and rich conditions, with a local minimum at the equivalence ratio associated with the maximum laminar burning velocity. This is caused by the temperature increase relative to the flame temperature being smaller in this region.

The temperature correlation can also be used as a tool to facilitate comparison with experimental results obtained at different temperatures. The temperature dependence was examined in Papers I-III. In Paper III, the temperature dependence was used to evaluate data reported in the literature, and to predict the laminar burning velocity at a higher temperature.

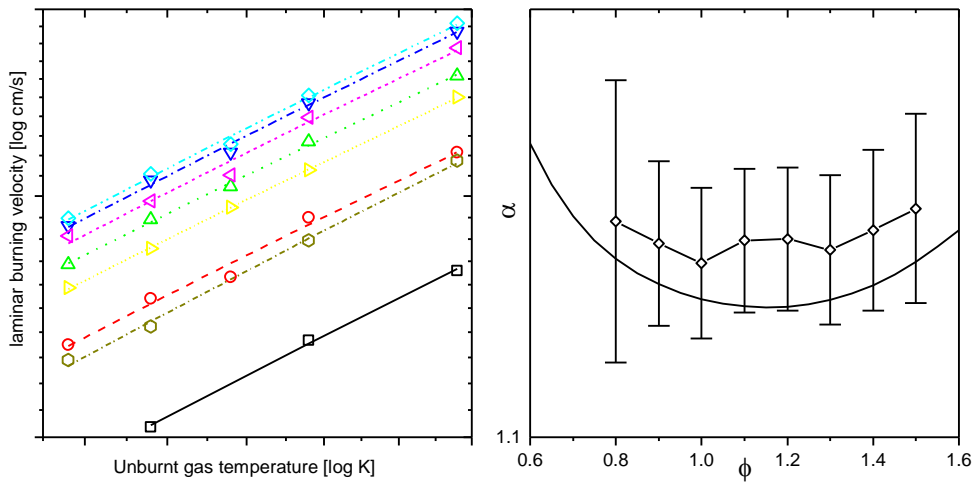


Figure 2: In (a) is an example of the experimental results, shown as symbols with its linear fit, shown as lines. The results are shown as the logarithms of the laminar burning velocity against the logarithm of the unburnt gas temperature for experimental results at various equivalence ratios. (b) shows  $\alpha$  (4) as a function equivalence ratio for methanol+O<sub>2</sub>+CO<sub>2</sub> as presented in Paper II. The temperature dependence of the laminar burning velocity can be used compare experimental results and modeling predictions, shown as a line.

## 2.2.4 Cellular structures

The flat qualities of a premixed laminar flame can be compromised by the presence of cellular structures over the surface of the flame front. Such structures consist of corrugations of the flame front. Examples of cellular flames together with examples of flat flames can be seen in Fig. 3. I laboratory scale flame, cellularity in flames can be caused by two types of mechanisms, the diffusive-thermal instability and hydrodynamic instability. The thermal expansion of the burned gas cause the hydrodynamic instability by introducing divergences in the laminar flow and local velocity gradients [15]. The diffusive-thermal instability can form inhomogeneities in the species concentrations at the flame front. In fuel+oxidizer mixtures the relationship between the thermal diffusion and the mass diffusion can affect the structure of the flame front. If there is an imbalance between the thermal diffusivity and the mass diffusion, this results in local regions in which there is an imbalance of mass- and heat flux. Then local hot spots of species and heat are formed at the flame front, due to the slow flux of heat from the flame as compared with the faster transportation of species to the flame front.

The relationship between thermal diffusion and mass diffusion can be described by the Lewis number ( $Le$ ) in Eq. (5) where the thermal diffusivity coefficient  $\alpha$  is divided by the mass diffusion coefficient,  $D$ . For Lewis numbers of less than unity, i.e.  $Le < 1$ , the thermal diffusion is lower than the mass transport.

$$Le = \alpha/D \quad (5)$$

In Papers I-III and in Paper V, cellular structures were formed at the flame front during the experiments at several measurement points. The implications of such cellular structures on flat flames and consequently of experimental measurements of laminar burning velocity and method of handling this issue is discussed further in Chapter 5.1.1 on the Heat flux method.



Figure 3: The pictures at the left show the flame front of a flat flame and the pictures at the right the flame front of a corrugated flame. Both flames are shown from the side as well as from above at an angle. The cone above the flames represents in each case the post flame zone. The flames in the pictures are ethanol+air flames mounted on a Heat flux burner.

## 2.3 Ignition

Ignition is the initiation of the burning part of the combustion process [16]. It describes the transition of the mixture from an unburnt gas to a burnt gas. Ignition can be described as an adiabatic thermal explosion. A thermal explosion can be described as:

A volume of gaseous fuel mixture is instantly heated to a high temperature. This initiation typically occurs by way of external energy transfer through temperature, either by directly applying a heat source or indirectly through increasing the temperature in a fuel mixture by means of a pressure increase. This activates some initial chain branching reactions that produce radicals. The initial reactions build up a pool of radicals. These initial reactions have only a marginal effect on the temperature and the pressure of the system. When a radical pool has been built up to sufficient degree, it ignites, resulting in a significant heat release. As the system is adiabatic, the heat is maintained in the mixture. The temperature and the reaction rates are accelerating each other mutually in a loop termed a thermal runaway. For ignition to occur the energy release from the radical pool must be greater than the heat loss due to diffusion and be able to raise a sufficiently large volume of the mixture up to the adiabatic flame temperature. If the concentrations of reactants are sufficient, then diffusion effects are negligible and the ignition is temperature controlled.

Information on the ignition behavior of a fuel has a high value for the scientific community as ignition is an important fundamental property for applications as monopropellants and fuels. As ignition is sensitive to the chemical structure of the fuel, it is appropriate for use in kinetic studies and for examining the relation of individual species to the ignition of a fuel.

Paper IV examines the ignition characteristics of nitromethane+O<sub>2</sub> through the measurement of ignition delay times.

### 2.3.1 Ignition delay time

The induction time between the initial activation of the combustion process to the moment of ignition, is referred to as the ignition delay time. This is the time required from the initiating reaction onwards. This induction-time is required for the process to build up a sufficient radical pool for ignition to occur and to be maintained. By measuring ignition delay times on a laboratory scale, the chemistry of explosions can be examined. From the ignition delay time, information, as the overall activation energy of the fuel and the effect of mixture composition can be derived. In Fig. 4(a) an example of ignition is presented as pressure and luminosity

over time and Fig. 4(b) the ignition delay times as a function of temperature is shown from Paper IV.

Ignition does not have a predetermined criterion. Instead the definition of ignition can vary between studies. In Paper IV, the ignition was examined through shock tube experiments, and the definition of ignition is discussed further with the results in Chapter 6.

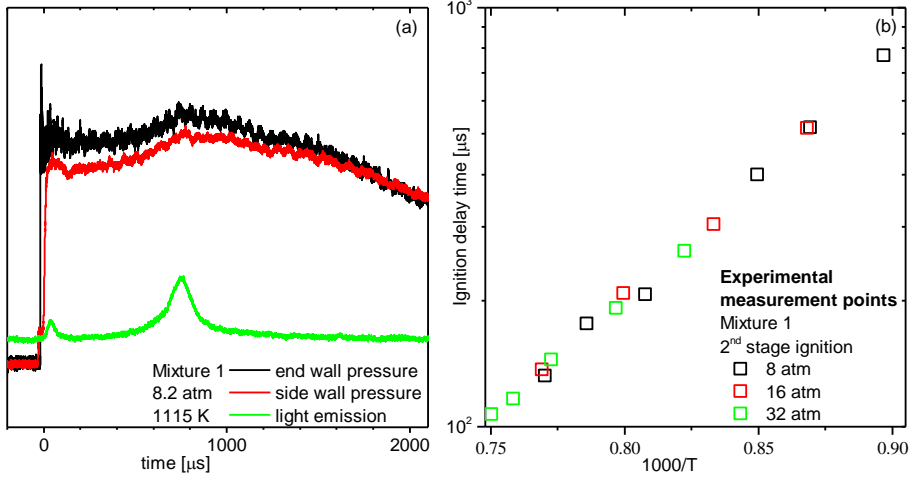


Figure 4: (a) an example of ignition, via pressure and luminosity profiles as a function of time for nitromethane+O<sub>2</sub>, and (b) experimental ignition delay times for nitromethane+O<sub>2</sub>, as presented in Paper IV.

### 2.3.2 Correlations of ignition delay time

With the help of correlations, the effect of the fuel, O<sub>2</sub> and diluent on the ignition delay times can be isolated and evaluated individually. Equation (6) exemplifies the structure of a correlation equation, with the exponents  $\beta$ ,  $\gamma$ ,  $\delta$  denoting the influence of the respective reactants.

$$\tau \propto e^{E_a/RT} [CH_3NO_2]^\beta [O_2]^\gamma [N_2]^\delta \quad (6)$$

The correlation coefficients provide a measure of how strong the effect of the concentrations of the initial reactants is on the ignition delay time. A positive sign of an exponent indicated that a lower concentration decreases the activity of the mixture, increasing the ignition delay time, whereas a negative sign of the exponent shows an increased activity in the mixture, resulting in shorter ignition delay times. In a correlation presented as a function of time the slope provides information of the global activation energy of the ignition, which is the energy

required for the mixture to ignite, released through the chemistry occurring prior to the ignition event.

Through the use of correlations, ignition delay times measured under different conditions can be compared. These correlations are also useful for rough estimations of the ignition delay times for a mixture without having to perform kinetic modeling. Different datasets can be processed in this way so as to obtain the global activation energy and composition dependence for a large range of conditions, or compare correlation coefficients so as to compare the ignition behavior under conditions that are not directly comparable.

# 3 Combustion chemistry

Understanding the chemistry behind combustion processes is key to unlocking knowledge on the behavior of combustion phenomena, such as flame properties and explosion characteristics. This knowledge can be used for simultaneously maximizing the output of thermal and kinetic energy from combustion processes, while minimizing its negative consequences.

The combustion process is essentially high temperature chemistry between the fuel and the oxidizer. The global process describes the overall reaction from initial reactants to final products, which consists of many different elementary reactions.

In an elementary reaction species interacts and transforms to other species through bond breaking or bond formation. The **transition state** describes the geometry of the interacting species, in between reactant and product, having the highest energy. For a reaction to occur it must pass through the transition state.

Combustion is dominated by radical chemistry. A **radical** is an atom or molecule that has one or more unpaired valence electrons and therefore highly reactive. Species with paired valence electrons, are considered as stable according to the terminology used in this thesis. **Stable species** can however still participate as reactants with radicals.

The chemistry can be divided up in terms of classes of reactions that have similar effects on the combustion, although with individual magnitude for the reactions involved within each class.

Combustion starts with an initial **chain-initiating reaction** taking place in the preheat zone. In chain-initiating reactions, radicals are formed from stable species, increasing the number of radicals in the system. These reactions are generally thermal decomposition reactions, which are endothermic because the reaction is essentially a bond breaking.

When one radical reacts to form two or more radicals what is called a **chain-branching reaction**. The reactivity of the system is increased as more radicals become available.

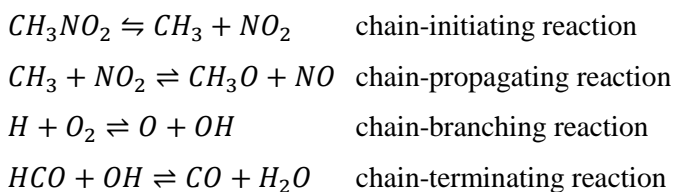
When a reaction generates as many radicals as it consumes it what is called a **chain-propagating reaction** occurs. This reaction maintains the combustion, but

does not affect the reactivity in other ways than replacing a radical with another. The nature of the radicals interchanging can affect the reactivity, however.

A **chain-terminating reaction** consumes more radicals than it produces, thus reducing the reactivity of the system.

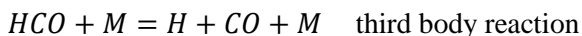
The same reactants can give different products when reacting. The **branching ratio** describes the relation between different product channels. These reactions often go through different transition states, with their activation energy and temperature dependence controlling the branching ratio.

Below are examples of the different types of reactions:



These reactions can occur consecutively or simultaneously, competing for the reactants.

In **third body reactions** the reaction is promoted by species that participate in the reaction but are not consumed. The third body lowers the activation energy of the reaction by forming a complex with the transition state and thereby promoting the reactions rate. Then the third body is released in its original form on the product-side of the reaction. Typically, stable species, which are abundant during the combustion process act as third bodies, for example product-species such as carbon dioxide and water, or diluents as molecular nitrogen or argon. Only the fraction of reactant which collide with the third body have the option of proceeding through the third body-complex. How large a portion of the reaction is affected depends on concentration of the third body. A third body reaction can belong to any of the classes mentioned above.



While both exothermic and endothermic reactions occur, the net effect of the combustion chemistry is exothermic. In combustion processes the chemistry is primarily thermally driven. Because of the high temperature during combustion, many reaction paths become readily available, potentially producing many

intermediate species and products. As the chemistry is thermally driven, the rate of the global process is higher in region of high temperature. The elementary reactions are activated by the heat. To a slight extent, radicals can activate reactions, after diffusing from high temperature regions to colder areas of the flame.

### 3.1 Flame- vs ignition-chemistry

It is generally the same chemistry present in both flames and explosions. However different reactions are important in flames as compared to ignition. Generally speaking, flame chemistry is governed by the reactions that sustain the flame, whereas self-ignition is controlled by the reactions building up the radical pool that ignites.

In flames the chemistry is affected by mass transport and thermal diffusion. A flame is dependent on the rate at which radicals are transported to the flame front. The fuel decomposes relatively quickly to form non-fuel-specific radicals. The chemistry within the flame front controls the propagation of the flame. Differences in flame properties, such as the laminar burning velocity, are largely controlled by the chemistry of the major radicals, because the flame is sustained by the reactions of these radicals. The flame front is carried and maintained by chain propagating chemistry, there being a balance between the chain branching and chain terminating reactions. Because of the fast fuel decomposition compared to the radical chemistry, the laminar burning velocity is insensitive to fuel specific chemical kinetics and fuel diffusion [17, 18]. High quality is required from the experimental results because of this insensitivity.

By studying ignition, combustion chemistry can be examined without considering mass transport and diffusion affecting the chemistry. It is the rate at which a sufficiently large radical pool for ignition is built up that controls the ignition delay time. Ignition is therefore more sensitive to the structure of the fuel and the rate of the chain initiation reactions. It is also sensitive to the branching ratio and to radical formation during the radical pool build up.

The temperature dependence of ignition is dominated by the temperature dependence of the initial reaction, as opposite to how temperature affects a flame front where the temperature drives the high rates of the reactions.

## 3.2 The role of carbon dioxide in combustion chemistry

In combustion chemistry carbon dioxide contributes with its thermal influence. The heat capacity (C) of carbon dioxide is higher than that of molecular nitrogen, which gives lower temperatures in a carbon dioxide-rich environment, as compared to a flame with corresponding amounts of molecular nitrogen.

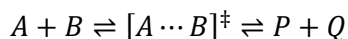
Carbon dioxide is also a chemically active species, which can participate in the chemistry as a reactant. Carbon dioxide commonly participates as a third body in reactions. A method of estimating the influence of a third body on a reaction was suggested by Warnatz [19]. In empirical observations Warnatz saw similarities in the effects of a third body for different reactions. A ranking of several third bodies according to their effect on the rate of reactions was suggested. The suggested magnitude of the third body is related to the bath gas used in the study measuring the rate constant.

The magnitude of these effects depends on which combustion property is studied as well as experimental conditions, such as mixture composition. From the literature on liquid fuel under CO<sub>2</sub>-rich conditions, it was shown that the laminar burning velocity was decreasing with CO<sub>2</sub>-dilution [20-22]. In Papers I-II the laminar burning velocity of methanol and ethanol, respectively, was measured with O<sub>2</sub>+CO<sub>2</sub>.

## 3.3 Kinetics

A reaction's kinetics describes the progression of the reaction, from reactants to products, in terms of rate.

A chemical system strives to reach equilibrium for each reaction between its reactants and product. Generally, a reaction has two directions, a forward and a reverse direction, with the respective reactions proceeding at different rates.



There are several variables that affect the rate of a reaction. The rate of a reaction is dependent on the concentration of the reactants. For a bimolecular reaction to occur, it is dependent on the reactants being in sufficiently close proximity for a collision to occur. Increasing concentration increases the probability of a collision, thereby increasing the likelihood of the reaction taking place. The activation energy (E<sub>a</sub>) is the energy difference between the reactants

and the transition state (denoted ‡). This is the minimum energy required to initiate the reaction. The rate of a reaction can be presented in the form of an Arrhenius expression in

$$k_1 = AT^n e^{-E_a/RT} \quad (7)$$

In the Arrhenius expression, properties of a reaction, in the form of its activation energy and its temperature dependence, are represented. The temperature dependence of  $A(T^n)$  together with  $e^{1/T}$  describes how the reaction rate varies with temperature. The pre-exponential factor ( $A$ ) is an empirical constant representing the likelihood that a collision, with the potential for initiate a reaction, will occur, in terms of collisional effect and steric effects. The exponential factor  $e^{E_a/RT}$  represents the Boltzman distribution, which describes the fraction of reactants that will have energy equal or higher than the activation energy at temperature  $T$ . It can be regarded as a measure of the likelihood of the reaction to proceed.  $R$  represents the gas constant.

# 4 Combustion modeling

To understand combustion phenomena, as explosions or flames, information on the chemistry behind these phenomena can provide valuable insight for understanding combustions underlying mechanisms [23]. The accelerated chemistry and the large number of species present make combustion chemistry complex to study experimentally. By complementing experiments with theoretical studies, much of the information otherwise inaccessible, can be accessed through predictions. One approach to investigating the complex chemistry in combustion theoretically is through the use of kinetic modeling of combustion phenomena.

This chapter discusses the approach to kinetic modeling used during the work presented in the thesis.

## 4.1 Detailed kinetic mechanisms

A detailed kinetic mechanism is a collection of the reactions believed to participate in the chemistry of the fuel of interest. The detailed kinetic mechanism represents the current knowledge about combustion chemistry. A kinetic mechanism can provide insight at a microscopic level on subjects which may not be accessible experimentally, while the mechanism at the same time is describing a macroscopic phenomenon. Although a kinetic mechanism is intended to describe the chemistry accurately, this can differ even between mechanisms created for the same conditions and fuels. This reflects different assumptions that are made in a mechanism, as the choice of which reactions are included, the choice of rate constant to describe a reaction, among other properties. In a detailed kinetic mechanism, the aim is to describe the chemistry behind the investigated combustion phenomena as accurately as possible, on a detailed level in the chemistry. Here lays a major challenge concerning detailed kinetic mechanism, in the assumptions made when choosing the relevant species and reactions to be included in a mechanism. As there is no universal knowledge on the correct chemistry behind each fuel or combustion phenomena, the choices in species and reaction included in a mechanism constitutes one of the differences between kinetic mechanisms.

Kinetic mechanism use rate constants to describe each reaction. Rate constants are often taken from the literature, where their numerical value is calculated or measured. In the absence on numerical value in the literature, educated estimations can be made. The choice of numerical value for individual rate constants is another difference between mechanisms.

Each species is also associated with both thermodynamic properties and transport properties. The thermodynamic data is in the form of species enthalpy, entropy, and specific heat capacity, with their dependence on temperature, in polynomial form. The reactions are commonly presented with rate constants in one direction. The software calculates the reverse rate from thermodynamic properties of the species involved and the forward rate constant. Pressure dependence and third bodies are represented by parameters describing their behavior. The transport and thermodynamic properties are also open to interpretations and selections to be made. These properties, are, however, not examined during the course of the work presented in the thesis, but accepted as is in the mechanisms. The exception being the mechanism of Mathieu et al. [24] when used in the study presented in Paper V. In the absence of transport data from Mathieu et al., transport data was taken from established kinetic mechanisms from the literature.

There is a variety of mechanisms with different interpretations of the chemistry, stemming of the choices made in kinetic mechanism. These choices regarding the chemistry can be based on assumptions, as for example, of their importance for the combustion phenomena which the mechanism aspire to describe, the condition of relevance, as range of pressure and temperature.

## 4.2 Modeling of combustion phenomena

Experimental studies are limited by the finite conditions covered in a given study and the limited range of experimental conditions, such as pressure and temperature. It is difficult to with certainty know whether the conclusions drawn on the basis of an experimental study are valid outside the experimental conditions.

Use of kinetic mechanisms enables the numerical value of a physical property, as the laminar burning velocity or the ignition delay time, to be predicted at conditions that have not yet been studied experimentally. The quality of these calculations is dependent on the kinetic mechanism, the choices made in the design of the mechanism, and the range of combustion phenomena the mechanism has the ambition to describe. To evaluate the quality of kinetic mechanisms, these can be compared to experimental studies on the basis of how well the kinetic mechanisms can reproduce the experimental results, and the conditions for which

it was designed. Ideally, with realistic chemistry, described by accurate rate constant, a kinetic mechanism should be able to reproduce experimental results over a range of different experimental conditions, at different temperatures and pressures. A realistic chemistry would ideally also have the capacity to predict different combustion phenomena accurately.

The modeling presented in the thesis was performed by using different modules provided in the software CHEMKIN IV [25], designed to emulate the conditions required for the combustion properties of interest.

### 4.3 Laminar burning velocity

The premixed laminar flame speed calculator in CHEMKIN IV [25] was used for the prediction of laminar burning velocity in Papers I-III, and in Paper V. The module assumes a freely propagating flame and simulates the adiabatic premixed stretch-free conditions required for determining the laminar burning velocity. The module provides a one dimensional output as a distance, not relative to any burner surface. The modeling should be extended over a distance that includes the entire reaction zone of the flame (until the temperature reached a plateau). When modeling the laminar burning velocity, it is important to consider multicomponent transport [26] and thermal diffusion for accurate description of the transport of species to the flame front. Multicomponent transport accounts for the diffusion of a given species relative to each individual species through the flame, in contrast to mixed average transport, where a species individual diffusion is related to the bulk of the gas. Thermal diffusion, also called the Soret effect, controls the mass flux through the temperature gradient of the flame. The thermal diffusion most strongly affects the hydrogen diffusion, which is important for the chemistry behind the laminar burning velocity. Both multicomponent transport and thermal diffusion were taken into account in the modeling presented in the thesis.

In Paper II, the effect of multicomponent transport and thermal diffusion was examined for both a methanol+O<sub>2</sub>+CO<sub>2</sub> flame, and a methanol+air flame. These factors were shown to affect the accuracy of the predictions.

The output from modeling also provides information as flame temperature, density, predicted species profiles at adiabatic conditions among others. Predicted temperature profiles and density profiles were used in the study presented in Paper III to reevaluate and recalculate the laminar burning velocity presented by Brequigny et al. [27] for nitromethane+air flames.

## 4.4 Ignition

The shock tube experiments presented in Paper IV were simulated using the homogeneous batch reactor in CHEMKIN IV [25] at constant volume and solving the energy equation. The module has zero dimensions with no spatial coordinate; the predicted activity is given as a function of time. The batch reactor emulates the uniformly distributed reactants in a confined volume in experiments with conserved mass. Adiabatic conditions are assumed during the modeling with the batch reactor module for the study presented in Paper IV. The transport of species are assumed to be infinitely fast and no input parameters for transport needing to be employed.

The maximum time step interval was set to  $0.1\ \mu\text{s}$  so as to ensure that the output provided an adequate number of gridpoints for describing the ignition over time with sufficient resolution.

## 4.5 Evaluating the effect of carbon dioxide

In the literature a fake carbon dioxide specie,  $\text{FCO}_2$ , has been used in kinetic modeling, aimed at evaluating the thermodynamic effect of carbon dioxide isolated from its chemistry [28-30]. During this procedure, the  $\text{FCO}_2$  is assigned the same thermal properties and transport properties as carbon dioxide, but is excluded from participating in any of the reactions as a reactant. In input parameters of the simulations, carbon dioxide is replaced by  $\text{FCO}_2$  as a reactant. By comparing the predictions with  $\text{FCO}_2$  to predictions with carbon dioxide, the effect from thermal properties on the output can be quantified.

In study presented in Paper II this approach was used to evaluate the effect of chemical activity of carbon dioxide on the laminar burning velocity of the methanol+ $\text{O}_2$ + $\text{CO}_2$  flames. The laminar burning velocity was found to increase dramatically, indicating that carbon dioxide was highly chemically active in the studied flames. This increase could not be counteracted by adding the  $\text{FCO}_2$  as a third body to all reactions, with the same collisional efficiency as for carbon dioxide.

## 4.6 Sensitivity to individual reactions and rate constants

The many reactions in a kinetic mechanism, all affect the examined property in different extent. Both to gain further knowledge on the chemistry, and to identify possible targets for improvements, it is of interest to quantify the effect from individual reactions on the combustion process as a whole.

Sensitivity analysis is a useful tool for evaluating how an individual reaction influences the predictions of a property from modeling. Sensitivity analysis gives a quantitative indication of how sensitive a property, such as the laminar burning velocity, is to change in the rate constant of an individual reaction. The sensitivity relates the relation of the change on the examined parameter to the change in magnitude of each rate coefficient. The sensitivity of a reaction can be defined as follows

$$s_i = \frac{\partial \ln x_i}{\partial \ln A_i} \quad (8)$$

The pre-exponential A-factor in the Arrhenius expression for a reaction (i) is modified ( $A_i$ ) for the reaction in the kinetic parameters of the mechanism. The resulting prediction ( $x_i$ ) is weighted in relation to the predictions ( $x$ ) from the unmodified mechanism. A sensitivity analysis can be performed either by brute force, or, as in the works presented in the thesis, through the CHEMKIN software [32].

In the studies presented in Papers I-II and in Paper V, sensitivity analysis was performed, and the reaction with the highest positive and negative sensitivity coefficients was identified as reactions with major influence on the laminar burning velocity.

## 4.7 Reaction path analysis

The chemistry of combustion is complex, reactions being able to occur either sequentially or simultaneously in a hierarchical structure. Those reactions occurring in a sequence are dependent on an initial reaction to form products which will act as reactants for a second reaction. Simultaneous reactions can either be competing for the same reactant, or promoting it by consuming a radical otherwise used in a competing reaction.

Reaction path analysis is used as a tool to illustrate how the species relate to one another and what path the combustion process takes from fuel to major products. Figure 5 illustrates the order in which the major intermediate species and products are formed, for an example of ethanol chemistry from the study presented in Paper I. The arrows represent the paths from one species to another, with the direction representing the net direction of the chemistry between the species. The paths consist of one or several reactions, involving both species, in both the forward and the reverse direction.

## 4.8 Rate of production

The amount of a species present during combustion is dependent on the overall rate at which it is produced, and the total rate of the reactions consuming it. The rate of production analysis treats the output from modeling and relates it to the rate of production of individual species and reactions. It provides information on the overall rate of production of a species and the rate at which each contributing reaction proceeds. A positive rate represents the production of a given species, whereas a negative rate means that the species is consumed faster than it is produced. By observing the rate of production over time or distance, information can be obtained on not only the rate but also the location of the chemistry. In the rate of production analysis, presented in Fig. 6(a), it can be seen how a species can vary from being produced to being consumed dependent on position in the flame, by an example for methanol from the study presented in Paper II. It also illustrates how a species can be predicted to behave differently between two mechanisms. In Fig. 6(b) the contribution of individual reactions to the total consumption rate can be seen, for an example of rate of production analysis of methanol in the study presented in Paper II.

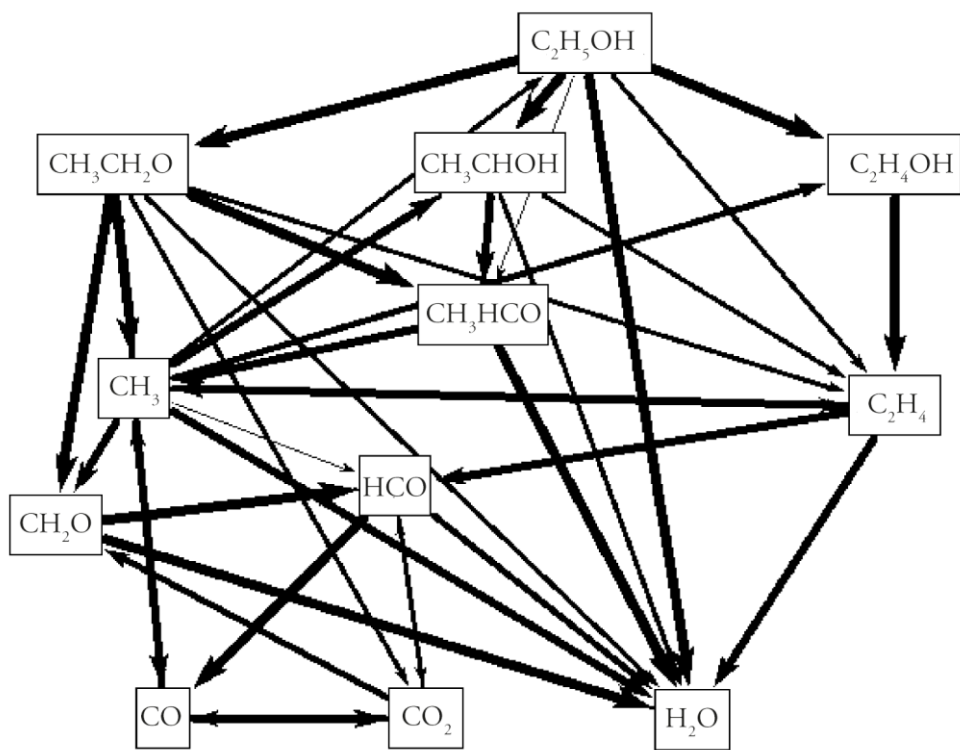


Figure 5: Reaction path analysis of the mechanism of Marinov for a stoichiometric ethanol+ $O_2$ + $CO_2$  flame as presented in Paper I.

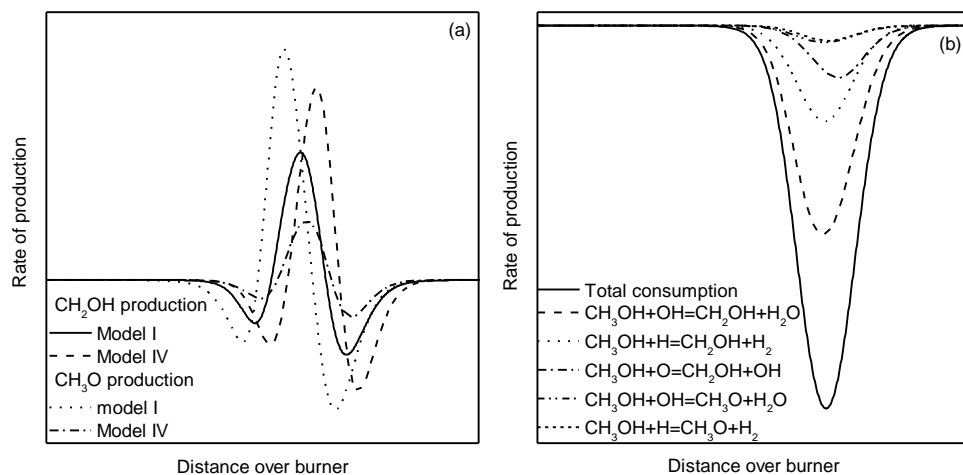


Figure 6: (a) A comparison of the total rate of production of  $CH_2OH$  and of  $CH_3O$  of the mechanisms and (b) the rate of production of methanol as presented in Paper II.

# 5 Experimental methods for quantifying combustion properties

The combustion inside real-life applications, such as an engine or a gas turbine, is complex. Many processes occur simultaneously, making individual properties challenging to distinguish. In such complex scenarios it is difficult to distinguish cause and effect, as well as secondary effect when examining variables. Fundamental properties are thus more easily examined in a laboratory setting, rather than in real-life combustion applications. Experiments for examining fundamental properties on a laboratory scale are designed to simplify the combustion process in order to isolate and distinguish the property of interest. The experimental designs are aimed at minimizing the number of variables present, and creating an environment in which the effect of variables can be studied individually.

## 5.1 Experimental methods for determining the laminar burning velocity

As laminar burning velocity is an important fundamental property, it is of interest to measure it experimentally. The challenge is to measure a velocity that fits the requirements of the theoretical definition as closely as possible [33]. Direct measurements of the laminar burning velocity require a flat flame under adiabatic conditions. Several techniques are available for determination of the laminar burning velocity, each with benefits and with issues to consider. Where the experimental methods do not meet the theoretical requirements, assumptions need to be made. The most common techniques are; the Heat flux method, spherically expanding flames and the stagnation flame method.

In the work presented in the thesis, laminar burning velocities measured using the Heat flux method and using spherically expanding flames were examined. In the study presented in Paper III laminar burning velocities obtained by these two methods were compared and discussed. The two methods are presented below.

### 5.1.1 Heat flux method

Since the Heat flux method has recently been examined by Alekseev et al. [34], the principle behind the method will only be briefly presented. The focus is on the extrapolation as performed in Papers I-II and Paper V, which distinguish the experiments performed from the conventional methodology when using the Heat flux method.

#### *Principles behind the Heat flux method*

The Heat flux method utilizes the heat transfer from the flame to the burner to find the adiabatic laminar burning velocity. The temperature over the burner plate surface represents the thermal interactions between the flame and the burner plate. At sub-adiabatic conditions, the flame is positioned closer to the burner and the heat gain of the burner plate from the flame being greater than its heat loss to the unburnt gas. This elevates the temperature in the center of the burner plate. The opposite is true under super-adiabatic conditions; here the heat gain from interactions with the flame is lower than the heat loss to the unburnt gas. Accordingly, the temperature is lower in the center of the burner plate than its edges.

The laminar burning velocity is indirectly measured by varying the velocity of the unburnt gas and measuring the temperature distribution across the burner surface. Thermocouples are utilized for measuring the temperature at different radii ( $r$ ) from the center of the burner plate. In Fig. 7, the various positions of the thermocouples are marked with red dots. Several measurements are taken at varied unburnt gas velocity. The measured temperatures across the burner surface are fitted to a parabolic function in Eq. (9). The burning velocity and the parabolic coefficient  $C$  are linearly dependent under sub- and super-adiabatic conditions close to the adiabatic condition. The adiabatic laminar burning velocity is found where the temperature is uniformly distributed over the burner surface, at  $C=0$ .

$$S_u = T_{center} + C * r^2 \quad (9)$$

This method is limited to unburnt gas temperatures  $\geq 10$  K below the temperature of the burner plate. Because of difficulties in maintaining a stable flame under high pressure conditions, the use of the method is also limited in working pressures.

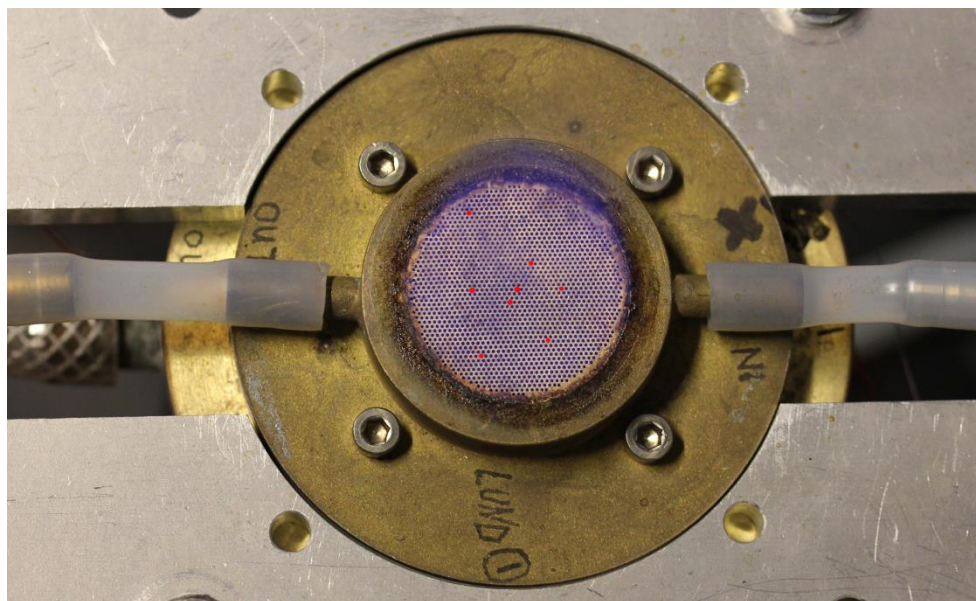


Figure 7: A photograph of the burner plate of a Heat flux burner from above. The red dots mark the positions of thermocouples in the burner plate and the blue area is an burning ethanol+air flame. This is burner T according to the nomenclature in Alekseev et al.

### *Extrapolation*

In Heat flux measurements, the adiabatic laminar burning velocity is commonly obtained through interpolation of the measurement points under sub- and super-adiabatic conditions near the adiabatic point. For the experimental work presented in Papers I-III and Paper V, however, in several measurement points, it was not possible to obtain a uniformly flat flame front under adiabatic conditions, due to cellular structures at the flame front. When these cellular structures were present in the flame front, accurate laminar burning velocity measurements were not possible due to the increase in flame front area. It has been shown by Konnov and Dyakov [35-37] that the measured flame propagation velocity is higher in cellular flames than in laminar flames.

To circumvent the problem of corrugations at the flame front, for these measurements, the adiabatic laminar burning velocity was obtained through linear extrapolation of the parabolic coefficient  $C$  in relation to flame velocity from sub-adiabatic conditions up to the highest velocity at which the flame front was planar. An example of an extrapolation to the laminar burning velocity is shown in Fig. 8. The points show the progression of the parabolic coefficient  $C$  in relation to flame velocity as mock points to illustrate the deviation from the experimental points found in a laminar flame. The parabolic coefficient for the corrugated flame deviates from the linear relationship of the experimental points from the flat flame.

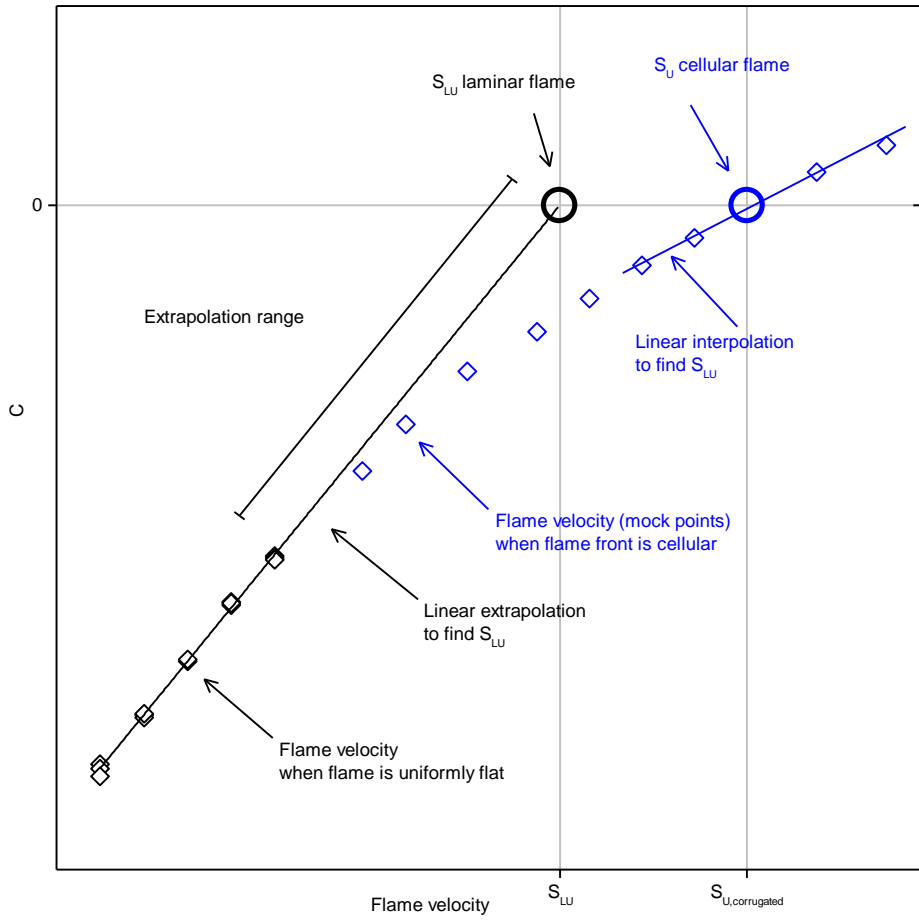


Figure 8: A schematic illustration of an extrapolation to the laminar burning velocity at adiabatic conditions for a measurement point for methanol+O<sub>2</sub>+CO<sub>2</sub> from Paper II.

The increase in the parabolic coefficient  $C$  with flame velocity shows a decreasing incline and fails to follow a linear relationship.

The extent of the extrapolation between experimental points varied with temperature and equivalence ratio. The general trend was that the flames were more prone to form cellular structures with increasing temperature and at rich mixtures, equivalence ratios  $>1$ . Accordingly the extrapolation was necessary when the cellular structures were formed under or just below adiabatic conditions.

Because of the extrapolation, additional uncertainty Eq. (10) was associated with these measurement points. The uncertainty is treated as a the error from the slope and intercept at  $C=0$  [38]. The uncertainty of the extrapolations is added to the overall uncertainty in the laminar burning velocity and the equivalence ratio of the measurement points.

$$error_{extr} = t_{0.05, n-2} * S * \sqrt{\frac{1}{n} + \frac{n(C^* - \bar{C})^2}{n \sum C_i^2 - (\sum x C_i)^2}} \quad (10)$$

where

$$\bar{C} = \frac{\sum C_i}{n} \quad (11)$$

and

$$S = \sqrt{\frac{\sum (U_{,i} - aC_i - b)^2}{n - 2}} \quad (12)$$

For each measurement point, individual t-distributions at 95% confidence interval was used, depending on the degrees of freedom ( $n-2$ ) for the number of experimental data points ( $n$ ) taken for each measurement point. The mean value of the parabolic coefficients of all the measurement points ( $\bar{C}$ ) and  $C^*=0$  was used in the calculating of errors. The deviation from a linear fit ( $S$ ) to each data point was calculated. The extrapolation process is presented in Paper II, and the fit to the linear equation to the measurement points is evaluated there, being found to contribute with  $\sim 0.2$  cm/s to the overall uncertainty in the laminar burning velocity for those particular flames.

### 5.1.2 Spherically expanding flames

The laminar burning velocity can also be determined using spherically expanding flames [14]. An illustration of a spherical flame can be seen in Fig. 9. The combustible gas is distributed uniformly within a confined spherical vessel. It is ignited at the center of the vessel and the flame expands outwards spherically, whilst consuming the mixture. The gas is stationary, and the increase of flame front's radius as a function of time defines the flame speed relative to the burnt gas. The velocity on the burnt side can be obtained by tracking the progression of the flame's outward expansion. Because of the curvature of the flame front, this output first needs to be corrected for stretch effects. The stretch effect can be corrected using linear or non-linear mathematical methods. The choice method for stretch correction can affect the resulting laminar burning velocity, however, stretch corrections are not examined in the work related to the thesis and will thus not be discussed further. Because of the confinement, as the flame progresses and products are formed, the pressure and temperature in the vessel increase. As both pressure and temperature affect the laminar burning velocity, the vessel needs to be sufficiently large to be able to assume that pressure and temperature effects are negligible, or it should be compensated for in the treatment of the output.

The unburnt laminar burning velocity can then be calculated from the stretch-corrected burnt flame speed. Assuming an infinitely thin flame front, the relationship between the mass densities of the unburnt gas and the burnt products can be used to obtain the unburnt laminar burning velocity.

$$S_{Lu} = S_{Lb} \frac{\rho_u}{\rho_b} \quad (13)$$

Equilibrium calculations can be used to obtain the densities at  $\pm\infty$  from the flame front. When assuming that the densities at  $\pm\infty$  holds true, it requires a sufficiently large reaction vessel to fit the flame front in its whole, and allow the flame front to expand. In Fig. 1(b) it is shown how the mass density decreases across the flame front and is lower in the burnt region behind the flame than in the unburnt region. The density decreases because the mass is conserved, but the gas is expanding as more species are formed. Issues can arise because of the width of the reaction zone, if the product formation is not completed within the reaction vessel. Spherically expanding flames are limited by the size of the vessel. Because of the pressure expansion of the burnt gas, the flame propagation can only be measured as long as the volume of the burnt gas is sufficiently small compared to the total volume of the vessel.

In paper III the effects of the definition of density in the processing of spherical nitromethane flames, and its implications for determining the laminar burning velocity of nitromethane+O<sub>2</sub> are addressed.

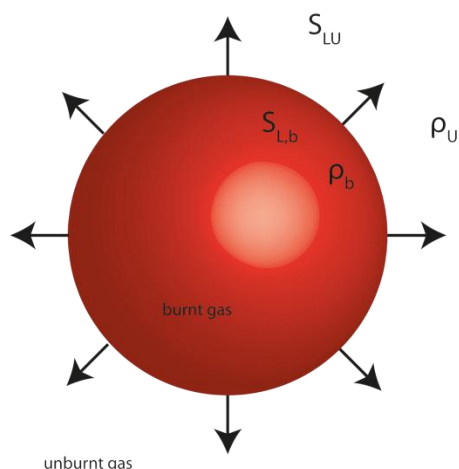


Figure 9: A schematic view of a spherically expanding flame.

## 5.2 Ignition

In order to study ignition on a laboratory scale shock tubes are commonly used. When ignition is studied on a laboratory scale, the goal is to emulate the ignition of an adiabatic thermal explosion, with conserved heat and mass and no boundary (wall) interactions. Shock tubes enable examination of ignition under conditions which reflect many real life applications of fuel combustion, such as high pressure and high temperatures.

Paper IV presents experiments performed in a shock tube using reflected shock waves.

### 5.2.1 Shock tube

Ignition properties as ignition delay time, examined in Paper IV, and kinetic studies of reactions can be readily studied using shock tube techniques. The experimental work in the study presented in Paper IV was performed during a research-visit at Combustion Chemistry Center at National University of Ireland in Galway, Ireland.

In essence, a shock tube is a cylindrical metal tube divided in to two sections separated by diaphragms, the driver section and the driven section. Figure 10 presents a schematic overview of a shock tube and the general principles of a shock tube experiment. The driver section is used to create the shock wave through use of an inert gas under high pressure. In the driven section the fuel mixture is kept in gas phase under lower pressures. It is in the driven section that the ignition will be examined. The incident shockwave is generated by bursting the diaphragms separating the two sections. The shock wave travels through the driven section. As the shock wave passes the fuel mixture it is instantly compressed and heated by the pressure rise. Pressure transducers mounted along the walls of the driven section to detect changes in pressure inside the shock tube. After hitting the end wall, the shock wave is reflected and travels back. The reflected shock wave passes the gas again and increases it heat and pressure a second time. From the output of the pressure transducers the velocity of the incident and reflective shock waves can be calculated.

The heating of the mixture from the shock wave initiates the ignition process. The conditions in the mixture after the reflected wave has passed cannot be measured, but is calculated from the output, considering the ideal gas law, the Rankine-Hugoniot conservation of mass, energy and momentum, Mach number and the ratio of the specific heat capacities.

As the reactants are in gas phase and are uniformly distributed within the driven section, there is no diffusion to consider in the results. The lack of diffusive and thermal effects makes shock tubes suitable for conducting kinetic experiments as any activity can be attributed solely to chemistry.

### *Definition of ignition*

The moment of ignition does not have a fixed definition but can be defined in different ways. The resulting ignition delay time depends on how the ignition is defined. A common definition is the maximum gradient of the pressure rise. This definition is well suited in cases where the ignition is clearly separated in time from the shock wave, and it is a fast process when ignition occurs in a single stage. Pressure has the advantage that it tracks all activity in the system sufficiently large to cause a change in pressure. However, as the shock wave itself also is a pressure wave, in some cases it can be difficult to distinguish from the pressure rise caused by chemical activity. Luminosity is also a common marker used for ignition in a shock tube. It can be utilized over a range of wavelengths, or filtered to a specific wavelength to track a specific species. Luminosity has the limitation that it can only detect activity which emits light in the detectable range. The limitations in detectable range of luminosity can also be used as an advantage. Combined with pressure, it can show if the ignition is controlled by chemistry in the detectable range or not, depending on how the pressure and luminosity signals behave over time. Filtering to a specific species, enables signals that are sharp and well-defined

over time to be obtained, and can also provide information on the chemistry of the ignition. In Chapter 6.2.2 the definition of ignition is discussed in light on the experimental ignition delay times measured for and presented in Paper IV.

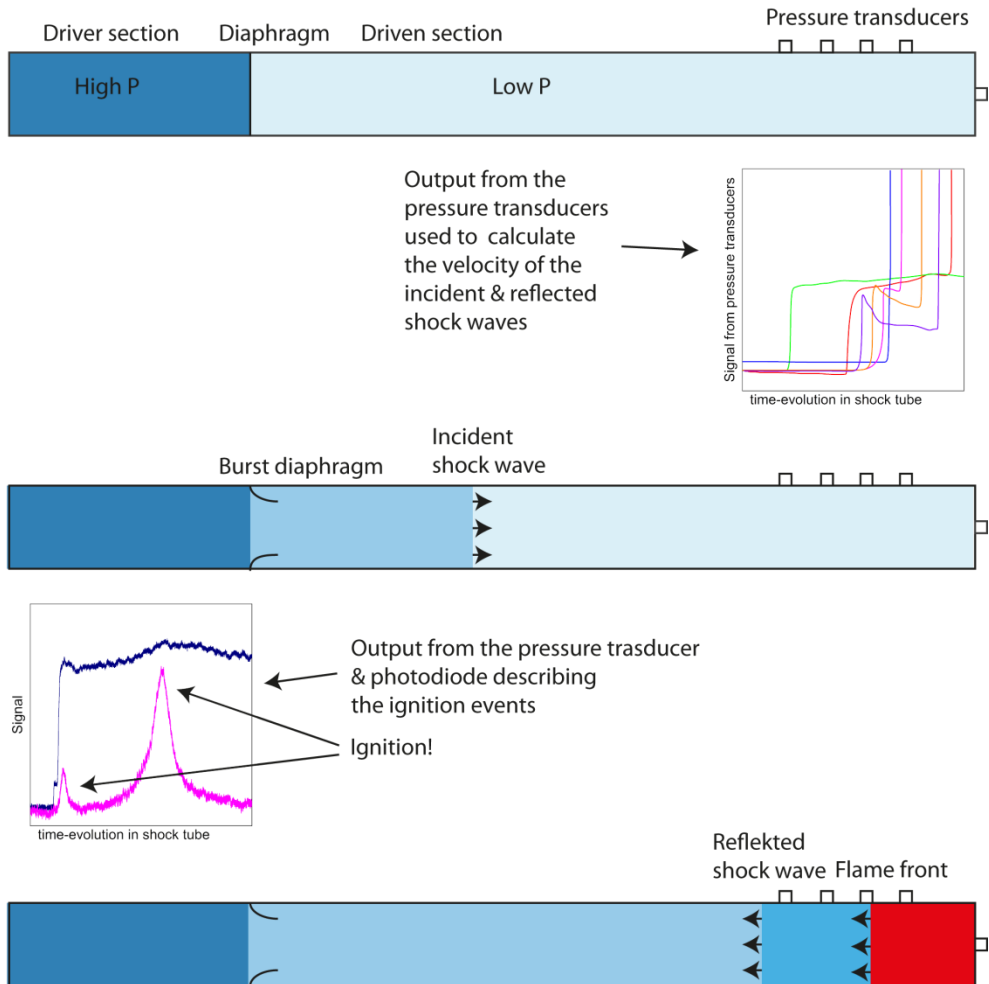


**Figure 10:** A schematic overview of a shock tube experiment. The tubes represents a shock tube, and its contents illustrates the progression of events occurring inside the shock tube during the course of a typical experiment, from the tube above to below. The signals are taken from a measurement of nitromethane+O<sub>2</sub>+N<sub>2</sub> ignition from Paper IV.

# 6 Results

In this chapter, the results from the studies behind the thesis are presented. The chapter is divided according to the studies, presented each of the separately. First the results from the two studies on alcohols at carbon dioxide-rich conditions are presented. Then the three studies concerning the combustion behavior of nitromethane are presented. For each section, the main findings from each study are presented and discussed.

## 6.1 Laminar burning velocity of alcohols at CO<sub>2</sub>-rich conditions

The laminar burning velocity has been measured with carbon dioxide in previous studies of gaseous fuels [21, 30, 35, 37, 39, 40]. The use of oxy-fuel-techniques is, however, not limited to the use of only gaseous fuels, but is pursued for use with many different types of fuels [41-44]. Therefore expanding the knowledgebase on fuels burnt at oxy-fuel conditions, with further studies on liquid fuels is of importance.

However, studies in the literature concerning the laminar burning velocity of liquid fuels under carbon dioxide-rich conditions are few. Zhou et al. [20] examined the adiabatic flame temperature and the laminar burning velocity of iso-octane+air diluted with carbon dioxide. In the study, the laminar burning velocity was found to decrease with increasing dilution. The decrease was then dampened at higher dilutions.

Two studies of alcohol combustion under carbon dioxide-rich conditions are presented in this chapter. Both studies aim primarily at providing the scientific community with new experimental data on laminar burning velocity of alcohols under carbon dioxide-rich conditions. Laminar burning velocity measurements for alcohols with O<sub>2</sub>+CO<sub>2</sub> was lacking in the literature previous to the studies presented in Paper I-II.

### 6.1.1 Ethanol+O<sub>2</sub>+CO<sub>2</sub>

The study presented in Paper I exemplifies how detailed kinetic mechanisms can handle a given set of combustion conditions differently, and illustrate the importance of validation against experimental results under different conditions.

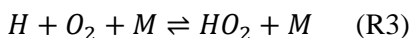
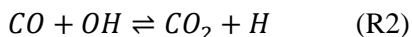
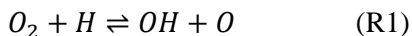
Experimental data on laminar burning velocity of ethanol+O<sub>2</sub>+CO<sub>2</sub> at 298, 318, and 338 K and atmospheric pressure was presented. The experimental results were limited in equivalence ratio to  $\leq 1$  by the limitations from the partial vapor pressure. Two experimental measurements series were presented, conducted one year apart, and in good agreement.

Three kinetic mechanisms were tested for their performance for ethanol+O<sub>2</sub>+CO<sub>2</sub>. The kinetic mechanisms of Leplat et al. (called LDTV in Paper I) [45], Saxena et al. (called San Diego in Paper I) [46] and Marinov [47] are well established in the literature, and all are validated against laminar burning velocity of ethanol+air flames and have documented predictive capabilities. The mechanisms of Saxena et al. and Marinov were validated against the same experimental data from Egolfopoulos et al. [48]. The mechanism of Leplat et al. was validated against the experiments of Liao et al. [49], whose results are  $\sim 2$  cm/s lower than those in the experiments of Egolfopoulos et al.

The performance of the mechanisms was evaluated by comparison of the predictions against the experimental results. The mechanisms showed the same predictive patterns as in their validation against air. The mechanisms of Marinov and Saxena et al. start in close agreement on the lean side at equivalence ratio 0.5. The mechanism of Saxena et al. shows the sharpest incline up to its maximum. Up to an equivalence ratio of 0.8, the mechanism of Saxena et al. is within the limits of the experimental uncertainty, whereas at equivalence ratio  $0.9 \leq 1.0$  its overpredicting. Predictions by the mechanism of Marinov are within the limits of the experimental uncertainty over the entire experimental range in equivalence ratio, whereas the mechanism of Leplat et al. underpredicted the experimental results. Above an equivalence ratio of 1.0 there are no experimental results, the mechanisms can only be compared with each other. The maximum laminar burning velocity was found at equivalence ratio 1.1 for the mechanisms of Leplat et al. and Saxena et al., at all three temperatures, but for the mechanism of Marinov the maximum was slightly shifted towards the lean side at an equivalence ratio of 1.05 at 298 and 338 K, but was in agreement at an equivalence ratio of 1.1 at 318 K. The mechanism of Saxena et al. peaked at the highest laminar burning velocity, the mechanism of Leplat et al. being just below the mechanism of Marinov. On the rich side, San Diego predicted the highest laminar burning velocities, whereas the mechanisms of Marinov and Leplat et al. were in close agreement with each other.

Sensitivity analysis based on the laminar burning velocity was performed for all three mechanisms for ethanol+O<sub>2</sub>+CO<sub>2</sub> and ethanol+air under stoichiometric conditions and at 298 K. Figure 11(a) shows ten reactions sensitivity most sensitive according to the predictions of the mechanism of Marinov for a stoichiometric flame at 298 K. In Fig. 11(b) a reaction path diagram illustrated the major paths from the predictions of the mechanism of Marinov et al. of It is interesting that there was a large difference between the mechanisms for ethanol+O<sub>2</sub>+CO<sub>2</sub>, whereas the sensitivity within the same mechanisms between ethanol+O<sub>2</sub>+CO<sub>2</sub> and ethanol+air were essentially identical in sensitive reactions. The difference between ethanol+O<sub>2</sub>+CO<sub>2</sub> and ethanol+air was found to be in the magnitude of the sensitivity coefficients.

The most sensitive reactions in all the mechanisms were found to be



The most sensitive reaction R1, showed a higher sensitivity in O<sub>2</sub>+CO<sub>2</sub> than in air for all the mechanisms. Reaction R2 was the only reaction directly involving CO<sub>2</sub> that was sensitive, its sensitivity decreasing drastically in O<sub>2</sub>+CO<sub>2</sub> as compared to air for all three mechanisms. This could be because at a high CO<sub>2</sub>-concentration R2 reaches a partial equilibrium with its reverse reaction.

The difference in how the mechanisms handle the ethanol+O<sub>2</sub>+CO<sub>2</sub> chemistry appears in the C<sub>2</sub>-chemistry. In the mechanisms of Marinov and Saxena et al. the formation of the vinyloxy radical (C<sub>2</sub>H<sub>3</sub>O) and ketene (CCO) was of importance, although these stemmed from different sources. The formation of acetaldehyde (CH<sub>3</sub>CHO) was of importance in the mechanism of Leplat.

The major differences in chemistry appear to be between the mechanism of Leplat et al. versus the mechanisms of Marinov and Saxena et al. The distribution of sensitivity over the chemistry also varied between mechanisms. In the mechanism of Marinov the six most sensitive reactions were more sensitive to O<sub>2</sub>+CO<sub>2</sub> than in air. Only R1 had a higher sensitivity in O<sub>2</sub>+CO<sub>2</sub> than in air for the mechanism of Leplat et al, all other reactions were more sensitive to air. For mechanism of saxena et al. the differences in sensitivity of the reactions between ethanol+O<sub>2</sub>+CO<sub>2</sub> and ethanol+air were minimal.

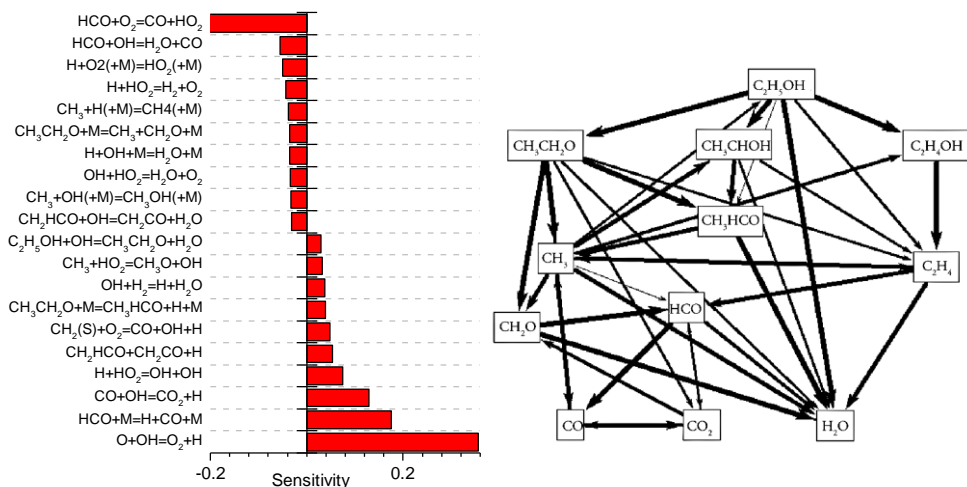


Figure 11: (a) The 20 most sensitive reactions in the mechanism of Marinov and (b) a reaction path diagram, for ethanol+O<sub>2</sub>+CO<sub>2</sub> at 298 K and under stoichiometric conditions from the study presented in Paper I.

### 6.1.2 Methanol+O<sub>2</sub>+CO<sub>2</sub>

Paper II concerns the question of how to expand the usefulness of an existing kinetic model designed for combustion with air, to the new experimental conditions of O<sub>2</sub>+CO<sub>2</sub> combustion. The article demonstrates how improvement in the performance at the O<sub>2</sub>+CO<sub>2</sub> conditions without compromising of the quality of the prediction at the original conditions, can be achieved.

Three kinetic mechanisms from literature were compared for their predictive capacity for methanol+air [50], as well as the new experimental results in Paper II. One of the examined mechanisms is a modified version of Li et al. [51], according to updates suggested by Klippenstein et al. [52]. All three examined mechanisms perform well in predicting the laminar burning velocity for methanol+air. The mechanism of Mittal et al. [53] over predicted the results when considering multicomponent transport and thermal diffusion, but performed well with mix average transport. Of the mechanisms all overpredicted the laminar burning velocity of methanol+O<sub>2</sub>+CO<sub>2</sub>. Both the mechanisms of Li et al. [51] and Li et al.+Klippenstein et al. were in agreement with the experimental results on the position of the maximum at an equivalence ratio of 1.2, whereas the mechanism of Mittal et al. predicts the maxima to occur under slightly richer conditions at an equivalence ratio of 1.3. The mechanisms of Li et al. and Li et al.+Klippenstein et al. were also in close agreement on the temperature dependence, and reasonable agreement on the dependence of the results on the equivalence ratio, with the mechanism of Li et al.+Klippenstein et al. in closer agreement with the experimental results.

The study continued to investigate the origin of the overprediction using modeling. First, it was examined how carbon dioxide affect the laminar burning velocity through chemistry and thermodynamical effects. This was examined using mechanism of Li et al. A procedure of replacing the carbon dioxide by a unreactive substitute, was proposed in the study by Liu et al. [54], and is discussed in Chapter 4.5. A fake species,  $\text{FCO}_2$ , was introduced in the mechanisms. This specie possessed the same thermodynamic properties and collisional efficiency as carbon dioxide, but did not participate as a reactant in any reactions. The removal of carbon dioxide as a reactant resulted in a dramatic increase in the predicted laminar burning velocity, to velocities high above the experimental results as can be seen in Fig. 13. Without carbon dioxide participating as a reactant the predicted reactivity from the mechanism increased, proving that carbon dioxide plays a significant role in the chemistry according to the mechanism from Li et al.

Sensitivity analysis and reaction path analysis for  $\text{methanol} + \text{O}_2 + \text{CO}_2$  were performed in order to identify the most important reactions. In light of the large amounts of carbon dioxide present in the oxidizer,  $\text{CO} + \text{OH} = \text{CO}_2 + \text{H}$  (R2) were examined for its effect on the laminar burning velocity. Its rate constant has been well determined and there is agreement in the literature. To investigate whether small differences in rate constants in R2 could affect the laminar burning velocity, several rate constants from the literature were tested in the mechanism of Li et al., without any significant effect on the laminar burning velocity.

The rate of production analysis and sensitivity analysis demonstrated the importance of H-abstraction chemistry from methanol. The rate of production analysis showed that in the mechanism of Li et al. the consumption of methanol was dominated by almost equal degree by H-abstraction from methanol, by reactions with OH through two branching channels, and with H to  $\text{CH}_2\text{OH}$ . To a lesser extent the H-abstraction of O to  $\text{CH}_2\text{OH}$  and from H to  $\text{CH}_3\text{O}$  also contribute to the consumption of methanol. Then the most important H-abstraction reactions, namely  $\text{CH}_3\text{OH} + \text{H}$  and  $\text{CH}_3\text{OH} + \text{OH}$  were studied in the literature on the rate constants. It was shown in the literature that the branching ratio of  $\text{CH}_3\text{O}$  and  $\text{CH}_2\text{OH}$  had not been examined experimentally, but theoretical work [55-57] suggests the branching ratio to be shifted towards  $\text{CH}_2\text{OH}$ . In the literature, data on the experimental rate constants for  $\text{CH}_3\text{OH} + \text{H}$  (R4) are scattered [58]. Calculated individual rate constants in the study by Meana-Pañeda et al. [56] for the branching channels of R4 suggest that at room temperature there is 100%  $\text{CH}_2\text{OH}$  formed, falling to 75% at 2500 K. Although the reaction rate of  $\text{CH}_3\text{OH} + \text{OH}$  (R5) is well established in the literature, the branching ratio is treated differently between studies. The rate constant from Xu and Lin [59] was chosen with an argument borrowed from the study by Mittal et al., that the rate constant is independent from carbon-chain length for methanol, ethanol and butanol, supporting the rate constant from the study by Xu and Lin. Changing the rate constants for R4-R5 resulted in a more accurate description of the  $\text{CH}_3\text{O}/\text{CH}_2\text{OH}$

branching, but resulted in underpredictions of the laminar burning velocity. Figure 13 also show the effect of updating the branching has on the laminar burning velocity for methanol+O<sub>2</sub>+CO<sub>2</sub> and methanol+air.

After the sensitivity was normalized against the uncertainty of its rate constant, HCO+M=H+CO+M (R6) was found to be highly sensitive. Its rate constant in the mechanism of Li et al. is derived from a wide range of experimental data obtained in different bath gases, He, Ar, N<sub>2</sub>, Ne, H<sub>2</sub>. But the major part of the experimental rate data was obtained with Ar and He as bath gases, as can be found in the references in the study from Li et al.

According to the observations of Warnatz, the effect of third bodies can be related to the bath gas used when measuring a rate constant experimentally as discussed in Chapter 0. In the mechanism of Li et al. all third body coefficients are in reasonable agreement with the observations of Warnatz, with the exception of water in R6. The numeric value used in the study by Li et al. is low in comparison to the observations of Warnatz. In the study presented in Paper II it is suggested to raise the collisional efficiency of water in R7 to 12, which is in reasonable agreement with the suggestions from Warnatz. The increase in collisional efficacy is still within the uncertainty limits of the rate constant. This change alone increased the predicted laminar burning velocity for methanol+O<sub>2</sub>+CO<sub>2</sub> and methanol+air to a high overprediction, as shown in Fig. 13.

Combining the suggested modifications of R4-R5 and the third body efficiency of H<sub>2</sub>O in R6 with the updates from the study by Klippenstein et al. and the mechanism of Li et al. improved the performance compared with the original version the mechanism of Li et al., as showed in Fig. 12. For the examined methanol+air flames, the modification did not influence the predictions more than cause a slight decrease over the entire range of equivalence ratios. In fact, the modified version predicts the laminar burning velocities within the experimental uncertainty at an equivalence ratio of  $\geq 1.0$ , providing a closer fit as compared to the original version of the mechanism of Li et al. At equivalence ratio of  $\leq 0.9$  the modified version underpredicts, but is close to the limits of the experimental uncertainty. The modified mechanism was found to predict the laminar burning velocities within the limits of the experimental uncertainty of the experimental results, providing a closer match to the experimental results of all the examined mechanisms.

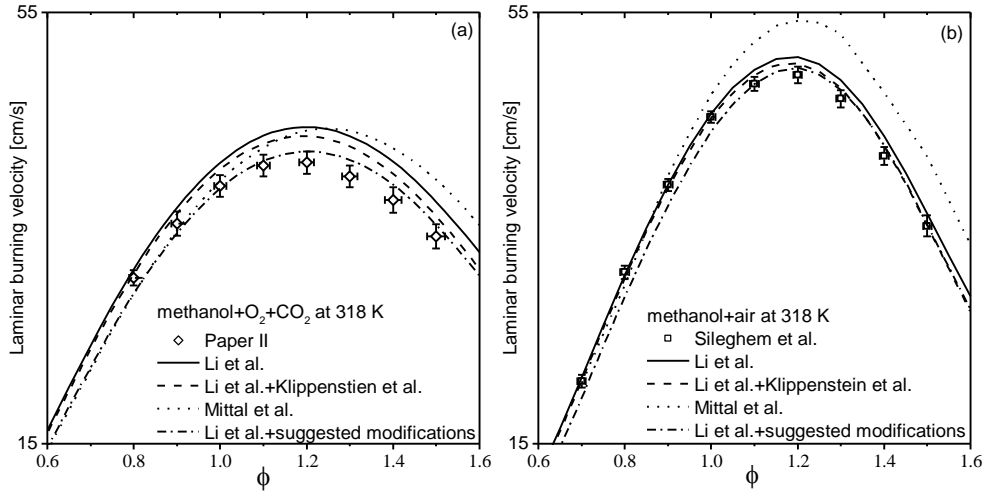


Figure 12: Experimental results compared with predictions for the laminar burning velocity of (a) methanol+O<sub>2</sub>+CO<sub>2</sub> and (b) methanol+air, from the study presented in Paper II.

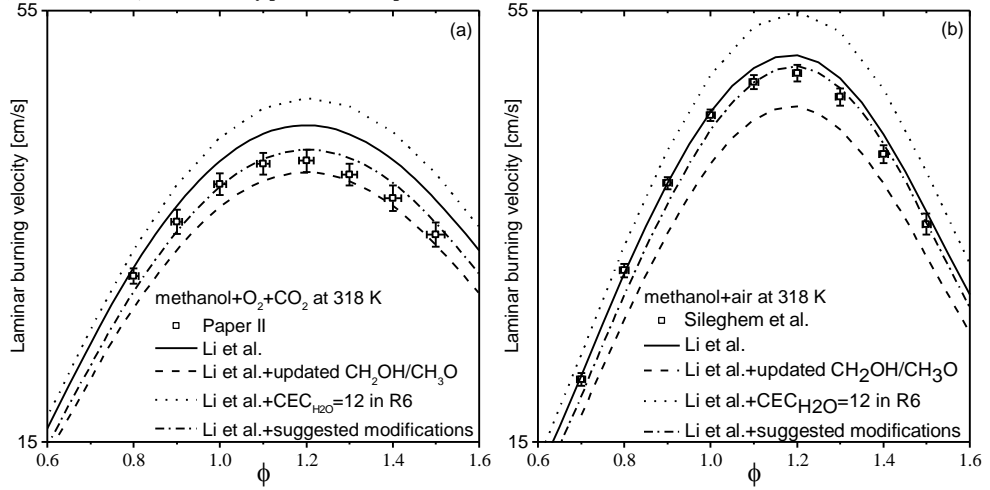


Figure 13: The effect of the suggested modifications of the mechanism of Li et al. on the predicted laminar burning velocity of (a) methanol+O<sub>2</sub>+CO<sub>2</sub> and (b) methanol+air, in comparison to the experimental results, taken from the study presented in Paper II.

## 6.2 Characterization of nitromethane combustion

To achieve the goal of providing new information on the combustion behavior of nitrogen containing fuels, a series of three studies was conducted. The studies examined and quantified the fundamental properties: the laminar burning velocity and the ignition of nitromethane+oxidizer.

Nitromethane is a potent fuel; used to boost the energy content of a fuel, as for example in drag racing where nitromethane is mixed with methanol. It is also a good representative of fuel-bound nitrogen due to its short carbon chain and nitrogen-carbon-bond.

Nitromethane exhibits the unusual property of reacting through a two stage process, as has been confirmed in both flame studies [60, 61] and ignition studies [62, 63]. Hall and Wolfhard [61] analyzed two reaction zones in nitromethane flames under low pressure. In the first zone, a yellow unidentified emission was observed. The authors reasoned that this was likely from  $\text{NO}_2^*$ . The emitted light from several radicals were observed in the second zone. A two stage process was also seen in the modeling from the studies of Boyer and Kuo [60] and study presented in Paper III. The study by Guirguis et al. [63] first noted that for a few of their measurements there were two pressure spikes from ignition observed, but did not investigate this further. The study by Djebaili-Chaumeix et al. [62] showed that nitromethane+ $\text{O}_2$  ignites through two stages. The authors concluded that the ignition first begins with the decomposition of nitromethane, and then a delayed ignition of the radical pool follows.

Clues on the structure of the two stage process can be found in species studies in the literature [60-65], as exemplified by the experimental studies discussed below. The combustion process starting with the thermal decomposition of nitromethane, predominantly to  $\text{CH}_3+\text{NO}_2$  has been demonstrated in shock tube studies [64]. In the study by Hall and Wolfhard emissions from  $\text{C}_2^*$ ,  $\text{CH}^*$ ,  $\text{CN}^*$ ,  $\text{OH}^*$ ,  $\text{NH}^*$  and  $\text{NO}^*$  was observed in the second stage of their flame.

The nitrogen proceeds from  $\text{NO}_2$  to  $\text{NO}$ . The reaction  $\text{NO}_2+\text{H}=\text{NO}+\text{OH}$  (R8) has been attributed as being the dominating exothermic step in detonation studies [66-69], where a two-stage process also was observed. It was found that in detonation these two stages proceeded at different velocities independent of one another.

In earlier nitromethane studies, the equivalence ratio was defined with the assumption being made that  $\text{N}_2$  is the final product [12]. However, in studies on nitromethane decomposition, in which  $\text{NO}$  was measured experimentally, it was shown that  $\text{NO}$  is one of the major product formed, but not consumed, and stable at high temperatures [70, 71]. This supports  $\text{NO}$  being considered as the final product from the thermal nitrogen in nitromethane and in the stoichiometric

balance for the equivalence ratio definition. The role of NO in nitromethane flames has been discussed by de Jaegere and van Tiggelen [72], as a non-reactive species in combustion. The study by Tian et al. [73] was the first to consider NO as being the major product for the nitrogen content of nitromethane. This definition of stoichiometry and equivalence ratio was also used in the following publication on low pressure nitromethane flames [74]. Considering this as a background to the work on nitromethane for this thesis the stoichiometric equation presented in Chapter 2.1, in which NO is the final product for nitrogen, was used to define the equivalence ratio.

### 6.2.1 Laminar burning velocity

In Paper III the laminar burning velocity was determined for nitromethane+air flames over an equivalence range of 0.8-1.6 at 338-358 K and atmospheric pressure. The laminar burning velocity was found to peak at an equivalence ratio of 1.2 for all three temperature-series, 33.04 cm/s at 338 K, 34.27 cm/s at 348 K, and 36.09 cm/s at 358 K. The exponent for the temperature dependence of the laminar burning velocity in the form of Eq. (4) was calculated. The experimental results were compared with predictions by the mechanisms of Zhang et al. [74] and Brequigny et al. [27] in Fig. 14.

The mechanism of Zhang et al. underpredicted the laminar burning velocity significantly under all experimentally examined conditions. The maximum at an equivalence ratio of 1.1 was shifted towards the lean side as compared to the experimental results. The mechanism of Brequigny could reproduce the position of the maxima in laminar burning velocity in terms of equivalence ratio, but not in magnitude. The laminar burning velocities were underpredicted for the entire experimental range in both temperature and equivalence ratio, but to a lesser extent than for the mechanism of Zhang et al.

#### *Reevaluation of the results from Brequigny et al.*

In Paper III it can be seen how information on the combustion behavior of a nitromethane is important for the interpretation of experimental data. It was shown that the width of the reaction zone of nitromethane+air is important to consider in the treatment of the output from spherical flames.

The study by Brequigny et al. measured laminar burning velocity at 423 K and 1-3 bar. Their experimental results at 1 bar were compared to the results in Paper III. As the two sets of experimental results were obtained at different temperatures, direct comparison was not possible. Instead predictions from the temperature dependence, derived from laminar burning velocities in Paper III, were compared to the experimental results from Brequigny et al. The comparison showed that the data from the study by Brequigny et al. did not fit the temperature dependence. To

understand the discrepancy, the experimental data from the study by Brequigny et al. were reexamined.

In the study by Brequigny et al. the laminar burning velocity was calculated using Eq.(13), from the experimental output with modeled densities calculated for  $\pm\infty$  distance from the flame front by equilibrium calculations assuming that the flame front fits within the combustion vessel and has reached completion. However, according to modeling performed in the study presented in Paper III, the reaction zone of the nitromethane flames presented in the study by Brequigny et al. is predicted as being stretched out in radii. In the modeling predictions for these flames at 1 bar presented in Paper III it was shown that for several equivalence ratios, the reaction zone is wider than the limitations placed on the radius of the closed vessel used in the study by Brequigny et al. to assume undisturbed flame propagation. The relationship between the flame front and the experimental limits on the radii can be seen in Fig. 15, in the form of predicted temperature as a function of distance across the flame structure, representing the predicted flame fronts for each measured equivalence ratio. For several measurements, the flame temperature profiles show that the temperature has not reached a plateau temperature, which would indicate that the chemistry has reached completion, but instead continues to rise. Then the assumption made in the study by Brequigny et al. that the combustion process has reached completion and the use of the densities at  $\pm\infty$  does not hold. The flames obtained at 1 bar in the study by Brequigny et al. were reexamined through modeling, at the experimental limitations in radius of the closed vessel. Predicted densities were taken at the positions in the flame for the maximum and the minimum in flame radius from modeling with the mechanism of Brequigny et al. This new use of densities were utilized in Eq. (13) to recalculate the laminar burning velocities for the limiting conditions resulting in a range where the laminar burning velocity is likely to be found, as can be seen in Fig. 15. After this treatment, the recalculated laminar burning velocities were in better agreement with the results presented in Paper III in accordance with the temperature dependence.

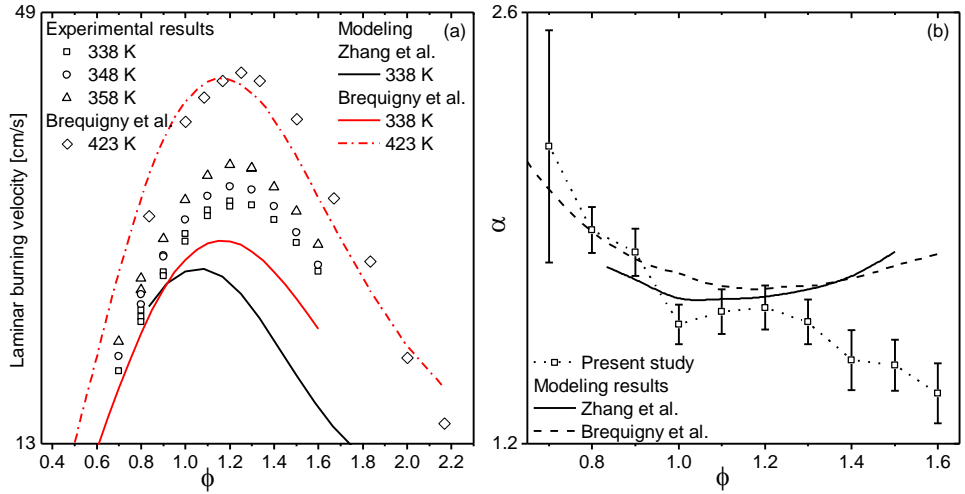


Figure 14: (a) The laminar burning velocity as a function of the equivalence ratio for the nitromethane+air flames from Paper III, together with the experimental results at 423 K and 1 bar from the study by Brequigny et al. Modeling predictions by the mechanism of Brequigny et al. is shown as lines. (b) The temperature dependence (4) as a function of the equivalence ratio for nitromethane+air, from both experimental results and modeling predictions from the study presented in Paper III.

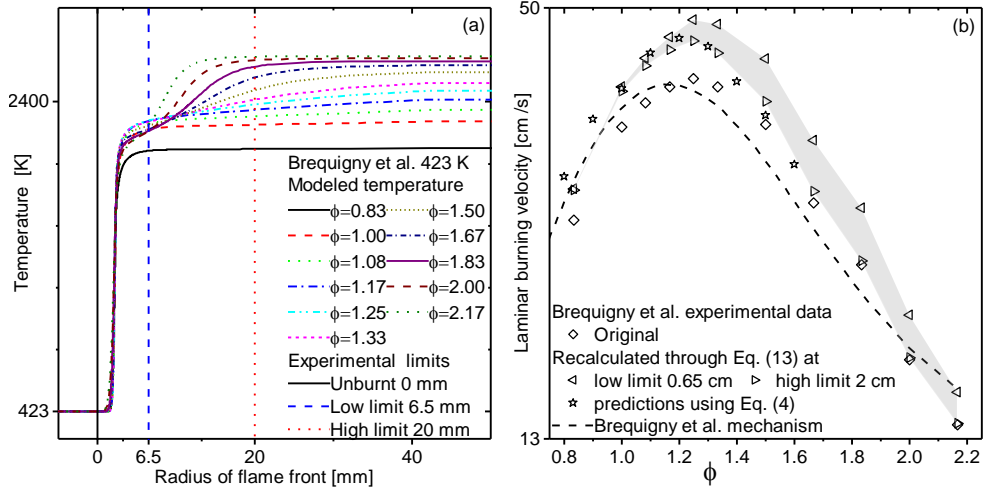


Figure 15: In (a) the flame front of the nitromethane+air flames examined in the study by Brequigny et al. at 423 K and 1 bar are presented in relation to the experimental limitations on the flame from the combustion vessel. The flames are represented by predicted temperature as a function of radii. and (b) its implication in the laminar burning velocity from the study by Brequigny et al. when modeled densities at the combustion vessels experimental limitations on the flame in radii was considered in (13). The results are taken from the study presented in Paper III.

### 6.2.2 Ignition

The study presented in Paper III led to the realization that the structure of the combustion process in a fuel+O<sub>2</sub> mixture is an important consideration in experimental measurements of other fundamental properties. The study presented in Paper IV is an effort to obtain knowledge on the fundamental structure of how nitromethane reacts. The study provided additional insight on the two stage process of nitromethane chemistry by examining both stages of the ignition of nitromethane+O<sub>2</sub>+N<sub>2</sub>. Through the analysis of the two stage behavior that occurs in nitromethane ignition and through discussions on correlations of the ignition delay times, the literature on nitromethane ignition and measured ignition delay times, which appeared to be scattered, came to consensus with the ignition of the two stages, as presented in Paper IV.

The ignition of nitromethane+O<sub>2</sub>+N<sub>2</sub> was studied in Paper IV through the use of luminosity and pressure over time to define the ignition characteristics. From the experimental traces, it was seen that the detected pressure rise was both fast, i.e. difficult to separate from the arrival of the shock wave, and stretched out over time. From the pressure traces it could be seen that there was an activity in the mixture extending over time, but the pressure traces could not independently prove that ignition had occurred. The luminosity traces showed that there were two ignition events separated in time. As the luminosity maxima were well defined, these were used to define ignition, with each maximum marking a separate ignition stage. The first stage appears shortly after the arrival of the shock wave, followed by a second ignition stage of greater intensity in luminosity. It was noted that the second luminosity maximum and the maximum in pressure coincided in time. Examples of pressure and luminosity over time for the three of the mixtures that were examined are shown in Fig. 16. As the pressure rise was gradual it would give a large uncertainty in the results. For this reason, in Paper IV the maximum intensity of unfiltered luminosity was used to define the ignition, as that signal was more clearly defined over time.

The two ignition stages were analyzed as on an individual basis, with their ignition delay time related to the arrival of the shock wave. The two ignition stages were analyzed as separate events through the experiments and in the modeling predictions.

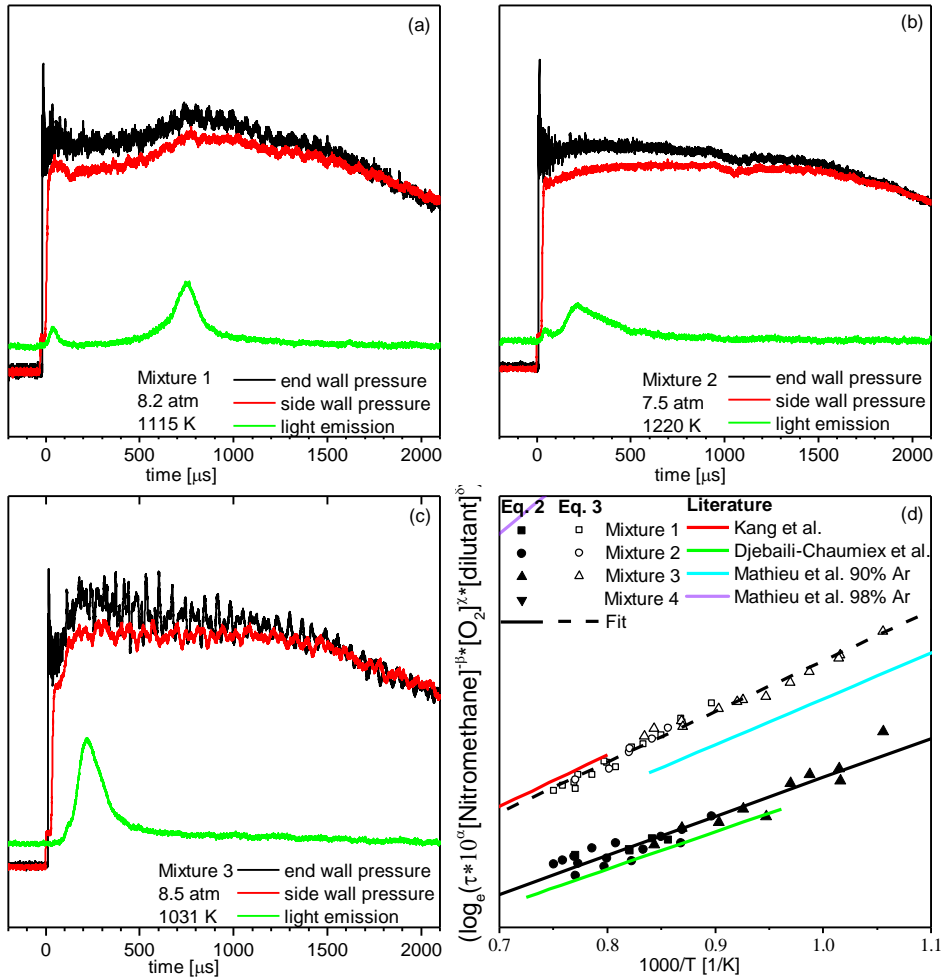


Figure 16: Pressure and luminosity profiles over time for (a-c) for measurement points exemplifying the ignition in Mixtures 1-3, from the study presented in Paper IV, and (d) correlations derived in the study presented in Paper IV with correlations from the literature shown as a function of time.

In Paper IV, correlation equations for both the first and second stage ignition were derived to quantify the effects of the mixture composition and obtain the global activation energy for nitromethane+O<sub>2</sub> ignition. The correlations showed that the first stage ignition is promoted primarily by the nitromethane content, and to lesser extent by the O<sub>2</sub> content. In the second ignition stage, the ignition is dampened by nitromethane, whereas it has unusual strong promotion by the O<sub>2</sub> content. The correlations obtained enabled comparison to be made with correlations presented in the literature [24, 62, 75] for ignition delay times measured under different conditions. The correlations are presented and compared in Fig. 16. The correlations indicate a close agreement of the ignition delay times

measured in the study by Kang et al. [75] with the second stage ignition. The correlation from the study by Djebaili-Chaumeix et al. [62] was in reasonable agreement with the first stage ignition. Mathieu et al. [24] presented two correlations, based on experiments performed with two different dilutions by Argon, neither dilution series were in agreement with the other correlations. Within the context of the results presented in Paper IV, the ignition studied in the study by Kang et al. and in the study by Djebaili-Chaumeix et al. can be in consensus to the two ignition stages. The apparent inconsistency in the literature was, after the literature was analyzed together, shown to be both consistent and to provide information on different aspects of nitromethane+O<sub>2</sub> ignition.

The two latest published kinetic mechanisms made for nitromethane combustion were compared, the mechanisms of Brequigny et al. [27] and Mathieu et al. [24]. It was shown that the mechanism of Brequigny et al. could reproduce both the trends in ignition delay in regards to mixture composition, as well as reproduced the ignition delay times in reasonably close agreement at 8 atm. The mechanism of Brequigny et al. was used for further modeling because of its better performance. However, as unfiltered emission was used for defining the ignition in the experiments of Paper IV, it was not possible to use the same definition in the modeling. To evaluate how to best compare the modeling predictions with the experimental ignition delay times, several definitions were compared and can be seen in Fig. 17. Because the mechanism from Brequigny et al. does not contain excited species, the maxima in concentration for precursor-species of those excited species which emit light within the range of the experimental luminosity, and the predicted maximum gradient in pressure were tested as markers for the ignition, and were examined over time. These precursors were compared with each other and to the experimental ignition delay times. It was demonstrated that maxima of the selected precursors was in close agreement in position over time, and that the choice of ignition marker did not influence quality in the interpretation of the modeling predictions of the study.

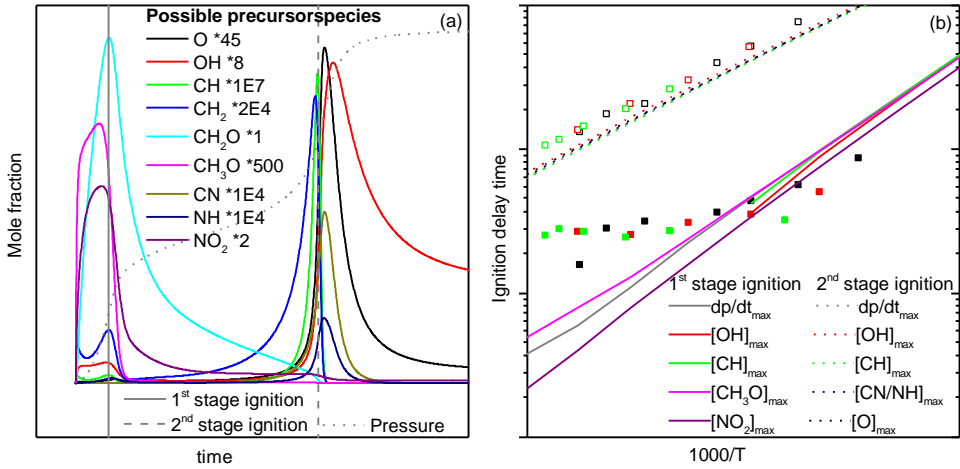


Figure 17: Specie profiles as a function of time are shown in relation to their position in time compared to pressure for modeling of a In (b) the ignition delay times using different definitions in the modeling of the first and second stage ignitions as a function of temperature are shown in comparison to the experimental results presented in the study in Paper IV.

### 6.2.3 Nitromethane under $CO_2$ -rich conditions

In Paper V, laminar burning velocity measurements for nitromethane+ $O_2$ + $CO_2$  were presented for the first time. The experiments were performed under atmospheric pressure using the Heat flux method at an equivalence ratio of 0.8-1.3 at 348 K, and equivalence ratio 0.8-1.6 at 358 K. The effect of the oxidizer was examined by varying the molecular oxygen fraction 30-40% for a stoichiometric flame at 358 K.

The experimental results were used as input in comparing predictions from two kinetic mechanisms from the literature, the mechanisms of Brequigny et al. [27] and Mathieu et al. [24]. There is a discrepancy in the quality of the modelling predictions between the  $CO_2$ -rich condition of the present study and in air, as can be seen in Fig. 18(a) as well as in Fig. 19(a-b). Both mechanisms underpredicts the laminar burning velocities of nitromethane+ $O_2$ + $CO_2$  presented in Paper V over the entire range of equivalence ratios and temperatures. The underprediction for the mechanism from Brequigny et al. was the greatest, with an underprediction of 6.4 cm/s, as compared to 3.6 cm/s for the mechanism of Mathieu et al. at an equivalence ratio of 1.1. The quality of the predictions from the two mechanisms was also evaluated based on predictions of the nitromethane+air flames from Paper III. The mechanism of Mathieu et al. managed to reproduce the laminar burning velocity for nitromethane+air, whereas the laminar burning velocity was underpredicted over the entire range of experimental results for nitromethane+ $O_2$ + $CO_2$ . The quality of the predictions for both mechanisms

appears to be dependent on both mixture composition and oxidizer composition. The influence of the content of molecular oxygen in the oxidizer was observed from the dilution series of a stoichiometric flame at 358 K, and by comparing the the increase in laminar burning velocity with increasing O<sub>2</sub> fraction for modeling predictions and experimental results. Both mechanisms predicted results under the experimental uncertainty, with the discrepancy deviating further with increasing molecular oxygen content.

Sensitivity analysis showed that the two mechanisms share the three most sensitive reactions, as can be seen in Fig. 18(b). The most sensitive reaction for both mechanisms is  $\text{H} + \text{O}_2 = \text{O} + \text{OH}$  (R1) for both nitromethane under carbon dioxide-rich conditions and for nitromethane+air. This reaction has a well determined rate constant, there being a solid agreement in the literature. The reaction is therefore not discussed here further.

The sensitivity of the reaction  $\text{CO} + \text{OH} = \text{CO}_2 + \text{H}$  (R2) is essentially the same for both the mechanisms in the examined cases. The rate constant from the study by Rasmussen et al. [76] used in the mechanism of Brequigny et al. is valid for 1 bar. No pressure dependence was employed, although rate constants for a variety of different pressures were provided in the study by Rasmussen et al. The study by Mathieu et al. used the rate constant from the study by Joshi and Wang [77] calculated for the temperature range 120-2500 K.

In the study presented in Paper V the temperature dependence for R2 was implemented in the mechanism of Brequigny et al. by implementing all the rate constants for R2 and its other branching channel provided by Rasmussen et al. As expected, as the flames in the present study are burnt at atmospheric pressure, no change in performance was observed.

The reaction  $\text{HCO} + \text{NO}$  (R4) showed the highest negative sensitivity in all the examined cases. Both mechanisms used the same rate constant from the study by Xu and Lin [79] and exhibit similar sensitivities, therefore this reaction was not considered further here.

Differences between the mechanisms are to be found in how the nitrogen chemistry is treated. The mechanism of Brequigny et al. is more sensitive to reactions involving HNO, whereas the mechanism of Mathieu et al. is more sensitive towards reaction involving conversion between NO and NO<sub>2</sub>. There are also differences in the sensitivity of the fuel reacting with radicals. The reaction  $\text{CH}_3\text{NO}_2 + \text{OH}$  is sensitive in the mechanism of Mathieu et al. under CO<sub>2</sub>-rich conditions and in air. The reaction  $\text{CH}_3\text{NO}_2 + \text{M}$  is sensitive for the case of nitromethane under carbon dioxide-rich conditions in the mechanism of Brequigny et al.

$\text{HCO} + \text{M} = \text{H} + \text{CO} + \text{M}$  (R3) is more sensitive in the mechanism of Brequigny et al. than in the mechanism of Mathieu et al., for nitromethane in air. Under CO<sub>2</sub>-

rich conditions this reaction is essentially equally sensitive between the two mechanisms; although there are differences in how this reaction is treated in the mechanisms. R3 is assigned the pressure dependent rate constant from the study by Hippler et al. [79] in the mechanism from Brequigny et al., whereas in the mechanism from Mathieu et al. the rate constant by Li et al. [51] is multiplied by 1.2 and used with different third body coefficients than chosen by Li et al. The low pressure rate constant from the study by Hippler et al. and the rate constant from the study by Li et al. are in acceptably close agreement, as is the multiplied rate constant used in the mechanism of Mathieu et al. However, because of the pressure dependence in the rate constant for R3 of Hippler et al., under atmospheric pressure the reaction occurs in its falloff regime. The unusual pressure dependence and the low pressure rate constant has been questioned by Krasnoperov et al. [80]. The reasoning of Krasnoperov et al. was as follows: Hippler et al. measured the formyl radical (HCO) decay rates in initial high concentrations, where bimolecular radical reactions can be expected to occur readily. Yet the formyl decay observed was attributed to solely the formyl decomposition reaction and interference from radical-radical reactions was neglected. For the performance under the conditions in the present study, the rate  $\sim 1$  atm could be of importance.

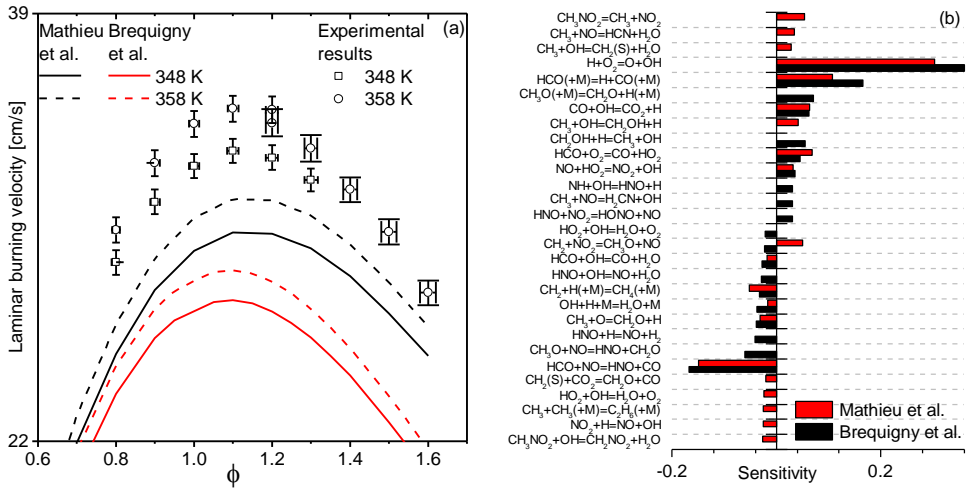


Figure 18: (a) The laminar burning velocity as a function of the equivalence ratio for the experimental results and modeling for nitromethane+ $O_2$ + $CO_2$  presented together with (b) sensitivity results for an equivalence ratio of 1.2, taken from the study presented in Paper V.

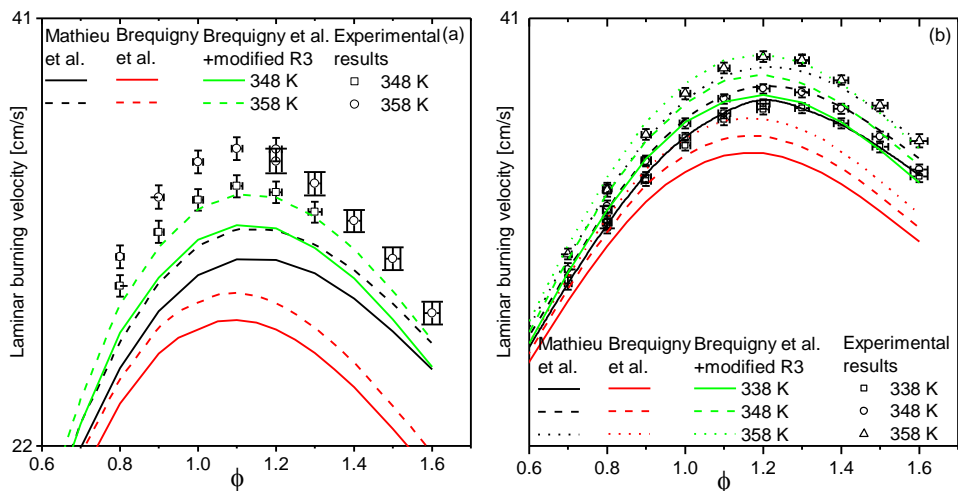


Figure 19: Effects of modifications of R3 on the laminar burning velocity of nitromethane+O<sub>2</sub>+CO<sub>2</sub> and of nitromethane+air, from the study presented in Paper V.

The mechanisms also dealt with the collisional efficiencies differently, most notably in the case of water, a third body which was shown to be of importance for flames at carbon dioxide-rich conditions in the study presented in Paper II on methanol+O<sub>2</sub>+CO<sub>2</sub> flames. Increasing the third body collisional efficiency for water in the mechanism of Brequigny et al. to 12, the same numerical values as employed by Mathieu et al. and in the study presented in Paper II were found to decrease the laminar burning velocity even further to a level below the experimental results as can be seen in Fig. 19

Using the rate constant at the low pressure limit would more realistically represent the conditions of the present study; therefore the rate constant from Li et al. multiplied by 1.2 as implemented by Mathieu et al., was implemented separately in Brequigny et al. and tested for its effect on the laminar burning velocity. This increased the predicted laminar burning velocity closer to the experimental results. Now the performance at carbon dioxide-rich conditions is improved to be better than Mathieu et al. as can be seen in Fig. 19(a). For the nitromethane+air flames, which can be seen in Fig. 19(b), the modified version of Brequigny et al. overpredicts the laminar burning velocity on the lean side at equivalence ratios 1 and below, while reproducing the laminar burning velocity successfully within the experimental uncertainty in the rich mixtures. The increase of laminar burning velocity with increased content of molecular oxygen in the oxidizer for the nitromethane+O<sub>2</sub>+CO<sub>2</sub> flames was reproduced within the experimental uncertainty by the modified version of Brequigny et al.

## 7 Summary and outlook

New experimental data were provided to the scientific community through the studies presented in the thesis. In Papers I-II and Paper V data on the first measurements of the laminar burning velocity of liquid fuels at carbon dioxide-rich conditions were presented. The laminar burning velocity of nitromethane was measured for nitromethane combusted with air as well as with  $\text{O}_2+\text{CO}_2$ , in Paper III and Paper V, respectively. In Paper IV the ignition of nitromethane+ $\text{O}_2$  was examined as a function of time, and ignition delay times were presented.

The combustion characteristics of nitromethane were explored through examining its laminar burning velocity and ignition in the studies presented in Papers III-V. The importance of knowledge of combustion characteristics of the fuel was highlighted through Paper III. It was shown that in a study from the literature, lack of knowledge on the combustion behavior of nitromethane was affecting the resulting laminar burning velocity from spherical flames in a negative way. The study presented in Paper III showed that because the reaction zone was predicted to be wider than the experimental limitations on the flame, the method used for calculating the laminar burning velocity was inapplicable. In Paper IV, the two stage ignition process was examined for the first time. From examining the two stage ignition of nitromethane+ $\text{O}_2+\text{N}_2$ , information as activation energy and the effect on mixture composition were derived from the experimental results, for both ignition stages. Previous to Paper IV, there was a seeming inconsistency in ignition delay times reported in the literature on nitromethane ignition. Through comparison to correlations from the study presented in Paper IV, it was shown that the different studies were likely to be accurately describing different stages of the ignition.

In all the presented studies, predictions from detailed kinetic mechanisms from the literature were explored and compared to the experimental results. It was shown that the examined mechanisms deal with the chemistry of the fuels in air and in  $\text{O}_2+\text{CO}_2$  similarly. The major differences were found to be between the different mechanisms. Paper II and Paper V emphasized the importance of validation of kinetic mechanisms against experimental results obtained with different diluents in the oxidizer. Both studies showed that water has a larger influence as a third body in the formyl decomposition in the flame chemistry with  $\text{O}_2+\text{CO}_2$  as compared to air as the oxidizer for their examined fuels. By validation of the combustion of

nitromethane, against different combustion properties, as the laminar burning velocity in the studies presented in Paper III and in Paper V, and ignition as presented the study in Paper IV, different aspects of the chemistry could be highlighted through the mechanisms. The studies revealed that with the current mechanisms for nitromethane, one mechanism cannot be used to describe both combustion properties accurately. This indicates that the full picture of nitromethane chemistry is not yet understood.

The studies presented in the thesis showed that the chemistry of the examined fuels, predicted with the current kinetic mechanisms from literature, cannot be directly translated to fuel+O<sub>2</sub>+CO<sub>2</sub> flames. The examined kinetic mechanisms were failing to accurately reproduce the experimental results, when changing the diluent to carbon dioxide, instead of molecular nitrogen from air.

Through the work presented in the thesis many gaps in the current knowledge were identified. Future studies can take direction from the thesis for relevant subjects which would benefit further examination, as for example the weak pressure dependence of nitromethane+O<sub>2</sub> ignition, or development of a kinetic mechanism with capacity to accurately reproduce flames burnt with carbon dioxide as the diluent.

# Acknowledgements

This thesis would not have been realized without the support of my supervisors, **Professor Alexander Konnov** and **Dr. Elna Heimdal-Nilsson**. **Alexander**, you have always challenged me to do better. I am truly impressed with the amounts of your knowledge. A major drive for me has been trying to find or prove something new, to get you to lean back and say “interesting...”. **Elna**, I appreciate that you have never told me how to do it, but instead had the “you can make it work”-attitude to supervising.

Thank you, **Professor Marcus Alden** for giving me this opportunity to pursue a PhD. Thank you to **Minna**, **Cecilia**, **Sven-Inge** and **Igor** for all the help. You are the framework that keeps the division running smooth.

My co-workers **Moah** and **Vladimir** were great companions during there years. We will drink that wine! Or at least open it! **Vladi**, you always had another perspective to offer on the science. After years of sharing and office with **Moah**, I feel that perhaps the most of what I have learnt comes from obsessing over details and articles, and the endless questioning of everything together.

Some of the most fun projects have been my collaborations with **Christian Brackmann**. Thank you Christian for all your support and sharing your experience with me.

I spent a month in Galway, working with **Professor Henry Curran** in his group. Thank you **Henry**, for the opportunity to work with your group. I learned a lot from you, and got to do super-fun-awesome science! **Professor John Simmie**, I appreciate that you generously shared your knowledge with me. An extra thank you to **Yang**, for our time together in the lab!

I want to thank everyone at the division for the chats, the laughs and the great support. A special thank you to my co-authors!

I would like to thank The Centre for Combustion Science and Technology (CECOST) and the Swedish Energy Agency (STEM) for financial support. Thanks to the Hierta-Retzius foundation for financial support for an extended research-trip to National University of Ireland, Galway.

Thank you **Anders**, for putting up with that I at times was also married to my research. **August** and **Liv**, you are the best life has to offer.

# References

- [1] Eurostat European Commission, Energy, transport and environment indicators, in, European union, Belgium, 2012.
- [2] A.K. Agarwal, Biofuels (alcohols and biodiesel) applications as fuels for internal combustion engines, *Prog. Energy Combust. Sci.*, 33 (2007) 233-271.
- [3] S.K. Thangavelu, A.S. Ahmed, F.N. Ani, Review on bioethanol as alternative fuel for spark ignition engines, *Renewable and Sustainable Energy Reviews*, 56 (2016) 820-835.
- [4] Efficient Shipping with low emissions <<http://www.effship.com>>
- [5] Alcohol (spirits) and ethers as marine fuel <<http://www.sspa.se/alternative-fuels/spireth-methanol-marine-fuel>>
- [6] Priority Project 21 on Motorways of the Sea <<http://ec.europa.eu/inea/ten-t/ten-t-projects/projects-by-priority-project/priority-project-21>>
- [7] K. Sekimoto, S. Inomata, H. Tanimoto, A. Fushimi, Y. Fujitani, K. Sato, H. Yamada, Characterization of nitromethane emission from automotive exhaust, *Atmospheric Environment*, 81 (2013) 523-531.
- [8] S. Inomata, Y. Fujitani, A. Fushimi, H. Tanimoto, K. Sekimoto, H. Yamada, Field measurement of nitromethane from automotive emissions at a busy intersection using proton-transfer-reaction mass spectrometry, *Atmospheric Environment*, 96 (2014) 301-309.
- [9] T. Edwards, Liquid Fuels and Propellants for Aerospace Propulsion: 1903-2003, *Journal of Propulsion and Power*, 19 (2003) 1089-1107.
- [10] K.W. McCown Iii, E.L. Petersen, Effects of nano-scale additives on the linear burning rate of nitromethane, *Combust. Flame*, 161 (2014) 1935-1943.
- [11] T. Powell, Racing experiences with methanol and ethanol-based motor-fuel blends, in, SAE International, 1975.
- [12] E.S. Starkman, Nitroparaffins as potential engine fuels, *Ind. Eng. Chem.*, 51 (1959) 1477-1480.
- [13] K.K. Kuo, *Principles of Combustion*, 2nd edition ed., Wiley, New York, 2005.
- [14] C.K. Law, *Combustion Physics*, Cambridge University Press, New York, USA, 2006.

- [15] S. Gutman, G.I. Sivashinsky, The cellular nature of hydrodynamic flame instability, *Physica D: Nonlinear Phenomena*, 43 (1990) 129-139.
- [16] J. Warnatz, U. Maas, R.W. Dibble, *Combustion*, 4th ed., Springer Berlin Heidelberg, New York, 2006.
- [17] H. Wang, D.A. Sheen, Combustion kinetic model uncertainty quantification, propagation and minimization, *Prog. Energy Combust. Sci.*, 47 (2015) 1-31.
- [18] A.T. Holley, X.Q. You, E. Dames, H. Wang, F.N. Egolfopoulos, Sensitivity of propagation and extinction of large hydrocarbon flames to fuel diffusion, *Proc. Comb. Inst.*, 32 (2009) 1157-1163.
- [19] J. Warnatz, Rate Coefficients in the C/H/O System, in: J.W.C. Gardiner (Ed.) *Combustion Chemistry*, Springer-Verlag New York Inc., New York, 1984, pp. 197-360.
- [20] J.X. Zhou, M. Cordier, C. Mounaïm-Rousselle, F. Foucher, Experimental estimate of the laminar burning velocity of iso-octane in oxygen-enriched and CO<sub>2</sub>-diluted air, *Combust. Flame*, 158 (2011) 2375-2383.
- [21] B. Galmiche, F. Halter, F. Foucher, P. Dagaut, Effects of Dilution on Laminar Burning Velocity of Premixed Methane/Air Flames, *Energy Fuels*, 25 (2011) 948-954.
- [22] F. Lacas, B. Leroux, N. Darabiha, Experimental study of air dilution in oxy-liquid fuel flames, *Proc. Comb. Inst.*, 30 (2005) 2037-2045.
- [23] Cleaner combustion - Developing detailed chemical kinetics models, (Ed.) F. Battin-Leclerc, J.M. Simmie, E. Blurock, Springer-Verlag, London, 2013.
- [24] O. Mathieu, B. Giri, A.R. Agard, T.N. Adams, J.D. Mertens, E.L. Petersen, Nitromethane ignition behind reflected shock waves: Experimental and numerical study, *Fuel*, 182 (2016) 597-612.
- [25] CHEMKIN IV 15101, Reaction Design, San Diego, 2010
- [26] G. Dixon-Lewis, Flame Structure and Flame Reaction Kinetics. II. Transport Phenomena in Multicomponent Systems, *Proc. R. Soc. London A: Mathematical, Physical and Engineering Sciences*, 307 (1968) 111-135.
- [27] P. Brequigny, G. Dayma, F. Halter, C. Mounaïm-Rousselle, T. Dubois, P. Dagaut, Laminar burning velocities of premixed nitromethane/air flames: An experimental and kinetic modeling study, *Proc. Comb. Inst.*, 35 (2014) 703-710.
- [28] T.L. Cong, P. Dagaut, Experimental and Detailed Kinetic Modeling of the Oxidation of Methane and Methane/Syngas Mixtures and Effect of Carbon Dioxide Addition, *Combust. Sci. Technol.*, 180 (2008) 2046-2091.

- [29] F. Halter, F. Foucher, L. Landry, C. Mounaïm-Rousselle, Effect of Dilution by Nitrogen and/or Carbon Dioxide on Methane and Iso-Octane Air Flames, *Combust. Sci. Technol.*, 181 (2009) 813-827.
- [30] F.S. Liu, H.S. Guo, G.J. Smallwood, The chemical effect of CO<sub>2</sub> replacement of N<sub>2</sub> in air on the burning velocity of CH<sub>4</sub> and H<sub>2</sub> premixed flames, *Combust. Flame*, 133 (2003) 495-497.
- [31] J.D. Naucier, L. Sileghem, E.J.K. Nilsson, S. Verhelst, A.A. Konnov, Performance of methanol kinetic mechanisms at oxy-fuel conditions *Combustion and Flame*, *Comb. Flame*, 162 (2014) 1717-1728.
- [32] CHEMKIN, Theory manual, CK-THE-10112-1112-UG-1, Reaction Design, San Diego, USA, 2011.
- [33] F.N. Egolfopoulos, N. Hansen, Y. Ju, K. Kohse-Hoinghaus, C.K. Law, F. Qi, Advances and challenges in laminar flame experiments and implications for combustion chemistry, *Prog. Energy Combust. Sci.*, 43 (2014) 36-67.
- [34] V.A. Alekseev, J.D. Naucier, M. Christensen, E.J.K. Nilsson, E.N. Volkov, L.P.H. de Goeij, A.A. Konnov, Experimental Uncertainties of the Heat Flux Method for Measuring Burning Velocities, *Combust. Sci. Technol.*, 188 (2016) 853-894.
- [35] A.A. Konnov, I.V. Dyakov, Measurement of propagation speeds in adiabatic flat and cellular premixed flames of C<sub>2</sub>H<sub>6</sub>+O<sub>2</sub>+CO<sub>2</sub>, *Combust. Flame*, 136 (2004) 371-376.
- [36] A.A. Konnov, I.V. Dyakov, Experimental study of adiabatic cellular premixed flames of methane (ethane, propane) plus oxygen plus carbon dioxide mixtures, *Combust. Sci. Technol.*, 179 (2007) 747-765.
- [37] A.A. Konnov, I.V. Dyakov, Measurement of propagation speeds in adiabatic cellular premixed flames of CH<sub>4</sub>+O<sub>2</sub>+CO<sub>2</sub>, *Exp. Therm. Fluid Sci.*, 29 (2005) 901-907.
- [38] J.L. Devore, Probability and Statistics for Engineering and the Sciences, 2nd edition ed., Brooks/Cole Publishing Company, Monterey, CA, 1987.
- [39] A.N. Mazas, D.A. Lacoste, T. Schuller, Asme, Experimental and numerical investigation on the laminar flame speed of CH<sub>4</sub>/O<sub>2</sub> mixtures diluted with CO<sub>2</sub> and H<sub>2</sub>O, 2010.
- [40] A.A. Konnov, I.V. Dyakov, J. de Ruyck, Nitric oxide formation in premixed flames of H<sub>2</sub>+CO+CO<sub>2</sub> and air, *Proceedings of the Combustion Institute*, 29 (2002) 2171-2177.
- [41] F. Normann, K. Andersson, F. Johnsson, B. Leckner, NO(x) reburning in oxy-fuel combustion: A comparison between solid and gaseous fuels, *Int. J. Greenh. Gas Control*, 5 (2011) S120-S126.
- [42] G. Scheffknecht, L. Al-Makhadmeh, U. Schnell, J. Maier, Oxy-fuel coal combustion—A review of the current state-of-the-art, *Int. J. Greenh. Gas Control*, 5, Supplement 1 (2011) S16-S35.

- [43] M.B. Toftegaard, J. Brix, P.A. Jensen, P. Glarborg, A.D. Jensen, Oxy-fuel combustion of solid fuels, *Prog. Energy Combust. Sci.*, 36 (2010) 581-625.
- [44] P. Wang, K. Casleton, S. Hedges, Effect of biomass blending on oxy-fuel coal combustion, in: 28th Annual International Pittsburgh Coal Conference 2011, PCC 2011, 2011, pp. 987-995.
- [45] N. Leplat, P. Dagaut, C. Togbe, J. Vandooren, Numerical and experimental study of ethanol combustion and oxidation in laminar premixed flames and in jet-stirred reactor, *Combust. Flame*, 158 (2011) 705-725.
- [46] P. Saxena, F.A. Williams, Numerical and experimental studies of ethanol flames, *Proceedings of the Combustion Institute*, 31 (2007) 1149-1156.
- [47] N.M. Marinov, A detailed chemical kinetic model for high temperature ethanol oxidation, *Int. J. Chem. Kinet.*, 31 (1999) 183-220.
- [48] F.N. Egolfopoulos, D.X. Du, C.K. Law, A Study on Ethanol Oxidation Kinetics in Laminar Premixed Flames, Flow Reactors, and Shock Tubes, *Proceedings of the Combustion Institute*, 24 (1992) 833-841.
- [49] S.Y. Liao, D.M. Jiang, Z.H. Huang, K. Zeng, Q. Cheng, Determination of the laminar burning velocities for mixtures of ethanol and air at elevated temperatures, *Appl. Therm. Eng.*, 27 (2007) 374-380.
- [50] L. Sileghem, V.A. Alekseev, J. Vancoillie, E.J.K. Nilsson, S. Verhelst, A.A. Konnov, Laminar burning velocities of primary reference fuels and simple alcohols, *Fuel*, 115 (2014) 32-40.
- [51] J. Li, Z.W. Zhao, A. Kazakov, M. Chaos, F.L. Dryer, J.J. Scire, A comprehensive kinetic mechanism for CO, CH<sub>2</sub>O, and CH<sub>3</sub>OH combustion, *Int. J. Chem. Kinet.*, 39 (2007) 109-136.
- [52] S.J. Klippenstein, L.B. Harding, M.J. Davis, A.S. Tomlin, R.T. Skodje, Uncertainty driven theoretical kinetics studies for CH<sub>3</sub>OH ignition: HO<sub>2</sub>+CH<sub>3</sub>OH and O<sub>2</sub>+CH<sub>3</sub>OH, *Proceedings of the Combustion Institute*, 33 (2011) 351-357.
- [53] G. Mittal, S.M. Burke, V.A. Davies, B. Parajuli, W.K. Metcalfe, H.J. Curran, Autoignition of ethanol in a rapid compression machine, *Combust. Flame*, 161 (2014) 1164-1171.
- [54] F. Liu, H. Guo, G.J. Smallwood, Ö.L. Gülder, The chemical effects of carbon dioxide as an additive in an ethylene diffusion flame: implications for soot and NO<sub>x</sub> formation, *Combust. Flame*, 125 (2001) 778-787.
- [55] J.F. Bott, N. Cohen, A shock tube study of the reactions of the hydroxyl radical with several combustion species, *Int. J. Chem. Kinet.*, 23 (1991) 1075-1094.

- [56] R. Meana-Pañeda, D.G. Truhlar, A. Fernández-Ramos, High-level direct-dynamics variational transition state theory calculations including multidimensional tunneling of the thermal rate constants, branching ratios, and kinetic isotope effects of the hydrogen abstraction reactions from methanol by atomic hydrogen, *The Journal of Chemical Physics*, 134 (2011) -.
- [57] E.F.V. Carvalho, A.N. Barauna, F.B.C. Machado, O. Roberto, Theoretical calculations of energetics, structures, and rate constants for the  $\text{H}+\text{CH}_3\text{OH}$  hydrogen abstraction reactions, *Chemical Physics Letters*, 463 (2008) 33-37.
- [58] D.L. Baulch, C.T. Bowman, C.J. Cobos, R.A. Cox, T. Just, J.A. Kerr, M.J. Pilling, D. Stocker, J. Troe, W. Tsang, R.W. Walker, J. Warnatz, Evaluated kinetic data for combustion modeling: Supplement II, *J. Phys. Chem. Ref. Data*, 34 (2005) 757-1397.
- [59] K. Xu, Z.F. Xu, M.C. Lin, Ab initio kinetic prediction of branching rate constants for reactions of H atoms with  $\text{CH}_3\text{O}$  and  $\text{CH}_2\text{OH}$ , *Molecular Physics*, 105 (2007) 2763-2776.
- [60] E. Boyer, K.K. Kuo, Modeling of nitromethane flame structure and burning behavior, *Proceedings of the Combustion Institute*, 31 (2007) 2045-2053.
- [61] A.R. Hall, H.G. Wolfhard, Multiple reaction zones in low pressure flames with ethyl and methyl nitrate, methyl nitrite and nitromethane, *Symposium (International) on Combustion*, 6 (1957) 190-199.
- [62] N. Djebaili-Chaumeix, S. Abid, C.E. Paillard, Shock tube study of the nitromethane decomposition and oxidation, in: A.F.P. Howing (Ed.) *Proceedings of the 21st international Symposium on Shock tubes and Shock Waves*, The University of Queensland, Australia, 1997.
- [63] R. Guirguis, D. Hsu, D. Bogan, E. Oran, A mechanism for ignition of high-temperature gaseous nitromethane—The key role of the nitro group in chemical explosives, *Combust. Flame*, 61 (1985) 51-62.
- [64] K. Glänzer, J. Troe, Thermische zerfallsreaktionen von nitroverbindungen I: Dissoziation von nitromethan, *Helvetica Chimica Acta*, 55 (1972) 2884-2893.
- [65] J.D. Nauglé, Y. Li, E.J.K. Nilsson, A.A. Konnov, H.J. Curran, Ignition of nitromethane+ $\text{O}_2$ + $\text{N}_2$  in a shock tube, in: *European Combustion Meeting*, Budapest, Hungary, 2015, pp. P4-05.
- [66] H.N. Presles, D. Desbordes, M. Guirard, Detonation in nitromethane and nitromethane-oxygen gaseous mixtures, *Proceedings of the Zeldovich Memorial-International Conference on Combustion*, (1994) 382-385.

- [67] H.N. Presles, D. Desbordes, M. Guirard, C. Guerraud, Gaseous nitromethane and nitromethane-oxygen mixtures: A new detonation structure, *Shock Waves*, 6 (1996) 111-114.
- [68] F. Joubert, D. Desbordes, H.N. Presles, Double cellular structure in the detonation of mixtures of compounds containing the NO<sub>2</sub> group, *Proceedings of the 19th ICDERS*, (2003).
- [69] M.O. Sturtzer, N. Lamoureux, C. Matignon, D. Desbordes, H.N. Presles, On the origin of the double cellular structure of the detonation in gaseous nitromethane and its mixtures with oxygen, *Shock Waves*, 14 (2005) 45-51.
- [70] L.J. Hillenbrand, M.L. Kilpatrick, The thermal decomposition of nitromethane, *Journal of Chemical Physics*, 21 (1953) 525-535.
- [71] J.N. Bradley, Shock-wave decomposition of nitroparaffins. Part 1.- Mass-spectrometric study of nitromethane decomposition, *Transactions of the Faraday Society*, 57 (1961) 1750-1756.
- [72] S. De Jaegere, A. Van Tiggelen, Comparative study of flame propagation in compounds containing nitrogen oxides, *Combust. Flame*, 3 (1959) 187-200.
- [73] Z.Y. Tian, L.D. Zhang, Y.Y. Li, T. Yuan, F. Qi, An experimental and kinetic modeling study of a premixed nitromethane flame at low pressure, *Proceedings of the Combustion Institute*, 32 (2009) 311-318.
- [74] K.W. Zhang, Y.Y. Li, T. Yuan, J.H. Cai, P. Glarborg, F. Qi, An experimental and kinetic modeling study of premixed nitromethane flames at low pressure, *Proceedings of the Combustion Institute*, 33 (2011) 407-414.
- [75] J.G. Kang, S.W. Lee, S.S. Yun, S.N. Choi, C.S. Kim, Ignition delay times of nitromethane-oxygen-argon mixtures behind reflected shock, *Combust. Flame*, 85 (1991) 275-278.
- [76] C.L. Rasmussen, J. Hansen, P. Marshall, P. Glarborg, Experimental measurements and kinetic modeling of CO/H-2/O-2/NO, conversion at high pressure, *Int. J. Chem. Kinet.*, 40 (2008) 454-480.
- [77] A.V. Joshi, H. Wang, Master equation modeling of wide range temperature and pressure dependence of CO + OH -> products, *Int. J. Chem. Kinet.*, 38 (2006) 57-73.
- [78] Z.F. Xu, C.H. Hsu, M.C. Lin, Ab initio kinetics of the reaction of HCO with NO: Abstraction versus association/elimination mechanism, *Journal of Chemical Physics*, 122 (2005).
- [79] H. Hippler, N. Krasteva, F. Striebel, The thermal unimolecular decomposition of HCO: effects of state specific rate constants on the thermal rate constant, *Physical Chemistry Chemical Physics*, 6 (2004) 3383-3388.
- [80] L.N. Krasnoperov, Comment on "The thermal unimolecular decomposition of HCO: effect of state specific rate constants on the

thermal rate constant" by H. Hippler, N. Krasteva and F. Striebel, Phys. Chem. Chem. Phys., 2004, 6, 3383, Physical Chemistry Chemical Physics, 7 (2005) 2074-2076.

# Summary of papers

**Paper I.** J. D. Nauc  r, M. Christensen, E. J. K. Nilsson, A. A. Konnov, Oxy-fuel combustion of ethanol in premixed flames, *Energy and Fuels* 26 (2012) 4269-4276

This study is the first to examine the laminar burning velocity of a flame from a liquid biofuel burnt with  $O_2+CO_2$ , without the presence of  $N_2$ . The laminar burning velocity was measured at 298, 318 and 338 K under atmospheric pressure using the Heat flux method. The experimental results were compared with predictions by three detailed kinetic mechanisms from the literature, the mechanisms of Marinov, Saxena et al. and Leplat et al. All three mechanisms were able to provide predictions in quantitative agreement with the experimental results. The chemistry as predicted by the mechanisms was compared through sensitivity analysis and reaction path analysis for ethanol with the present oxidizer mixture and ethanol with air. In the reaction path analysis it can be seen that the mechanisms shares major reaction paths. It was shown that the same major reactions, in air and in  $O_2+CO_2$ , are involved in each, but that the respective reactions differ in sensitivity.

*I performed the measurements as well as the modeling, and carried out the sensitivity analysis. The manuscript was written in collaboration with my coauthors.*

**Paper II:** J. D. Nauc  r, L. Sileghem, E. J. K. Nilsson, S. Verhelst, A. A. Konnov, Performance of methanol kinetic mechanism at oxy-fuel conditions, *Combust. Flame* 162 (2015) 1719-1728

The laminar burning velocity of methanol+ $O_2+CO_2$  was measured in this study using the heat flux method for the first time. The experimental conditions cover  $\phi=0.8-1.5$  over a temperature range of 308-358 K at atmospheric pressure. Three detailed kinetic mechanisms were compared in terms of their predictive capabilities for accurately reproducing the laminar burning velocity of the experimental results of the present study and of methanol+air. The examined mechanisms were the mechanisms of Li et al. Li et al. with the suggested updates from Klippenstein et al., and Mittal et al. All the examined mechanisms overpredicted the laminar burning velocity of methanol+ $O_2+CO_2$ . The decomposition of formyl was shown to be sensitive in methanol+ $O_2+CO_2$ , but not in air. Sensitivity analysis was used to examine the chemistry of the mechanisms of importance for methanol+ $O_2+CO_2$ . It was shown that updating the reactions of

methanol with H and OH, and use the updates suggested by Klippenstein et al., together with modification of the third body efficiency of water in the decomposition of formyl in line with the suggestions of Warnatz, improved the performance of the mechanism of Li et al. for methanol combustion in  $O_2+CO_2$  as well as air.

*In this study the experiment were carried out by L. Sileghem and myself. The modeling was performed by me. The analysis of the kinetic mechanism, and suggested improvements was done by me. I wrote the major part of the manuscript, which was finalized by E. J. K. Nilsson and A. A. Konnov.*

**Paper III:** J. D. Nauc  r, E. J. K. Nilsson, A. A. Konnov, Laminar burning velocities of nitromethane+air: a comparison of flat and spherical flames, Combust. Flame 162 (2015) 3801-3807

Experimental measurements of the laminar burning velocities of nitromethane+air at 338-358 K at atmospheric pressure using the Heat flux method were presented in this paper. The results were compared with laminar burning velocities obtained from spherical flames at 423 K and 1 atm by Brequigny et al. The temperature dependence in the present study, and kinetic modeling carried out were used to facilitate the comparison. The predicted temperature profiles showed that the width of the reaction zone of nitromethane flames needs to be considered in the processing the laminar burning velocity of spherical flames. The conventional approach of considering the ratios of calculated equilibrium densities at infinite distance from the flame front was found unsuitable for these particular flames. After recalculating the data from Brequigny et al., using predicted densities at the experimental limits for flame radii, the results obtained were found to be in closer agreement with the present study. The article does not claim that the recalculated laminar burning velocities represent true numerical values, but instead that they point to an issue to consider when working with nitromethane flames.

*I measured the laminar burning velocities and performed the modeling. The data analysis and reinterpretation of literature data were performed by me. I was responsible for preparing the manuscript, which was finalized by A. A. Konnov.*

**Paper IV:** J. D. Nauc  r, Y. Li, E. J. K. Nilsson, H. J. Curran, A. A. Konnov, An experimental and modeling study of nitromethane+ $O_2+N_2$  ignition in a shock tube, Fuel 186 (2016) 629-638

This study examines the ignition of nitromethane+ $O_2+N_2$ . The ignition was investigated in a shock tube over a temperature range of 947-1333 K at 8, 16 and 32 atm for three different mixtures. From pressure and luminosity traces over time, two ignition stages were identified and were examined further. Both ignition stages were examined in terms of their respective temperature and pressure dependence. The influence of mixture composition and activation energy was

investigated through calculation of correlation equations for each ignition stage by tracking the ignition delay times. The experiments revealed that within the examined range of pressures, both ignition stages have very weak pressure dependence. The activation energies derived from the experimental results were found to be 15.16 kcal/molK and 20.89 kcal/molK for the first and second ignition stages, respectively. The first ignition stage was demonstrated to be driven mainly by fuel content, indicating this stage to be primarily controlled by the products from the thermal decomposition of nitromethane. The second ignition stage was promoted by the molecular oxygen content, and was dampened by nitromethane. The mechanism of Brequigny et al. was used in an attempt to reproduce the experimental ignition delay times. The modeling was able to reproduce the two stage ignition and the activation energy of the second stage ignition. It failed, however, to reproduce both the pressure independence of both ignition stages, and the activation energy of the first stage ignition.

*The experiments were performed by me together with Y. Li. The analysis of the data from the literature was done by me. I performed the modeling and the data processing. I was responsible for the manuscript, which all of the co-authors contributed to.*

**Paper V:** J. D. Nauc  r, E. J. K. Nilsson, A. A. Konnov, An experimental and modeling study of nitromethane flames at CO<sub>2</sub>-rich conditions, submitted to Energy and Fuels

Laminar burning velocities for nitromethane+O<sub>2</sub>+CO<sub>2</sub> were measured for the first time. Experimental results for equivalence ratio of 0.8-1.3 at 348 K, and for equivalence ratio of 0.8-1.6 at 358 K, under atmospheric pressure were presented. The measurements were performed using the Heat flux method. The experimental results were used as input in comparing two contemporary mechanisms in terms of their performance at the conditions of the present study. Through sensitivity analysis it was shown that there were larger differences in the treatment of the chemistry between the two mechanisms than between combustion in O<sub>2</sub>+CO<sub>2</sub> versus in air. The reaction of HCO+M was updated in the mechanism of Brequigny et al. to the rate constant from Li et al. multiplied by 1.2 as used in the mechanism of Mathieu et al, with associated third body coefficients. The update resulted in improved performance for the flames presented in the current study, and for the nitromethane+air flames from the study in Paper III.

*Both the experimental work and all of the modeling presented were performed by me. I was responsible for the manuscript, which all co-authors contributed to.*







## Oxy-fuel Combustion of Ethanol in Premixed Flames

Jenny D. Nauclér, Moah Christensen, Elna J. K. Nilsson,\* and Alexander A. Konnov

Division of Combustion Physics, Department of Physics, Lund University, Post Office Box 118, SE-221 00 Lund, Sweden

**ABSTRACT:** First measurements of the adiabatic laminar burning velocities of lean ethanol + oxygen + carbon dioxide flames, at 1 atm and initial gas mixture temperatures of 298, 318, and 338 K, are presented. The oxygen content  $O_2/(O_2 + CO_2)$  in the artificial air was 35%. The laminar burning velocities were determined using the heat flux method, where a non-stretched flame is stabilized under adiabatic conditions. The measurements were found in qualitative agreement with modeling performed using the Marinov model, the San Diego model, and the model by Leplat et al. In comparison to experimental data, the Marinov model gave the best quantitative agreement. Notable quantitative differences between the models were analyzed using sensitivity analysis and reaction path diagrams. Reaction path analysis showed that the Marinov and the San Diego models have the same 12 most important species. Among the 12 most important species in the model of Leplat et al., 10 species are in common with the other two models. According to predictions of the Marinov model, combustion of ethanol in air and at oxy-fuel conditions proceeds via the same reaction path; however, the sensitivities of the key reactions are different.

### INTRODUCTION

Carbon dioxide ( $CO_2$ ) is one of the atmospheric gases contributing to the greenhouse effect. Reducing the levels of  $CO_2$  in the atmosphere is an important part of efforts to prevent global warming. Oxy-fuel combustion, where air is replaced by recirculated flue gas and  $O_2$ , is considered to be of strategic importance because it offers a pathway for  $CO_2$  capture. Besides this, oxy-fuel combustion has shown to have the additional benefit of reducing the formation of  $NO_x$  pollutants in the emissions.<sup>1–3</sup> Implementation of this approach to combustion of solid fossil and gaseous fuels has motivated a significant number of recent investigations reviewed, e.g., in ref 3.

Combustion of liquid fuels under oxy-fuel conditions has been considered in a few studies, examples are diesel engines for underwater applications<sup>4</sup> and iso-octane/air combustion diluted by  $CO_2$ .<sup>5</sup> In the recent work by Zhou et al.,<sup>5</sup> oxygen as well as  $CO_2$  (in the range of 0–28%) dilution was varied and the effect on the laminar burning velocity and the adiabatic flame temperature was investigated. The main conclusion concerning  $CO_2$  dilution was that, as the  $CO_2$  percentage increases, the laminar burning velocity decreases, with the decrease slowing as the  $CO_2$  dilution was increased.

In a work by Lacas et al.,<sup>6</sup> the influence of oxidizer dilution in oxy-liquid ethanol flames was investigated. They report that increasing the nitrogen mixing ratio lead to a decrease in the laminar flame speed and, as a result of this, a less stable flame.

Galmiche et al.<sup>7</sup> report on effects of dilution on the laminar burning velocity of methane/air flames. When dilution by  $N_2$ ,  $CO_2$ , and  $H_2O$  is compared, it is seen that  $CO_2$  results in a significantly large decrease in the laminar burning velocity compared to the other two diluents. The origin of this effect was investigated, and it was concluded that, for  $CO_2$ , there is both thermal and chemical effects, with the thermal effect dominating at higher dilution percentages.

No attempts to investigate flames of liquid biofuels in the oxidizing mixtures of  $O_2$  in  $CO_2$  have been reported thus far, to the best of the authors' knowledge. In principle, combustion of

renewable fuels under oxy-fuel conditions with subsequent sequestration could be considered as a negative source of  $CO_2$  and, thus, positively addresses environmental concerns. Any endeavor to develop this technology, however, is hampered by the lack of the background knowledge of the relevant combustion characteristics.

The adiabatic laminar burning velocity is a fundamental parameter of each combustible mixture, with dependence upon the stoichiometric ratio, pressure, temperature, and composition of the oxidizer. At standard conditions, i.e., atmospheric pressure and an initial temperature of 298 K, the laminar burning velocity is valuable for the characterization of combustion properties of a given fuel, for understanding the underlying chemistry and validation of models. An important aspect of the oxidizer composition is the fact that nitrogen, argon, and helium present in air are not chemically reactive in combustion, while  $CO_2$  is reactive and participates in chemical processes.<sup>7</sup>

Studying ethanol flames under oxy-fuel conditions is of high relevance because it is a popular alternative to traditional fuels.<sup>8</sup> The laminar burning velocities for ethanol + air at atmospheric pressure have been measured using a range of experimental techniques, including the heat flux method used in the present study. For a summary of available literature data, we refer to refs 9 and 10 and references therein.

The aim of the present study is the determination of the laminar burning velocities of ethanol under oxy-fuel conditions, using the heat flux method,<sup>11–14</sup> under conditions when the net heat loss of the flame was zero. In addition, the flames are modeled using chemical kinetic schemes commonly used for ethanol + air flames. Modeling was performed using the original version of the Marinov model,<sup>15</sup> the San Diego model,<sup>16</sup> and the model by Leplat et al.,<sup>17</sup> in the following referred to as the LDTV model. These three models are well-known and have

Received: May 10, 2012

Revised: June 14, 2012

Published: June 19, 2012

been validated for ethanol combustion. The qualitative and quantitative predictability and the sensitivities toward important reactions for the three different models are discussed in detail. Similarities and differences between the models are identified and used to draw conclusions on their performance.

The Marinov model is included in the present work because it was created for ethanol combustion and is likely the one most extensively used for applications concerning engine studies. The LDTV model has recently been used to describe ethanol combustion in flames, a jet-stirred reactor, and shock-tube measurements.<sup>17</sup> The San Diego model was validated against, among other characteristics, laminar burning velocities at 1 atm and several initial temperatures.<sup>18</sup>

In the following section, the experimental setup and procedure are outlined. This is followed by a section on modeling details, including relevant background information concerning the three models used. The measurements of the adiabatic laminar burning velocities of ethanol + oxygen + carbon dioxide flames are then presented and compared to kinetic modeling results. Sensitivity analyses of the three models are presented and discussed to elucidate similarities and differences than can possibly explain their performance in the present context. Finally, the sensitivity analysis from the modeling of ethanol flames under oxy-fuel conditions is compared to the case of ethanol + air flames.

## ■ EXPERIMENTAL SECTION

The heat flux method was used to measure laminar burning velocities for ethanol + CO<sub>2</sub> + O<sub>2</sub> at atmospheric pressure. An oxidizer mixture of 35 mol % O<sub>2</sub> was chosen to be compatible with the earlier studies in methane (ethane and propane) + oxygen + carbon dioxide mixtures.<sup>19</sup> As originally developed for measurements on gaseous fuel, the method, including a discussion on uncertainties, has been reported in detail elsewhere.<sup>11–14</sup> First, measurements using a heat flux setup for liquid fuels were studied on ethanol + air combustion.<sup>9</sup> The setup used for the present experiments is essentially an improved version of the setup described by Konnov et al.<sup>9</sup> Validation and testing of this setup were reported by van Lipzig et al.<sup>10</sup>

The perforated burner plate is kept at 358 K using a heating jacket. The heat flux method builds on the principle that heat is transferred to the unburnt gas, cooling the plate, while heat transfer from the flame heats the plate. At the flow rate equal to the adiabatic burning velocity, the heat loss and the heat gain are equally large, giving a uniform temperature distribution over the burner plate. The temperatures at various distances from the center of the burner plate are measured by thermocouples placed in the holes perforating the plate. As discussed by van Lipzig et al.,<sup>10</sup> temperature measurements close to the edge of the burner plate are not reliable, and therefore, the outermost thermocouple is placed at 12.6 mm from the center of the plate. Two sets of experiments were performed within the present study with the interval of 1 year. For the first set, a burner with six thermocouples within the acceptable distance from the center was used, and in the second measurement campaign, a burner with eight thermocouples within the same distance was used. The thermocouple readings are acquired by a 16-channel thermocouple input module, National Instrument 9213.

A mixing panel is used to control the composition of the fuel and oxidizer mixture. The oxidizer stream is provided from a gas bottle and, after passing a buffer vessel split into two streams, regulated by two mass flow controllers (MFCs) from Bronkhorst B.V. The fuel is pressurized with N<sub>2</sub>, and the flow is controlled and regulated by a mini CORI-FLOW from Bronkhorst B.V. The fuel is carried to the controlled evaporator mixer (CEM) from Bronkhorst B.V., where it is diluted with the oxidizer stream from MFC 1 and evaporated from the liquid state to the gaseous state at 423 K. After the evaporator, the gas stream is further diluted with the oxidizer stream from MFC 2 and mixed in a 1 m long and 12 mm thick tube before reaching the plenum

chamber of the burner. The temperature of the unburnt gas mixture is determined by the temperature of the cooling jacket surrounding the plenum chamber. The temperatures of this cooling jacket as well as that of the heating jacket of the burner plate are regulated by thermostatted water baths.

As mentioned above, sources of uncertainties for the heat flux method in general<sup>11–14</sup> and its application to liquid fuels<sup>9</sup> have been assessed previously. In the following, only uncertainties related to composition of the oxidizer mixture and metering of gases and liquid in the present work are described, while in the final error assessment, all possible uncertainties are included, as outlined by Bosschaart and de Goey.<sup>14</sup>

The MFCs were originally calibrated for air flows, and a correction needs to be applied for the use of a different oxidizer mixture. The first set of measurements was performed with factory settings recalculated to O<sub>2</sub>/(O<sub>2</sub> + CO<sub>2</sub>) = 0.35 by coefficients supplied by Bronkhorst B.V.<sup>20</sup> Before the second set of measurements, a calibration for the oxidizer mixture used in the present study was performed for the MFCs using a drum-type rotameter TG 05 model 10 from Ritter Apparatebau GmbH. A third degree polynomial obtained from calibration was used to calculate the gas flows during the second set of experiments. The same polynomial was used to recalculate the first set of data, because calibration was more accurate than the coefficients originally used. The uncertainty in the composition of the 35.0 mol % O<sub>2</sub> oxy-fuel gas mixture used was  $\pm 0.7\%$ . The ethanol (Merck) used had a purity of 99.9 mol % with less than 0.1 mol % water content. To prevent water exchange with the atmosphere, fresh unopened bottles were used. During experiments, the ethanol was stored in a nitrogen atmosphere in the fuel tank, which minimized the exposure to air and water exchange to the short time of filling the fuel tank.

The CORI-FLOW MFC, controlling the fuel flow, has a maximum deviation of 0.2% from the set flow. The gas MFCs have a 0.8% deviation from the set flow. For this to be accurate, it is recommended to work with flows higher than 10% of the maximum flow. The drum used for calibration has an uncertainty of 0.5%. The absolute error from the MFCs affecting the adiabatic burning velocity was previously estimated to less than 0.5 cm s<sup>-1</sup> for an identical setup.<sup>9</sup> The relative error from the MFCs introduces an uncertainty typically of  $\pm 0.02$  in the equivalence ratio. In the error estimation of the laminar burning velocity, uncertainties from the mass flows, the drum calibration, the temperature readings by thermocouples, the polynomial fit of the laminar burning velocity calculations, and the CEM operating temperature were taken into account. The errors are calculated in the same manner as by Bosschaart and de Goey.<sup>14</sup> The overall uncertainties for the measured laminar burning velocities are estimated to be typically about  $\pm 1$  cm s<sup>-1</sup> for 298 K,  $\pm 0.7$  cm s<sup>-1</sup> for 318 K, and  $\pm 0.65$  cm s<sup>-1</sup> for 338 K, which are slightly higher than was evaluated earlier.<sup>9,10</sup>

## ■ CHEMICAL KINETICS MODELING

**Modeling Details.** The ethanol + O<sub>2</sub> + CO<sub>2</sub> flames were modeled using CHEMKIN-PRO.<sup>21</sup> Thermal diffusion and multicomponent transport were taken into account. Adaptive mesh parameters were GRAD = 0.04 and CURV = 0.5. The laminar burning velocities were modeled for  $\Phi = 0.5$ –1.6 in steps of 0.05 for 298, 318, and 338 K for each model. Sensitivity analysis for the flow rate was performed for each model. Reaction path analysis was performed at 298 K and an equivalence ratio  $\Phi = 0.85$  for the 12 most important species of each model. The reaction paths were determined at a position in the flame where there is 50% consumption of ethanol.

**Marinov Mechanism.** The mechanism developed by Marinov<sup>15</sup> and published in 1999 is likely the most widely used mechanism for modeling of ethanol combustion. This detailed model consists of 56 species and 351 reversible reactions. In the original publication, the mechanism was validated against data for laminar burning velocities, ignition

Table 1. Experimentally Determined Laminar Burning Velocities,  $u_L$ , of Ethanol +  $O_2$  +  $CO_2$  at Different Initial Temperatures

298 K		318 K		338 K	
$\phi$	$u_L$ (cm s <sup>-1</sup> )	$\phi$	$u_L$ (cm s <sup>-1</sup> )	$\phi$	$u_L$ (cm s <sup>-1</sup> )
0.56 ± 0.02	15.46 ± 0.36	0.56 ± 0.02	17.25 ± 0.47	0.56 ± 0.02	19.35 ± 0.88
0.60 ± 0.02	18.99 ± 1.05	0.60 ± 0.01	23.47 ± 0.68	0.60 ± 0.013	23.63 ± 0.64
0.67 ± 0.02	22.82 ± 0.43	0.67 ± 0.02	25.85 ± 0.44	0.67 ± 0.02	28.45 ± 0.47
0.70 ± 0.02	26.04 ± 1.05	0.70 ± 0.02	27.22 ± 0.68	0.70 ± 0.02	30.93 ± 0.64
		0.78 ± 0.21	32.56 ± 0.39	0.79 ± 0.02	35.50 ± 0.40
		0.80 ± 0.02	33.00 ± 0.68	0.80 ± 0.02	36.23 ± 0.64
		0.90 ± 0.02	37.64 ± 0.43	0.90 ± 0.03	40.61 ± 0.42
		0.90 ± 0.02	36.52 ± 0.68	0.90 ± 0.02	40.06 ± 0.64
		1.00 ± 0.02	38.59 ± 0.68		
		1.01 ± 0.03	39.69 ± 0.39		

delays, and oxidation in both a flow reactor and jet-stirred reactor,<sup>15</sup> with good agreement. The mechanism was built on previously published mechanisms for hydrogen and alkane combustion, in large part published in two papers by Marinov and co-workers,<sup>22,23</sup> with minor updates. The reaction subset for ethanol oxidation includes species  $C_2H_5OH$ ,  $C_2H_4OH$ ,  $CH_3CH_2O$ ,  $CH_3CHOH$ , and  $CH_3HCO$  and is based on literature data, rate constant calculations, and analogy to similar reactions. In addition, reactions for  $HCOOH$  are included in the C1 chemistry subset because this species is produced in the ethanol oxidation mechanism. Branching ratios for a large part of the reactions were not experimentally available at that time and were estimated, often on the basis of low-temperature branching ratios.

With regard to laminar burning velocities for ethanol + air at conditions relevant to the present study, the model was validated against the experimental data by Gülder<sup>24</sup> at 1 atm and 300 K and a data set from Egolfopoulos et al.,<sup>25</sup> extrapolated from measurements at higher temperatures. The agreement of the model with these two data sets is good but with an underprediction by 2 cm s<sup>-1</sup> at  $\Phi = 1.05$ – $1.15$ <sup>15</sup> and an overprediction of laminar burning velocity of 3 cm s<sup>-1</sup> at  $\Phi = 0.70$ – $0.75$ .

**San Diego Mechanism.** This mechanism was developed and validated by Saxena and Williams.<sup>16,18</sup> It consist of 288 elementary reactions among 57 species, including nitrogen and C3 chemistry. The mechanism is presented with validation against ignition delay, laminar burning velocity, diffusion flame extinction, and structure of partially premixed and diffusion flames. The mechanism is an extension of a mechanism developed for a range of other compounds, including propane<sup>26</sup> and methanol.<sup>27,28</sup> To enable simulation of ethanol combustion, 55 new reactions involving  $C_2H_5OH$ ,  $CH_3CHOH$ ,  $CH_3CH_2OH$ ,  $CH_3CH_2O$ ,  $CH_3CHO$ , and  $CH_3CO$  were added. A large part of the added reactions is adopted from the mechanism by Li,<sup>29</sup> with the exception of the initial decomposition of  $C_2H_5OH$ . Saxena and Williams conclude that ethylene and acetaldehyde are important stable intermediates in ethanol combustion, under all investigated conditions.<sup>18</sup>

The laminar burning velocity for ethanol + air at 1 atm and 300 K is validated against the same data set by Egolfopoulos et al.<sup>25</sup> as was used for validation of the Marinov mechanism. The San Diego mechanism reproduces the experimental data well around stoichiometry<sup>18</sup> but shows overestimation by a few centimeters per second for lean flames at  $\Phi = 0.7$ – $0.9$ . This means that the San Diego mechanism gives higher laminar burning velocities than the Marinov mechanism, over the whole range of equivalence ratios.

**LDTV Mechanism.** This mechanism consists of 252 reversible reactions among 36 species. It has adopted the GRI<sup>30</sup> mechanism subsets for  $H_2/O_2$ , C1 species, and C2 non-oxygenated species. Decomposition of ethanol is largely taken from the Marinov mechanism,<sup>15</sup> with parameters for hydrogen abstraction reactions updated on the basis of theoretical calculations.<sup>31–34</sup> Also, reactions with  $CH_3$  radicals are increased by a factor of 3, and the acetaldehyde submechanism is updated in comparison to that of the Marinov mechanism. A range of other modifications and additions were made, for example the addition of hydrogen atom abstraction by the oxygen atom on  $C_2H_4$ .<sup>17</sup>

Laminar burning velocities of ethanol + air at 0.1 MPa and 300 K recently published by Liao et al.<sup>35</sup> were used for validation of the mechanism. The mechanism reproduces the experimental data well,<sup>17</sup> but it is important to note that these experimental results are significantly lower than the results by Gülder<sup>24</sup> and Egolfopoulos et al.<sup>25</sup> used for the validation of the Marinov and San Diego mechanisms.

## RESULTS

**Experimental Results and Comparison to Models.** The experimental results with associated uncertainties are summarized in Table 1. In Figures 1–3, these experimental data for

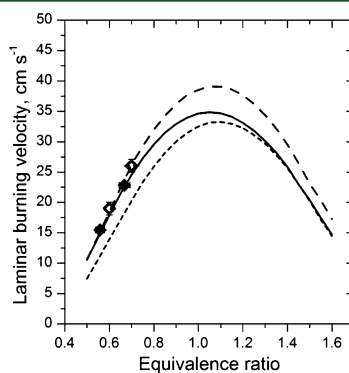
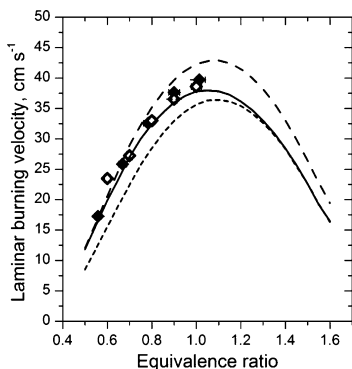
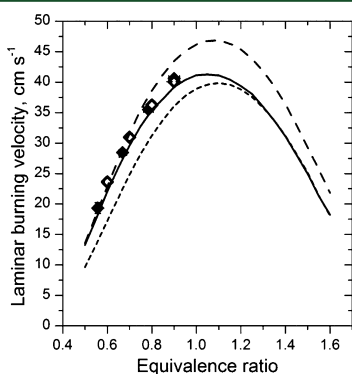


Figure 1. Laminar burning velocity versus equivalence ratio for ethanol +  $O_2$  +  $CO_2$  at 298 K. ( $\diamond$ ) First set of experimental data and ( $\blacklozenge$ ) second set of experimental data. Lines represent modeling: (—) Marinov model, (---) San Diego model, and (···) LDTV model.



**Figure 2.** Laminar burning velocity versus equivalence ratio for ethanol + O<sub>2</sub> + CO<sub>2</sub> at 318 K. (◇) First set of experimental data and (◆) second set of experimental data. Lines represent modeling: (—) Marinov model, (---) San Diego model, and (···) LDTV model.



**Figure 3.** Laminar burning velocity versus equivalence ratio for ethanol + O<sub>2</sub> + CO<sub>2</sub> at 338 K. (◇) First set of experimental data and (◆) second set of experimental data. Lines represent modeling: (—) Marinov model, (---) San Diego model, and (···) LDTV model.

three initial gas mixture temperatures, 298, 318, and 338 K, are presented together with the modeling results. For 298 K (Figure 1), the equivalence ratio,  $\Phi$ , was varied in the range of 0.5–0.7. At higher equivalence ratios, partial vaporization pressure of ethanol would lead to condensation of the fuel at this temperature.<sup>9,36</sup> The two measurement series conducted with 1 year between show consistent results and are in qualitative agreement with the modeling, considering existing experimental uncertainty and a rather narrow range of the measurements. The Marinov and San Diego models show agreement with the experimental results, while the LDTV model underpredicts the laminar burning velocity in the investigated range. The maximum of the burning velocity calculated using the Marinov model appears at  $\Phi = 1.05$ , with a value of  $34.9 \text{ cm s}^{-1}$ . The San Diego and LDTV models predict the maximum at  $\Phi = 1.1$ , with values of  $39.1$  and  $33.2 \text{ cm s}^{-1}$ , respectively.

To extend the range of accessible  $\Phi$ , the initial temperature of the mixture was increased to 318 and 338 K, results of the experiments and modeling are presented in Figures 2 and 3. The maximum equivalence ratios accessible at these temperatures, 1.0 at 318 K and 0.9 at 338 K, were limited by the full range of the CORI-FLOW. The Marinov model is in quantitative agreement with the experimental results at all temperatures and equivalence ratios, while the San Diego model overpredicts the results at equivalence ratios above 0.7. The LDTV model gives consistently lower laminar burning velocities than the experiments. At 318 K, the three models agree on the position of the maximum,  $\Phi = 1.1$ , but give different values of the burning velocity of  $42.9$ ,  $37.8$ , and  $36.4 \text{ cm s}^{-1}$  for the San Diego, Marinov, and LDTV models, respectively. At 338 K, the San Diego and LDTV models give maximums of  $46.8$  and  $39.9 \text{ cm s}^{-1}$ , respectively, at  $\Phi = 1.1$ . For the Marinov model, the position is shifted to  $\Phi = 1.05$  at 338 K, with a maximum velocity of  $41.3 \text{ cm s}^{-1}$ .

As described in the above sections on the three models, they have all been validated for ethanol + air flames. When the results of the three models are compared, it is notable that they show the same relation concerning the oxy-fuel ethanol flames as they do for ethanol + air. Under identical conditions, the San Diego mechanism predicts the highest laminar burning velocity, while the LDTV model shows the lowest, with a difference of about  $6 \text{ cm s}^{-1}$  at the maximum. The performance of the models in the present study shows trends similar to those in the ethanol + air cases; over- and underpredictions compared to experimental results in ethanol + air flames are seen in an analogous way for the ethanol + O<sub>2</sub>/CO<sub>2</sub> flames. In an attempt to understand the differences in the performance of the models when applied to oxy-fuel conditions, they are investigated further using sensitivity analysis and reaction path analysis.

**Sensitivity and Reaction Path Analyses.** Sensitivity analysis was performed to identify the reactions that have a predominant effect on the laminar burning velocity. To find the routes of the ethanol conversion into products and identify important intermediary species, reaction path analysis was performed. The left-hand side panels of Figures 4–6 present the 20 most sensitive reactions for the Marinov, San Diego, and LDTV models, and the right-hand side panels show the reaction paths from ethanol to H<sub>2</sub>O and CO<sub>2</sub>, including the 12 most important species of each mechanism.

From Figure 4–6, it can be seen that the Marinov and San Diego models have the same important species, while the LDTV model differs by the lack of the radical CH<sub>3</sub>CH<sub>2</sub>O and the emerging importance of the radicals CH<sub>3</sub>CO and CH<sub>3</sub>O. The important differences in the reaction of the fuel C<sub>2</sub>H<sub>5</sub>OH are the insignificance of a step producing CH<sub>3</sub>CH<sub>2</sub>O in the LDTV model and the fact that, in both the Marinov and LDTV models, there are direct paths to CH<sub>3</sub>CHO not seen in the San Diego model. The parameters used to represent hydrogen abstraction from C<sub>2</sub>H<sub>5</sub>OH in the LDTV mechanism are based on recent theoretical calculations by Lin and co-workers.<sup>31–34</sup> According to Leplat et al.,<sup>17</sup> a good agreement of the LDTV model with experimental concentrations of CH<sub>3</sub>HCO, CH<sub>2</sub>CO, and CH<sub>3</sub> justify the choice of parameters. The choices of hydrogen abstraction reaction rates and branching ratios have implications for the production of smaller species further down the oxidation chain.

HCO is not present among the 12 most important species in the reaction path of the LDTV model. In both the Marinov and San Diego models, HCO produced from C<sub>2</sub>H<sub>4</sub> and form-

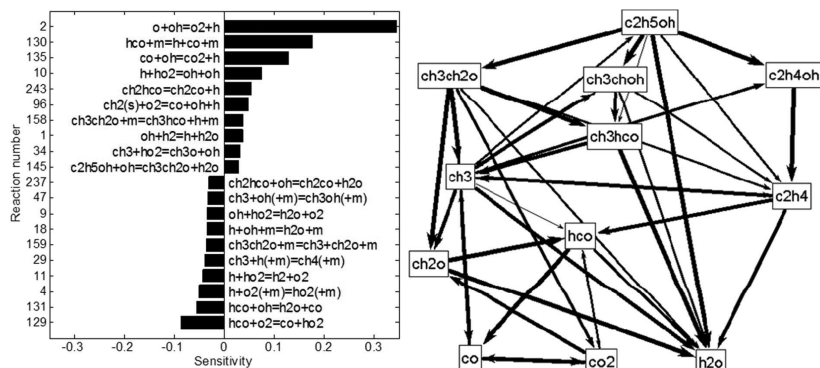


**Figure 4.** (Left panel) Twenty most sensitive reactions for ethanol + O<sub>2</sub> + CO<sub>2</sub> flame at 298 K and Φ = 0.85 for the Marinov model. (Right panel) Reaction path for the 12 most important species at half consumption of ethanol.

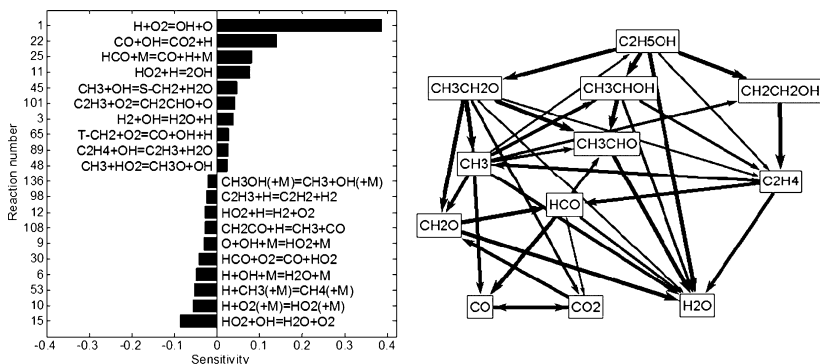


**Figure 5.** (Left panel) Twenty most sensitive reactions for ethanol + O<sub>2</sub> + CO<sub>2</sub> flame at 298 K and Φ = 0.85 for the San Diego model. (Right panel) Reaction path for the 12 most important species at half consumption of ethanol.

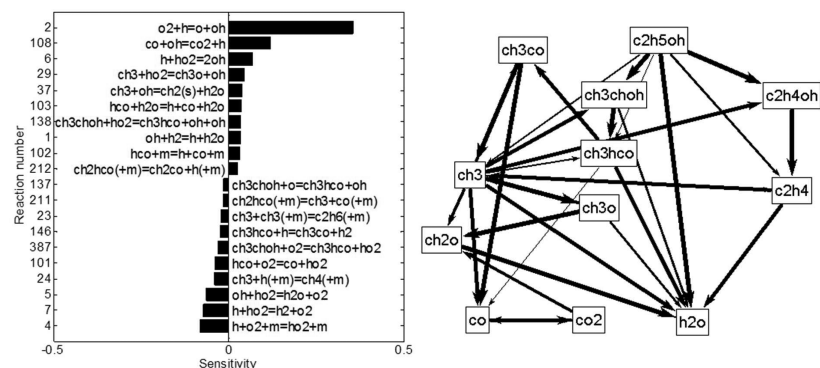


**Figure 6.** (Left panel) Twenty most sensitive reactions for ethanol + O<sub>2</sub> + CO<sub>2</sub> flame at 298 K and Φ = 0.85 for the LDTV model. (Right panel) Reaction path for the 12 most important species at half consumption of ethanol.

aldehyde are of importance. For all three mechanisms, the formation of water and  $\text{CH}_3$  from  $\text{C}_2\text{H}_4$  is important. In the San Diego model, formyl radical recombines with methyl to form  $\text{CH}_3\text{CHO}$ .

In all three models,  $\text{CH}_3\text{CHOH}$  is oxidized to form water in both a direct path and through the intermediate,  $\text{CH}_3\text{HCO}$ . In all three mechanisms,  $\text{C}_2\text{H}_4$  is to some extent formed directly from  $\text{C}_2\text{H}_5\text{OH}$ . In the LDTV model,  $\text{C}_2\text{H}_4$  is also formed from  $\text{C}_2\text{H}_4\text{OH}$ . In the Marinov and San Diego models,  $\text{C}_2\text{H}_4$  is mainly formed from  $\text{C}_2\text{H}_4\text{OH}$  and  $\text{CH}_3$  but also from  $\text{CH}_3\text{CHOH}$  and  $\text{CH}_3\text{CH}_2\text{O}$ . In the LDTV mechanism, the production of  $\text{CH}_3\text{CH}_2\text{O}$  is a minor path for  $\text{C}_2\text{H}_5\text{OH}$  oxidation (7%),<sup>17</sup> which is significantly lower than the branching calculated by Marinov and used in the Marinov mechanism.<sup>15</sup>

The sensitivity spectra shown in Figures 4–6 corroborate and extend reaction path analysis. The normalized sensitivities are defined as  $(\delta \ln u_i / \delta \ln k_i)$ , where  $u_i$  is the laminar flame speed and  $k$  is the rate constant of reaction  $i$ . Reaction numbering in the present work corresponds to the Marinov mechanism, although in Figures 5 and 6, reaction numbers on the sensitivity panels are taken from the San Diego and LDTV models, respectively. Not surprisingly, the most sensitive reaction in all models is



Typically, for hydrocarbons and oxygenated fuels, reaction



shows one of the highest positive sensitivities, while reaction



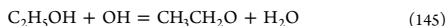
has one of the most negative sensitivities, because it competes with reaction  $-2$  for H atoms. A similar competition for the formation of H atoms and less reactive  $\text{HO}_2$  radicals occurs in reactions



These and other reactions from hydrogen and C1 submechanism appear in all sensitivity spectra, albeit not always in the same order of importance. A striking difference between three models is manifested in fuel-specific reactions of C2 species. In the LDTV model, reactions



compete for the consumption of  $\text{CH}_3\text{CHOH}$  radicals and the formation of two reactive hydroxyls or less-reactive  $\text{HO}_2$ . These reactions do not appear in the sensitivity spectra of the San Diego and Marinov models. Instead, the formation of vinyloxy radical and, subsequently, ketene is of key importance in the last two mechanisms. However, in the San Diego model, they originate from the vinyl radical, while in the Marinov model, they originate from acetaldehyde. Finally, reaction



forming  $\text{CH}_3\text{CH}_2\text{O}$  and subsequent competing decomposition reactions

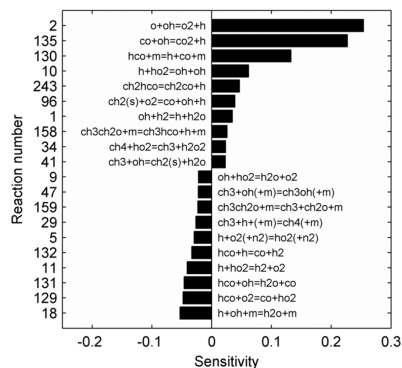
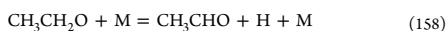


Figure 7. Twenty most sensitive reactions for ethanol + air flame at 298 K and  $\Phi = 0.85$  for the Marinov model.

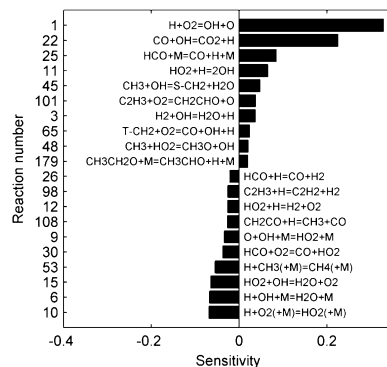


Figure 8. Twenty most sensitive reactions for ethanol + air flame at 298 K and  $\Phi = 0.85$  for the San Diego model.

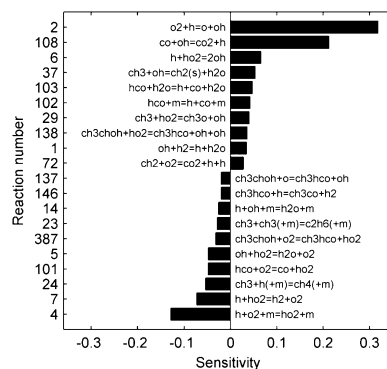


Figure 9. Twenty most sensitive reactions for ethanol + air flame at 298 K and  $\Phi = 0.85$  for the LDTV model.

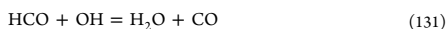


are of importance in the Marinov model, as clearly manifested in the reaction path analysis as well.

**Comparison to Ethanol + Air.** To better understand the difference between conventional ethanol combustion in air and under oxy-fuel conditions, it is instructive to compare sensitivity analysis and reaction path analysis. The 20 most sensitive reactions for ethanol + air flames in all three models are shown in Figures 7–9. Reaction path diagrams for ethanol + air combustion are essentially identical to those shown in Figures 4–6 and are therefore not shown. In general, the comparison of the sensitivity spectra for ethanol burning in  $\text{O}_2/(\text{O}_2 + \text{CO}_2)$  and air shows that they share major sensitive reactions but with differences in the sensitivity and reaction order.

When comparing the sensitive reactions and the magnitude of the sensitivity, there are a few trends that are in common for all three models. The sensitivity of the most sensitive reaction, reaction –2, is higher for oxy-fuel conditions compared to combustion in air; the increase is most pronounced for the Marinov mechanism. The sensitivity to the important reaction converting CO into  $\text{CO}_2$ , reaction 135, show a significant decrease for oxy-fuel conditions. It is apparently due to the high concentration of  $\text{CO}_2$  that leads to partial equilibration with the reverse reaction, reaction –135.

There are also some trends that are different for the three mechanisms. A general comment regarding the San Diego mechanism is that it does not show as much difference in either sensitivity or the order of sensitive reactions compared to the other two mechanisms. For the 5–6 most sensitive reactions, the Marinov mechanism displays a generally higher sensitivity for ethanol flames under oxy-fuel conditions compared to ethanol flames in air. The opposite is true for the LDTV mechanism, for which only the most sensitive reaction show higher sensitivity under oxy-fuel conditions. An example of this is that the Marinov mechanism has a higher sensitivity for reactions involving HCO consumption under oxy-fuel conditions, reactions 129, 130, and



For the LDTV mechanism, all reactions involving HCO consumption show lower sensitivity under oxy-fuel conditions.

## CONCLUSION

The laminar burning velocity for ethanol +  $\text{O}_2$  +  $\text{CO}_2$  was measured at 1 atm and 298, 318, and 338 K. The experimental data were compared to the modeling performed with the LDTV, San Diego, and Marinov mechanisms. The models showed discrepancies of up to  $7 \text{ cm s}^{-1}$  compared to each other. The best agreement with the experimental results was found for the Marinov model, even though this is the one of the three models based on the oldest chemical kinetics data. Reaction path analyses showed that the San Diego and Marinov models have the same important species, while the LDTV model has a different set of important species. In the LDTV model,  $\text{CH}_3\text{CH}_2\text{O}$  and HCO radicals did not appear in this set; instead,  $\text{CH}_3\text{CO}$  and  $\text{CH}_3\text{O}$  have importance. Pathways of fuel-specific radical conversion are also different between the models. In the Marinov and San Diego models, the formation of vinyloxy radical and ketene are of importance, although the models have different sources for these intermediates. In the LDTV model, reactive hydroxyls are formed from  $\text{CH}_3\text{CHOH}$ . A comparison of the models for ethanol + air and ethanol +  $\text{O}_2$

+  $\text{CO}_2$  resulted in the same important species from reaction path analysis. Sensitivity analysis showed that the sensitivities of the reactions were different in air and oxy-fuel conditions, with higher sensitivity for the Marinov mechanism and generally lower sensitivity for the LDTV mechanism. Common for all three mechanism was that the sensitivity toward the most sensitive reaction,  $\text{O} + \text{OH} = \text{O}_2 + \text{H}$ , was higher under oxy-fuel conditions.

## AUTHOR INFORMATION

### Corresponding Author

\*E-mail: elna.heimdal\_nilsson@forbrf.lth.se.

### Notes

The authors declare no competing financial interest.

## ACKNOWLEDGMENTS

Financial support of the Foundation for Strategic Research (SSF, Sweden), Swedish Energy Agency (Energimyndigheten), and the Swedish Research Council (VR) are gratefully acknowledged.

## REFERENCES

- (1) Flamme, M. *Energy Convers. Manage.* **2001**, 42 (15–17), 1919–1935.
- (2) Normann, F.; Andersson, K.; Leckner, B.; Johnsson, F. *Fuel* **2008**, 87 (17–18), 3579–3585.
- (3) Normann, F.; Andersson, K.; Leckner, B.; Johnsson, F. *Prog. Energy Combust. Sci.* **2009**, 35 (5), 385–397.
- (4) Hawley, J. G.; Ashcroft, S. J.; Patrick, M. A. *Trans. Inst. Mar. Eng.* **1993**, 106, 61–75.
- (5) Zhou, J. X.; Cordier, M.; Mounaim-Rousselle, C.; Foucher, F. *Combust. Flame* **2011**, 158 (12), 2375–2383.
- (6) Lacas, F.; Leroux, B.; Darabiha, N. *Proc. Combust. Inst.* **2005**, 30, 2037–2045.
- (7) Galmiche, B.; Halter, F.; Foucher, F.; Dagaut, P. *Energy Fuels* **2011**, 25 (3), 948–954.
- (8) Farrell, A. E.; Plevin, R. J.; Turner, B. T.; Jones, A. D.; O'Hare, M.; Kammen, D. M. *Science* **2006**, 311 (5760), 506–508.
- (9) Konnov, A. A.; Meuwissen, R. J.; de Goey, L. P. H. *Proc. Combust. Inst.* **2011**, 33, 1011–1019.
- (10) van Lipzig, J. P. J.; Nilsson, E. J. K.; de Goey, L. P. H.; Konnov, A. A. *Fuel* **2011**, 90 (8), 2773–2781.
- (11) de Goey, L. P. H.; van Maaren, A.; Quax, R. M. *Combust. Sci. Technol.* **1993**, 92, 201–207.
- (12) van Maaren, A.; Thung, D. S.; de Goey, L. P. H. *Combust. Sci. Technol.* **1994**, 96, 327–344.
- (13) van Maaren, A.; de Goey, L. P. H. *Combust. Sci. Technol.* **1995**, 102, 309–314.
- (14) Bosschaart, K. J.; de Goey, L. P. H. *Combust. Flame* **2003**, 132, 170–180.
- (15) Marinov, N. M. *Int. J. Chem. Kinet.* **1999**, 31 (3), 183–220.
- (16) *The San Diego Mechanism, Version 20051201*; <http://maeweb.ucsd.edu/combustion/>.
- (17) Leplat, N.; Dagaut, P.; Togbe, C.; Vandooren, J. *Combust. Flame* **2011**, 158 (4), 705–725.
- (18) Saxena, P.; Williams, F. A. *Proc. Combust. Inst.* **2007**, 31 (1), 1149–1156.
- (19) Dyakov, I. V.; Konnov, A. A. *Combust. Sci. Technol.* **2007**, 179, 747–765.
- (20) *Fluidat Database*; <http://www.fluidat.com>.
- (21) Reaction Design. *CHEMKIN-PRO 15101*; Reaction Design: San Diego, CA, 2010.
- (22) Marinov, N. M.; Westbrook, C. K.; Pitz, W. J. *Transport Phenomena in Combustion*. In *Eighth International Symposium on Transport Properties*; Chen, S. H., Ed.; Lawrence Livermore National Laboratory (LLNL): Livermore, CA, 1996; p 118.

- (23) Marinov, N. M.; Pitz, W. J.; Westbrook, C. K.; Castaldi, M. J.; Senkan, S. M. *Combust. Sci. Technol.* **1996**, 116-117, 211–287.
- (24) Gülder, O. L. *Proc. Combust. Inst.* **1982**, 19, 275.
- (25) Egolfopoulos, F. N.; Du, D. X.; Law, C. K. *Proc. Combust. Inst.* **1992**, 24, 833–841.
- (26) Petrova, M. V.; Williams, F. A. *Combust. Flame* **2006**, 144, 526–544.
- (27) Li, S. C.; Williams, F. A. *Proc. Combust. Inst.* **1996**, 26, 1017–1024.
- (28) Li, S. C.; Williams, F. A. *Proc. Combust. Inst.* **1998**, 27, 485–493.
- (29) Li, J. Ph.D. Thesis, Princeton University, Princeton, NJ, 2004.
- (30) Smith, G. P.; Golden, D. M.; Frenklach, M.; Moriarty, N. W.; Eiteneer, B.; Goldenberg, M.; Bowman, C. T.; Hanson, R. K.; Song, S.; Gardiner, W. C.; Lissianski, V.; Qin, Z. *GRI-Mech 3.0*; [http://www.me.berkeley.edu/fri\\_mech](http://www.me.berkeley.edu/fri_mech).
- (31) Park, J.; Xu, Z. F.; Lin, M. C. *J. Chem. Phys.* **2003**, 118, 9990–9996.
- (32) Xu, Z. F.; Park, J.; Lin, M. C. *J. Chem. Phys.* **2004**, 120, 6593–6599.
- (33) Xu, S.; Lin, M. C. *Proc. Combust. Inst.* **2007**, 31, 159–166.
- (34) Wu, C. W.; Lee, Y. P.; Xu, S.; Lin, M. C. *J. Phys. Chem. A* **2007**, 111, 6693–6703.
- (35) Liao, S. Y.; Jiang, D. M.; Huang, Z. H.; Zeng, K.; Cheng, Q. *Appl. Therm. Eng.* **2007**, 27 (2–3), 374–380.
- (36) Bradley, D.; Lawes, M.; Mansour, M. S. *Combust. Flame* **2009**, 156 (7), 1462–1470.

## Paper II





# Performance of methanol kinetic mechanisms at oxy-fuel conditions



Jenny D. Naucner<sup>a,\*</sup>, Louis Sileghem<sup>b</sup>, Elna J.K. Nilsson<sup>a</sup>, Sebastian Verhelst<sup>b</sup>, Alexander A. Konnov<sup>a</sup>

<sup>a</sup> Division of Combustion Physics, Department of Physics, Lund University, P.O. Box 118, SE-221 00 Lund, Sweden

<sup>b</sup> Department of Flow, Heat and Combustion Mechanics, Ghent University, Sint-Pietersnieuwstraat 41, B-9000 Gent, Belgium

## ARTICLE INFO

### Article history:

Received 25 June 2014

Received in revised form 25 November 2014

Accepted 25 November 2014

Available online 18 December 2014

### Keywords:

Methanol

Kinetic model

Laminar flame

Sensitivity analysis

CO<sub>2</sub>

## ABSTRACT

Methanol premixed flames were studied under oxy-fuel conditions for the first time. Laminar burning velocities were measured with the heat flux method at atmospheric pressure for unburnt gas temperatures of 308–358 K within a stoichiometric range of  $\phi = 0.8$ –1.5. A linear relationship between temperature and laminar burning velocity on a log–log scale was observed. The experimental results are discussed by comparison to modeling results from three kinetic mechanisms. All models gave an overprediction of the laminar burning velocity. It was demonstrated that implementation of recently advised rate constants for reactions of methanol with O<sub>2</sub>, HO<sub>2</sub>, H and OH, together with modification of the third-body efficiency for H<sub>2</sub>O in the decomposition of the formyl radical, significantly improves model performance both for methanol combustion in air and at oxy-fuel conditions.

© 2014 The Combustion Institute. Published by Elsevier Inc. All rights reserved.

## 1. Introduction

An approach to deal with emissions of the greenhouse gas carbon dioxide, CO<sub>2</sub>, is carbon capture and sequestration (CCS). A novel and promising way to implement CCS is the oxy-fuel technology where air is replaced by molecular oxygen (O<sub>2</sub>) and CO<sub>2</sub>. The CO<sub>2</sub> is recycled from the flue gas and mixed with O<sub>2</sub>. The high concentration of CO<sub>2</sub> in the gas downstream the burner facilitates separation of CO<sub>2</sub> for sequestration. As external gas recirculation creates CO<sub>2</sub>-rich combustion conditions, combustion studies of fuel at these conditions is of high relevance. Also, many internal combustion engines employ External Gas Recirculation (EGR) regimes which creates CO<sub>2</sub>-rich conditions. In special applications, like submarine engines, oxy-fuel combustion of liquid fuels is directly implemented.

Methanol's popularity as an alternative fuel for engines is increasing. In China, 6–8% of the transportation fuel pool is methanol (coal-based) in an effort to reduce dependency on imported oil. Methanol is used both as a blending component (with gasoline) and as a pure fuel in methanol cars. Methanol is also being considered as a viable alternative fuel for shipping (mainly in Europe). The Scandinavian EFFSHIP project [1], investigated a number of alternative fuels and advanced methanol as the most promising one. Within the SPIRETH project [2], a “spin-off” from EFFSHIP, a main engine was run on methanol in a laboratory setting, and an auxiliary diesel engine on a Swedish RoPax vessel was fueled with

a blend of primarily di-methyl ether (DME), with some residual methanol from the onboard fuel conversion process. Within a 2012 TEN-T Multi-Annual Programme funded project [3], an existing passenger vessel was retrofitted for operation on methanol.

In combustion research methanol is used as a model fuel for studying alcohol chemistry. A strength of methanol as a model fuel for kinetic studies is that the chemistry of the H-abstraction products CH<sub>2</sub>OH and CH<sub>2</sub>O is relatively isolated from methyl radical chemistry. This background gives value to methanol studies, not only for its own merits but as a representative for alcohol chemistry.

When changing the oxidizer from conventional air to CO<sub>2</sub> rich conditions the prerequisites for the combustion process are altered. CO<sub>2</sub> not only acts as a diluent for O<sub>2</sub>, it changes combustion properties such as heat capacity and flame temperature and participates as a reactant in the combustion reactions [4–7].

Chemical kinetic models are commonly validated for combustion in normal air. To enable further understanding and development of oxy-fuel technology the performance of the models under CO<sub>2</sub>-rich conditions need to be investigated and possibly improved. The present paper is part of a study of C1–C2 alcohols under oxy-fuel conditions; in a previous publication it was shown that models for ethanol + air overpredicted laminar burning velocities for ethanol under oxy-fuel conditions [8].

In the current work, the laminar burning velocity of methanol flames at atmospheric pressure and elevated temperatures under oxy-fuel conditions are presented for the first time. The temperature dependence of the laminar burning velocity ( $S_L$ ) is interpreted using the relation  $S_L = S_{L0} (T/T_0)^x$ , where  $S_{L0}$  is the laminar burning

\* Corresponding author. Fax: +46 46 222 45 42.

E-mail address: [jenny.naucner@forbrf.lth.se](mailto:jenny.naucner@forbrf.lth.se) (J.D. Naucner).

velocity at standard conditions,  $T$  is the temperature and  $T_0$  is the reference temperature at standard conditions. The laminar burning velocities are modeled using kinetic mechanisms by Li et al. [9], Li et al. with changes according to Klippenstein et al. [10], and Aramco 1.3 [11]. Using sensitivity and rate of production analyses the mechanisms are evaluated for the  $\text{CO}_2$ -rich conditions of the study, aiming at the identification of possible improvements in reaction rate parameters.

## 2. Experimental

Premixed methanol +  $\text{O}_2$  +  $\text{CO}_2$  flames were stabilized using the heat flux method [12–14]. The principle of the method is based on a thermodynamic exchange between the flame, burner head and unburnt gas. The burner has a heated plenum chamber and a heated burner plate with 0.5 mm diameter holes. Heating jackets and thermostatically controlled water is used to keep the burner head at a constant temperature of 368 K and the plenum chamber at the desired unburnt gas temperature.

At the adiabatic laminar burning velocity, the net flux of the heat exchange is zero and the temperature profile of the burner plate is uniform. The temperature profile as a function of the radius of the burner plate is given by  $T_p(r) = T_c + Cr^2$ , where  $T_c$  is the temperature at the center of the burner plate;  $C$  is a coefficient in the fit and  $r$  the radius of the burner plate [14]. The adiabatic laminar burning velocity is found at  $C = 0$ . The temperature profile is measured by eight thermocouples (type T) inserted in holes at different radial positions of the burner plate and collected by a National Instrument 9213 thermocouple input module.

The flames were studied at atmospheric pressure, temperatures of 308, 318, 328, 338 and 358 K and equivalence ratios ( $\phi$ ) in the range 0.8–1.5. The laminar burning velocity at 298 K was not measured due to the limitations in the partial vapor pressure for methanol. The oxidizer mixture consisted of 35%  $\text{O}_2$  and 65%  $\text{CO}_2$ , chosen to approximately match the flame temperature of equivalent methanol flames with air as an oxidizer [15,16].

The gases were taken from gas bottles, passing through a buffering vessel before a mass flow controller (MFC). To control the fuel flow, a liquid mass flow controller (Mini-Cori-Flow) was used. The fuel was mixed with the oxidizer gas and evaporated in a controlled evaporator mixer (CEM). All components of the experimental setup are schematically presented in Fig. 1. The MFC, CEM and Mini-Cori-Flow are all from Bronkhorst. The MFC used for the oxidizer mixture was originally calibrated for air, recalibration was performed with a piston meter Definer 220 from Bios, USA. From the calibration a third degree polynomial was obtained and used to recalculate the gas flow settings for the oxidizer mixture.

The methanol from Merck had a purity of 99.9 mol% with less than 0.1% water content. The oxidizer gas was premixed at AGA mixing plant, at 35.0 mol%  $\text{O}_2$  in  $\text{CO}_2$  within an accuracy of 0.7%.

One should note that variation of the oxygen content in the oxidizer of the order of 1% may significantly change the measured laminar burning velocity, as was experimentally demonstrated by, e.g., Dyakov et al. [17]. To eliminate this uncertainty, two series of measurements at 308 K and 328 K were performed with on-site mixing of  $\text{O}_2$  and  $\text{CO}_2$  using separate MFCs. As will be demonstrated in the following, both types of oxidizer preparation (from the plant or on-site) yield consistent results.

### 2.1. Experimental uncertainties

Experimental uncertainties are mainly due to uncertainties in gas mixture composition and scatter in temperature reading. These uncertainties need to be accurately quantified to evaluate the error in the results. Uncertainties in the equivalence ratio stem from the

accuracy of the flows of oxidizer and fuel, and are quantified in the same manner as by Bosschaart and de Goeij [14]. The uncertainty in the laminar burning velocities is dependent on the accuracy of the flows of oxidizer and fuel, and the scatter in the temperature distribution of the thermocouples. The uncertainty from the temperature distribution is represented by the standard deviation from the thermocouples. This is calculated by a least square fit of the scatter in the temperature distribution. A mean value of the standard deviations of the  $C$  coefficient for each of the measured points is then calculated. This mean value is then divided by the slope from the fit of  $C$  vs. flow rate to produce the errors in  $C$ .

Due to tendencies of cell formation in flames burned with  $\text{O}_2$  +  $\text{CO}_2$  [18], all data were obtained at sub-adiabatic conditions and extrapolated to the laminar burning velocity. The experimental data points,  $C$  vs. laminar burning velocity, at a specific gas mixture composition show a linear relationship in the measured interval and based on the work of Bosschaart and de Goeij [14] it is assumed that this linearity is valid to the adiabatic conditions ( $C = 0$ ). At least four measurement points were taken to make sure the trend was indeed linear. A linear fit to the data was made, followed by an extrapolation to  $C = 0$ . The extent of the extrapolation range varies for different flame conditions with respect to equivalence ratio and unburnt gas temperature. At higher temperatures and richer conditions the flames had a tendency to form cellular structure around conditions that are expected to be adiabatic, and therefore the conditions at which the flame was uniformly flat and suitable for data collection are further below the adiabatic state compared to colder and leaner conditions. For the measurements at unburnt gas temperature of 308 K the extent of the extrapolation is 0.3–0.7  $\text{cm s}^{-1}$  from the determined adiabatic laminar burning velocity, while at 358 K it is as far as 1.7–2  $\text{cm s}^{-1}$ . This is clearly within the linear region as shown by Bosschaart and de Goeij [14].

The highest initial temperature of the fresh gases, 358 K, was only 10 K lower than the temperature of the burner head, 368 K. Hermanns [19] noted that the measured laminar burning velocity does not depend on the temperature difference between the plenum chamber and the burner head, yet a difference smaller than about 30 K may lead to flame instabilities. This effect is manifested in the present work in the slightly increased uncertainty of the laminar burning velocity at 358 K due to the more extensive extrapolation, as explained in the previous paragraph. The procedure for evaluation of associated uncertainties is described in the Supplementary material.

In addition to the described major uncertainties in gas mixture composition and as a result of scatter in temperature readings, there are a number of other uncertainties. Examples are edge effects at limiting equivalence ratios, flow uniformity, radiative heat losses (discussed in the following), limited range of possible measurements defined by the perforation pattern of the burner plate, etc. The uncertainties are summarized and analyzed elsewhere [20,21] with advises of the methods to control them and the best laboratory practice to follow.

The uncertainties in the power exponent,  $\alpha$ , are evaluated by considering the uncertainties from the laminar burning velocity for each experimental point. Each experimental  $S_L$  value is changed to its uncertainty limits,  $\Delta S_L$ , and a new  $\alpha_i$  is recalculated for each case. This is done for each experimental point individually in a sequence. Since:

$$\alpha = f(S_{L_1}, S_{L_2}, \dots, S_{L_n}) \quad (1)$$

then the contribution of each measured flame speed to the total uncertainty in  $\alpha$  equals  $\Delta\alpha(S_{L_i}) = \alpha_i - \alpha_0$ , where  $\alpha_0$  is the original power exponent  $\alpha$ , calculated from the experimental data. The total

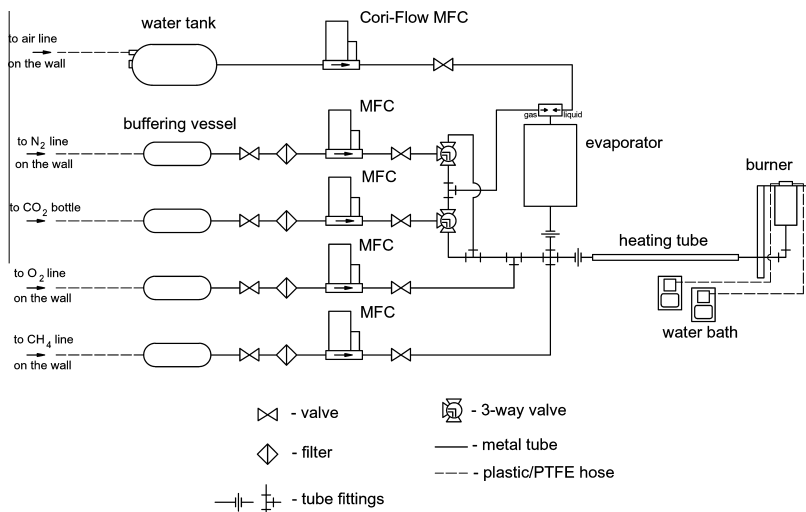


Fig. 1. A schematic overview of the experimental setup.

uncertainty can therefore be estimated from the squared error addition rule:

$$\Delta\alpha = \sqrt{\sum_i [\Delta\alpha(S_{li})]^2} \quad (2)$$

All standard deviations are calculated with a 95% confidence interval.

### 3. Kinetic modeling

Three detailed kinetic mechanisms were evaluated in the present work, from here on referred to as Models I–III.

**Model I:** The mechanism by Li et al. [9], which is well established for methanol combustion and validated for the diluting gas  $N_2$  [22]. Here a version further updated by Li et al. is used: the rate constant for reaction  $CO + HO_2 = CO_2 + OH$  was changed [23]. This mechanism contains 84 reactions with 20 species.

**Model II:** This mechanism is based on Model I with modifications advised by Klippenstein et al. [10]. The H-abstraction from methanol by  $HO_2$  and  $O_2$  was updated with new rate constants, and a new product channel for methanol +  $HO_2$  to  $CH_3O + H_2O_2$  was included. This mechanism contains 85 reactions with 20 species.

**Model III:** Aramco 1.3 from Mittal et al. [11] is a recently developed mechanism for oxidation of small hydrocarbons and oxygenates. This mechanism contains 1542 reactions with 253 species.

The flames were modeled using Chemkin IV [24]. The parameters GRAD = 0.03 and CURV = 0.01 were used to ensure a grid-independent solution with a typical number of grid points of ~700. Multicomponent transport and thermal diffusion options were taken into account.

A sensitivity analysis of the calculated burning velocities was performed at 318 K and  $\phi = 0.6, 1.0$  and 1.4 for each of the models. The rate of production was also studied for key species and analyzed to find production and consumption pathways for each mechanism at 318 K and  $\phi = 0.6, 1.0$  and 1.4.

### 4. Results and discussion

First, experimental results for the laminar burning velocity of methanol under oxy-fuel conditions are presented. These results are subsequently used as a base to study how the models handle the methanol +  $O_2$  +  $CO_2$  chemistry. The focus of the discussion is on the differences between the models and how these differences affect the calculated laminar burning velocity. Finally modifications to Model I are proposed to improve its agreement with the experimental results. This updated version of Model I is in the following named Model IV.

#### 4.1. Laminar burning velocity

Experimentally determined laminar burning velocities vs. equivalence ratio ( $\phi$ ) for initial temperatures of 308, 318, 328, 338 and 358 K are shown in Fig. 2. Maximum laminar burning velocities are found at  $\phi = 1.2$  at all initial gas mixture temperatures. Error bars in Fig. 2 show evaluated uncertainties in equivalence ratio and in the burning velocity. While the heat flux method generally gives errors of  $\sim 1 \text{ cm s}^{-1}$ , the uncertainty from each experimental point is calculated individually, ranging from 0.63 to  $1.23 \text{ cm s}^{-1}$ , dependent on  $\phi$  and unburnt gas temperature, as presented in Tables 1 and 2. The temperature dependence of the laminar burning velocity is commonly described by the relation:  $S_L = S_{L0}(T/T_0)^\alpha$ , which was probably first suggested by Heime [25]. Elucidation of the temperature dependence is important both from practical and fundamental points of view. Many engineering and CFD codes implement this relation to evaluate burning velocity at the elevated temperatures often not covered in laboratory experiments; comparison of the power exponents  $\alpha$  obtained from experiments and derived from different models provides an independent validation tool; finally interpreting measurements obtained at different temperatures using this relation helps to check that the data are not biased by some systematic errors [25]. Presented on a log–log scale, the experimental results are

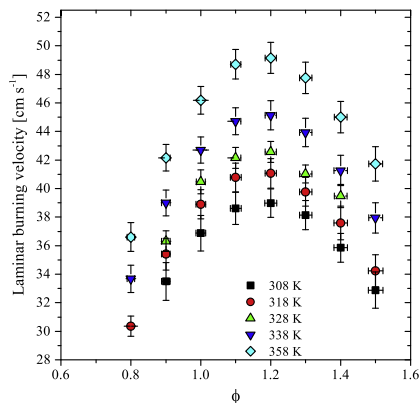


**Fig. 2.** Laminar burning velocity vs. equivalence ratio for methanol + O<sub>2</sub> + CO<sub>2</sub> flames for temperatures 308 K (square), 318 K (circle), 328 K (triangle), 338 K (diamond), and 358 K (pentagon).

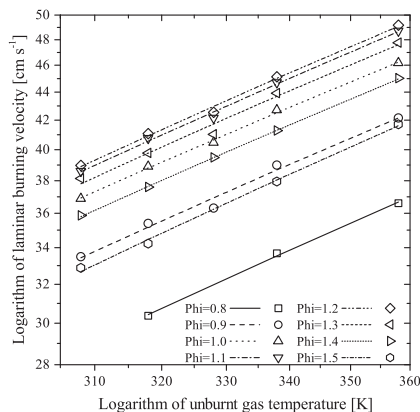


**Fig. 3.** The logarithms of laminar burning velocity vs. unburnt gas temperature for methanol + O<sub>2</sub> + CO<sub>2</sub> flames.

**Table 1**

Experimental laminar burning velocity,  $S_L$ , for methanol + O<sub>2</sub> + CO<sub>2</sub> flames at initial temperatures 308, 318 and 328 K.

308 K		318 K		328 K	
$\phi$	$S_L$ (cm s <sup>-1</sup> )	$\phi$	$S_L$ (cm s <sup>-1</sup> )	$\phi$	$S_L$ (cm s <sup>-1</sup> )
–	–	0.8 ± 0.011	30.36 ± 0.72	–	–
0.9 ± 0.012	33.50 ± 1.32	0.9 ± 0.012	35.40 ± 1.12	0.9 ± 0.012	36.32 ± 0.72
1.0 ± 0.014	36.88 ± 1.24	1.0 ± 0.014	38.91 ± 1.02	1.0 ± 0.013	40.47 ± 0.83
1.1 ± 0.015	38.61 ± 1.12	1.1 ± 0.015	40.78 ± 1.01	1.1 ± 0.015	42.15 ± 0.73
1.2 ± 0.017	38.98 ± 0.99	1.2 ± 0.017	41.07 ± 1.04	1.2 ± 0.016	42.56 ± 0.73
1.3 ± 0.018	38.14 ± 1.03	1.3 ± 0.018	39.77 ± 1.01	1.3 ± 0.017	41.03 ± 0.63
1.4 ± 0.019	35.85 ± 1.01	1.4 ± 0.019	37.58 ± 1.18	1.4 ± 0.019	39.47 ± 0.81
1.5 ± 0.021	32.89 ± 1.23	1.5 ± 0.021	34.24 ± 1.13	–	–

**Table 2**

Experimental laminar burning velocity,  $S_L$ , for methanol + O<sub>2</sub> + CO<sub>2</sub> flames at initial temperatures, 338 and 358 K and power exponent  $\alpha$ .

338 K		358 K		$\alpha$
$\phi$	$S_L$ (cm s <sup>-1</sup> )	$\phi$	$S_L$ (cm s <sup>-1</sup> )	
0.8 ± 0.011	33.68 ± 0.96	0.8 ± 0.011	36.60 ± 1.00	1.58 ± 0.28
0.9 ± 0.012	39.00 ± 0.90	0.9 ± 0.012	42.15 ± 0.93	1.47 ± 0.16
1.0 ± 0.014	42.70 ± 0.92	1.0 ± 0.013	46.19 ± 0.98	1.45 ± 0.15
1.1 ± 0.015	44.72 ± 0.94	1.1 ± 0.015	48.71 ± 1.04	1.50 ± 0.14
1.2 ± 0.016	45.13 ± 1.02	1.2 ± 0.016	49.16 ± 1.10	1.52 ± 0.14
1.3 ± 0.018	43.93 ± 1.01	1.3 ± 0.017	47.75 ± 1.11	1.54 ± 0.15
1.4 ± 0.019	41.27 ± 1.06	1.4 ± 0.019	45.01 ± 1.10	1.56 ± 0.16
1.5 ± 0.020	37.95 ± 1.06	1.5 ± 0.020	41.73 ± 1.21	1.67 ± 0.19

expected to have a linear relationship, which is seen in Fig. 3. Experimental values obtained with different types of oxidizer preparation (on-site at 308 K and 328 K and from the plant at 318 K, 338 K and 358 K) accurately follow the linear trend lines confirming the consistency of the measurements and allowing to neglect any variation of the oxidizer composition. From the slope of the linear fit, the power exponent  $\alpha$  was derived, see Fig. 4. The scattering of experimental values of  $\alpha$  and the magnitude of the error-bars is too large to draw any certain conclusions on its relationship to  $\phi$  from the measurements only. Also shown in Fig. 4 are power exponents  $\alpha$  derived from different models, further discussed in the following.

#### 4.2. Comparison and analysis of the models

Predictions of the three models outlined above have been compared with the measurements of methanol + air flames [26] and with the results at oxy-fuel conditions obtained in the present work. Results for the initial gas mixture temperature of 318 K are used to illustrate the behavior of the models.

The performance of Models I–III is evaluated by comparing laminar burning velocities of methanol + air flames at 318 K to results from a previous study in the same laboratory [18], as presented in Fig. 5. The experimental uncertainties reported in that work are about 0.5–1 cm s<sup>-1</sup>. As the heat flux method generally gives a reproducibility of ~1 cm s<sup>-1</sup> the laminar burning velocities are presented with 1 cm s<sup>-1</sup> error bars in Fig. 5. At the lean side Models I–III are all in agreement with the experimental values. Models I–II shows minor overpredictions of about 2 and 1 cm s<sup>-1</sup>, respectively, at stoichiometric conditions, while the overprediction of Model III is as large as ~5 cm s<sup>-1</sup>. On the rich side Model III overpredicts the laminar burning velocity by ~4 cm s<sup>-1</sup>, while Models I–II predictions are in agreement with the experimental results. One should note that when using mixture-average transport instead of multi-component transport, Model III is in considerably better agreement with the experimental results. Models I and II are much less sensitive to the choice of transport properties. Figures S5 and S6 available in the Supplementary material illustrate the performance of Models I–IV with different transport properties taken into account.

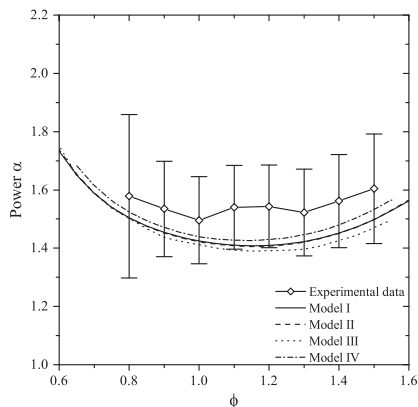


**Fig. 4.** Power exponent  $\alpha$  vs. equivalence ratio. Squares are experimental results and the lines are modeled results, Model I (solid), Model II (dash), Model III (dot) and Model IV (dash dot).

The experimental and modeling results from Models I–III for methanol +  $O_2$  +  $CO_2$  with an unburnt gas temperature of 318 K are presented in Fig. 6. For lean and stoichiometric conditions, Models I–II give results just above the experimental uncertainties, while Model III gives predictions within experimental uncertainties. At the experimental maximum laminar burning velocity, at  $\phi = 1.2$ , Models I–III overpredict significantly as compared to the experimental results. On the rich side all three models significantly overpredict experimental results. Figures S1–S4 presenting the model performance at all other measured temperatures are available as [Supplementary material](#).

As shown in Fig. 4, all three models predict the same non-linear temperature dependency for  $\phi = 0.5$ –1.6, with a minimum at  $\phi = 1.2$ ; i.e. the same  $\phi$  as where the maximum of the laminar burning velocities was found. Since the models predict similar

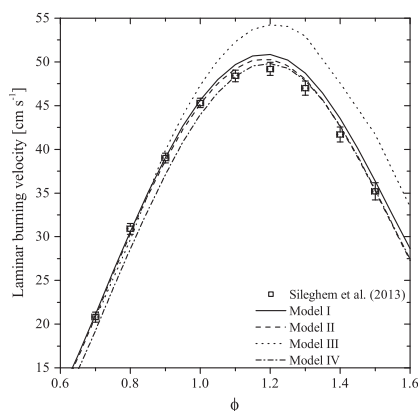


**Fig. 5.** Comparison between experimental results (symbols) [26] and modeling results (lines) for methanol + air at 318 K. The models are Model I (solid), Model II (dash), Model III (dot) and Model IV (dash dot).

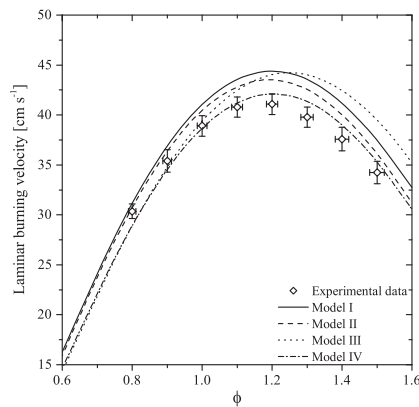


**Fig. 6.** Comparison between experimental results (symbols) and modeling results (lines) for methanol +  $O_2$  +  $CO_2$  at 318 K. The models are Model I (solid), Model II (dash), Model III (dot) and Model IV (dash dot).

temperature dependency, temperature is likely not an important factor affecting the difference in performance of the models at the present conditions. As the uncertainty of the experimentally determined  $\alpha$  is large, and the model predictions are within this uncertainty no conclusion can be drawn with any certainty.

The different models' performance for methanol burning in air or at oxy-fuel conditions can stem from differences in flame temperatures, radiative properties or chemical involvement of  $CO_2$ . Model I was used as a platform to examine these effects. The calculated adiabatic temperature for the methanol flames under oxy-fuel conditions is slightly higher (by about 100 K) than for methanol + air at  $\phi = 1.0$  and an unburnt gas temperature of 318 K. This difference in temperature is insignificant compared to the flame temperature. The deteriorated performance of the models with  $O_2$  +  $CO_2$  as oxidizer as compared to air thus cannot be explained as an effect of the shift of the flame temperature window.

With the amounts of  $CO_2$  present in the oxidizer mixture, the effect of radiative heat loss from the flame could possibly be of importance. Planck's mean absorption coefficients from an optically thin model for  $CO_2$ ,  $CO$  and  $H_2O$  [27], were incorporated in Model I to examine this effect. 1-D freely propagating flames were modeled using Chemkin IV [24] and solving the energy equation, which includes heat losses from the burnt gases to the surroundings at room temperature. In this simplified numerical setup the presence of the burner plate and reabsorption of the radiation by the fresh gas mixture are not considered. Inclusion of those would decrease the effect and therefore the results obtained here provide a conservative upper limit of the possible effect. It was found that the radiation from the flame has a minor influence on the calculated burning velocity which is only reduced by  $\sim 0.5 \text{ cm s}^{-1}$ , as can be seen in Fig. 7. In real measurements up to 50% of the radiative heat losses may reflect from the burner surface and further re-absorb by the fresh gas mixture making this effect even less important. Radiative heat loss, therefore, is neglected in the continued evaluation of the models. It is interesting to note that in relevant studies of the radiation-induced uncertainty of the burning velocity derived from spherical flames (see e.g. [28] and references therein) the one-sided bias was found within 5% and 2% for mixtures propagating faster than  $12 \text{ cm s}^{-1}$  and  $26 \text{ cm s}^{-1}$ , respectively. The predicted effect is therefore somewhat higher in spherical flames (about  $0.6 \text{ cm s}^{-1}$  [28]) since it includes contributions

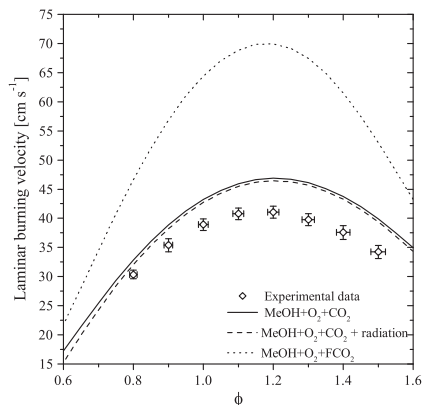


Fig. 7. Comparison between experimental results (symbols) and modeling results (lines) for methanol +  $O_2$  +  $CO_2$  at 318 K. Baseline modeling with Model I (solid), with radiative losses (dash) and flames with  $CO_2$  replaced with fake  $CO_2$ ,  $FCO_2$  (dot).

from temperature reduction of the flame front and negative flow speed of the burned gases. On the other hand, Yu et al. [28] admitted that their evaluation is also a conservative upper limit, since they did not take into account wall-reflected radiation.

To investigate whether  $CO_2$  chemistry has a significant impact on the model performance,  $CO_2$  was replaced with a substitute, fake  $CO_2$  ( $FCO_2$ ), with the same thermal properties, but which does not participate in the chemistry. This procedure has been proposed by Liu et al. [5]. The result was a drastic increase in the modeled laminar burning velocity, by about  $25 \text{ cm s}^{-1}$  at stoichiometric conditions, as illustrated in Fig. 7. As a second test, collisional efficiency coefficients for  $FCO_2$  were included in the  $FCO_2$  model. The coefficients were added to all third body reactions within Model I and set to the corresponding value as the  $CO_2$  coefficients. This gave an increase in the laminar burning velocity of  $\sim 1\%$  as compared to the  $FCO_2$ -modeling without changes in the third body coefficients. These results are thus a strong indication that  $CO_2$  is highly chemically active in the flame.

The methanol + air mixtures exhibit higher burning velocities than the corresponding oxy-fuel mixtures (with 35%  $O_2$  and 65%  $CO_2$ ) as seen in Figs. 5 and 6. One should note, however, that methanol + air and methanol +  $O_2$  +  $CO_2$  are different systems, where a number of factors differ, as heat capacity of inert, amount of oxygen in the oxidizer and radical composition in the reaction zone.

The sensitivity and rate of production of species related to methanol consumption, have been analyzed to further elucidate the reactions involved. The twenty most sensitive reactions for Models I–III under oxy-fuel conditions, at  $\phi = 1.0$  and 318 K, are presented in Fig. 8. Figure 9 shows the twenty sensitive reactions multiplied with uncertainty factors from Baulch et al. [29]. The reaction numbering corresponds to the mechanism of Li et al. [9]. The sensitivity spectra are similar for Models I–II, with the exception of four minor reactions which differ between Models I and II,  $HO_2 + HO_2 = H_2O_2 + O_2$  (14),  $CH_3O + OH = HCO + H_2O$  (44),  $CH_3 + OH = CH_2O + H$  (61) and  $CH_3OH + HO_2 = CH_2OH + H_2O_2$  (91). The most sensitive reaction is  $H + O_2 = O + OH$  (1), but despite its high sensitivity (1) is not considered further as this reaction rate is well studied and thus has a low uncertainty [29]. An important difference in sensitivity is related to the reaction of methanol with the hydroxyl radical, where the isomeric products formed differ in

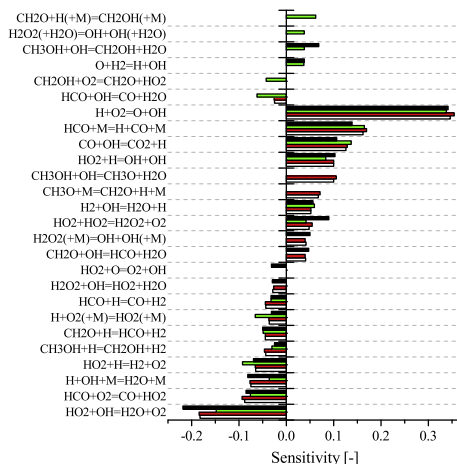


Fig. 8. The twenty most sensitive reactions for methanol +  $O_2$  +  $CO_2$  at  $\phi = 1.0$  with Model I (white), Model II (red), Model III (green) and Model IV (black).

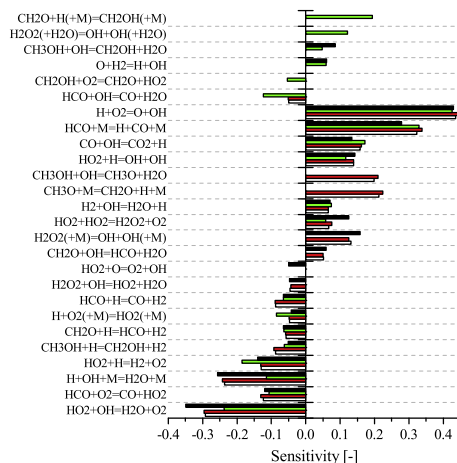


Fig. 9. Combined uncertainty and sensitivity affecting calculated  $S_L$  for methanol +  $O_2$  +  $CO_2$  at  $\phi = 1.0$  with Model I (white), Model II (red), Model III (green) and Model IV (black). (For interpretation of the references to colour in this figure legend, the reader is referred to the web version of this article.)

Model III compared to Models I–II. Models I–II are sensitive to reaction  $CH_3OH + OH = CH_3O + H_2O$  (78) at  $\phi = 1.0$ . As this reaction is flame promoting, and one of the most important methanol-consuming reactions in Models I–II, an erroneous rate constant is expected to have a large impact on the laminar burning velocity. Model III is sensitive to reaction  $CH_3OH + OH = CH_2OH + H_2O$  (79). Reaction  $CH_3OH + H = CH_2OH + H_2$  (75) is among the 20 most sensitive reactions with similar sensitivity in all three models. Reaction  $CH_2OH + O_2 = CH_2O + HO_2$  (57) is among the sensitive

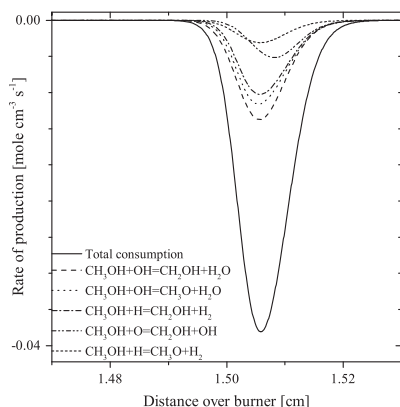


Fig. 10. Consumption profile for methanol +  $\text{O}_2$  +  $\text{CO}_2$  at  $\phi = 1.0$  and 318 K for Model I.

reactions in Model III only, for both air and oxy-fuel conditions. The decomposition reaction  $\text{CH}_3\text{O} + \text{M} = \text{CH}_2\text{O} + \text{H} + \text{M}$  (63) is sensitive in Models I–II.

The production and consumption rates of key species in the three models were compared. The consumption of methanol can be linked directly to the calculated laminar burning velocity, especially in the lean flames, where the fuel is the limiting species. Figure 10 shows the consumption profiles for methanol in Model I at  $\phi = 1.0$  and 318 K via the most dominant reactions. The H-abstraction by OH (78–79), H (75) and  $\text{CH}_3\text{OH} + \text{H} = \text{CH}_3\text{O} + \text{H}_2$  (76), and  $\text{CH}_3\text{OH} + \text{O} = \text{CH}_2\text{OH} + \text{OH}$  (77), are the dominant methanol consuming reactions, but the ratio between them vary in the three models. In Models I–II the dominating reactions are H-abstraction with branching to  $\text{CH}_2\text{OH}$  and  $\text{CH}_3\text{O}$ .  $\text{CH}_2\text{OH}$  is produced by reaction with OH (78), O (77) and H (75), while  $\text{CH}_3\text{O}$  is mainly from OH (79). In Model III, the methanol consumption is dominated by the formation of  $\text{CH}_2\text{OH}$  (75, 79). Reaction with OH (79) is dominating in the methanol consumption, at  $\phi = 1.0$ , with ~60% of the overall rate. Reaction (75) consumes ~30% of methanol.

In Models I–II the production of  $\text{CH}_2\text{OH}$  and  $\text{CH}_3\text{O}$  as a result of H-abstraction from methanol are close to equal, while for Model III the production of  $\text{CH}_2\text{OH}$  is almost 10 times higher than that of  $\text{CH}_3\text{O}$ . The ratio between (79) and (75) can be part of the explanation of the lower laminar burning velocity of Model III at lean conditions, as reaction (79) is chain propagating, and reaction (75) leads to chain branching. In Models I–II reaction (79) has an equal contribution to the methanol consumption as reaction (75), increasing the laminar burning velocity of Models I–II, by having a higher chain-branching contribution to the methanol consumption, than in Model III. In Models I–III,  $\text{CH}_2\text{OH}$  is consumed mainly by reaction (57). Reaction (57) has the same rate constant in Models I–III, therefore the sensitivity is presumably a response to reactions (75, 77, 79) producing  $\text{CH}_2\text{OH}$ .  $\text{CH}_3\text{O}$  consumption is dominated by the unimolecular decomposition to  $\text{CH}_2\text{O} + \text{H}$  (63) with a minor contribution from reaction with  $\text{O}_2$  (67). Different rate constants of reaction (67) are used in the mechanisms considered. In Model III a slower rate constant is used compared to Models I–II.

Carbon dioxide reacts with radicals to form carbon monoxide. It will compete with  $\text{O}_2$  to react. From the sensitivity profiles, there are no major differences in how the mechanisms deal with  $\text{CO}_2$

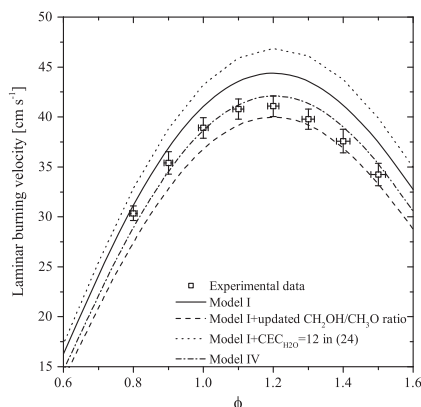


Fig. 11. The effect on the modifications suggested in Section 4.3 on the modeled laminar burning velocity of methanol +  $\text{O}_2$  +  $\text{CO}_2$  flames.

and CO. There are five shared sensitive reactions involving CO, with no major differences in sensitivity. The most sensitive of the CO reactions is  $\text{CO} + \text{OH} = \text{CO}_2 + \text{H}$  (23) which is also the major reaction consuming  $\text{CO}_2$  in the reverse direction. Reaction (23) has a different rate constant in Model III compared to Models I–II.

Additional sensitivity analyses are illustrated in Figs. S17–S27 in the Supplementary material.

#### 4.3. Modifications analyzed

From the sensitivity and rate of production analyses presented above, key parameters potentially affecting the mechanism performance at oxy-fuel conditions, were identified. Model I is a well-established model for methanol flames, and was chosen as the base for modifications aiming at improving the performance at oxy-fuel conditions. The modified version of Model I is called Model IV and the modifications are described below. The attempted modifications resulted in a very good agreement with experimental data for flames in air as well as under oxy-fuel conditions. The results can be seen in Figs. 5 and 6. In Figs. 10 and 11 the effect of the suggested modifications on the predictions of the laminar burning velocity for Model I is illustrated. The modifications are incorporated in Model I first separately and then together, to produce Model IV. The following modifications have been attempted.

##### 4.3.1. Reaction (23)

Previous studies of oxy-fuel combustion have identified  $\text{CO}_2 + \text{H} \rightarrow \text{CO} + \text{OH}$  (23) as an important step in  $\text{CO}_2$  formation and consumption [4–7]. Under  $\text{O}_2/\text{N}_2$  combustion  $\text{N}_2$  is not contributing to chain branching other than as a third body, while as it is replaced by a high concentration of  $\text{CO}_2$  the reactivity increases since  $\text{CO}_2$  is ready to react with radicals, mainly via reaction (23). This reaction is well determined with consistently good agreement between rate constants published in the literature [29]. Reaction (23) exhibits a near temperature independent behavior at low temperatures. Above ~500 K the reaction rate increases with temperature. The rate constant from Li et al. [9], used in Model I, is derived from experimentally determined rate constants from the literature. Selected rate constants can be seen in Fig. S12 in the Supplementary material. A change in the rate constant for reaction (23) was attempted to examine if the small differences between selected

expressions would have any impact at the present  $\text{CO}_2$  rich conditions. Expressions implemented in other models [30–32] were tested, selected as these rate constant exhibit qualitatively different temperature dependency profiles. This did not give any significant change, thus the rate constant was left unaltered.

#### 4.3.2. H-abstraction from methanol

From the rate of production and sensitivity analyses the product branching as a result of H-abstraction from  $\text{CH}_3\text{OH}$ , was identified as a candidate for model improvement. H-abstraction reactions are the main methanol consumption reactions as illustrated in Fig. 10 for Model I. The branching in these reactions is important as the isomers methoxy,  $\text{CH}_3\text{O}$ , and hydroxyl methyl,  $\text{CH}_2\text{OH}$ , have different consumption paths; the radical pool is highly dependent on the accuracy of this branching ratio. Although both isomers produce mainly  $\text{CH}_2\text{O}$ , dependent on the isomer either  $\text{HO}_2$  or H is formed in the competing reactions with  $\text{O}_2$  or decomposition. No experimental studies shed light on the branching ratio issue. However  $\text{CH}_2\text{OH}$  is thermodynamically a more stable species than  $\text{CH}_3\text{O}$ . Published theoretical studies suggest that the  $\text{CH}_2\text{OH}$  radical is more prominently formed than its isomer  $\text{CH}_3\text{O}$  [33–35]. In recent works by Mittal et al. [11], Model III, and Klippenstein et al. [10], Model II, branching ratios for reactions of methanol with OH, H,  $\text{HO}_2$  and  $\text{O}_2$  have been updated compared to the ones used in Model I.

The H-abstraction reactions in Model I were updated with the new rate constants for reactions with H from Meana-Pañeda et al. [34], and with OH from Xu and Lin [36]. Meana-Pañeda et al. [34] presented reaction rates for H-abstraction from methanol by H where the product channels have individually calculated rate constants [34,37]. This gave a branching ratio shifted toward  $\text{CH}_2\text{OH}$ , with the formation of  $\text{CH}_2\text{OH}$  faster than  $\text{CH}_3\text{O}$ . The branching ratio is predicted to be temperature dependent, with close to 100%  $\text{CH}_2\text{OH}$  at room temperature falling to 75% at 2500 K. The calculation by Meana-Pañeda et al. [34] for this rate constant predicts a temperature dependent activation energy for the reaction and based on this the authors argue that because of this temperature dependence in activation energy, the rate constants from experimental work as Warnatz [38] among others, suffers from a too low activation energy. The experimentally determined rate constants found in the literature are scattered, as reviewed by Baulch et al. [29].

The overall rates for methanol with OH are well determined. The main difference is in the treatment of the branching ratio between product channels. Xu and Lin [36] derived individual rate constants and product branch ratio from ab initio calculations of the  $\text{CH}_3\text{OH} + \text{OH}$  reactions. Using the Xu and Lin [36] rate constants will not change the total reaction rate, only the branching ratio as compared to Bott and Cohen [33], but the product branching toward  $\text{CH}_2\text{OH}$  will be strongly favoured with more than 90% of the total rate. The branching ratio by Xu and Lin [36] is nearly temperature independent, a major difference compared to Bott and Cohen [33] where the branch ratio is strongly decreasing with increasing temperature. As argued in Mittal et al. [11] with references therein, the reaction rate is independent of alkyl chain length for methanol, ethanol and butanol, which supports the rate constants from Xu and Lin [36].

Rate constants for reactions with  $\text{O}_2$  and  $\text{HO}_2$  were adopted from Klippenstein et al. [10]. Implementation of the rate constant from Alecu and Truhlar [39] for H-abstraction with  $\text{HO}_2$  did not affect the performance in any significant way, as can be seen in Figs. S10 and S11 in the Supplementary material. In Fig. 13, the consumption paths for  $\text{CH}_3\text{OH}$  in Model IV are illustrated, showing the total consumption for  $\text{CH}_3\text{OH}$  at oxy-fuel conditions, 318 K and  $\phi = 1.0$ , together with the 5 reactions with the highest consumption rates. The  $\text{CH}_2\text{OH}$  formation is dominating the  $\text{CH}_3\text{OH}$

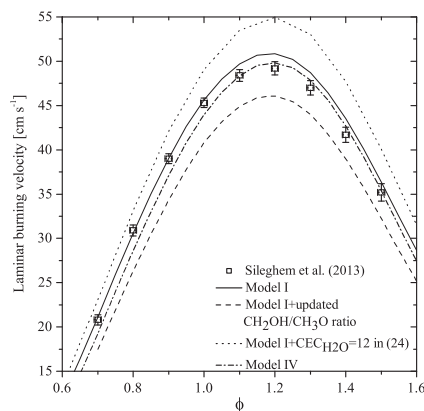


Fig. 12. The effect on the modifications suggested in Section 4.3 on the modeled laminar burning velocity of methanol + air flames.

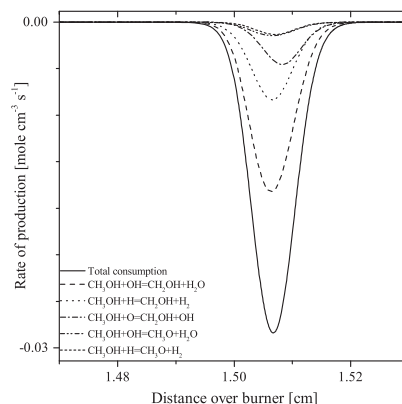


Fig. 13. Consumption profile for methanol +  $\text{O}_2$  +  $\text{CO}_2$  conditions at  $\phi = 1.0$  and 318 K for Model IV.

consumption. Comparing Fig. 12, with Fig. 10, it can be seen that these modifications affect both the total consumption of methanol and the production of  $\text{CH}_2\text{OH}$  and  $\text{CH}_3\text{O}$ . This modification of Model I results in significantly lower laminar burning velocities compared to the original version, underestimating the experimental results. This effect is illustrated in Figs. 11 and 12. The rate constants discussed above are summarized in Table S1 in the Supplementary material.

#### 4.3.3. Collisional efficiency coefficient for reaction (24)

After weighting the sensitivity against the rate constant uncertainty (Fig. 9), reaction  $\text{HCO} + \text{M} = \text{H} + \text{CO} + \text{M}$  (24) emerges as a highly sensitive reaction. The rate constant for (24) from Li et al. [9], used in Models I–III, is derived by fitting a wide range of experimental data obtained in different bath gases, He, Ar,  $\text{N}_2$ , Ne,  $\text{H}_2$  [40–53]. For the determination of collisional efficiency coefficients

(CEC) for third body reactions like (24), the experimental conditions with respect to bath gas composition have to be considered [38]. In Model I a CEC of 6 is used for  $\text{H}_2\text{O}$ . Given that the primary diluents used in the original experiment and calculations were Ar and He, one may argue that a higher value for  $\text{H}_2\text{O}$  would better describe this reaction. The CEC for  $\text{H}_2$ , CO and  $\text{CO}_2$  have values which are reasonable according to the theory of Warnatz. The uncertainty of (23) by Baulch et al. [54] is estimated to be a factor of 2. A doubling of the value for CEC, compared to the value used in Model I, result in a rate constant within this uncertainty.

A CEC of 12 for  $\text{H}_2\text{O}$  in reaction (24) was implemented in the modified version of Model I, reflecting the wide range of bath gases from the underlying experimental data. This modification resulted in a significantly increased laminar burning velocity, as seen in Fig. 11 and 12. The performance of Model IV is significantly improved compared to Model I, for oxy-fuel conditions the results can be seen in Fig. 6. For the methanol + air flames, seen in Fig. 5, predictions from Model IV results in a fit on the lean side by  $\sim 1 \text{ cm s}^{-1}$  below the experimental values but close to the lower limit of the experimental uncertainty whereas it fits well with the experimental velocities at  $\phi = 1.0$ –1.5.

#### 4.3.4. Collisional efficiency of $\text{CO}_2$

To examine the third body effect of  $\text{CO}_2$ , the collisional efficiency coefficient for  $\text{CO}_2$  in the sensitive reactions  $\text{H} + \text{OH} + \text{M} = \text{H}_2\text{O} + \text{M}$  (8),  $\text{H} + \text{O}_2 + \text{M} = \text{HO}_2(+\text{M})$  (9),  $\text{H}_2\text{O}_2(+\text{M}) = \text{OH} + \text{OH}(+\text{M})$  (15), (24), and  $\text{CH}_3\text{O} + \text{M} = \text{CH}_2\text{O} + \text{H} + \text{M}$  (63) was altered for each reaction individually by doubling and reducing by 50% sequentially. This scaling of the original coefficients is in the same order of magnitude as the differences between the original bath gases in the experimental determinations of the rate constants with different third bodies. The modifications had an impact on the predictions of the methanol +  $\text{O}_2$  +  $\text{CO}_2$  flames, but did not change the predictions for methanol + air flames. The collisional efficiency coefficients for  $\text{CO}_2$  were therefore left unaltered.

The effects on prediction of laminar burning velocity by altering the collisional efficiency coefficients are presented in Figs. S7 and S8 in the Supplementary material [38].

## 5. Conclusions

Novel experimental data for laminar burning velocity for pre-mixed methanol +  $\text{O}_2$  +  $\text{CO}_2$  flames are presented for temperatures 308–358 K and pressure of 1 atm. The experimental laminar burning velocities show a linear temperature dependency on a log–log-scale. In light of these new experimental results, the performance of three kinetic models was examined. Modifications to the mechanism of Li et al. [9] (Model I) were suggested to improve the prediction capabilities for methanol +  $\text{O}_2$  +  $\text{CO}_2$  flames. These modifications include: (a) recommendations from Klippenstein et al. [10] for the rate constants of reactions (80, 82a) and  $\text{CH}_3\text{OH} + \text{HO}_2 = \text{CH}_3\text{O} + \text{H}_2\text{O}_2$  (82b). (b) Changing the branching ratio of H-abstraction by the two major methanol consuming species, H and OH. (c) The decomposition of the formyl radical was given a higher collisional efficiency coefficient for the third body  $\text{H}_2\text{O}$ . As a result of the modifications the product formation was shifted toward formation of  $\text{CH}_2\text{OH}$  at the expense of  $\text{CH}_3\text{O}$  with new rate constants from Meana-Pañeda et al. [34] and Xu and Lin [36]. It appears that the site of the H-abstraction has a large effect in the combustion of methanol. These changes resulted in a more accurate reproduction of laminar burning velocity of methanol for both air and oxy-fuel conditions at 1 atm.

One should note that the present analysis is pertinent to atmospheric pressure only; further studies at higher pressures relevant to possible applications are required.

## Acknowledgments

The authors are grateful to Prof. F.L. Dryer and Dr. M. Chaos for fruitful discussions. Thanks also to the Swedish Energy Agency and the Foundation for Strategic Research, (SSF) through the Center of Combustion Science and technology (CECOST) for financial support. L. Sileghem gratefully acknowledges a Ph.D. fellowship (FWO11/ASP/056) and a grant for a long stay abroad at Lund University provided by the Research Foundation Flanders.

## Appendix A. Supplementary material

Supplementary data associated with this article can be found, in the online version, at <http://dx.doi.org/10.1016/j.combustflame.2014.11.033>.

## References

- [1] Efficient Shipping with low emissions. <<http://www.effship.com>>.
- [2] Alcohol (spirits) and ethers as marine fuel. <<http://www.spireth.com>>.
- [3] [http://inea.ec.europa.eu/en/news\\_events/newsroom/eu-to-co-fund\\_pilot\\_action\\_on\\_methanol\\_for\\_maritime\\_transport.htm](http://inea.ec.europa.eu/en/news_events/newsroom/eu-to-co-fund_pilot_action_on_methanol_for_maritime_transport.htm).
- [4] A.R. Masri, R.W. Dibble, R.S. Barlow, Combust. Flame 91 (1992) 285–309.
- [5] F.S. Liu, H.S. Guo, G.J. Smallwood, O.L. Gulder, Combust. Flame 125 (2001) 778–787.
- [6] F.S. Liu, H.S. Guo, G.J. Smallwood, Combust. Flame 133 (2003) 495–497.
- [7] P. Glarborg, L.L.B. Bentzen, Energy Fuels 22 (2008) 291–296.
- [8] J.D. Naucier, M. Christensen, E.J.K. Nilsson, A.A. Konnov, Energy Fuels 26 (2012) 4269–4276.
- [9] J. Li, Z.W. Zhao, A. Kazakov, M. Chaos, F.L. Dryer, J.J. Scire, Int. J. Chem. Kinet. 39 (2007) 109–136.
- [10] S.J. Klippenstein, L.B. Harding, M.J. Davis, A.S. Tomlin, R.T. Skodje, Proc. Combust. Inst. 33 (2011) 351–357.
- [11] G. Mittal, S.M. Burke, V.A. Davies, B. Parajuli, W.K. Metcalfe, H.J. Curran, Combust. Flame 161 (2014) 1164–1171.
- [12] L.P.H. de Goeij, A. van Maaren, R.M. Quax, Combust. Sci. Technol. 92 (1993) 201–207.
- [13] D.S.T.A. van Maaren, L.P.H. de Goeij, Combust. Sci. Technol. 96 (1994) 327–344.
- [14] K.J. Bosschaert, L.P.H. de Goeij, Combust. Flame 132 (2003) 170–180.
- [15] F. Normann, K. Andersson, B. Leckner, F. Johnsson, Fuel 87 (2008) 3579–3585.
- [16] A.A. Konnov, I.V. Dyakov, Combust. Flame 136 (2004) 371–376.
- [17] I.V. Dyakov, A.A. Konnov, J. De Ruyck, K.J. Bosschaert, E.C.M. Brock, L.P.H. de Goeij, Combust. Sci. Technol. 172 (2001) 81–96.
- [18] A.A. Konnov, I.V. Dyakov, Combust. Sci. Technol. 179 (2007) 747–765.
- [19] R. Hermanns, Doctoral Dissertation, Laminar Burning Velocities of Methane–Hydrogen–Air Mixtures, Technische Universiteit Eindhoven, 2007.
- [20] <http://www.heatfluxburner.org/>.
- [21] V.A. Alekseev, J.D. Naucier, M. Christensen, E.J.K. Nilsson, A.A. Konnov, Experimental uncertainties of the heat flux method for measuring burning velocities, 2014 (in preparation).
- [22] J. Vancollie, M. Christensen, E.J.K. Nilsson, S. Verhelst, A.A. Konnov, Energy Fuels 26 (2012) 1557–1564.
- [23] F.L. Dryer, CO,  $\text{CH}_2\text{O}$ ,  $\text{CH}_3\text{OH}$ , and Syngas: A “C1 Model A Comprehensive Kinetic Mechanism for CO,  $\text{CH}_2\text{O}$ ,  $\text{CH}_3\text{OH}$  Combustion”. <[http://www.princeton.edu/mae/people/faculty/dryer/homepage/kinetic\\_models/c1-model/](http://www.princeton.edu/mae/people/faculty/dryer/homepage/kinetic_models/c1-model/)>.
- [24] CHEMKIN IV 15101, Reaction Design, San Diego, 2010.
- [25] S. Heimeil, Effects of Initial Mixture Temperature on Burning Velocity of Hydrogen–air Mixtures with Preheating and Simulated Preburning, NACA Technical Note 4156, 1957.
- [26] L. Sileghem, V.A. Alekseev, J. Vancollie, E.J.K. Nilsson, S. Verhelst, A.A. Konnov, Fuel 115 (2014) 32–40.
- [27] Y.G. Ju, H.S. Guo, F.S. Liu, K. Maruta, J. Fluid Mech. 379 (1999) 165–190.
- [28] H. Yu, W. Han, J. Santner, X. Gou, C.H. Sohn, Y. Ju, Z. Chen, Combust. Flame 161 (2014) 2815–2824.
- [29] D.L. Baulch, C.T. Bowman, C.J. Cobos, R.A. Cox, T. Just, J.A. Kerr, M.J. Pilling, D. Stocker, J. Troe, W. Tsang, R.W. Walker, J. Warnatz, J. Phys. Chem. Ref. Data 34 (2005) 757–1397.
- [30] C.L. Rasmussen, J. Hansen, P. Marshall, P. Glarborg, Int. J. Chem. Kinet. 40 (2008) 454–480.
- [31] P. Dagaut, Phys. Chem. Chem. Phys. 4 (2002) 2079–2094.
- [32] A.V. Joshi, H. Wang, Int. J. Chem. Kinet. 38 (2006) 57–73.
- [33] J.F. Bott, N. Cohen, Int. J. Chem. Kinet. 23 (1991) 1075–1094.
- [34] R. Meana-Pañeda, D.G. Truhlar, A. Fernández-Ramos, J. Chem. Phys. 134 (2011).
- [35] E.F.V. Carvalho, A.N. Barauna, F.B.C. Machado, O. Roberto, Chem. Phys. Lett. 463 (2008) 33–37.
- [36] S. Xu, M.C. Lin, Proc. Combust. Inst. 31 (2007) 159–166.
- [37] S.C. Li, F.A. Williams, Symp. (Int.) Combust. 26 (1996) 1017–1024.

- [38] J. Warnatz, in: J.W.C. Gardiner (Ed.), *Combustion Chemistry*, Springer-Verlag New York Inc., New York, 1984, pp. 197–360 (Chapter 5).
- [39] I.M. Alecu, D.G. Truhlar, *J. Phys. Chem. A* 115 (2011) 14599–14611.
- [40] R.R. Baldwin, D. Jackson, A. Melvin, B.N. Rossiter, *Int. J. Chem. Kinet.* 4 (1972) 277–292.
- [41] C.T. Bowman, *Combust. Sci. Technol.* 2 (1970) 161–172.
- [42] W.G. Browne, R.P. Porter, J.D. Verlin, A.H. Clark, *Symp. (Int.) Combust.* 12 (1969) 1035–1047.
- [43] I.M. Campbell, B.J. Handy, *J. Chem. Soc. Faraday Trans. 1: Phys. Chem. Condens. Phases* 74 (1978) 316–325.
- [44] M.A. Cherian, P. Rhodes, R.J. Simpson, G. Dixon-Lewis, *Symp. (Int.) Combust.* 18 (1981) 385–396.
- [45] P.H. Cribb, J.E. Dove, S. Yamazaki, *Combust. Flame* 88 (1992) 169–185.
- [46] G. Friedrichs, J.T. Herbon, D.F. Davidson, R.K. Hanson, *Phys. Chem. Chem. Phys.* 4 (2002) 5778–5788.
- [47] H. Hippler, N. Krasteva, F. Striebel, *Phys. Chem. Chem. Phys.* 6 (2004) 3383–3388.
- [48] C.J. Hochanadel, T.J. Sworski, P.J. Ogren, *J. Phys. Chem.* 84 (1980) 231–235.
- [49] L.N. Krasnoperov, E.N. Chesnokov, H. Stark, A.R. Ravishankara, *J. Phys. Chem. A* 108 (2004) 11526–11536.
- [50] G.S. Pearson, *J. Phys. Chem.* 67 (1963) 1686–1692.
- [51] R.S. Timonen, E. Ratajczak, D. Gutman, A.F. Wagner, *J. Phys. Chem.* 91 (1987) 5325–5332.
- [52] H.Y. Wang, J.A. Eyre, L.M. Dorfman, *J. Chem. Phys.* 59 (1973) 5199–5200.
- [53] C.K. Westbrook, J. Creighton, C. Lund, F.L. Dryer, *J. Phys. Chem.* 81 (1977) 2542–2554.
- [54] D.L. Baulch, C.J. Cobos, R.A. Cox, C. Esser, P. Frank, T. Just, J.A. Kerr, M.J. Pilling, J. Troe, R.W. Walker, J. Warnatz, *J. Phys. Chem. Ref. Data* 21 (1992) 411–734.

## Paper III





# Laminar burning velocity of nitromethane + air flames: A comparison of flat and spherical flames

Jenny D. Nauc  r, Elna J.K. Nilsson, Alexander A. Konnov\*

Division of Combustion Physics, Department of Physics, Lund University, Lund, Sweden

## ARTICLE INFO

### Article history:

Received 6 May 2015

Revised 13 July 2015

Accepted 14 July 2015

Available online 31 July 2015

### Keywords:

Laminar burning velocity

Nitromethane

Temperature dependence

Modelling

## ABSTRACT

Laminar burning velocities,  $S_L$ , of nitromethane and air flames at 1 atm and initial gas temperatures,  $T$ , of 338 K, 348 K, and 358 K were determined using the heat flux method. Measurements were performed in non-stretched flames, stabilized on a perforated plate burner under adiabatic conditions. The comparison of these new experimental data and recent literature results obtained in spherical flames at 423 K was guided by the analysis of the temperature dependence of  $S_L$  using expression  $S_L = S_{L0}(T/T_0)^{\beta}$ , and also by kinetic modelling of premixed flames employing detailed mechanisms suggested in the literature. It was demonstrated that conventional recalculation of the flame front speed into the burning velocity using density ratio of the unburned and burned gases at equilibrium is inappropriate for spherical nitromethane flames. Both the laminar burning velocities and the power exponents,  $\alpha$ , were compared with predictions of the kinetic mechanisms. Remaining discrepancies of the modelling and reconciled experimental data were highlighted.

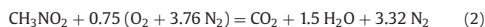
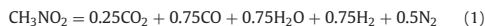
  2015 The Combustion Institute. Published by Elsevier Inc. All rights reserved.

## 1. Introduction

Combustion chemistry of nitromethane,  $\text{CH}_3\text{NO}_2$ , is important in several aspects. Nitromethane is considered as one of the simplest fuel-nitrogen species with one C–N single bond that facilitates understanding of the reactions relevant to mutual sensitized oxidation of hydrocarbons and nitrogen oxides [1]. It was proposed as a potential monopropellant [2] that motivated extensive studies of nitromethane thermal decomposition, e.g., [3–6], and detonation [7]. Moreover, nitromethane is also a fuel with practical applications as for example in race cars both pure [8] or mixed, commonly with methanol [9]. When added to gasoline or surrogate fuels, nitromethane reduces motor and research octane numbers [10], and may reduce soot formation at certain conditions [11]. Fells and Rutherford investigated the effect of nitromethane addition to methane + air mixtures (up to 3% of the total flow) and observed an increase or decrease of the burning velocity in lean and rich flames, respectively [12]. Relative modification of the burning velocity, though, was rather modest as compared to other additives studied, that was discussed in terms of a dual fuel-oxidant action of nitromethane due to its own oxygen content.

Remarkably, different stoichiometric equations for decomposition and oxidation of nitromethane coexist in the literature. In engine-oriented studies [8,9,13,14] and earlier studies of the thermal decomposition, e.g., [3], it was assumed that molecular nitrogen is the final

product as:



It was, however, soon realized that thermal decomposition both at moderate [4] and high [5] temperatures mostly produces NO, not  $\text{N}_2$ , according to equation



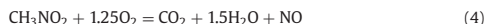
Formation of NO as a stable product of nitromethane self-ignition was supported in the modelling of Guirguis et al. [15]. However, the mechanism of Boyer and Kuo [2] predicted that for liquid nitromethane burning without the presence of  $\text{O}_2$ , NO formed would act as an oxidizer and be consumed for pressures above 3 MPa. The authors claimed good agreement with their own and literature experimental results [16] on the burning rates up to 15 MPa. The simulations [2] revealed three separate reactions zones of the process. The consumption of nitromethane takes place in the first reaction zone, forming radicals and intermediates reacting in the following two zones. Interestingly, two clearly separated zones have been observed in nitromethane + oxygen and in nitromethane + air premixed flames stabilized at about 0.1 atm [17].

The very first measurements of the laminar burning velocity of  $\text{CH}_3\text{NO}_2 + \text{O}_2 + \text{N}_2$  mixtures with variable ratio of  $\text{CH}_3\text{NO}_2/(\text{CH}_3\text{NO}_2 + \text{O}_2)$  and different dilution by nitrogen have been performed using Bunsen burner and Schlieren imaging at atmospheric

\* Corresponding author.

E-mail address: [alexander.konnov@forbrf.lth.se](mailto:alexander.konnov@forbrf.lth.se) (A.A. Konnov).

pressure [18]. Flame temperatures were measured employing sodium line reversal method to investigate apparent activation energy of the flame propagation. De Jaegere and van Tiggelen [18] did not formulate the equivalence ratio, yet discussed that NO formed in the flames is not a reactive species. Explicit stoichiometric equation of nitromethane burning in the presence of O<sub>2</sub> and considering NO, CO<sub>2</sub> and H<sub>2</sub>O as the major products



was first used by Tian et al. [19]. In this work and its follow-up [20], the structure of stoichiometric and several rich nitromethane + O<sub>2</sub> + Ar flames at low pressures close to 4.66 kPa was studied using synchrotron photoionization and molecular beam mass-spectrometry. A number of intermediates, not observed in the previous studies of nitromethane combustion, were detected that prompted extension and development of the kinetic model by Glarborg et al. [1]. The mechanism advanced in these studies [19,20] and further extended for nitroethane low-pressure flames [21] was found in reasonable agreement with the experimental species profiles for low-pressure flames of nitromethane and nitroethane.

The model of Zhang et al. [21] is essentially a result of progressive improvement of the quantitative understanding of nitromethane combustion mechanism starting with early works of Perche et al. [22,23] devoted to nitromethane pyrolysis. The same authors [24] have subsequently extended this mechanism to simulate gas phase oxidation of nitromethane in a static vessel at moderate temperatures (700–740 K). Further model development was based on dedicated experiments in shock tubes [15,25–27] that brought up experimentally determined rate constants of the key pertinent reactions and led to construction of the mechanism by Glarborg et al. [1].

Several modifications to the mechanism of Zhang et al. [20] were made by Brequigny et al. [14], who measured laminar burning velocity of nitromethane + air flames at 423 K, within a pressure range from 0.5 to 3 bar. First, the rate constants of 26 reactions (most of them were not fuel-specific) were replaced by expressions taken from other publications of Glarborg and colleagues arguing that these modifications are required for the modelling at atmospheric and higher pressures. Second, the rate constants for three reactions were taken from other sources to improve the agreement of the model predictions with experimental data. They were:  $\text{HNO} + \text{O}_2 = \text{HO}_2 + \text{NO}$ ,  $\text{HCO} + \text{NO} = \text{HNO} + \text{CO}$  and  $\text{CH}_3 + \text{OH}$ . One should note that although reaction between methyl and hydroxyl radicals is cited by Brequigny et al. [14] as  $\text{CH}_3 + \text{OH} = \text{CH}_2\text{OH} + \text{H}$ , the products really implemented in the mechanism file are singlet methylene CH<sub>2</sub>(S) and H<sub>2</sub>O. The authors showed that modifications implemented did not deteriorate the ability of the mechanism in prediction of the species profiles in low-pressure flames of Zhang et al. [20].

Brequigny et al. [14] investigated and analysed pressure dependence of the laminar burning velocity of nitromethane + air flames at a fixed temperature. The goal of the present study was to determine  $S_L$  of nitromethane + air flames at 1 atm and different initial gas temperatures, to analyse its temperature dependence, and to compare with the data of Brequigny et al. [14]. Two mechanisms were tested and compared, those of Zhang et al. [21] and of Brequigny et al. [14].

## 2. Modelling details

The model of Brequigny et al. [14] contains 88 species and 701 reactions; it was used without modifications since mentioning of  $\text{CH}_2\text{OH} + \text{H}$  as the products of reaction between CH<sub>3</sub> and OH is an apparent misprint in the paper text. The model of Zhang et al. [21] contains 115 species and 729 reactions; it was obtained from the authors because the transport parameters associated with this mechanism have not been provided in the original publication.

The modelling was performed with CHEMKIN IV [28] using the premixed laminar flame speed calculation module. The parameters

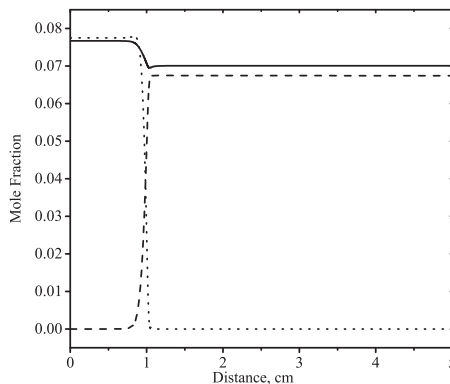


Fig. 1. Profiles of N<sub>2</sub> (solid line), NO (dashed line) and nitromethane (dotted line) in nitromethane + air flame at 358 K and  $\phi = 0.5$ , calculated using the mechanism of Brequigny et al. [14]. The concentration of N<sub>2</sub> is divided by a factor of 9.5.

GRAD = 0.03 and CURV = 0.02 were used, to ensure grid-independent solutions, with typical number of grid points above 900. Multicomponent transport and thermal diffusion options were taken into account. The modelling was performed over 8 cm domain, to ensure that wide reaction zones of nitromethane flames are covered in the modelling.

Laminar burning velocity is a fundamental property of a fuel + oxidizer mixture and is dependent only on equivalence ratio,  $\phi$ , pressure and temperature. In the present work the definition of equivalence ratio according to Eq. (4) is adopted. To prove that this is applicable not only to low-pressure flames [19,20], but is the only correct definition, flame structure of lean,  $\phi = 0.5$ , nitromethane + air flame with initial gas temperature of 358 K was calculated using the mechanism of Brequigny et al. [14]. Fig. 1 shows the calculated profiles of CH<sub>3</sub>NO<sub>2</sub>, N<sub>2</sub>, and NO in this flame having excess of oxygen to ensure complete oxidation. The NO and nitromethane profiles are at the same scale, while the N<sub>2</sub> profile is scaled down by a factor of 9.5 to facilitate comparison between them. The mechanism predicts negligible formation of N<sub>2</sub> in this flame; the small decrease in the mole fraction of nitrogen after the flame front in Fig. 1 is merely a diluting effect as the total number of species is increased, see Eq. (4). It is thus obvious that nitromethane is almost quantitatively converted into NO. Minor deficiency in the final NO concentration is due to re-burning, possible even in lean flames, e.g., [29].

## 3. Experimental details

The heat flux method was used to determine the laminar burning velocity of premixed nitromethane + air flames at atmospheric pressure and initial gas temperatures of 338 K, 348 K and 358 K. The flames were studied over the equivalence ratio range of 0.8–1.6. The partial vapour pressure of nitromethane limits the lower experimental unburnt gas temperature to 338 K.

The principle behind the heat flux method is a thermodynamic exchange of heat between the burner plate, flame and unburnt gas [30]. Cross-section of the burner head comprising all essential elements is shown in Fig. 2. The burner has a plenum chamber and a heated perforated burner plate of brass with 0.5 mm diameter holes. The temperature of the unburnt gas and the burner plate is controlled by water baths. The unburnt gas temperature was varied, while the burner plate was kept at 368 K.

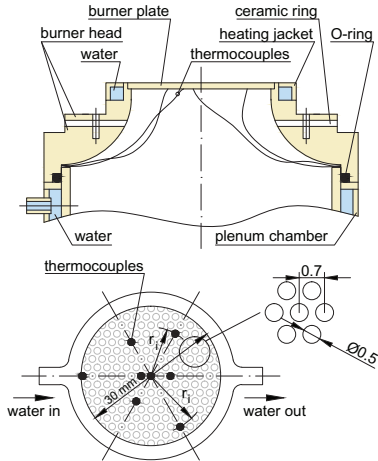


Fig. 2. Cross-section and top view of the heat flux burner head.

It has been shown that the temperature distribution over the burner plate reflects the adiabatic state of the flame [30]. By heating the burner plate the flame can be stabilized at unburnt gas velocities,  $V_g$ , above and below the adiabatic laminar burning velocity. Gas mixture velocities lower than the adiabatic laminar burning velocity yield a higher heat gain from the flame than the heat loss to the unburnt gas, and vice versa for velocities higher than the adiabatic velocity. Under the conditions of the gas mixture velocity equal to the adiabatic burning velocity, there is no net heat transfer and the temperature within the burner plate is uniform. Thus, through monitoring the burner plate temperature, the laminar burning velocity can be determined. Thermocouples of type T are mounted in the perforation holes at different radii from the centre of the burner plate,  $r$ , see Fig. 2. Temperature readings from the thermocouples are fitted to the form [30]

$$T = T_c + Cr^2 \quad (5)$$

A typical procedure of measurements of the burning velocity consists in determination of the parabolic coefficient,  $C$ , as a function of unburnt gas velocity,  $V_g$ . This is illustrated in Fig. 3, which shows experimental temperature profiles approximated by parabolic fits (Eq. (5)) for  $V_g$  lower than  $S_L$  ( $V_g = 27.5$  cm/s,  $C = -0.131$  K/mm<sup>2</sup>), close to  $S_L$  ( $V_g = 29.5$  cm/s,  $C = -0.007$  K/mm<sup>2</sup>), and higher than  $S_L$  ( $V_g = 29.8$  cm/s,  $C = 0.012$  K/mm<sup>2</sup>). Setting points of  $V_g$  are taken close to the adiabatic laminar burning velocity and a linear relationship between the parabolic coefficient,  $C$ , and  $V_g$  is used to determine the adiabatic laminar burning velocity at  $C = 0$ , as shown in Fig. 4. Typically at least four different setting points of  $V_g$  were chosen for each laminar burning velocity measured. These measurement points were sampled more than three times. For all measurements,  $C$  was linearly dependent on the gas velocity. Data collected at initial gas temperature of 338 K can be processed via interpolation, as shown in Fig. 4, and the burning velocity is then directly obtained at the location of  $C = 0$ . Due to tendencies of cell formation at adiabatic ( $C = 0$ ) and super-adiabatic (positive  $C$ ) conditions of rich flames, sometimes extrapolation from sub-adiabatic conditions has to be used. Extrapolation procedure is also illustrated in Fig. 4 for initial gas temperature of 358 K. Parabolic coefficients,  $C$ , were recorded at sub-adiabatic conditions only; thus they are all negative. The extrapolation

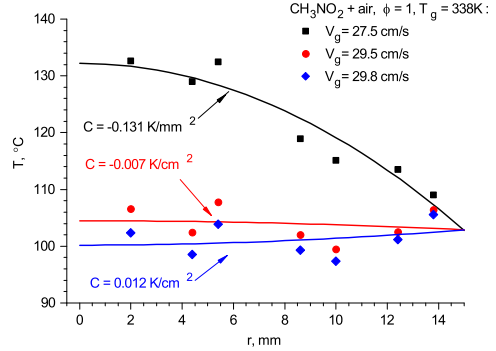


Fig. 3. Temperature distribution in the burner plate for stoichiometric nitromethane + air flame at different gas velocities. Symbols: experimental, lines: parabolic fits with Eq. (5).

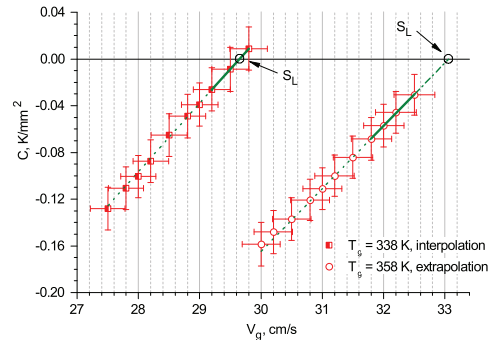


Fig. 4. Determination of  $S_L$  from the dependences of  $C$  ( $V_g$ ) in stoichiometric nitromethane + air flames having different initial gas temperatures.

procedure assumes that dependence of the  $C$  coefficient, Eq. (5), from the unburnt gas velocity  $V_g$  is linear at least close to  $C = 0$ , where the adiabatic laminar burning velocity is found. This linearity was experimentally confirmed even for a larger range of  $V_g$  variation, see Fig. 4.

For the measurements at the unburnt gas temperature of 338 K, only  $\phi = 1.2$  required extrapolation. The extent of the extrapolation was 0.59 cm/s from the closest setting of  $V_g$  to the laminar burning velocity. All measurement points at 348 K, except  $\phi = 0.8$  and 1.0, required extrapolation within a range of 0.12–1.17 cm/s. At the highest unburnt gas temperature, 358 K, all laminar burning velocities were obtained from extrapolation. The extrapolation was extended 0.01–0.99 cm/s from the closest setting of  $V_g$  to the laminar burning velocity. The extrapolation to find  $C = 0$  results in a larger standard deviation compared to the interpolation procedure, but in the present work this increase was found to be negligible compared to the overall experimental uncertainty, which was typically below  $\pm 0.5$  cm/s.

In Fig. 5, a schematic drawing of the experimental setup is presented. The gas flows are controlled by mass flow controllers, MFC from Bronkhorst. The flow of the fuel is controlled by a Mini Cori-Flow MFC, then the fuel is evaporated in a controlled evaporator mixer, CEM (both from Bronkhorst). To ensure and verify the accuracy of the flow, the MFC used for the oxidizer (air) was calibrated with a piston

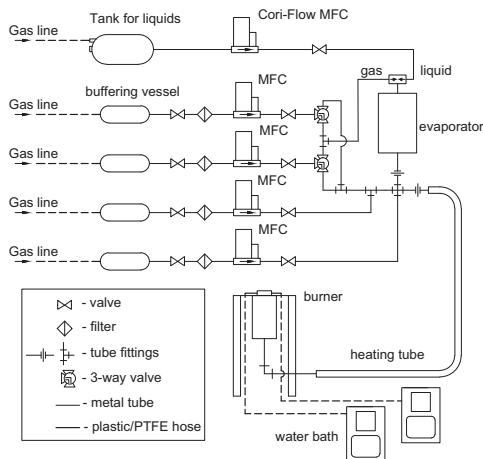


Fig. 5. A schematic overview of the experimental setup.

meter, Definer 220 (Bios DryCal Tech.). From the calibration a third degree polynomial was obtained and used to calculate the gas flow settings for the oxidizer. Experimental uncertainties in both equivalence ratio and in the determined burning velocity are defined by the accuracy of the MFCs and by the scattering of the thermocouple readings. Extended discussion of these experimental uncertainties as well as of the data processing is available elsewhere [31–33].

## 4. Results and discussion

### 4.1. Flat flames

The laminar burning velocities of nitromethane + air flames determined in the present study with associated experimental uncertainties can be seen in Fig. 6 and listed in Table 1. In the present work

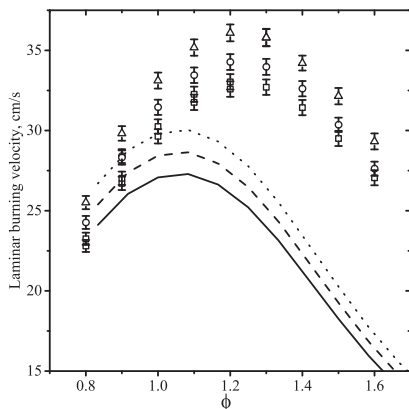


Fig. 6. Laminar burning velocity vs.  $\phi$  for flat nitromethane + air flames. Symbols: present experiments, lines: predictions of the model of Zhang et al. [21]. Solid lines: 338 K, dashed lines: 348 K, dotted lines: 358 K. Squares: 338 K, circles: 348 K, triangles: 358 K.

Table 1  
Experimental laminar burning velocities in cm/s at 338 K, 348 K, and 358 K, and the power exponent  $\alpha$ .

$\phi$	338 K	348 K	358 K	$\alpha$
$0.8 \pm 0.011$	$23.25 \pm 0.38$	$24.27 \pm 0.41$	$25.51 \pm 0.41$	$1.78 \pm 0.34$
$0.8 \pm 0.011$	$22.80 \pm 0.38$	–	–	–
$0.9 \pm 0.012$	$27.03 \pm 0.42$	$28.41 \pm 0.43$	$29.82 \pm 0.45$	$1.82 \pm 0.32$
$0.9 \pm 0.012$	$26.71 \pm 0.42$	$28.32 \pm 0.43$	–	–
$1.0 \pm 0.014$	$30.25 \pm 0.45$	$31.45 \pm 0.47$	$33.12 \pm 0.50$	$1.75 \pm 0.31$
$1.0 \pm 0.014$	$29.64 \pm 0.44$	–	–	–
$1.1 \pm 0.015$	$32.26 \pm 0.48$	$33.45 \pm 0.48$	$35.18 \pm 0.51$	$1.63 \pm 0.31$
$1.1 \pm 0.015$	$31.76 \pm 0.48$	–	–	–
$1.2 \pm 0.016$	$33.04 \pm 0.48$	$34.27 \pm 0.49$	$36.09 \pm 0.53$	$1.64 \pm 0.31$
$1.2 \pm 0.016$	$32.59 \pm 0.48$	–	–	–
$1.3 \pm 0.018$	$32.70 \pm 0.48$	$33.97 \pm 0.50$	$35.79 \pm 0.54$	$1.60 \pm 0.31$
$1.3 \pm 0.018$	–	–	$35.80 \pm 0.54$	–
$1.4 \pm 0.019$	$31.43 \pm 0.48$	$32.61 \pm 0.47$	$34.21 \pm 0.47$	$1.47 \pm 0.36$
$1.5 \pm 0.020$	$29.51 \pm 0.47$	$30.36 \pm 0.45$	$32.15 \pm 0.51$	$1.49 \pm 0.39$
$1.6 \pm 0.022$	$27.06 \pm 0.47$	$27.62 \pm 0.44$	$29.32 \pm 0.50$	$1.40 \pm 0.42$

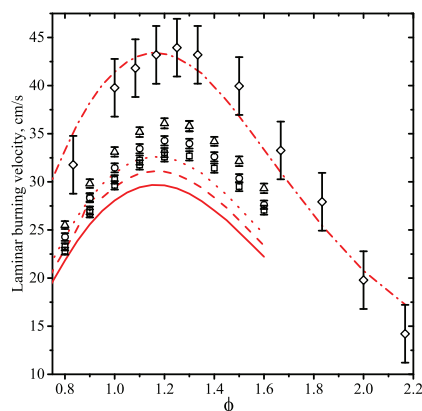


Fig. 7. Laminar burning velocity vs.  $\phi$  for nitromethane + air flames. Symbols: experiments, lines: predictions of the model of Brequigny et al. [14]. Solid lines: 338 K, dashed lines: 348 K, dotted lines: 358 K, dash-dot line: 423 K. Squares: 338 K, circles: 348 K, triangles: 358 K, all present study; diamonds: 423 K [14].

the definition of equivalence ratio according to Eq. (4) is adopted. To check the repeatability of the experimental setup, two separate series of measurements have been performed at 338 K, both are presented in Table 1. For the case of  $\phi = 0.9$  at 348 K and  $\phi = 1.3$  at 358 K two values are presented in the table, in these cases the two measurements were conducted on the same day. The two different datasets at 338 K, as well as the datapoints repeated within the measurement series at 348 K and 358 K, were found consistent within overlapping uncertainties. The maximum laminar burning velocity was found at  $\phi = 1.2$  for all three temperature series.

Brequigny et al. [14] used the definition of equivalence ratio according to Eq. (2) and found the maximum burning velocity at  $\phi$  around 0.75 that inspired an extended discussion of possible reasons of this unexpected behaviour. When their equivalence ratios are recalculated according to Eq. (4), the maximum is shifted towards rich flames close to  $\phi = 1.25$ , in qualitative agreement with the present data. These measurements obtained from spherically propagating flames at 423 K and 1 bar are shown in Fig. 7 with "statistical errors" [14] of  $\pm 3$  cm/s.

The burning velocities calculated using two mechanisms, [21,14], are presented in Figs. 6 and 7, respectively, together with the experimental data. The model of Zhang et al. [21] significantly under

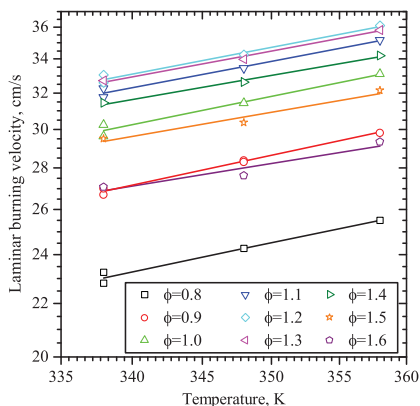


Fig. 8. Laminar burning velocities of nitromethane + air flames in a log–log scale.

predicts experimental results at all conditions except fortuitous coincidence at  $\phi = 0.8$ , and shows a maximum at  $\phi = 1.1$ , which is shifted towards the lean side as compared to the present data. The model of Brequigny et al. [14] shows better agreement in reproducing the variation of the burning velocities determined in the present work with equivalence ratio; yet significant underprediction is seen in all rich mixtures. This model was tuned to match experimental data at initial temperature of 423 K at 1 bar (Fig. 7) and other pressures in the range 0.5–3 bars [14]. Thus, through direct comparison of the kinetic modeling and two independent sets of measurements shown in Fig. 7, one may conclude that either the mechanism of Brequigny et al. [14] does not reproduce temperature dependence of nitromethane burning velocity, or experimental datasets are inconsistent for some reason.

Analysis of the temperature dependence of the burning velocity is an efficient tool for comparison of measurements performed at different temperatures. In addition, the analysis may reveal possible deficiencies in the ability of the model [14] to predict laminar burning velocities for temperatures other than 423 K that it was initially developed for. To evaluate the effect of initial gas temperature on the laminar burning velocity, the following empirical equation is commonly used

$$S_L = S_{L0}(T/T_0)^\alpha \quad (6)$$

where  $S_{L0}$  denotes the burning velocity at a reference temperature,  $T_0$ , in the present study set to 338 K. It follows from Eq. (6) that, when plotted on a log–log scale as a function of temperature,  $S_L$  should follow a linear trend and the slope of the linear relations results in the power exponent,  $\alpha$ . Figure 8 presents the burning velocities determined in the present study, and indeed illustrates linear trends at all equivalence ratios and temperatures covered.

The power exponents derived from the slope of the linear regressions for each measured  $\phi$  are shown in Fig. 9 and listed in Table 1. The error bars associated with the power exponents were calculated by taking the uncertainty of each burning velocity value (see Table 1) as well as the uncertainty of the least squares fit into account. Transitional slopes,  $\alpha_i$ , were calculated by changing each experimental value of  $S_L$  to its uncertainty limit,  $\Delta S_L$ . To evaluate the contribution of the uncertainties in the laminar burning velocity, the original power exponent,  $\alpha_0$ , is subtracted from each transitional  $\alpha_i$ , which

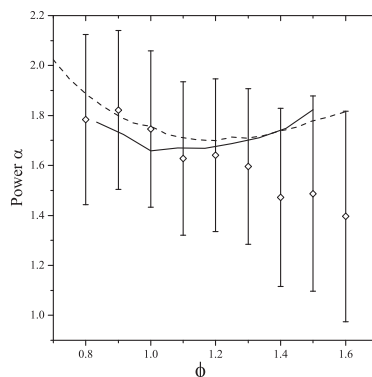


Fig. 9. Power exponents  $\alpha$  vs.  $\phi$  for nitromethane + air flames. Symbols with error bars: present experiments. Lines: model predictions. Solid line: [21], dashed line: [14].

yields  $\Delta\alpha(S_{Li})$ . The total uncertainty can then be written as [32]

$$\Delta\alpha = \sqrt{\sum_i [\Delta\alpha(S_{Li})]^2} \quad (7)$$

Also shown in Fig. 9 are the power exponents derived from the calculations using the mechanisms of Zhang et al. [21] and of Brequigny et al. [14]. The models predict similar values of  $\alpha$ , in contrast to the very different values of  $S_L$ , as shown in Figs. 6 and 7. This is not surprising and has been earlier observed for methane [34], ethanol [35], methyl formate [32] and other fuels. Christensen et al. [32] analysed why the mechanisms showing large difference in prediction of the burning velocities can be very close with respect to the prediction of the power exponents  $\alpha$ . It was explained by the fact that normalized sensitivity coefficients for  $\alpha$  are roughly one order of magnitude smaller than commonly used normalized sensitivity coefficients for the burning velocity.

The experimental power exponents do not contradict to those derived from the modelling from lean to moderately rich mixtures, Fig. 9. Together with the robustness and insensitivity of two different mechanisms in calculation of the power exponents  $\alpha$ , this strongly indicates that the models are not deficient in predicting the temperature dependence of nitromethane flames. Discrepancies of the modelling and present experiments seen in Fig. 7, are then, likely, due to their inconsistency with the measurements in spherical flames [14].

Experimental linear regressions for each measured  $\phi$  (Fig. 8) can be extrapolated up to 423 K. These extrapolated values, in the following called “expected  $S_L$ ”, possess somewhat higher uncertainty than the present measurements (typically  $\pm 0.5$  cm/s) due to rather narrow temperature range covered (20 K) and its extension by 75 K. The uncertainty of the expected  $S_L$  shown in Fig. 10 is thus evaluated to be  $\pm 1.5$ –2 cm/s and even higher at  $\phi > 1.4$ . In fact, extrapolation of the measurements performed at lower temperatures up to 423 K does not require multiple datasets (at 338, 348 and 358 K), but can be done from experimental data at one temperature guided by kinetic modelling over a wider temperature range. For instance,  $S_L(423\text{ K})$  can be obtained using Eq. (6) with the present experimental data at 338 K as the reference ( $T_0, S_{L0}$ ) combined with calculated values of the power exponent  $\alpha$  predicted by the mechanism of Brequigny et al. [14]. These  $S_L$  values, in the following called “expected  $S_L$  set 2”, are shown in Fig. 10. The difference between two sets of expected  $S_L$  does not exceed 1.2 cm/s thus confirming consistency of

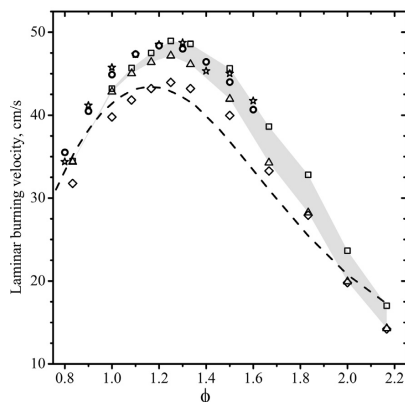


Fig. 10. Comparison of the original measurements (diamonds) and model prediction (line) from Brequigny et al. [14] with expected  $S_L$  (stars), expected  $S_L$  set 2 (circles), and recalculated with expansion ratios  $\epsilon_{6.5}$  (squares) and  $\epsilon_{20}$  (triangles).

the present measurements and validity of comparison through extrapolation. Two sets of expected  $S_L$  at 423 K are obviously higher than both experimental data and model predictions of Brequigny et al. [14] in lean, stoichiometric and moderately rich mixtures. This inconsistency prompted for the analysis of experimental limitations of the measurements performed in spherical flames [14] as described below.

#### 4.2. Spherical flames

Experiments in spherical flames have been performed and described by Brequigny et al. [14]. Contemporary procedure for determination of the burning velocity in spherical flames consists of the following steps: (a) measurements of the flame propagation speed within chosen range of radii; (b) extrapolation of these speeds towards unstretched flame speed,  $V_0$ , using linear or non-linear theoretical models; (c) the burning velocity is then obtained multiplying  $V_0$  by the expansion factor,  $\epsilon$ , defined as the ratio of the densities of product gas,  $\rho_p$ , and fresh mixture,  $\rho_u$

$$\epsilon = \rho_p / \rho_u \quad (8)$$

In the work of Brequigny et al. [14] the measurements were limited to the range of radii [36] (not diameters, as stated in the paper) from 6.5 till 20 mm. The data at smaller and larger radii were ignored, since they may be affected by ignition spark, or by pressure rise in the vessel, respectively. The appropriateness of the selected range was not explored further, and probably reflects the best practice choice based on previous studies. Non-linear model for stretch correction proposed by Kelly and Law [37] was implemented to determine the unstretched flame speed,  $V_0$ . Finally, the expansion factor  $\epsilon$  was determined [14] using EQUIL code [38], which calculates thermodynamic equilibrium essentially corresponding to the flame conditions at  $\pm$  infinity, not accessible in real experiments. Such a procedure, combined with the limited range of radii investigated, assumes that flame thickness is much smaller than 6.5 mm and combustion is thus complete. This premise can easily be checked by numerical modelling. Figure 11 shows calculated temperature profiles for nitromethane flames with initial temperature of 423 K at 1 atm at different equivalence ratios using the model of Brequigny et al. [14]. Interestingly, rich flames clearly exhibit two separate reaction zones observed earlier in low-pressure flames by Hall and Wolfhard [17].

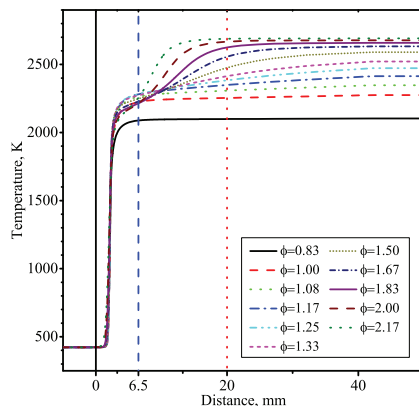


Fig. 11. Calculated temperature profiles for nitromethane + air flames with initial temperature of 423 K at 1 atm at different equivalence ratios using the model of Brequigny et al. [14].

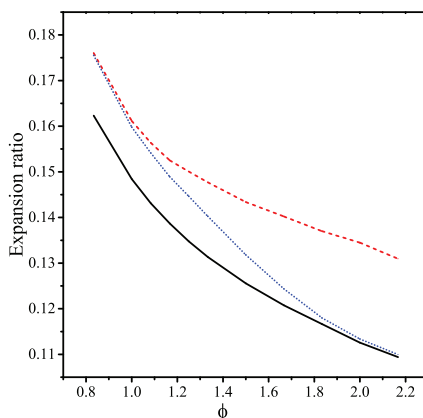


Fig. 12. Expansion ratios in nitromethane + air flames with initial temperature of 423 K at 1 atm. Solid line: equilibrium values [14], dashed line:  $\epsilon_{6.5}$ , dotted line:  $\epsilon_{20}$ .

Even more important, the temperature profiles are not levelled off in atmospheric pressure flames neither at 6.5 mm, nor at 20 mm.

To quantify an impact of incomplete combustion on the real density of the burned gases, the expansion ratio was calculated at the limiting distances for each  $\phi$ . The cold boundary, at which  $\rho_u$  is taken, was defined as the point in the flame where the density is decreased by a factor of  $(1 + 10^{-6})$ . Two new expansion ratios were calculated at the limits of the experimental boundaries, 6.5 mm ( $\epsilon_{6.5}$ ) and 20 mm ( $\epsilon_{20}$ ) from the cold boundary, as indicated in Fig. 11 by vertical lines. The calculated expansion ratios are compared to those implemented by Brequigny et al. [14] in Fig. 12. All expansion factors are decreasing as the flames become richer. There is a substantial deviation of both expansion ratios,  $\epsilon_{6.5}$  and  $\epsilon_{20}$ , from the original equilibrium values used in [14].

In attempt to reconcile the expected  $S_L$  values at 423 K obtained from the temperature dependence of flat flames (Fig. 10) and the

measurements performed in spherical flames, the unstretched flame speeds  $V_0$  from Brequigny et al. [14] were multiplied by the expansion ratios  $\varepsilon_{6.5}$  and  $\varepsilon_{20}$ , as shown in Fig. 10. The recalculated values indicate the limits of where the actual laminar burning velocity most probably can be found. This area is highlighted in Fig. 10 as a grey area. Remarkably good agreement between the expected  $S_L$  values and those recalculated is seen from stoichiometric to moderately rich flames around maximum burning velocity at 423 K. The recalculated burning velocities, however, have large uncertainty, especially in rich mixtures due to considerable difference between  $\varepsilon_{6.5}$  and  $\varepsilon_{20}$ . The reconsideration of the expansion ratios described above is straightforward if linear stretch correction for the data processing was employed, since the variation of the observable flame speed versus stretch is simply scaled up. When non-linear model of the stretch correction is considered, the dependence of the observable flame speed on the stretch is not linear [37]. Modification of the effective expansion ratios along this dependence can be manifested in the change of its curvature that in turn can introduce additional error in extrapolation toward  $V_0$ .

Predictions of the Brequigny et al. [14] mechanism are consistently lower than corrected or expected  $S_L$  values in spherical flames (Fig. 10), as well as the burning velocities determined in flat flames (Fig. 7). Although the measurements of de Jaegere and van Tiggelen [18] were performed in Bunsen flames, and no stretch or variable curvature corrections were considered, they were tentatively modelled using the same mechanism. The calculated laminar burning velocity of  $\text{CH}_3\text{NO}_2 + \text{O}_2 + \text{N}_2$  mixtures with variable ratio of  $\text{CH}_3\text{NO}_2/(\text{CH}_3\text{NO}_2 + \text{O}_2)$  and different dilution by nitrogen were found lower by 40–60% than the measurements.

## 5. Conclusions

The laminar burning velocities of nitromethane + air flames at 1 atm and initial gas temperatures of 338 K, 348 K, and 358 K were determined in non-stretched flat flames using the heat flux method. The comparison of these new experimental data and recent literature results obtained in spherical flames at 423 K [14] was guided by the analysis of the temperature dependence of  $S_L$ , and also by kinetic modelling of premixed flames employing detailed mechanisms of Zhang et al. [21] and of Brequigny et al. [14]. It was demonstrated that conventional recalculation of the flame front speed into the burning velocity using density ratio of the unburned and burned gases at equilibrium is inappropriate for spherical nitromethane flames since the flame thickness is comparable to the range of flame radii covered experimentally. The measurements in flat and spherical flames were reconciled using calculated density ratios, yet with rather high uncertainty. Both kinetic mechanisms tested [14,21] significantly under predict the laminar burning velocities of nitromethane + air flames. It should also be noted that burning velocities derived from spherical flames [14] and recalculated using modified expansion ratios  $\varepsilon_{6.5}$  and/or  $\varepsilon_{20}$  cannot be considered as ultimately corrected values; original raw data ( $r - t$  traces) should be re-processed and other sources

of uncertainty pertinent to spherical flames [39] should be taken into account as well.

## Acknowledgements

The authors would like to acknowledge the financial support from the Centre for Combustion Science and Technology (CECOST), and Swedish Research Council (VR) via Grant 621-2010-4975. The help and valuable discussions of M. Christensen and V.A. Alekseev are gratefully acknowledged.

## References

- [1] P. Glarborg, A.B. Bendtsen, J.A. Miller, *Int. J. Chem. Kinet.* 31 (1999) 591–602.
- [2] E. Boyer, K.K. Kuo, *Proc. Combust. Inst.* 31 (2007) 2045–2053.
- [3] H.A. Taylor, V.V. Vessilovsky, *J. Phys. Chem.* 39 (1934) 1095–1101.
- [4] L.J. Hillenbrand, M.L. Kilpatrick, *J. Chem. Phys.* 21 (1953) 525–535.
- [5] J.N. Bradley, *Trans. Faraday Soc.* 57 (1961) 1750–1756.
- [6] A. Perche, J.C. Tricot, M. Lucquin, *J. Chem. Res.-S* (1979) 116–117.
- [7] R. Menikoff, M.S. Shaw, *Combust. Flame* 158 (2011) 2549–2558.
- [8] E.S. Starkman, *Ind. Eng. Chem.* 51 (1959) 1477–1480.
- [9] G.J. Germane, A technical review of automotive racing fuels, SAE Technical Paper Series, SAE 852129, 1985.
- [10] R.F. Cracknell, J.C.G. Andrae, L.J. McAllister, M. Norton, H.L. Walmsley, *Combust. Flame* 156 (2009) 1046–1052.
- [11] T. Gl nzler, M. Collet, M. Kahandawala, S.-Y. Lee, D. Liscinsky, K. McNesby, R. Pawlik, M. Roquemore, R. Santoro, S. Sidhu, S. Stouffer, *Combust. Sci. Technol.* 183 (2011) 739–754.
- [12] I. Fells, A.G. Rutherford, *Combust. Flame* 13 (1969) 130–138.
- [13] Q. Zhang, W. Li, D.-C. Lin, N. He, Y. Duan, J. Hazard. Mater. 185 (2011) 756–762.
- [14] P. Brequigny, G. Dayma, F. Halter, C. Mounaim-Rousselle, T. Dubois, P. Dagaut, *Proc. Combust. Inst.* 35 (2015) 703–710.
- [15] R. Guirguis, D. Hsu, D. Bogan, E. Oran, *Combust. Flame* 61 (1985) 51–62.
- [16] S. Kelzenberg, N. Eisenreich, W. Eckl, V. Weiser, *Propellants Explosives Pyrotechn.* 24 (1999) 189–194.
- [17] A.R. Hall, H.G. Wolfhard, *Symp. (Int.) Combust.* 6 (1957) 190–199.
- [18] S. De Jaegere, A. Van Tiggelen, *Combust. Flame* 3 (1959) 187–200.
- [19] Z.Y. Tian, L.D. Zhang, Y.Y. Li, T. Yuan, F. Qi, *Proc. Combust. Inst.* 32 (2009) 311–318.
- [20] K.W. Zhang, Y.Y. Li, T. Yuan, J.H. Cai, P. Glarborg, F. Qi, *Proc. Combust. Inst.* 33 (2011) 407–414.
- [21] K. Zhang, L. Zhang, M. Xie, L. Ye, F. Zhang, P. Glarborg, F. Qi, *Proc. Combust. Inst.* 34 (2013) 617–624.
- [22] A. Perche, J.C. Tricot, M. Lucquin, *J. Chem. Res.-S* (1979) 304–305.
- [23] A. Perche, M. Lucquin, *J. Chem. Res.-S* (1979) 306–307.
- [24] J.C. Tricot, A. Perche, M. Lucquin, *Combust. Flame* 40 (1981) 269–291.
- [25] K. Gl nzler, J. Troe, *Helvet. Chim. Acta* 55 (1972) 2884–2893.
- [26] D.S.Y. Hsu, M.C. Lin, *J. Energ. Mater.* 3 (1985) 95–127.
- [27] Y.X. Zhang, S.H. Bauer, *J. Phys. Chem. B* 101 (1997) 8717–8726.
- [28] CHEMKIN IV 15101, Reaction Design: San Diego, 2010.
- [29] D.A. Knyazkov, A.G. Shmakov, I.V. Dyakov, O.P. Korobinichev, J. De Ruyck, A.A. Konnov, *Proc. Combust. Inst.* 32 (2009) 327–334.
- [30] K.J. Bosschaert, L.P.H. de Goeij, *Combust. Flame* 132 (2003) 170–180.
- [31] J.D. Nauc ler, L. Sileghem, E.J.K. Nilsson, S. Verhelst, A.A. Konnov, *Combust. Flame* 162 (2015) 1719–1728.
- [32] M. Christensen, E.J.K. Nilsson, A.A. Konnov, *Fuel* 157 (2015) 162–170.
- [33] V.A. Alekseev, J.D. Nauc ler, M. Christensen, E.J.K. Nilsson, A.A. Konnov, Experimental uncertainties of the heat flux method for measuring burning velocities, In preparation.
- [34] A.A. Konnov, *Fuel* 89 (2010) 2211–2216.
- [35] A.A. Konnov, R.J. Meuwissen, L.P.H. de Goeij, *Proc. Combust. Inst.* 33 (2011) 1011–1019.
- [36] P. Brequigny, *Person. Commun.* (2014).
- [37] A.P. Kelly, C.K. Law, *Combust. Flame* 156 (2009) 1844–1851.
- [38] Equil: A Chemkin Implementation of Stanjan for Computing Chemical Equilibria, Sandia National Laboratories, Livermore, CA, 1992, p. 94551.
- [39] Z. Chen, *Combust. Flame* 162 (2015) 2442–2453.



## Paper IV





## Full Length Article

An experimental and modeling study of nitromethane + O<sub>2</sub> + N<sub>2</sub> ignition in a shock tubeJ.D. Nauclér<sup>a,\*</sup>, Y. Li<sup>b</sup>, E.J.K. Nilsson<sup>a</sup>, H.J. Curran<sup>b</sup>, A.A. Konnov<sup>a</sup><sup>a</sup> Division of Combustion Physics, Department of Physics, Lund University, Lund, Sweden<sup>b</sup> Combustion Chemistry Centre, National University of Ireland, Galway, Ireland

## ARTICLE INFO

## Article history:

Received 18 April 2016

Received in revised form 20 July 2016

Accepted 2 September 2016

## Keywords:

Nitromethane

Multistage ignition

Modeling

## ABSTRACT

The ignition of nitromethane/O<sub>2</sub>/N<sub>2</sub> mixtures was investigated via shock tube experiments in the temperature range 947–1333 K at reflected shock pressures near 8, 16 and 32 atm. The ignition was recorded as the intensity maxima of unfiltered luminosity in the range 240–530 nm. Under the experimental conditions of the present study, ignition was found to proceed via a two stage process. Dependencies on concentration, pressure and temperature were examined and discussed. The two ignition stages were separated in time, with individual concentration and temperature dependence. The two experimentally determined ignition stages were found to be pressure independent over the pressure range investigated. The activation energy was derived to be  $16.15 \pm 1.57$  kcal mol<sup>-1</sup> for the first stage ignition and  $20.89 \pm 0.82$  kcal mol<sup>-1</sup> for the second stage. Modeling using the mechanism by Brequigny et al., published in Proceedings of the Combustion Institute (2014) 703–710, could predict the magnitude of the ignition delay times at 8 atm, but it could not reproduce the temperature dependence of the first stage ignition or the pressure independence of both ignition stages. The measurements are discussed in relation to data from the literature.

© 2016 Elsevier Ltd. All rights reserved.

## 1. Introduction

Nitromethane, CH<sub>3</sub>NO<sub>2</sub>, is a simple nitrogen containing fuel, which is used in mixtures with methanol or as a pure fuel in racing cars and in model engines [1]. It is also considered as a fuel additive [2–4] in engines, promoting their efficiency and reducing soot from their exhaust. Because of the oxygen content in the molecule, nitromethane can act as both a fuel and as an oxidizer in combustion processes, as noted in the study by Fells and Rutherford [5], where the effect of nitromethane addition on the burning rate of methane flames was investigated. These dual fuel-oxidizer properties motivate studies of combustion characteristics of nitromethane as a single component as well as in mixtures with other oxidizers. Due to its potential as a monopropellant [6], nitromethane has been extensively studied, focusing on thermal decomposition [7–17], and detonation [18–22]. The combustion chemistry of nitromethane is also of interest from a fundamental research viewpoint since it is the simplest representative for fuel-nitrogen species, and as such can facilitate understanding of

the reactions relevant to the mutually sensitized oxidation of hydrocarbons and nitrogen oxides [11].

The decomposition of nitromethane has been investigated mainly by kinetic studies of its thermal decomposition in shock tubes [11–17,23]. A common experimental approach is to track the formation of NO<sub>2</sub>, and it is well established that NO<sub>2</sub> + CH<sub>3</sub> are the significant decomposition products that then undergo further reactions [12,13,16]. It was experimentally shown by Zaslonko et al. [12] that in the temperature and pressure ranges 1030–1580 K and 1.0–2.8 atm, the thermal decomposition produced CH<sub>3</sub>O and CH<sub>3</sub>ONO. The latter was explained as the result of recombination of CH<sub>3</sub> and NO<sub>2</sub>. In the thermal decomposition study of Hsu and Lin [15] NO and CO profiles were measured in the temperature range 940–1520 K at pressures 0.4–1 atm. From the NO and CO profiles the authors showed that NO is formed early during ignition, while CO is formed at a later stage. Kuznetsov et al. [16] monitored the formation of NO<sub>2</sub> in nitromethane decomposition through shock tube experiments in the temperature range 1190–1490 K at 1.5 atm. The authors confirmed that the NO<sub>2</sub> profile had a convex shape consistent with a typical decomposition product, and that the disappearance of nitromethane and the formation of NO<sub>2</sub> coincided. Through theoretical analysis it was also concluded that isomerization of nitromethane to CH<sub>3</sub>ONO was

\* Corresponding author at: P.O. Box 118, SE-221 00 Lund, Sweden.

E-mail address: [jenny.naucler@forbrf.lth.se](mailto:jenny.naucler@forbrf.lth.se) (J.D. Nauclér).

not competitive compared to thermal decomposition. The thermal decomposition of nitromethane has been shown to be pressure dependent in the pressure range of 0.1–40 atm [12,13,17,23].

An interesting aspect of nitromethane combustion is that experiments and modeling indicate that it proceeds via two or three steps; detonation has been shown to be a two-step process [19–22,24], a similar pattern is seen in low-pressure flames [25] and in the case of flames of liquid nitromethane three reaction zones have been identified [6].

From detonation studies it is known that fuels and mixtures containing NO<sub>2</sub> propagate in a double cellular structure [20–22,24]. Presles et al. [20,21] showed a sub-structure within the first part of the main cell during detonation of pure nitromethane and rich nitromethane/O<sub>2</sub> mixtures ( $1.3 < \phi < 1.75$ ) at 390 K and 0.05–1.7 bar. This sub-structure behaved independently of the main cell in terms of velocity and structure. Sturtzer et al. [19] compared their numerical results of pure nitromethane and nitromethane + O<sub>2</sub> detonation with the experimental results from Presles et al. [20,21]. It was suggested that the origin of the double cellular structure is an endothermic step of fuel decomposition into CH<sub>3</sub> and NO<sub>2</sub>, followed by two independent exothermic steps and attributed the reaction NO<sub>2</sub> + H = NO + H<sub>2</sub> as the main exothermic source in the first step of detonation.

Experimental and theoretical studies on nitromethane flames have shown a wide total reaction zone, with the chemistry divided into multiple separated zones [6,25]. By performing modeling studies Boyer and Kuo [6] identified three reaction zones in a pure liquid nitromethane flame at pressures of 3–6 MPa. Indications of a two stage ignition process for pure nitromethane were presented [14,26,27]. Guirguis et al. [27] noted that in their study of 100% nitromethane pyrolysis behind reflected shock waves, for some of the measurements there were two separated pressure spikes where the second was higher in intensity. The presence of a second pressure spike was however not given any further attention. In light of modeling results for flames from previous studies [6,28] and detonation studies [20–22,24], the second pressure spike could indicate that a second stage ignition occurred in the experiments of Guirguis et al. [27].

In the study by Hall and Wolfhard [25] multiple reaction zones in methyl- and ethyl nitrate, methyl nitrite and nitromethane flames were examined at low pressures. It was concluded that these flames had up to three separate reaction zones. The emission from the reaction zones was analyzed and characterized in terms of emitting species. A nitromethane/O<sub>2</sub> flame was analyzed at 323 K and ~0.1 atm, and two reaction zones were detected. A yellow undefined emission was observed in the first reaction zone, and it was argued by the authors that this was likely due to NO<sub>2</sub>. In the second reaction zone, emissions from C<sub>2</sub>, CH\*, CN\*, OH\*, NH\* and NO\* were identified. No emission from formaldehyde was observed for nitromethane/O<sub>2</sub> flames.

Laminar burning velocities of nitromethane/air flames have been determined using the Bunsen flame method [29], spherically expanding flames [30], and the heat flux method [28]. In the work of Nauc  r et al. [28] laminar burning velocities of nitromethane/air flames were measured using the heat flux method in the temperature range 338–358 K at pressure of 1 atm. The width of the reaction zone of these nitromethane flames was examined using modeling and implications for experimental determinations of laminar burning velocity were discussed. The modeling by Nauc  r et al. [28] implied that a two-stage process occurred.

Oxidation studies of nitromethane are not as numerous as compared to detonation and decomposition studies. Oxidation in a static vessel was investigated by Tricot et al. [31] by studying nitromethane explosion limits in the temperature range 700–740 K. Flame structure has been investigated in low-pressure nitromethane/O<sub>2</sub>/Ar flames [32,33].

The ignition of nitromethane in the presence of O<sub>2</sub> has been considered as a one-stage process in studies by Borisov et al. [14] and Kang et al. [26]. A two-stage process in the ignition of nitromethane/O<sub>2</sub> was indicated in the literature [34,35], and later shown by the authors of the present work [36] in a conference-publication for the 7th European Combustion Meeting 2015. The two-stage ignition process was independently confirmed by Mathieu et al. [37].

A shock tube study on nitromethane + O<sub>2</sub> + Ar at conditions of  $0.5 < \phi < 2$ , 875–1595 K and 1.71–35.8 atm, by Mathieu et al. [38], was published after the original submission of the present work. The study showed two ignition stages, detected by emission from OH\*. Ignition delay times were determined for the second ignition stage by both the maximum OH\* signal and the maximum gradient in the OH\* signal. A kinetic mechanism was presented, which performed satisfactorily for the conditions of the study. In addition, a correlation based on equivalence ratio and pressure at 90% and 98% Ar dilution was presented.

Borisov et al. [14] measured the autoignition of nitromethane/O<sub>2</sub> mixtures in a by-pass apparatus with the diluents Ar, N<sub>2</sub> and He at 700–1300 K in order to determine the rate constant for the thermal decomposition of nitromethane. Kang et al. [26] examined the ignition delay times of nitromethane/O<sub>2</sub>/Ar mixtures in a shock tube by tracking the von Neuman pressure spike in the temperature-range 1250–1900 K at a pressure of about 0.2 atm for several different nitromethane/O<sub>2</sub>/Ar compositions. A correlation between mixture composition and ignition delay times was presented by Kang et al. [26]. The overall activation energy was calculated to be  $21.36 \pm 0.51$  kcal mol<sup>−1</sup> through multiple regression analysis. The authors concluded that the presence of oxygen in the NO<sub>2</sub>-group in the fuel molecule reduced the role of O<sub>2</sub> as an ignition promoter compared to other hydrocarbon fuels. The decomposition of pure nitromethane, and its ignition in the presence of O<sub>2</sub> was investigated in a shock tube [34] and presented by Djebaili-Chaumeix et al. [35]. Absorption at 235 nm and emission at 235 nm and 306 nm were observed and treated as ignition delay times.

In summary based on the literature discussed above, nitromethane + O<sub>2</sub> ignition occurs in at least two stages. The work of Djebaili-Chaumeix et al. [35] showed that ignition begins with a rapid decomposition of nitromethane and, after a buildup of the radical pool, a second stage of oxidation of the decomposition products follows.

However, the two stages in ignition have not yet been examined and compared. As mentioned above the two-stage behavior was indicated by the present authors in a conference publication [36] where ignition delay times from a shock tube study in the temperature range of 947–1333 K and at pressures in the range 8–32 atm were presented. In the present paper, that study is discussed in detail. A characterization of the ignition of nitromethane/O<sub>2</sub> over time is conducted by studying pressure and luminosity profiles to understand the ignition process. Aspects of nitromethane ignition, such as pressure dependence and effects of fuel and oxidizer composition at the same equivalence ratio, are examined. A recent kinetic model developed for nitromethane flames [30] was used in an attempt to interpret the ignition characteristics.

## 2. Experimental details

Experiments were performed in a high-pressure shock tube at NUI Galway. The experimental setup is described in detail in the work of Nakamura et al. [39].

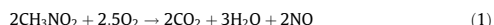
The experimental pressure profiles were recorded using two pressure transducers, one at the endwall and the other at the side wall, 10 mm from the endwall. The measurable time range in this

experimental setup is 4000  $\mu$ s. The ignition was tracked using unfiltered light emission from an optical window at the side wall, 10 mm from the endwall. The window is transparent within a wavelength range of 150–2000 nm and the emission was recorded with a Photodiode array detector (PDA) within the range 240–530 nm. Ignition delay times were measured from the time that the reflected shock wave triggered the pressure transducer at the endwall to the maximum intensities in the luminosity trace. This choice of ignition delay definition is further discussed in Section 4.1.

Four different gas compositions with varying fuel and O<sub>2</sub> content were studied, see Table 1. The gas mixtures were prepared and continuously stirred in a mixing tank at low pressure, at a temperature of 323 K. The shock tube driven section was maintained at the same temperature. Partial pressure was used to control the mixture compositions. An issue when working with nitromethane is the risk of condensation. To avoid this, the liquid nitromethane (Sigma-Aldrich Ireland Limited, 95% purity) was gradually injected into the mixing tank with close monitoring of the pressure. Between each injection the fuel was left to vaporize and equilibrate. The partial pressure of the nitromethane was kept about three times lower than the saturation pressure of nitromethane. The O<sub>2</sub> (99.5%) and N<sub>2</sub> (99.99%) were supplied by BOC Ireland Limited.

The experiments were performed in the temperature range 947–1333 K at approximately 8, 16 and 32 atm. As explained in detail later, the ignition of nitromethane was found to have two separate stages of ignition with the two stages observed to be pressure independent. Therefore experimental results with pressures deviating from the target pressure were included in the presentation of the experimental results. The pressures were within 90–105% of the target pressures, with larger deviations for Mixture 1 at 32 atm, with three deviating pressures at 38.8, 39.5 and 44.9 atm, and Mixture 3 at 8 atm, with two deviating pressure of 9.2 and 9.7 atm. All experimental measurements are available in tabulated form as Supplementary material.

Traditionally N<sub>2</sub> has been regarded as the final product for nitromethane combustion [1,7]. For nitromethane flames, NO has been shown to be formed but not consumed [32,33]. For this reason, NO was chosen as the final product for nitromethane-containing nitrogen in the definition of  $\phi$ , as further discussed in the work of Nauc  r et al. [28].



The experimental uncertainties, as estimated by Nakamura et al. [39], are  $\pm 15$  K in reflected shock temperature,  $T_5$ ,  $\pm 15\%$  in ignition delay time,  $\tau$ , and  $\pm 2\%$  in mixture concentration.

### 3. Modeling details

The shock tube experiments were modeled using the batch reactor module of CHEMKIN IV [40] at constant volume and at a variety of pressure conditions. Two recent kinetic mechanisms were used in modeling nitromethane combustion, one from Brequigny et al. [30] and the second from Mathieu et al. [38].

The Brequigny et al. mechanism [30] contains 88 species and 701 reactions, of which the nitromethane subset involves 13

reactions. The mechanism is an adaptation of a mechanism by Glarborg et al. [11,33], developed to describe oxidation in low-pressure flames, validated for pressures in the range 0.5–3.0 bar.

The Mathieu et al. mechanism [38] contains 166 species and 1204 reactions. This mechanism is an adaptation of the nitromethane subset from Brequigny et al. [30], updated with new rate constants from the literature. The mechanism was developed for the self-ignition of nitromethane + O<sub>2</sub> mixtures, and validated in the pressure range of 1.71–35.8 atm.

### 4. Results and discussion

The ignition was investigated for various conditions with respect to gas mixture composition, equivalence ratio and pressure. The experimental conditions presented in Table 1 are chosen to provide a matrix of parameters covering a relevant range of pressures and mixture compositions. In the following discussion the experimentally measured properties pressure and luminosity, over time, are first evaluated. It is shown that luminosity has two time-separated maxima, which is treated as two separate ignition stages. These stages are discussed separately from both an experimental and a modeling perspective. Correlation equations are calculated for both of the ignition stages and compared to correlations from the literature [26,35,38]. The effects of mixture composition and pressure on ignition delay times are discussed.

#### 4.1. Experimental traces of pressure and luminosity

To accurately define the ignition, profiles of pressure and luminosity over time are explored. Mixtures 1–4 are discussed separately with respect to the characteristics of each mixture. Figs. 1–4 are typical examples of the measured pressure and luminosity profiles, clearly illustrating the similarities and differences characterizing the different mixtures. Fig. 1 presents the experimental pressure and luminosity profiles of Mixture 1 at  $\phi = 1$ , at a pressure of 8.2 atm and a temperature of 1115 K. From the pressure trace in Fig. 1, it can be seen that after the distinct pressure rise resulting from the arrival of the shock wave, there is a smooth pressure rise with a maximum. The pressure rise indicates that there is a prolonged activity in the gas mixture after the reflected shock wave reaches the end-plate but the pressure trace cannot be used independently to determine if ignition has occurred. In the luminosity trace in Fig. 1 two luminosity maxima separated in time, are evident. First there is a luminosity maximum shortly after the arrival of the shock wave, with a maximum intensity occurring in a time scale smaller than 40  $\mu$ s. This is followed by a second luminosity peak with a higher maximum intensity and with a broader distribution over time. The second maximum intensity in light emission roughly coincides in time with the pressure maximum. The difference in intensity between the first and second luminosity maxima can be explained either by a higher concentration of light emitting species during the second luminosity maximum, or by different light emitting species present in the two luminosity maxima.

Mixture 2 has  $\phi = 0.5$ , with the same oxygen content but with a 50% reduction in nitromethane as compared to Mixture 1. Example

**Table 1**  
Experimental conditions visited with respect to mixture composition and pressure. Mixture components are given as mole%.

Mixture	CH <sub>3</sub> NO <sub>2</sub>	O <sub>2</sub>	N <sub>2</sub>	$\phi$	Pressure [atm]
1	4	5	91	1	7.4–8.2, 15.9–16.8, 32.5–44.9
2	2	5	93	0.5	7.3–8.2
3	4	10	86	0.5	7.7–9.7, 14.4–15.6
4	4	2.5	93.5	2	14.8–16.6

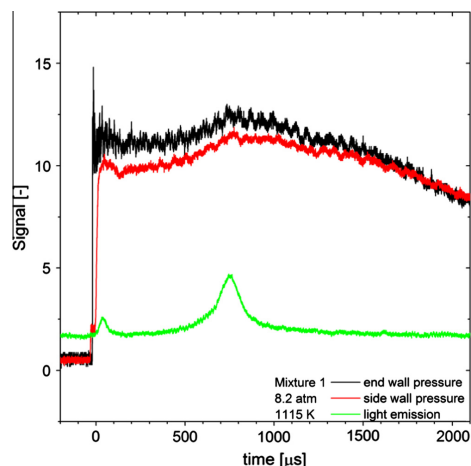


Fig. 1. Traces from pressure and light emission from the ignition of Mixture 1 at 1115 K and 8.2 atm.

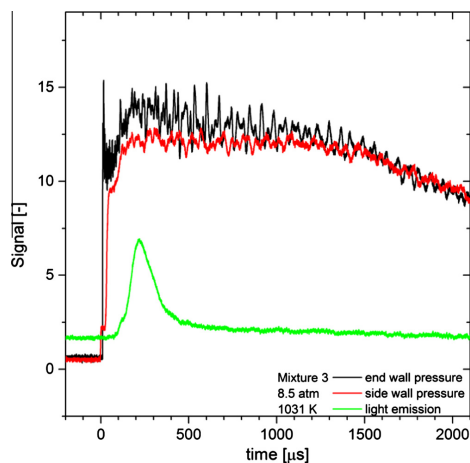


Fig. 3. Traces from pressure and light emission from the ignition of Mixture 3 at 1031 K and 8.5 atm.

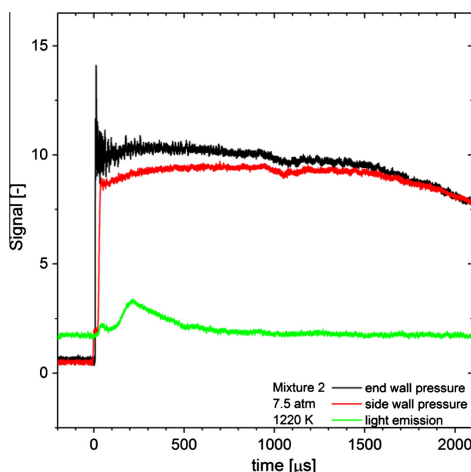


Fig. 2. Traces from pressure and light emission from the ignition of Mixture 2 at 1220 K and 7.5 atm.

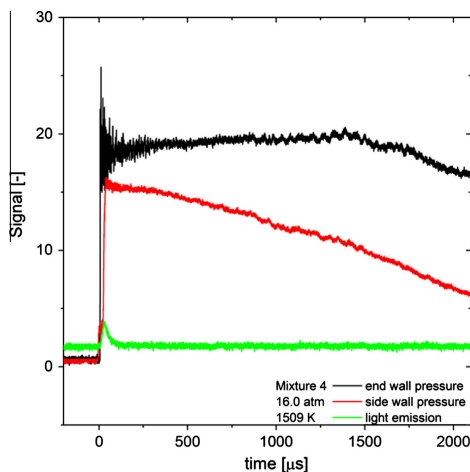


Fig. 4. Traces from pressure and light emission from the ignition of Mixture 4 at 1509 K and 16 atm.

pressure and luminosity profiles, representing a measurement for Mixture 2 at 1220 K and 8.5 atm, are shown in Fig. 2. Unlike the pressure in Mixture 1 there is no clearly defined pressure rise after the arrival of the shock wave, indicating that there is no major change in volume during the ignition, or that no ignition occurs. The chemical activity in this mixture is apparently too low to be detected from the pressure traces. However, from the luminosity traces it is evident that ignition does occur. A similar pattern as in the luminosity profiles from Mixture 1 is seen, with two separated maxima. The first maximum occurs shortly after the arrival of the reflected shock wave, while the second maximum is delayed. The second stage has a stronger emission intensity and wider dis-

tribution over time. Considering both the pressure and luminosity traces gives an indication that the lower fuel amount in Mixture 2 decreases the intensity of the luminosity, while preserving similar characteristics over time compared to Mixture 1.

Mixture 3 has  $\phi = 0.5$ , which is the same as for Mixture 2, with the same nitromethane content as in Mixture 1 but with the  $O_2$  content doubled. There is no pressure rise after the arrival of the shock wave for Mixture 3 in the measurements at temperatures  $>1032$  K. Measurements at 984 K and 1031 K show a rise in pressure, coinciding in time with the luminosity peaks. Fig. 3 shows the pressure and luminosity traces for Mixture 3 at 1031 K and 8.5 atm. In the luminosity traces for Mixture 3, it can be seen that

both luminosity maxima are close together in time, and are almost indistinguishable. The ignition does not start at the arrival of the shock wave in the measurements at  $\leq 1186$  K, but there is a time delay, as can be seen in Fig. 3.

Mixture 4 has  $\phi = 2.0$ , with the same nitromethane content as Mixture 1 but it contains 50% of the  $O_2$  content. This mixture was investigated in the temperature range 1109–1780 K at 16 atm. As can be seen in Fig. 4 the experimental pressure traces shows no significant pressure rise after the arrival of the shock wave. In contrast to the other conditions investigated, luminosity profiles for Mixture 4 show only one peak. This can be either the first stage ignition with the second ignition stage outside the time restrictions in the present study, or the two maxima collapsed to one luminosity peak. From the pressure and luminosity traces it cannot be conclusively determined if the ignition of Mixture 4 corresponds to the first or second stages identified in the luminosity profiles of the other mixtures. In the coming sections the information gained from the analysis of the other conditions are used to elucidate the ignition behavior of Mixture 4.

In the experimental pressure profiles of Mixtures 1–3, the pressure rise after the arrival of the shock wave occurs gradually or not at all, in contrast to the sharp pressure rise commonly used to identify ignition in shock tube experiments. Thus, if ignition were to be defined based on the pressure profiles measured in the present study, there would be a high degree of uncertainty. The luminosity profiles have well defined maxima; therefore the experimental ignition is defined as the maxima of the luminosity profiles, with each maximum marking separate ignition events.

In the above it was shown that the ignition of nitromethane in the presence of oxygen exhibits an unusual ignition behavior with two separate ignition stages at the majority of the experimental conditions in the present study, as exemplified by the luminosity profiles in Figs. 1–3. Under these conditions the first stage ignition is fast, with a luminosity maximum at  $< 40$   $\mu s$ , with the exception of Mixture 3 at 984 and 1031 K, while the second stage had a delayed ignition in all mixtures and experimental conditions. This multi stage ignition is considered analogous to the multi stage chemistry found in flames [6,25,28] and in detonations [19]. Both the first and second stages are investigated further.

#### 4.1.1. Ignition delay determination

The ignition delay times for first- and second-stage ignition were determined for Mixtures 1–3 in the temperature range 947–1333 K. Fig. 5 shows that the ignition delay times for the first stage ignition are the same magnitude for Mixtures 1–3 over the temperature range studied, indicating that the initial gas mixture composition does not affect the ignition delay times. The activation energy for the first stage ignition is similar for the three mixtures. As a result of experimental uncertainties and the short ignition times of this ignition stage scatter in the results are likely not to be attributed to pressure effects. Mixture 4 shows a fast ignition and the results are plotted in Fig. 5 together with the first stage ignition from Mixtures 1–3. The ignition delay times measured for Mixture 4 are of the same order of magnitude as those for Mixtures 1–3, therefore the single stage ignition in Mixture 4 is likely the first stage ignition.

In Fig. 6 the experimental data for the second stage ignition is presented for Mixtures 1–3. The experimental second stage ignition delay decreases with temperature, as the reactivity increases. Reducing the nitromethane content by half has a small activating effect on the second stage ignition by decreasing ignition delay times. By doubling the  $O_2$  content the effect on the ignition delay was considerably stronger with a reduction of the ignition delay times by  $\sim$ four times compared to Mixture 1. The effective activation energy of the second stage ignition of Mixture 3 is weaker than that for Mixtures 1 and 2.

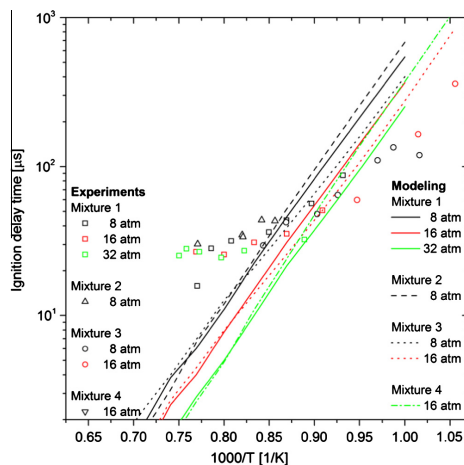


Fig. 5. The experimental results for the ignition delay times for the first stage ignition with predictions from the mechanism of Brequigny et al.

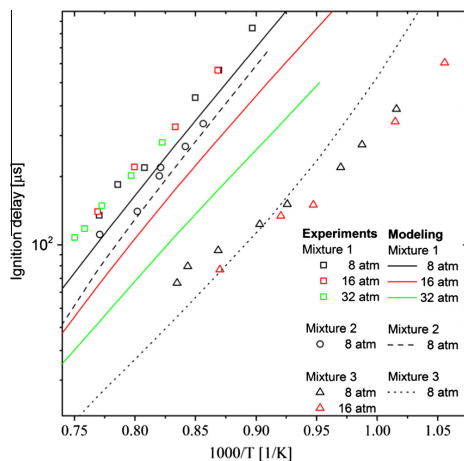


Fig. 6. Experimental results and predictions from the mechanism of Brequigny et al. for the second stage ignition in Mixtures 1–3 at 8, 16 and 32 atm.

Mixture 1 and Mixture 3 were examined in the pressure range of 7.4–44.9 atm and 7.7–15.6 atm, respectively. For many fuels, the ignition is sensitive to pressure [41]. As a result of the higher concentrations of fuel and  $O_2$  in the gas mixture, ignition is typically faster at higher pressures. However, no change in ignition delay times with pressure is observed for either of the two ignition stages over the pressure range investigated.

#### 4.1.2. Correlation equations based on mixture composition

The use of correlation equations allows comparison of datasets obtained at different conditions as the correlations quantify the

**Table 2**

The correlation coefficients from Eqs. (2)–(7).

Coefficients	Djbaili-Chaumeix et al. (Eq. (5))	Kang et al. (Eq. (4))	Mathieu et al. 90% Ar (Eq. (6)) 98% Ar (Eq. (7))	Breigny et al. mechanism 1st stage	Breigny et al. mechanism 2nd stage	Present study 1st stage (Eq. (2))	Present study 2nd stage (Eq. (3))
$10^{-\alpha}$	8.43	1.11	1.80	2.91	4.94	4.54	1.71
$E_a$ (kcal)	15.44	21.36	19.8	37.5	40.3	32.29	16.15
$[NM]^{\beta}$	–1.02	0.59	0.72	1.55	–0.01	0.71	–0.31
$[O_2]^{\gamma}$	–1.08	–0.72	–0.72	–1.55	–0.09	–3.01	–0.02
$[diluant]^{\delta}$	1.42	0	0.06	–0.26	–0.54	1.41	0.48

dependence of the ignition delay on the concentration of fuel, oxidizer and inert gas over a range of conditions. The quality of a correlation depends on the range and quality of data used in deriving it. All correlations discussed below are summarized in Table 2. In the present work correlation equations were obtained by fitting an expression to the experimental results from Mixtures 1–3 of the present study for both the first (Eq. (2)) and second (Eq. (3)) stage ignition. Mixture 4 was not included since the single ignition stage cannot be conclusively attributed to one or the other ignition stages identified in the other mixtures. The effect of temperature and mixture composition was evaluated by multiple regression analysis. The concentrations are in  $\text{mol m}^{-3}$ , temperature in K and R in  $\text{kcal mol}^{-1}\text{K}^{-1}$ .

$$\tau = 10^{-1.71} e^{-16.15/RT} [\text{CH}_3\text{NO}_2]^{-0.31} [\text{O}_2]^{-0.02} [\text{N}_2]^{0.48} \quad (2)$$

$$\tau = 10^{-3.38} e^{-20.98/RT} [\text{CH}_3\text{NO}_2]^{0.59} [\text{O}_2]^{-2.35} [\text{N}_2]^{1.64} \quad (3)$$

The overall activation energy,  $E_a$ , was determined to be  $16.15 \pm 1.57 \text{ kcal mol}^{-1}$  for the first-stage ignition and  $20.89 \pm 0.82 \text{ kcal mol}^{-1}$  for the second stage ignition. The pressure dependence derived from Eqs. (2) and (3) is weak,  $P^{0.15}$  and  $P^{-0.12}$  respectively. It can be seen in Fig. 7 that the correlations from the present study, Eqs. (2) and (3), represent the experimental results satisfactorily, with an exponential agreement. The ignition delay times determined for Mixture 4 were evaluated by comparison to Eqs. (2) and (3). The agreement with the correlation of the first stage ignition, Eq. (2), was good for the measurements at 1109 K and 1258 K, but the measurements at 1509 K and 1779 K did not fit the correlation. However, because there are no other mixtures examined in the temperature range 1500–1700 K, it not possible to determine whether these measurements are faulty or are an accurate description of the first stage ignition at these temperatures. The fit of Mixture 4 were considerably lower than of the second stage ignition, Eq. (3).

The present analysis predicts a promoting effect of  $\text{O}_2$  on both ignition stages, as evident from the negative sign on the exponents.  $\text{O}_2$  has a minor influence on the first stage ignition,  $[\text{O}_2]^{-0.02}$ . However, the second stage ignition exhibits an unusually large influence of  $\text{O}_2$ ,  $[\text{O}_2]^{-2.35}$ . Commonly the influence of  $\text{O}_2$  on ignition is in the order of  $[\text{O}_2]^{-0.5}$  to  $[\text{O}_2]^{-1.5}$  [26]. Nitromethane concentration has a positive influence on the ignition in the first stage,  $[\text{CH}_3\text{NO}_2]^{-0.31}$ , while it has a dampening effect on the second stage ignition,  $[\text{CH}_3\text{NO}_2]^{0.59}$ , according to the correlation analysis in Eqs. (2) and (3). Nitrogen is predicted to have a more pronounced dampening effect on the second stage ignition with a positive exponential dependence of 1.64, compared to the first stage ignition with a dependence of 0.48.

The correlations for the first and second ignition stage were compared to correlations from the literature [26,35,38]. Kang et al. [26] determined the ignition delay at  $\sim 0.2 \text{ atm}$  by tracking the spike in pressure. The pressure profile presented by Kang et al. has the von Neuman spike, not the gradual increase seen in the present study. As mentioned in the discussion of pressure profiles, the second stage ignition detected by peaks in luminosity, in

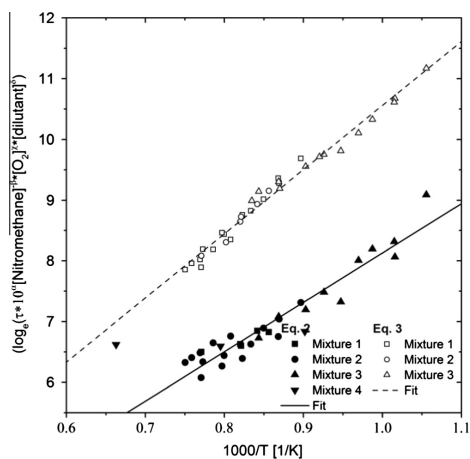


**Fig. 7.** The experimental data from the present study presented in the form of Eq. (2) for the first stage ignition and Eq. (3) for the second stage ignition.

many cases were accompanied with a pressure increase. In light of this, the ignition delays from Kang et al., derived from pressure profiles, could be interpreted as the second stage ignition. Any indication of a fast ignition stage, near the arrival of the shock wave in time, is absent in the work by Kang et al. However, this can be a question of detection limits and equipment sensitivity. Their results were presented in the form of a correlation equation Eq. (4), derived from the ignition delay data obtained from mixtures with  $\phi \approx 0.8$ –3.12. The experimental data was collected for mixture compositions with 8.0–37.8% nitromethane, 8.6–39.5%  $\text{O}_2$ , 33.3–80% Ar in the temperature range 1250–1900 K at  $\sim 0.2 \text{ atm}$ .

$$\tau = 10^{-1.11} e^{-21.36/RT} [\text{CH}_3\text{NO}_2]^{0.59} [\text{O}_2]^{-0.72} [\text{Ar}]^0 \quad (4)$$

In the study by Djebaili-Chaumeix et al. [35], the ignition delay times were determined from a delayed emission signal at 235 nm. The correlation, Eq. (5), was derived from ignition delay times for mixture compositions 3.56–6.4% nitromethane, 3.2–12.4%  $\text{O}_2$ , 84–91.97% Ar, and measured at 1040–1380 K at 0.8–2.8 atm.

$$\tau = 10^{-8.43} e^{-15.44/RT} [\text{CH}_3\text{NO}_2]^{-1.02} [\text{O}_2]^{-1.08} [\text{Ar}]^{1.42} \quad (5)$$

The similar activation energies determined in the present study and that of Kang et al., with the uncertainty of both  $E_a$ , supports the hypothesis of the present study that the ignition detected in the pressure profiles by Kang et al. is corresponding to the second stage ignition identified in the present study. The trends in nitromethane and  $\text{O}_2$ , are the same for Eqs. (3) and (4), although with different magnitudes.

The correlation Eq. (5) behaves considerably differently compared to the correlations for the second stage ignition, Eqs. (3) and (4). According to Eq. (5), the ignition is promoted by both oxygen and nitromethane. This behavior is similar to that of the first stage ignition of the present study, Eq. (2). The activation energy in Eq. (5), is significantly lower than in Eqs. (3) and (4), and is in good agreement with the first stage ignition of the present study, Eq. (2), within its uncertainty.

By comparing the correlations for the second stage ignition, Eqs. (3) and (4), it can be seen that O<sub>2</sub> is predicted to have a larger influence on the ignition in the present study, as compared to the analysis by Kang et al. When inserting the experimental results for the second stage ignition into Eq. (4), Mixtures 1 and 2 are well represented, but Mixture 3 is not. This could be attributed to the fact that the equations are generated at different conditions, where Eq. (4) was calculated from predominantly richer mixtures and higher temperatures than in the present study with one stoichiometric mixture and two mixtures with  $\phi = 0.5$ , at 947–1333 K. As the activation energies in Eqs. (3) and (4) are in close agreement, the difference in temperature dependency between the studies could be due to differences in mixture composition.

Mathieu et al. [38] presented ignition delay times for mixtures in the range  $0.5 < \phi < 2$  at temperatures in the range 875–1595 K and at pressures in the range 1.71–35.8 atm. The experimental results with 90% and 98% Ar dilution were used to calculate two correlations, Eqs. (6) and (7). In the work of Mathieu et al. the correlations are based on  $\phi$  and pressure. Here, the coefficients are directly translated to dependences on reactants and diluent, respectively, to facilitate comparison.

$$\tau = 10^{-1.80} e^{-19.8/RT} [\text{CH}_3\text{NO}_2]^{0.72} [\text{O}_2]^{-0.72} [\text{Ar}]^{0.06} \quad (6)$$

$$\tau = 10^{-2.91} e^{-37.5/RT} [\text{CH}_3\text{NO}_2]^{1.55} [\text{O}_2]^{-1.55} [\text{Ar}]^{-0.26} \quad (7)$$

The activation energies at 90% and 98% Ar dilution have different magnitudes. With higher dilution, the activation energy increased by 89%. The influence of the reactant also increased with higher dilution.

Correlations based on the predictions of the Brequigny et al. [30] mechanism were calculated in the present study. The predictions were performed in the same temperature and pressure ranges as the corresponding experimental mixtures, with  $\sim 50$  K steps. The coefficients can be seen in Table 2. Even though the mechanism could capture the ignition delay times at 8 atm for the examined mixtures, the correlation, containing other pressures, cannot capture the influence of the reactants nor the experimental activation energy.

The data from Borisov et al. [14] cannot be directly compared with the correlations obtained in shock tubes. In fact, earlier measurements performed in a by-pass apparatus were affected by significant heat losses during ignition delay as was revealed and discussed by the same authors [42,43]. Due to heat losses the temperature of the mixture was not equal to the temperature of the walls that affects interpretation of both ignition delays and the apparent activation energy [42,43].

By interpreting the data in light of the present study, where two ignition stages were observed in the same measurements, it is plausible that discrepancies that exist in the literature [26,35] could be due to observations of different stages in the ignition.

## 4.2. Ignition modeling

### 4.2.1. Possible origin of luminosity

The presence of two luminosity maxima indicate that the ignition of nitromethane in the presence of O<sub>2</sub> occurs in several zones or steps, as previously seen in detonation [19] and flame [6,25]

studies. The possible origins of the luminosity maxima were explored using kinetic modeling and information about the chemiluminescence from excited species in the light emitting wavelength range [44]. When identifying species, considerable experimental work [12,13,25,26,44–46] and the book of Gaydon [44] was considered. Candidate species were those which emit light within the experimentally detectable range of the present study, 240–530 nm.

In the work of Hall and Wolfhard [25] two zones were detected in a nitromethane/air flame. In the first zone the species C<sub>2</sub>, CH\*, CN\*, OH\*, NH\* and NO\* were observed, but not CH<sub>2</sub>O\*. In the shock tube study of Kang et al. [26] the authors mention that the species CH<sub>2</sub>O\*, OH\*, and NO\* were detected through emission after the reflected shock had passed, which was referenced in [26] as a publication in preparation but is, to the best of our knowledge, not yet published. In the shock tube study of nitromethane decomposition by Zaslonko et al. [12] CH<sub>2</sub>O\* was detected, and used as proof of the presence of CH<sub>3</sub>O radical early in the ignition. In the combustion of liquid nitromethane strong signals of OH\* were detected with somewhat smaller signals of CN\* [46]. Dong et al. [45] investigated emission from nitromethane/O<sub>2</sub> mixtures in a shock tube and observed emission of CH<sub>3</sub>O\* and OH\* appearing simultaneously. In the shock tube study of Mathieu et al. a weak OH\* signal was detected [38].

NO<sub>2</sub> is a likely candidate for the first stage emission that is detected as it is established in the literature that ground state NO<sub>2</sub> is produced from the thermal decomposition of nitromethane [12,13], and emits light in the detectable region.

Formaldehyde CH<sub>2</sub>O\* emits light in the range 370–480 nm. It was generally considered that the reaction CH<sub>3</sub>O + CH<sub>3</sub>O = CH<sub>2</sub>O\* + CH<sub>3</sub>OH is a source of excited formaldehyde [13].

In the present study, the possibility that luminosity originated from OH\* was examined by OH\*-filtering. No luminosity signal was detected in the filtered experiments. Based on this lack of signal it is, however, not possible with certainty to rule out the presence of OH\*, since the signal might be weaker than the detection limit. As OH\* radicals have been detected in previous studies, it is considered among the possible luminosity sources. Precursors to OH\* are primarily  $\dot{\text{O}} + \text{H} = \text{OH}^*$  and  $\text{CH} + \text{O}_2 = \text{CO} + \text{OH}^*$ , and to a minor extent  $\text{N}_2\text{O} + \text{H} = \text{N}_2 + \text{OH}^*$ .

NO does not decompose at the present temperatures and would therefore not result in one or several concentration maxima with a constrained time interval, but rather be distributed over a wide range in time. The same behavior was also predicted by the model. Considering this NO was excluded as a possible source of the luminosity peaks. The species left for consideration are, CN\*, NH\* and C<sub>2</sub>. These species all emit light in the experimentally detectable range of the present study; CN\* at 388.3 and 359 nm, NH\* at 337 nm, C<sub>2</sub> with two swanbands within the detectable region of the present study at 473.7 and 516.2 nm.

The excited species C<sub>2</sub> is produced from  $\text{CH} + \dot{\text{C}} = \text{C}_2^* + \text{H}$  and  $\text{CH}_2 + \dot{\text{C}} = \text{C}_2^* + \text{H}_2$  [47]. Through the reaction  $\text{CH} + \text{NO} = \text{NH}^* + \text{CO}$  the excited species NH\* can be formed [48]. The formation of CN\* is, to the best of the authors' knowledge, not well established in the literature. Therefore its ground state equivalents are examined further.

Excited species are not present in the chemical kinetic mechanism used to simulate the present results, but the ignition is evaluated using the precursors for the excited species discussed above. Modeling shows two regions of species maxima that could possibly be related to the first- and second-stage ignition, as shown in Fig. 8. The first and second ignition stages are defined as the maximum pressure rises according to the model, and marked in Fig. 8. CH<sub>3</sub>O and NO<sub>2</sub> peak almost simultaneously at the first ignition stage, with the presence of CH<sub>3</sub>O indicating that CH<sub>2</sub>O\* can be formed. CN has a maximum at the second stage ignition, while NH has two maxima corresponding in time with both the first

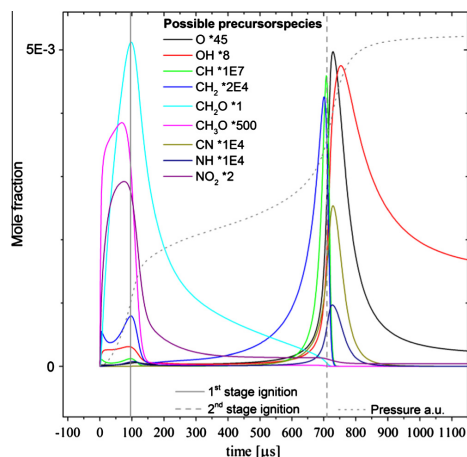


Fig. 8. Predicted concentrations over time for selected precursors to plausible light emitting species in Mixture 1 at 1100 K and 8 atm. The predictions are from the mechanism of Brequigny et al.

and second stage ignition events. At both ignition stages, maxima from OH radical can be found. The radical CH is of interest as a precursor for OH\* and C<sub>2</sub> and NH\*. CH<sub>2</sub> acts as a precursor to C<sub>2</sub>. The OH, CH and CH<sub>2</sub> radicals have three maxima. First there is a maximum at times <5 ms, followed by two delayed maxima corresponding in time with the two ignition stages respectively. The first two maxima are predicted to have a lower molar fraction than the third maximum. Atomic oxygen, O, is studied as a precursor to OH\*, it has a maximum at both ignition stages. The luminosity of both ignition stages is probably emission from a mixture of several of the excited species discussed above.

#### 4.2.2. Definition of ignition delay in the modeling

The choice of marker to define the ignition delay time is important when evaluating the performance of the mechanism. In light of the previous discussion, several definitions of ignition were tested in our modeling. Precursors to the radicals considered as likely sources of emission have been tested. These include:  $dp/dt_{\max}$ ,  $[\text{OH}]_{\max}$  and  $[\text{CH} + \text{CH}_2]_{\max}$  for both ignition stages,  $[\text{CH}_3\text{O}]_{\max}$  and  $[\text{NO}_2]_{\max}$  for the first stage ignition, and  $[\text{CN}]_{\max}$ ,  $[\text{NH}]_{\max}$  and  $[\text{N}_2\text{O}]_{\max}$  for the second stage ignition. The definitions  $dp/dt_{\max}$ ,  $[\text{OH}]_{\max}$  and  $[\text{CH} + \text{CH}_2]_{\max}$  were chosen as they have all been established in the literature as markers for ignition, and are formed within the explosion and consumed relatively fast. The results are plotted in Fig. 9 and one can see that there are no major differences in ignition delay time using the different definitions, for either the first or second stage ignition events. The pressure profiles versus time resulted in two pressure rises separated in time; a maximum gradient in pressure  $dp/dt_{\max}$  was calculated for both pressure rises. The first maximum for OH and CH + CH<sub>2</sub> appears at times considerably shorter than the first experimental maximum. This can contribute to the width of the luminosity maximum, but is unlikely to be an appropriate marker for the maximum. Therefore the second maximum was tested as a marker for the first stage ignition. At temperatures >1150 K, these two first maxima were difficult to distinguish. Therefore the ignition delay times for the first stage ignition were only calculated up to 1150 K for OH and CH + CH<sub>2</sub>. For the second stage ignition the

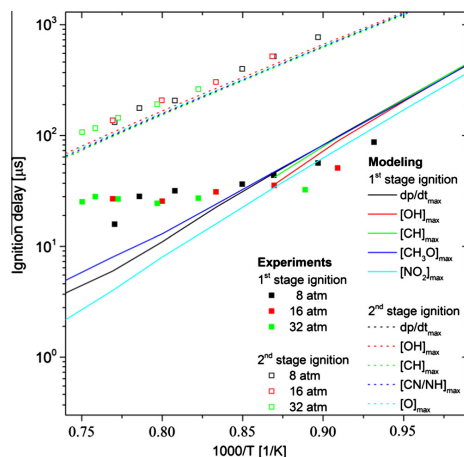


Fig. 9. Comparison of different definitions of the predicted ignition delay time for the first and second stage ignition in Mixture 1. The predictions are from the mechanism of Brequigny et al.

ignition delay time from  $[\text{O}]_{\max}$  and  $[\text{OH}]_{\max}$  were slightly longer compared to predictions using  $dp/dt_{\max}$ ,  $[\text{CN}/\text{NH}]_{\max}$  and  $[\text{CH} + \text{CH}_2]_{\max}$ , but negligible on the logarithmic scale, as seen in Fig. 8. As there is negligible difference between the definitions for both ignition stages, the choice of ignition marker in modeling the data is of little consequence and does not influence the interpretation of the mechanism's performance. The maximum pressure gradient  $dp/dt_{\max}$  was used for the modeling predictions as the origin of the experimental luminosity was not experimentally proven.

#### 4.3. Comparison between experimental results and modeling

First, two contemporary kinetic mechanisms by Brequigny et al. [30] and Mathieu et al. [38] are compared for their ability to reproduce the experimental ignition delay times. The mechanism of Brequigny et al. accurately reproduced the trends in ignition delay times from all mixture compositions at 8 atm. An important point is that the small reduction in ignition delay time when decreasing the nitromethane content was successfully reproduced. The Mathieu et al. mechanism did not reproduce the ignition delay times as well as that of Brequigny et al. in the present work. Therefore the Brequigny et al. mechanism has been chosen in our further discussion. In Supplementary material, the performance of the mechanism of Mathieu et al., at the condition of the present study, is presented for both ignition stages.

When comparing the experimental results with the modeling predictions for the first stage ignition, the activation energy in the predictions is higher for all mixtures examined, as seen in Fig. 5. The predicted first stage ignition ranges between 1 and 544  $\mu\text{s}$  in the temperature range 1000–1500 K for Mixture 1 at 8 atm, and coincides with the experimental results ~1100 K. There are minor differences between the predicted activation energy of the first stage ignition for the different mixtures, which is slightly lower in Mixture 3 and negligibly higher in Mixture 2 and Mixture 4, as compared to Mixture 1. These differences in activation energy between the different mixtures are small compared to the experimental activation energy.

For Mixtures 1 and 2 the experiments and modeling are in reasonable agreement with the second stage ignition at 8 atm.

Moreover, in the simulated second stage ignition the temperature dependence is stronger than observed in the experimental temperature dependence for Mixture 3, as seen in Fig. 6.

The pressure dependence was examined at 8, 16 and 32 atm for Mixture 1. Unlike the pressure independence in the experimental results, the model predicts decreasing ignition delay times (faster reactivity) for both ignition stages with increasing pressure for Mixture 1.

## 5. Conclusions

The ignition of nitromethane/O<sub>2</sub>/N<sub>2</sub> mixtures was characterized as a two-stage process under our experimental conditions. The ignition profiles were examined with respect to pressure and luminosity versus time. Some pressure traces showed a continuous rise stretched over time with one maximum, rather than a sharp von Neuman spike, while some traces had no significant pressure rise at all. From the luminosity traces two maxima were identified; the second coinciding in time with the pressure maximum. The luminosity was used to define the experimental ignition, with the ignition delay times taken at the maximum intensity of the luminosity peaks. Firstly, a fast ignition stage occurs, followed by a second stage ignition with higher luminosity intensity and a larger spread over time. The two-stage ignition process, seen also in detonations [19], and possibly corresponding to the occurrence of several reaction zones in modeled flames [6,28], is thereby proven experimentally in self ignition. Both the first- and second-stage ignition was examined for pressure and mixture composition dependence. An unusual aspect of nitromethane ignition is that over the conditions examined in the current study, there was no pressure dependence in the ignition delay times for either the first or second stage ignition. Mixture composition had no measurable effect on the first stage ignition delay times. However, for the second stage ignition, the ignition delay time was decreased by a factor of approximately four by doubling the O<sub>2</sub> content of the mixture, but reducing the nitromethane content by half only marginally reduced the ignition delay times.

Possible excited species generating the emission were identified as possible ignition markers for simulations from a theoretical discussion based on species observed in the literature. It was shown that the definition of ignition did not affect the evaluation of the performance for the mechanism of Brequigny et al. [30].

Modeling could reproduce the magnitude of the first stage ignition in reasonable agreement, but the temperature dependence was steeper than for the experimental results. For the second stage ignition the model predictions reproduce the temperature dependence well, and also reproduces well the ignition delay times at 8 atm but under-predicts them at 16 and 32 atm. The mechanism could not reproduce the pressure independence seen in the experimental results for either the first or second stage ignition. The kinetics of nitromethane/O<sub>2</sub>/N<sub>2</sub> ignitions cannot be fully explained, and warrants further investigation.

The experimental temperature and mixture dependence was analyzed in terms of a correlation fit for each ignition stage, Eqs. (2) and (3). From this analysis the first stage ignition was concluded to be mainly promoted by the concentration of nitromethane, suggesting that this ignition stage is controlled by the thermal decomposition of nitromethane and its neighboring chemistry. In the second stage ignition O<sub>2</sub> has a strong promoting effect on the reactivity, while nitromethane has a mild dampening effect on the ignition. From the correlations the overall activation energy was calculated to be  $16.15 \pm 1.57$  kcal mol<sup>-1</sup> for the first stage ignition, and  $21.45 \pm 0.82$  kcal mol<sup>-1</sup> for the second stage. Compared to the correlation from Kang et al. [26], the second-stage ignition is in the present study predicted to be more influenced by O<sub>2</sub> and

diluent concentrations. The activation energy for the second stage ignition is in good agreement with the activation energy calculated in the work of Kang et al. In the correlation from Djebaili-Chaumeix et al. [35] the activation energy is in good agreement with the first stage ignition of the present study.

The ignition in Mixture 4 was attributed to a first stage ignition, but the measurement points at 1509 K and 1779 K where differentiated as the ignition delay times do not follow the general trend of first stage ignition found in the temperature range 947–1333 K.

The chemistry behind ignition of nitromethane/O<sub>2</sub> warrants further studies, in order to elucidate the pressure independence of the ignition and improve capabilities to reproduce this through simulations.

## Acknowledgements

The author would like to thank The Centre for Combustion Science and Technology (CECOST) and the Swedish Energy Agency (STEM) for financial support. Special thanks to the Hierta-Retzius foundation for financial support for an extended research-trip of JDN to National University of Ireland, Galway. Discussions and feedback from Prof. John Simmie are gratefully acknowledged.

## Appendix A. Supplementary material

Supplementary data associated with this article can be found, in the online version, at <http://dx.doi.org/10.1016/j.fuel.2016.09.003>.

## References

- [1] Starkman ES. Nitroparaffins as potential engine fuels. *Ind Eng Chem* 1959;51:1477–80.
- [2] Litzinger T, Colket M, Kahandawala M, Lee SY, Liscinsky D, McNesby K, et al. Fuel additive effects on soot across a suite of laboratory devices, Part 2: Nitroalkanes. *Combust Sci Technol* 2011;183:739–54.
- [3] Cracknell RF, Andrae JCG, McAllister LJ, Norton M, Walmsley HL. The chemical origin of octane sensitivity in gasoline fuels containing nitroalkanes. *Combust Flame* 2009;156:1046–52.
- [4] Jia Z, Wang Z, Cheng Z, Zhou W. Experimental and modeling study on pyrolysis of n-decane initiated by nitromethane. *Combust Flame* 2016;165:246–58.
- [5] Fells I, Rutherford AG. Burning velocity of methane-air flames. *Combust Flame* 1969;13:130–8.
- [6] Boyer E, Kuo KK. Modeling of nitromethane flame structure and burning behavior. *Proc Combust Inst* 2007;31:2045–53.
- [7] Taylor HA, Vesselsky VV. The thermal decomposition of nitromethane. *J Phys Chem* 1934;39:1095–101.
- [8] Hillenbrand TJ, Kilpatrick ML. The thermal decomposition of nitromethane. *J Chem Phys* 1953;21:525–35.
- [9] Bradley JN. Shock-wave decomposition of nitroparaffins. Part 1. –Mass-spectrometric study of nitromethane decomposition. *Trans Faraday Soc* 1961;57:1750–6.
- [10] Perche A, Tricot JC, Lucquin M. Pyrolysis of nitromethane.1. Experimental study - nitromethane alone and in the presence of additives. *J Chem Res-S* 1979;116–7.
- [11] Glarborg P, Bendtsen AB, Miller JA. Nitromethane dissociation: Implications for the CH<sub>3</sub> + NO<sub>2</sub> reaction. *Int J Chem Kinet* 1999;31:591–602.
- [12] Zaslanko IS, Kogarko SM, Mozzhukin EB, Petrov Y. Thermal decomposition of nitromethane in shock waves. *Kinet Catal (Engl Transl)* 1972;13:1001–5.
- [13] Gl  nzer K, Troe J. Thermische zerfallsreaktionen von nitroverbindungen. I: Dissoziation von nitromethan. *Helv Chim Acta* 1972;55:2884–93.
- [14] Borisov AA, Kogarko SM, Skachkov GI. Thermal decomposition of nitromethane. *Kinet Catal (Engl Transl)* 1966;7:521–6.
- [15] Hsu DSY, Lin MC. Laser probing and kinetic modeling of NO and CO production in shock-wave decomposition of nitromethane under highly diluted conditions. *J Energ Mater* 1985;3:95–127.
- [16] Kuznetsov NM, Petrov YP, Turetskii SV. Kinetics of NO<sub>2</sub> formation upon the decomposition of nitromethane behind shock waves and the possibility of nitromethane isomerization in the course of the reaction. *Kinet Catal* 2012;53:1–12.
- [17] Zaslanko IS, Petrov YP, Smirnov VN. Thermal decomposition of nitromethane in shock waves: the effect of pressure and collision partners. *Kinet Catal* 1997;38:321–4.
- [18] Menikoff R, Shaw MS. Modeling detonation waves in nitromethane. *Combust Flame* 2011;158:2549–58.
- [19] Sturzer MO, Lamoureux N, Matignon C, Desbordes D, Presles HN. On the origin of the double cellular structure of the detonation in gaseous nitromethane and its mixtures with oxygen. *Shock Waves* 2005;14:45–51.

- [20] Presles HN, Desbordes D, Guirard M. Detonation in nitromethane and nitromethane-oxygen gaseous mixtures. In: Proceedings of the Zeldovich memorial-international conference on combustion. 1994. p. 382–5.
- [21] Presles HN, Desbordes D, Guirard M, Guerraud C. Gaseous nitromethane and nitromethane-oxygen mixtures: a new detonation structure. *Shock Waves* 1996;6:111–4.
- [22] Khasainov B, Viot F, Presles HN, Desbordes D. Parametric study of double cellular detonation structure. *Shock Waves* 2013;23:213–20.
- [23] Petrov YP, Karasevich YK, Turetskii SV. Decomposition of nitromethane in shock waves: the primary stage and the kinetics of decomposition at pressures of about 40 atm. *Russ J Phys Chem B* 2010;4:566–73.
- [24] Joubert F, Desbordes D, Presles H-N. Detonation cellular structure in  $\text{NO}_2/\text{N}_2\text{O}_4$ -fuel gaseous mixtures. *Combust Flame* 2008;152:482–95.
- [25] Hall AR, Wolfhard HC. Multiple reaction zones in low pressure flames with ethyl and methyl nitrate, methyl nitrite and nitromethane. *Symp (Int) Combust* 1957;6:190–9.
- [26] Kang JG, Lee SW, Yun SS, Choi SN, Kim CS. Ignition delay times of nitromethane/oxygen/argon mixtures behind reflected shock. *Combust Flame* 1991;85:275–8.
- [27] Guirgis R, Hsu D, Bogan D, Oran E. A mechanism for ignition of high-temperature gaseous nitromethane—the key role of the nitro group in chemical explosives. *Combust Flame* 1985;61:51–62.
- [28] Nauc  r JD, Nilsson EJK, Konnov AA. Laminar burning velocity of nitromethane + air flames: a comparison of flat and spherical flames. *Combust, Flame* 2015;162:3803–9.
- [29] De Jaegere S, Van Tiggelen A. Comparative study of flame propagation in compounds containing nitrogen oxides. *Combust Flame* 1959;3:187–200.
- [30] Brequigny P, Dayma G, Halter F, Mounaim-Rousselle C, Dubois T, Dagaut P. Laminar burning velocities of premixed nitromethane/air flames: an experimental and kinetic modeling study. *Proc Combust Inst* 2014;35:703–10.
- [31] Tricot JC, Perche A, Lucquin M. Gas-phase oxidation of nitromethane. *Combust Flame* 1981;40:269–91.
- [32] Tian ZY, Zhang LD, Li YY, Yuan T, Qi F. An experimental and kinetic modeling study of a premixed nitromethane flame at low pressure. *Proc Combust Inst* 2009;32:311–8.
- [33] Zhang KW, Li YY, Yuan T, Cai JH, Glarborg P, Qi F. An experimental and kinetic modeling study of premixed nitromethane flames at low pressure. *Proc Combust Inst* 2011;33:407–14.
- [34] Seljeskog M. Shock tube experiments on nitromethane and promotion of chemical reactions by nonthermal plasma. In: Faculty of Engineering Science and Technology Department of Thermal Energy and Hydropower, The Norwegian University of Science and Technology, Trondheim. 2002. p. 328.
- [35] Djebaili-Chaumeix N, Abid S, Paillard CE. Shock tube study of the nitromethane decomposition and oxidation. In: Howing AFP, editor. Proceedings of the 21st international symposium on shock tubes and shock waves. Australia: The University of Queensland; 1997.
- [36] Nauc  r JD, Li Y, Nilsson EJK, Konnov AA, Curran HJ. Ignition of nitromethane +  $\text{O}_2$  +  $\text{N}_2$  in a shock tube. In: European combustion meeting, Budapest, Hungary. 2015. p. P4–P05.
- [37] Mathieu O, Giri B, Mertens JD, Petersen EL. Nitromethane ignition behind reflected shock waves. In: 25th ICDERS, Leeds, UK. 2015.
- [38] Mathieu O, Giri B, Agard AR, Adams TN, Mertens JD, Petersen EL. Nitromethane ignition behind reflected shock waves: experimental and numerical study. *Fuel* 2016;182:597–612.
- [39] Nakamura H, Darcy D, Mehl M, Tobin CJ, Metcalfe WK, Pitz WJ, Westbrook CK, Curran HJ. An experimental and modeling study of shock tube and rapid compression machine ignition of n-butylbenzene/air mixtures. *Combust Flame* 2014;161:49–64.
- [40] CHEMKIN IV 15101. Reaction Design: San Diego; 2010.
- [41] Westbrook CK, Curran HJ, Pitz WJ, Griffiths JF, Mohamed C, Wo SK. The effects of pressure, temperature, and concentration on the reactivity of alkanes: experiments and modeling in a rapid compression machine. In: Burgess AR, Dryer FL, editors. Symposium (international) on combustion. Pittsburgh: Combustion Institute; 1998. p. 371–8.
- [42] Borisov AA, Knorre VG, Kudryashova EL, Skachkov GI, Troshin KY. On temperature measurements in the induction of homogenous gas mixtures in a static admittance apparatus. *Chem Phys Rep c/c Khimicheskaja Fizika* 1998;17:1323–32.
- [43] Borisov AA, Skachlov GI, Troshin KY. Ignition and combustion kinetics of simple C1–C3 hydrocarbons in their mixtures with air. *Chem Phys Rep* 1999;18:1665–82.
- [44] Gaydon AG. The spectroscopy of flames. 2nd ed, London (UK): Chapman and Hall Ltd; 1974.
- [45] Dong H, Yong-Guo W, Hong-Bin L, Zhu-Mei S. Studies on high speed reaction spectrum of nitromethane under high temperature and high pressure. *Chin J High Press Phys* 1994;8:296–301.
- [46] Kelzenberg S, Eisenreich N, Eckl W, Weiser V. Modelling nitromethane combustion. *Propel Explos Pyrotech* 1999;24:189–94.
- [47] Grebe J, Homann KH. Blue-green Chemiluminescence in the system  $\text{C}_2\text{H}_2/\text{O}/\text{H}$ . Formation of the emitters  $\text{CH}(\text{A}^2\Delta)$ ,  $\text{C}_2(\text{d}^3\Pi_g)$  and  $\text{C}_2\text{H}^+$ . *Ber Bunsenges Phys Chem* 1982;86:587–97.
- [48] Lichten DA, Berman MR, Lin MC.  $\text{NH}(\text{A}^3\Pi \rightarrow \text{X}^3\Sigma^-)$  Chemiluminescence from the  $\text{CH}(\text{X}^2\Pi) + \text{NO}$  reaction. *Chem Phys Lett* 1984;108:18–24.

## Paper V



**Paper submitted to Energy and Fuels**

# An experimental and modelling study of nitromethane flames at CO<sub>2</sub>-rich conditions

*J. D. Naclér, E. J. K. Nilsson\*, A. A. Konnov*

Division of Combustion Physics, Department of Physics, Lund University, Lund, Sweden

\* E. J. K. Nilsson

P.O. Box 118

SE-221 00 Lund

Sweden

Phone: +46 46 222 14 03

Email: elna.heimdal\_nilsson@forbrf.lth.se

## ABSTRACT

The laminar burning velocity for nitromethane+O<sub>2</sub>+CO<sub>2</sub> was measured for  $\phi=0.8-1.3$  at 348 K and  $\phi=0.8-1.6$  for 358 K at atmospheric pressure using the Heat flux method. Oxidizer composition was 35% O<sub>2</sub> and 65% CO<sub>2</sub>. In addition, the effect of the oxidizer composition was examined for a stoichiometric flame at 358 K by varying oxygen fraction from 30% to 40%. Two kinetic mechanisms from the literature were examined for their predictive capabilities against the experimental laminar burning velocities for flames of nitromethane+O<sub>2</sub>+CO<sub>2</sub> and nitromethane+air. The mechanism by Mathieu et al. (*Fuel* **2016**, 182, 597), previously not validated for flames, was able to reproduce experimental laminar burning velocities for nitromethane+air but underpredicted new results at O<sub>2</sub>+CO<sub>2</sub> conditions. The mechanism by Brequigny et al. (*Proc. Combust. Inst.* **2014**, 35, 703) underpredicted experimental results significantly at all investigated conditions. Sensitivity analysis revealed that one of the most sensitive reactions is  $\text{HCO}+\text{M}=\text{CO}+\text{H}+\text{M}$ , for which different rate constant expressions were implemented in the two mechanisms. When replacing the rate constant for that reaction in the mechanisms of Brequigny et al., with the one used by Mathieu et al., significantly better agreement with experimental data was obtained.

**Keywords:** nitromethane, oxy-fuel, laminar burning velocity, kinetic modelling

## 1. INTRODUCTION

A contemporary challenge due to continuous use of combustion for energy production is the emission of greenhouse gases, in particular carbon dioxide ( $\text{CO}_2$ ), and dealing with its consequences. To address the issue of  $\text{CO}_2$ -emissions through technical advances methods for carbon capture and sequestration (CCS), where the  $\text{CO}_2$  is not released into the atmosphere, are under development. In CCS the  $\text{CO}_2$  can be recirculated in the combustion process as a diluent instead of molecular nitrogen ( $\text{N}_2$ ), resulting in a high- $\text{CO}_2$  flue gas that is suitable for sequestration. In application with fossil fuels, these techniques are regarded as carbon-neutral<sup>1</sup>. Biofuels combined with CCS-techniques have a potential to result in a negative net  $\text{CO}_2$ -balance, making it a viable option for dealing with the large  $\text{CO}_2$ -emissions from combustion. Research on biofuels combusted at oxy-fuel conditions, both as the primary fuel and together with coal, is presently pursued with promising results<sup>2-3</sup>.

Oxy-fuel combustion has the subordinate but important effect of reducing  $\text{NO}_x$  emissions, compared to combustion in air. This is partly because there is no  $\text{N}_2$  present that can form  $\text{NO}_x$  at high combustion temperatures, but also a result of that the fate of fuel-nitrogen (fuel-N) under oxy-fuel conditions can be different compared to combustion with air, as reviewed for combustion of fossil fuels<sup>3-5</sup>. Shaddix and Molina<sup>6</sup> investigated  $\text{NO}_x$ -conversion from fuel-N in pulverized coal with  $\text{CO}_2$  or  $\text{N}_2$  as diluents. It was seen that at equivalent amounts of  $\text{CO}_2$  or  $\text{N}_2$ , less of the fuel-N was converted to  $\text{NO}_x$  when burnt in  $\text{CO}_2$ . Most studies have focused on the  $\text{NO}_x$  emissions from fuel-N in combustion of real fossil fuels, containing a range of different fuel-N-species. Fossil fuels and biomass yield different fuel-N compounds and it has been shown that biomass release more of its nitrogen content at lower temperatures, as compared to fossil fuels, as discussed by Glarborg et al.<sup>5</sup>.

To better understand the chemistry of fuel-N at oxy-fuel conditions, further studies on fundamental properties of individual fuel-nitrogen compounds are necessary. Because of its short carbon-chain and single bond between the nitrogroup and the carbon, nitromethane ( $\text{CH}_3\text{NO}_2$ ) is an excellent representative for fuel-N chemistry. The literature on the effect of carbon dioxide on nitromethane combustion is at present limited to one study where the effect of  $\text{CO}_2$  as a collision partner in the decomposition of nitromethane was investigated in a shock tube<sup>7</sup> at 1050-1400 K and 0.2-40 atm. A ratio of 1:3 ( $\text{Ar}:\text{CO}_2$ ) for the third body collisional efficiency was presented for the low pressure rate constant of the thermal decomposition.

Kinetic mechanisms for modeling of nitromethane+ $\text{O}_2$  combustion in the diluents Ar or  $\text{N}_2$  are available in literature, the recent ones are outlined in the following. A mechanism for low pressure nitromethane+ $\text{O}_2$ +Ar flames was presented by Zhang et al.<sup>9</sup>, together with experimental temperature and species profiles for  $\phi=1.0$ , 1.5 and 2.0, at 4.655 kPa. The model predictions were in satisfactory agreement with the experimental results. Brequigny et al.<sup>10</sup> adapted the mechanism from Zhang et al.<sup>9</sup> to pressures in the range 0.5-3 bar, by updating selected rate constants. The mechanism was validated against laminar burning velocities for nitromethane+air at 423 K and 0.5-3 bar. Naucler et al.<sup>11</sup>, have shown that the mechanism of Brequigny et al.<sup>10</sup> underpredicted the laminar burning velocity at unburnt gas temperatures 338-358 K and atmospheric pressure. A study on nitromethane+ $\text{O}_2$ + $\text{N}_2$  ignition at 947-1333 K in the pressure range 7.3-44.9 atm<sup>12</sup>, showed that the mechanism of Brequigny et al.<sup>10</sup> agrees with the experimentally determined effects of mixture compositions on ignition delay times at 8 atm, but failed to reproduce the weak pressure dependence of the experimental results. The latest published mechanism, from Mathieu et al.<sup>13</sup> was developed for self-ignition of nitromethane, and ignition delay times for nitromethane+ $\text{O}_2$ +Ar at 2-34 atm were reproduced with satisfactory

agreement. Nauc  r et al.<sup>12</sup> tested the mechanism of Mathieu et al.<sup>13</sup> against ignition delay times at 947-1333 K in the pressure range 7.3-44.9 atm for nitromethane+O<sub>2</sub>+N<sub>2</sub> mixtures. Predicted trends of variation in ignition delay times with mixture composition were far from the measurements. The mechanism was also shown to be more reactive at the conditions covered by Nauc  r et al.<sup>12</sup>, with significantly shorter predicted ignition delay times as a result. This mechanism has not been validated for nitromethane flames so far.

The laminar burning velocities of nitromethane with N<sub>2</sub> as the diluent have been examined in three previous studies. De Jaeger et al.<sup>14</sup> measured the laminar burning velocity using a Bunsen burner and Schlieren imaging for nitromethane+O<sub>2</sub>+N<sub>2</sub> at various N<sub>2</sub> dilutions. Brequigny et al.<sup>10</sup> utilized the closed bomb technique to measure the laminar burning velocity for nitromethane+air at 423 K in the pressure range 0.5-3 bar. They defined equivalence ratio assuming N<sub>2</sub> as the final nitrogen-product, resulting in a maximum laminar burning velocity at lean conditions,  $\phi \sim 0.75$ . Nauc  r et al.<sup>11</sup> showed that by defining the equivalence ratio with NO as the final product, the maximum appears at rich conditions,  $\phi \sim 1.2$ , in line with many other fuels. Laminar burning velocities for nitromethane+air in the temperature range 338-358 K at atmospheric pressure, were determined using the heat flux method<sup>11</sup>. Through modeling it was shown that the width of the reaction zone of nitromethane+air flames needs to be considered when using the closed bomb technique<sup>11</sup>. The experimental results at 1 bar from Brequigny et al.<sup>10</sup> were reprocessed, considering the predicted width of the reaction zone, which improved the agreement between the studies.

Fundamental properties of fuel-N species has yet to be characterized at oxy-fuel conditions. To improve the knowledge on fuel-N conversion at CO<sub>2</sub>-rich conditions, the present study provides new experimental data on laminar burning velocity for nitromethane+O<sub>2</sub>+CO<sub>2</sub> flames which

have not been examined experimentally before. The results are used to validate and compare two contemporary kinetic mechanisms for nitromethane combustion. The performance of the mechanisms is evaluated based on the capability to accurately predict the present CO<sub>2</sub>-enriched flames as well as the laminar burning velocities for nitromethane+air<sup>11</sup>. To shed light on the differences or similarities between the mechanisms and their respective performance, sensitivity analysis is performed.

## 2. EXPERIMENTAL DETAILS

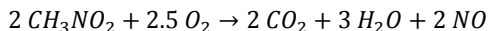
Laminar burning velocities of nitromethane+O<sub>2</sub>+CO<sub>2</sub> flames at atmospheric pressure were determined using the heat flux method. Initial gas mixture temperatures were 348 K and 358 K, and equivalence ratios visited were in the range  $\phi=0.8$ -1.6. At 348 K measurements were limited to a highest equivalence ratio of 1.3, due to low vapor pressure and thus a risk for condensation of the fuel at higher equivalence ratios at this temperature. The oxidizer mixture had a composition of 35% O<sub>2</sub> and 65% CO<sub>2</sub> for experiments over the whole accessible range of equivalence ratios. In addition, the effect of oxidizer composition was examined for a stoichiometric flame at 358 K by varying oxygen fraction from 30% to 40%.

The experimental setup and methodology used were described in detail by Alekseev et al.<sup>15</sup>. The burner used in the present study was designated “N”<sup>15</sup>. For this burner the adiabatic laminar burning velocities from the present study and from Nauc  r et al.<sup>11</sup> were corrected for burner surface area variation by multiplication by a factor of 1.023, as suggested by Alekseev et al.<sup>15</sup> The liquid nitromethane was mixed with CO<sub>2</sub> during evaporation as the gas flow through the evaporator. Just downstream the evaporator O<sub>2</sub> was added to the gas mixture. All gases were then allowed to mix as they passed through a heated hose set at the desired temperature of the

unburnt gas, 348 K or 358 K. The O<sub>2</sub> and CO<sub>2</sub> were provided by AGA with purities 99.5% and 99.8%, respectively. The nitromethane was from Sigma-Aldrich with a purity of 99.8%.

At adiabatic conditions (overall zero heat loss of the flame to the burner) the flame front was corrugated, an issue previously discussed by Nauc  r et al.<sup>11, 16</sup>. Following the methodology outlined in these previous works the flames were studied at sub-adiabatic conditions and extrapolated to the adiabatic laminar burning velocity. This extrapolation was up to 2.8 cm/s from the adiabatic laminar burning velocity at most, with a linear relationship between the measurement points.

In the present study, the only source of nitrogen is in the nitrogroup of nitromethane. In past research N<sub>2</sub> has been considered as the final product from nitromethane combustion<sup>17</sup>. However, for nitromethane flames, NO has been shown to be formed but not consumed<sup>9, 18</sup>. For this reason, NO was chosen as the final product for nitromethane-containing nitrogen in the definition of  $\phi$ , as discussed in the work of Nauc  r et al.<sup>11</sup>.



### 3. MODELING DETAILS

Modelling was performed using the premixed laminar flame speed calculation module in CHEMKIN IV<sup>19</sup>, with thermal diffusion and multicomponent transport taken into account. The parameters GRAD and CURV were kept sufficiently small to generate a grid of >800 gridpoints over 8 cm domain.

The flames were modelled using the detailed kinetic mechanisms of Brequigny et al.<sup>10</sup> and Mathieu et al.<sup>13</sup>. The latter did not provide transport parameters, which are necessary to perform

flame simulations. Transport parameters were mainly adopted from the mechanism of Konnov<sup>20</sup> and, for species not included in the Konnov mechanism, from Aramco 2.0<sup>21</sup>.

#### 4. RESULTS AND DISCUSSION

In this section the new experimental results for nitromethane+O<sub>2</sub>+CO<sub>2</sub> flames are first presented. This is followed by an evaluation of the ability of two mechanisms, by Brequigny et al.<sup>10</sup> and Mathieu et al.<sup>13</sup>, to reproduce the new experimental results as well as the measurements for nitromethane+air flames<sup>11</sup>. Discrepancies between experimental results and modelling are further investigated using sensitivity analysis and the most sensitive reactions are discussed.

##### *4.1 Experimental results*

Experimentally determined laminar burning velocities for nitromethane+O<sub>2</sub>+CO<sub>2</sub> are presented as symbols in Figure 1, with error bars showing the individual uncertainty in  $\phi$  and velocity for each measurement point. The maximum laminar burning velocity was reached at  $\phi=1.1$  with 32.8 cm/s at 348 K and 34.4 cm/s at 358 K. The position of the maximum laminar burning velocity is shifted to slightly leaner mixtures,  $\phi=1.1$ , as compared to nitromethane+air flames which peak at  $\phi=1.2$ . Laminar burning velocities of nitromethane+air flames<sup>11</sup> are provided in Figure 2.

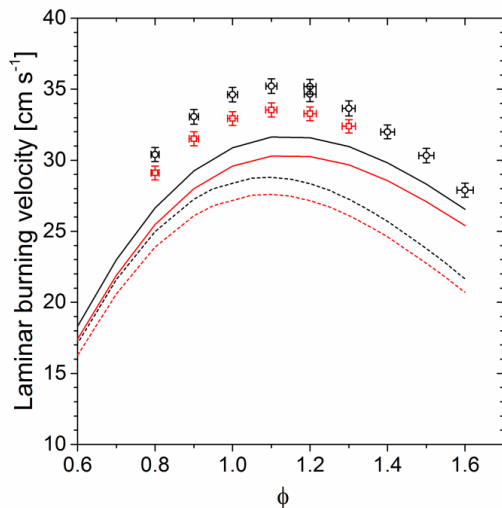


Figure 1. Laminar burning velocities at 1 atm for nitromethane+O<sub>2</sub>+CO<sub>2</sub>. Symbols: present study at 348 K (red squares) and 358 K (black circles). Lines: modeling using the mechanisms of Brequigny et al.<sup>10</sup> (dashed) and Mathieu et al.<sup>13</sup> (solid) at 348 K (red) and 358 K (black).

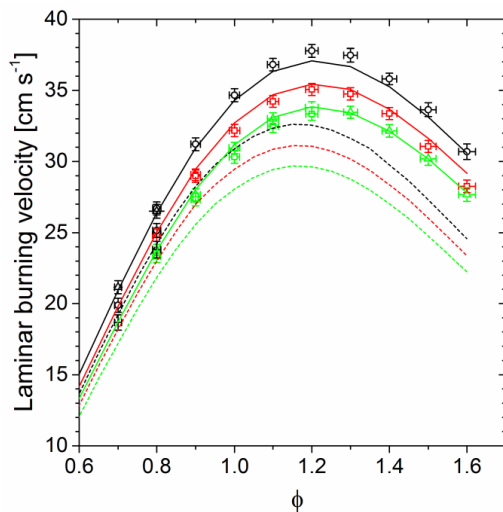


Figure 2. Laminar burning velocities at 1 atm for nitromethane+air. Symbols: measurements<sup>11</sup> at 338 K (green triangles), 348 K (red squares) and 358 K (black circles). Lines: modeling using the

mechanisms of Brequigny et al.<sup>10</sup> (dashed) and Mathieu et al.<sup>13</sup> (solid) at 338 K (green) 348 K (red) and 358 K (black).

Figure 3 shows how the laminar burning velocity at stoichiometric conditions and 358 K varies with fraction of O<sub>2</sub> in the oxidizer, O<sub>2</sub>/(O<sub>2</sub>+CO<sub>2</sub>), in the range 0.30 to 0.40. The laminar burning velocity exhibits close to linear increase with increasing O<sub>2</sub> content in the investigated range.

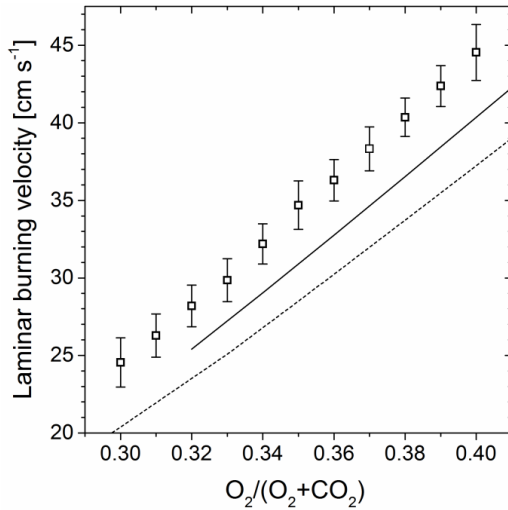


Figure 3. The laminar burning velocity for nitromethane+O<sub>2</sub>+CO<sub>2</sub> at stoichiometric conditions and 358 K as a function of O<sub>2</sub> fraction in the oxidizer. Lines: modeling using the mechanisms of Brequigny et al.<sup>10</sup> (dashed) and Mathieu et al.<sup>13</sup> (solid).

#### 4.2 Modelling results

For nitromethane+O<sub>2</sub>+CO<sub>2</sub> flames, modelling results from the mechanisms of Brequigny et al.<sup>10</sup> and Mathieu et al.<sup>13</sup> are presented together with the experimental data in Figure 1. As

evident from the figure the laminar burning velocity is consistently underpredicted by modelling, with the results from the mechanism by Brequigny et al.<sup>10</sup> substantially lower than those of the mechanism by Mathieu et al.<sup>13</sup>. The extent of the underprediction decreases towards richer conditions for the mechanism by Mathieu et al.<sup>13</sup>, going from 3.8 cm/s at  $\phi=0.8$  to 1.3 cm/s at  $\phi=1.6$ , at 358 K. The corresponding numbers for the mechanism of Brequigny et al.<sup>10</sup> show an opposite trend with respect to equivalence ratio, going from 5.4 cm/s at  $\phi=0.8$  to 6.2 cm/s at  $\phi=1.6$ , at 358 K. It is important to note that for both mechanisms the underpredictions are well outside the uncertainty limits of the experimental results.

The influence of O<sub>2</sub>-content in the oxidizer can be observed by comparing the slopes of the experimental results (symbols) and the model predictions (lines) in Figure 3. At all oxygen concentrations considered here the mechanisms give results below the lower uncertainty limits and the modelling results deviate further from the measurements with increasing O<sub>2</sub>-fraction.

Experimental laminar burning velocities for nitromethane+air from Naulé et al.<sup>11</sup>, are presented together with the model predictions from the two mechanisms in Figure 2. The mechanism of Mathieu et al.<sup>13</sup> successfully reproduces laminar burning velocities inside the experimental uncertainty over the entire investigated range of  $\phi$ . The mechanism of Brequigny et al.<sup>10</sup> underpredicts the laminar burning velocity for nitromethane+air, with a trend of increasing deviation at richer conditions.

#### *4.3 Sensitivity analysis*

From the comparisons between modelled and experimental laminar burning velocities, discussed above, it is seen that the two mechanisms show different quantitative and qualitative performance. To elucidate which reactions are responsible for the differences observed,

sensitivity analyses were carried out for nitromethane flames burnt with  $O_2+CO_2$  and with air at  $\phi=1.2$  and 358 K, for both mechanisms. The ten reactions with highest positive and ten reactions with most negative sensitivity were identified for each case and the results are presented in Figures 4 and 5 for the mechanisms of Brequigny et al.<sup>10</sup> and Mathieu et al.<sup>13</sup>, respectively. In the Supplementary material the same data are presented but with results for  $O_2+CO_2$  from both mechanisms shown in Figure S1 and the corresponding results for air in Figure S2.

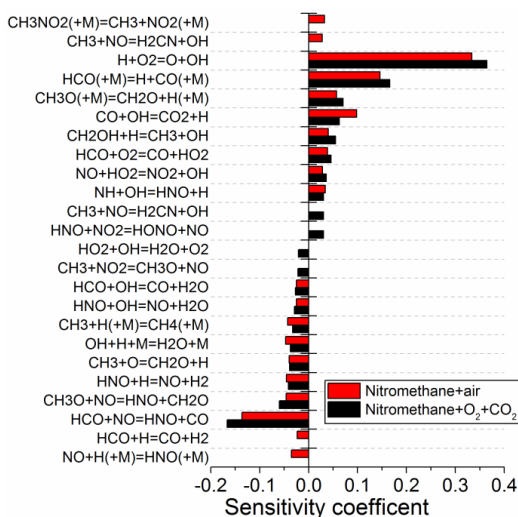


Figure 4. The 20 most sensitive reactions for nitromethane+ $O_2+CO_2$  and nitromethane+air according to the mechanism by Brequigny et al.<sup>10</sup>, at  $\phi=1.2$  and 358 K.

The four most sensitive reactions for flames of nitromethane+air are the same for the two mechanisms:  $H+O_2=O+OH$  (R1),  $CO+OH=CO_2+H$  (R2) and  $HCO+M=H+CO+M$  (R3) with positive sensitivities and  $HCO+NO=HNO+CO$  (R4) with negative sensitivity, as evident from Figure S2. At  $CO_2$ -rich conditions, Figure S1, the sensitive reactions are essentially the same but

for the mechanism of Brequigny et al.<sup>10</sup> the reaction  $\text{CH}_3\text{O}(+\text{M})=\text{CH}_2\text{O}+\text{H}(+\text{M})$  appear with a slightly higher sensitivity than R2. The rate data implemented in the two mechanisms for reactions R1-R4 are collected in Table S3 in the Supplementary material.

The sensitivity spectra comparing the two mechanisms reveal some differences in how the nitrogen chemistry is treated: the mechanism from Brequigny et al.<sup>10</sup> is more sensitive to reactions involving  $\text{HNO}$ , while the mechanism of Mathieu et al.<sup>13</sup> is more sensitive towards a few reactions involving conversion between  $\text{NO}$  and  $\text{NO}_2$ . There are also differences in the sensitivity of the fuel reacting with radicals, but with small sensitivities compared to the four most sensitive reactions.

The most sensitive reaction, R1, has a well determined rate constant with a solid agreement in literature, as discussed by Alekseev et al.<sup>22</sup> The mechanisms tested in the present study use rate constant expressions from different sources, but these are in agreement, as can be seen in Figure S3 in the Supplementary material. It is not likely to be responsible for the different results by the two mechanisms in the present study, and is therefore not further discussed.

The sensitivity for  $\text{CO}+\text{OH}=\text{CO}_2+\text{H}$  (R2) is similar for  $\text{O}_2+\text{CO}_2$  and air combustion, presented in Figures 4 and 5, respectively. Also for this reaction different sources for the rate constant expressions are used in the two mechanisms, but the resulting rate constants are in fairly good agreement, as presented in Figure S4 of the Supplementary material. The rate constant from Rasmussen et al.<sup>23</sup> used by Brequigny et al.<sup>10</sup> is valid for 1 bar. No pressure dependence was implemented, although rate constants at a range of pressures were provided by Rasmussen et al.<sup>23</sup> Since the present study is conducted at only atmospheric pressure this choice is not expected to be important. Mathieu et al.<sup>13</sup> implemented the rate constant from Joshi and Wang<sup>24</sup> calculated for the temperature range 120-2500 K.

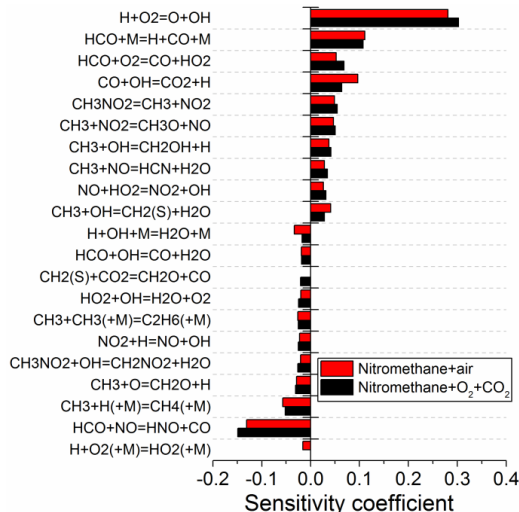


Figure 5. The 20 most sensitive reactions for nitromethane+O<sub>2</sub>+CO<sub>2</sub> and nitromethane+air according to the mechanism by Mathieu et al.<sup>13</sup>, at  $\phi=1.2$  and 358 K.

For nitromethane+air the reaction  $\text{HCO}+\text{M}=\text{H}+\text{CO}+\text{M}$  (R3) has a large sensitivity for the mechanism by Brequigny et al.<sup>10</sup>, at both oxidizer conditions, see Figure 4. The reaction is treated differently in the two mechanisms and is therefore a likely candidate for discrepancies. In the mechanism of Brequigny et al.<sup>10</sup> R3 is assigned the pressure dependent rate constant from Hippler et al.<sup>25</sup>, while in the mechanism of Mathieu et al.<sup>13</sup> the rate constant from Li et al.<sup>26</sup>, multiplied by a factor of 1.2, is used. Rate constants are presented in Figure S5 of the Supplementary material. The low pressure rate constant from Hippler et al.<sup>25</sup> and the rate constant from Li et al.<sup>26</sup> are in reasonable agreement. However, the pressure dependence of the rate constant for R3 by Hippler et al.<sup>25</sup> implies that at 1 atm, the reaction occurs in the falloff regime. The unusual pressure dependence and the low pressure rate constant were questioned by Krasnoperov et al.<sup>27</sup>. The reasoning of Krasnoperov et al.<sup>27</sup> was as follows: Hippler et al.<sup>25</sup> measured the HCO decay rates in initial high concentrations, where bimolecular radical reactions

can be expected to occur readily. Yet the HCO decay observed were attributed to solely the HCO decomposition reaction and interference from radical-radical reactions were neglected. In the present study atmospheric pressure is considered and therefore the rate  $\sim 1$  atm is of importance.

Using a rate constant at the low pressure limit would more realistically represent the conditions of the present study; therefore the rate constant used by Mathieu et al.<sup>13</sup>, was implemented in the mechanism of Brequigny et al.<sup>10</sup>. This increased significantly the predicted laminar burning velocity, now in better agreement with the experimental results, as can be seen in Figure 6. Also the nitromethane+air flames were rerun with the updated rate constant, as presented in Figure 7. The laminar burning velocity is now overpredicted by the modified mechanism of Brequigny et al.<sup>10</sup> on the lean side, while reproducing the laminar burning velocity successfully within the experimental uncertainty in rich mixtures.

Reaction R4 shows the largest negative sensitivity for all cases. The two mechanisms use the same rate constant and therefore this reaction was not considered further.

The two mechanisms treat the collisional efficiencies in R3 differently, most notably for H<sub>2</sub>O, which was shown to be of importance for flames at CO<sub>2</sub>-rich conditions in methanol+O<sub>2</sub>+CO<sub>2</sub> flames<sup>16</sup>. Increasing the third body collisional efficiency for reaction R3 in the mechanism of Brequigny et al.<sup>10</sup> to 12, the same numeric value as employed by Mathieu et al.<sup>13</sup> and Nauc  r et al.<sup>16</sup> decreased the laminar burning velocity further below the experimental results, as can be seen in Figure 6.

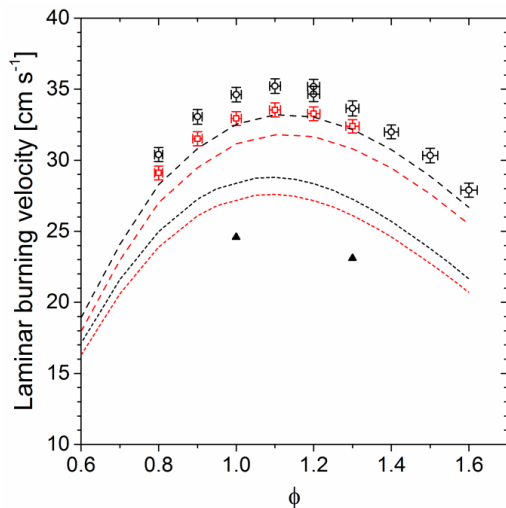


Figure 6. Laminar burning velocities at 1 atm for nitromethane+O<sub>2</sub>+CO<sub>2</sub>. Open symbols: measurements at 348 K (red squares) and 358 K (black circles). Lines: modeling using the mechanism of Brequigny et al.<sup>10</sup> with original value on R3 (short dash) and with R3 adopted from Mathieu et al.<sup>13</sup> (long dash) at 348 K (red) and 358 K (black). The black triangles represent modeling with the mechanism of Brequigny et al.<sup>10</sup>, at 358 K, using a collisional coefficient of 12 for H<sub>2</sub>O.

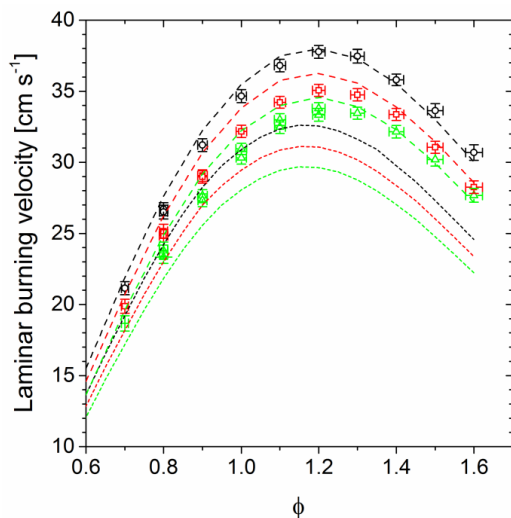


Figure 7. Laminar burning velocities at 1 atm for nitromethane+air. Symbols: measurements from Naucler et al.<sup>11</sup> at 338 K (green triangles), 348 K (red squares) and 358 K (black circles). Lines: modeling using the mechanism of Brequigny et al.<sup>10</sup> with original value on R3 (short dash) and with R3 adopted from Mathieu et al.<sup>13</sup> (long dash) at 338 K (green) 348 K (red) and 358 K (black).

## 5. CONCLUSIONS

The first experimental determination of the laminar burning velocities of nitromethane+O<sub>2</sub>+CO<sub>2</sub> flames was presented. Two kinetic mechanisms were tested for the ability to reproduce the experimental results of the present study and previously published results for nitromethane+air flames<sup>11</sup>. The mechanism by Mathieu et al.<sup>13</sup> successfully reproduced the data for nitromethane+air flames, while underpredicting the laminar burning velocities at CO<sub>2</sub> rich conditions. The mechanism by Brequigny et al.<sup>10</sup> underpredicts the laminar burning velocity for

both examined cases. The behaviour of both mechanisms varies with mixture composition and oxidizer composition.

A sensitivity analysis revealed that the impacts of individual reactions were similar for the laminar burning velocity for nitromethane with air and CO<sub>2</sub>-rich combustion. In the sensitivity analysis the reaction  $\text{HCO} + \text{M} = \text{CO} + \text{H} + \text{M}$  was the second most sensitive at all conditions, and since the rate constants for this reaction were different in the two mechanisms it was considered as a candidate for modification. The unusual pressure dependence in the rate constant used by Brequigny et al.<sup>10</sup> was questioned in literature<sup>27</sup> and replacing it with the rate constant implemented by Mathieu et al.<sup>13</sup>, significantly improved the performance of the mechanism from Brequigny et al.<sup>10</sup>.

It is concluded that the mechanism of Mathieu et al.<sup>13</sup>, previously not validated for flames, accurately predict laminar burning velocities of nitromethane+air flames at atmospheric pressure. The original mechanism by Brequigny et al.<sup>10</sup> showed significant underpredictions at all conditions, but upon modification of the rate constant for reaction  $\text{HCO} + \text{M} = \text{CO} + \text{H} + \text{M}$  performance is significantly improved with good agreement for nitromethane+air flames and only a minor underprediction for nitromethane+O<sub>2</sub>+CO<sub>2</sub> flames.

## **Acknowledgements**

The authors would like to acknowledge the financial support from the Centre for Combustion Science and Technology (CECOST), Sweden

## **References**

- (1) Habib, M. A.; Nemitallah, M.; Ben-Mansour, R. *Energy Fuels* **2013**, 27 (1), 2-19.
- (2) Wang, P.; Casleton, K.; Hedges, S. In *Effect of biomass blending on oxy-fuel coal combustion*, 28th Annual International Pittsburgh Coal Conference 2011, PCC 2011, 2011; pp 987-995.
- (3) Toftegaard, M. B.; Brix, J.; Jensen, P. A.; Glarborg, P.; Jensen, A. D. *Prog. Energy Combust. Sci.* **2010**, 36 (5), 581-625.
- (4) Normann, F.; Andersson, K.; Leckner, B.; Johnsson, F. *Prog. Energy Combust. Sci.* **2009**, 35 (5), 385-397.
- (5) Glarborg, P.; Jensen, A. D.; Johnsson, J. E. *Prog. Energy Combust. Sci.* **2003**, 29 (2), 89-113.
- (6) Shaddix, C. R.; Molina, A. *Proc. Combust. Inst.* **2011**, 33, 1723-1730.
- (7) Zaslonko, I. S.; Petrov, Y. P.; Smirnov, V. N. *Kinet. Catal.* **1997**, 38 (3), 321-324.
- (8) Glarborg, P.; Bendtsen, A. B.; Miller, J. A. *Int. J. Chem. Kinet.* **1999**, 31 (9), 591-602.
- (9) Zhang, K. W.; Li, Y. Y.; Yuan, T.; Cai, J. H.; Glarborg, P.; Qi, F. *Proc. Combust. Inst.* **2011**, 33, 407-414.
- (10) Brequigny, P.; Dayma, G.; Halter, F.; Mounaïm-Rousselle, C.; Dubois, T.; Dagaut, P. *Proc. Combust. Inst.* **2014**, 35 (1), 703-710.
- (11) Naucclér, J. D.; Nilsson, E. J. K.; Konnov, A. A. *Combust. Flame* **2015**, 162 (10), 3803-3809.
- (12) Nauccler, J. D.; Li, Y.; Nilsson, E. J. K.; Curran, H. J.; Konnov, A. A. *Fuel* **2016**, 186, 629-638.
- (13) Mathieu, O.; Giri, B.; Agard, A. R.; Adams, T. N.; Mertens, J. D.; Petersen, E. L. *Fuel* **2016**, 182, 597-612.
- (14) De Jaegere, S.; Van Tiggelen, A. *Combust. Flame* **1959**, 3 (2), 187-200.

- (15) Alekseev, V. A.; Naucler, J. D.; Christensen, M.; Nilsson, E. J. K.; Volkov, E. N.; de Goey, L. P. H.; Konnov, A. A. *Combust. Sci. Technol.* **2016**, *188* (6), 853-894.
- (16) Naucler, J. D.; Sileghem, L.; Nilsson, E. J. K.; Verhelst, S.; Konnov, A. A. *Combust. Flame* **2015**, *162* (5), 1719-1728.
- (17) Starkman, E. S. *Ind. Eng. Chem.* **1959**, *51* (12), 1477-1480.
- (18) Tian, Z. Y.; Zhang, L. D.; Li, Y. Y.; Yuan, T.; Qi, F. *Proc. Combust. Inst.* **2009**, *32* (1), 311-318.
- (19) *CHEMKIN IV 15101*, Reaction Design: San Diego, 2010.
- (20) Fomin, A.; Zavlev, T.; Alekseev, V. A.; Rahinov, I.; Cheskis, S.; Konnov, A. A. *Combust. Flame* **2016**, *171*, 198-210.
- (21) Zhou, C.-W.; Li, Y.; O'Connor, E.; Somers, K. P.; Thion, S.; Keese, C.; Mathieu, O.; Petersen, E. L.; DeVerter, T. A.; Oehlschlaeger, M. A.; Kukkadapu, G.; Sung, C.-J.; Alrefae, M.; Khaled, F.; Farooq, A.; Dirrenberger, P.; Glaude, P.-A.; Battin-Leclerc, F.; Santner, J.; Ju, Y.; Held, T.; Haas, F. M.; Dryer, F. L.; Curran, H. J. *Combust. Flame* **2016**, *167*, 353-379.
- (22) Alekseev, V. A.; Christensen, M.; Konnov, A. A. *Combust. Flame* **2015**, *162* (5), 1884-1898.
- (23) Rasmussen, C. L.; Hansen, J.; Marshall, P.; Glarborg, P. *Int. J. Chem. Kinet.* **2008**, *40* (8), 454-480.
- (24) Joshi, A. V.; Wang, H. *Int. J. Chem. Kinet.* **2006**, *38* (1), 57-73.
- (25) Hippler, H.; Krasteva, N.; Striebel, F. *Phys. Chem. Chem. Phys.* **2004**, *6* (13), 3383-3388.
- (26) Li, J.; Zhao, Z. W.; Kazakov, A.; Chaos, M.; Dryer, F. L.; Scire, J. J. *Int. J. Chem. Kinet.* **2007**, *39* (3), 109-136.

(27) Krasnoperov, L. N. *Phys. Chem. Chem. Phys.* **2005**, 7 (9), 2074-2076.



